Technische Universität München

Fakultät für Chemie

Bayerisches NMR Zentrum

Lehrstuhl für Biomolekulare NMR-Spektroskopie

Natural products and derivatives as novel scaffolds targeting PTP1B

Eleni Kyriakou

Vollständiger Abdruck der von der Fakultät für Chemie der Technischen Universität München zur Erlangung des akademischen Grades eines Doktors der Naturwissenschaften genehmigten Dissertation.

Vorsitzender:		Prof. Dr. Franz Hagn
Prüfer der Dissertation:	1.	Prof. Dr. Michael Sattler
	2.	Prof. Dr. Dierk Niessing

Die Dissertation wurde am 18.10.2017 bei der Technischen Universität München eingereicht und durch die Fakultät für Chemie am 04.12.2017 angenommen.

Table of Contents

Abstract

Type 2 diabetes (T2D) is one of the most serious metabolic disorders of our time that is characterized by hyperglycemia and insulin resistance. Patients with T2D are usually obese and consequently there is a direct link between T2D and obesity. Although, there are many therapeutic approaches developed for both diseases individually, there are no drugs that target both disorders at the same time. It has been suggested that a combination of antidiabetic and anti-obesity medication may be more effective for the treatment of both T2D and obesity. Protein tyrosine phosphatase 1B (PTP1B) is a negative regulator of insulin and leptin signaling pathways. It is an attractive drug target for T2D and obesity since it was reported that PTP1B knockout (KO) mice exhibit increased insulin sensitivity and are resistant to high-fat diet-induced obesity. It has been also shown that neuronal PTP1B knockout mice have increased leptin sensitivity, reduced body weight and increased energy expenditure. These results suggest that PTP1B specific inhibitors may thus be therapeutically beneficial in obesity as well as in T2D.

PTP1B inhibitors development has been proven to be challenging due to specificity and cell permeability problems. Lack of selectivity is based on the high homology that protein tyrosine phosphatases (PTPs) share in their catalytic domains. TCPTP is the most homologous phosphatase to PTP1B. Following different strategies many potent and selective PTP1B inhibitors have been produced with desirable physiochemical properties. However, there is no effective inhibitor of PTP1B that has been passed successfully Phase II clinical trials.

In this work I attempt to identify modulators of PTP1B and TCPTP that can be used as scaffolds for the development of potent drug candidates. For this purpose, I followed a structured-based drug discovery approach, using a combination of biochemical and biophysical methods.

Chapter 1 introduces the biological background of T2D and obesity and the current available therapeutic. Main focus is given on the role of PTP1B on T2D and obesity and previously known data about the drug development for PTP1B inhibitors is highlighted. Chapter 2 includes basic theory of NMR spectroscopy and some of its applications used in this study. Chapter 3 presents the material used in this study and describes the methods providing experimental details.

Chapter 4 provides the biochemical methods results concerning the best conditions for protein expression and purification, NMR applications and the assays used in this study. It is also shows the backbone assignment of PTP1B.

Chapter 5 focuses in the preparation of a compound library containing mainly natural products with antidiabetic and anti-obesity properties and its use in different screenings. The compounds have been classified according to their biosynthetic origin into three classes: triterpenoids, steroids and other compounds. Their interaction with PTP1B has been tested using ligand-based NMR approaches (1D screening and STDs) and their inhibitory activity over PTP1B has been determined using a colorimetric assay (pNPP assay). I have found interesting compounds that modulate differently PTP1B and its highly homologous phosphatase, TCPTP, in low micromolar range. The binding site of 18β-glycyrrhetinic acid, cholesterol sulfate and trodusquemine were mapped on the 3D structure of PTP1B using NMR. All three compounds were found to bind to different binding sites on PTP1B, most probably allosteric. Using a cellular assay in collaboration with Paul Pfluger (IDO, HMGU), it was found that our best hits also enhance insulin sensitivity.

Chapter 6 unravels the mechanism through which compound celastrol induces loss of body weight. Using an activity assay (DiFMUP assay), NMR spectroscopy approaches and Mass spectrometry was shown that celastrol is a reversible non-competitive inhibitor of both PTP1B and TCPTP in both reduced and oxidized conditions. Mapping the binding site of celastrol onto the 3D structure of PTP1B revealed that binds close to the catalytic site but not directly in it. Using the same cellular assay, celastrol was found to enhance insulin sensitivity. In addition, our collaborators (Michael Cowley, Stephanie Simonds, Monash University, Australia) show using mice with genetically deletion of PTP1B, TCPTP and SOCS3 that the weight lowering effects of celastrol are due to hypothalamic PTP1B and TCPTP inhibition that regulate appetite in the brain.

In summary, this thesis demonstrates the role of new triterpenoid scaffolds targeting PTP1B and TCPTP as anti-obesity and antidiabetic agents. The collected structural information of the most important binding groups of each scaffold class can be used in the future for the development of new more efficient inhibitors. Regulation of PTPs via non-competitive, allosteric inhibition using celastrol or structurally related compounds may offer an efficacious way to overcome these challenges, such as poor cell permeability, selectivity and in vivo efficacy, enhancing leptin action and offering a path forward toward a clinical anti-obesity trial. In addition,

the role of some hormones and vitamins as activators or inhibitors can provide new information about regulation of biological signaling pathways not previously described.

1. Introduction I: Biological background

1.1 Diabetes mellitus type 2

Diabetes mellitus is a chronic metabolic disorder in which the body is unable to regulate blood glucose levels (Dixon et al. 2017). Diabetes is one of the largest global epidemic of our time. As of 2015, the International Diabetes Federation estimated the number of people with diabetes worldwide to be nearly 415 million (International Diabetes Federation: *IDF Diabetes Atlas 7th edition*, 2015 [article online available from www.idf.org.]) This number is expected to exceed 642 million by 2040. There are three main type of diabetes: type 1 diabetes (T1D), type 2 diabetes (T2D) and gestational diabetes.

T1D known as "insulin-dependent diabetes mellitus" or "juvenile diabetes" is an autoimmune disorder of the pancreatic beta cells leading to insufficient insulin production and resulting in high blood glucose levels (Los and Wilt 2017). People with T1D must receive daily insulin which is usually administrated through injections (Cefalu 2004).

Gestational diabetes appears during pregnancy, it can lead to serious health risks for both the mother and child and it is associated with an increased risk of both mother and child developing T2D later in life (McCance 2015).

T2D is the metabolic disease in which the body doesn't respond properly to insulin that sometimes can be combined with reduced insulin secretion (Sorli 2014). It is the most dominant type of diabetes, which is directly linked to lifestyle factors.

Many therapeutic approaches have been developed for T2D (Nguyen et al. 2011). There are 13 classes of FDA approved antidiabetic agents for the treatment of T2D, which are alpha-glucosidase inhibitors, amylin analogues, biguanide (metformin), bile acid sequestrant, dopamine agonist, incretin mimetics (or GLP-1 receptor agonists), insulin preparations, nonsulfonylurea secretagogues, first and second generation sulfonylureas, thiazolidinediones, sodium-glucose cotransporter-2 inhibitors (SGLT-2 inhibitors) (Nguyen et al. 2011). All of them have either no effect on weight loss or they increase the body weight. The only exceptions are the amylin analogues, the incretin mimetics,DPP-4 inhibitors and the SGLT-2 inhibitors (Nguyen et al. 2011; Esquivel and Lansang 2017). Among the FDA approved drugs for T2D, metformin is the most effective drug. It decreases the hepatic glucose, while it increases peripheral glucose uptake (Y.-

W. Wang et al. 2017; Sanchez-Rangel and Inzucchi 2017). However, most of these drugs are not providing an appropriate glycemic control to patients with chronic T2D. There are another new 6 drug classes with new mechanisms of action that aim to improve patients' outcome. These new classes include, 11 beta-hydroxysteroid dehydrogenase, glycogen phosphorylase inhibitors, glucokinase activators, G protein-coupled receptor 119 agonists, glucagon-receptor antagonists and protein tyrosine phosphatase 1B inhibitors. Some representatives of the last categories are in clinical trials.

T2D is closely associated with obesity and patients with T2D are usually overweight or obese (Smyth and Heron 2006; Esquivel and Lansang 2017). The most effective treatment against obesity until now is considered the bariatric surgery (Schauer et al. 2017). However, several drugs have been approved for weight loss, and although their effect on weight tends to be moderate, some have been shown to reduce the incidence of T2D and improve diabetic control (Saltiel 2016; Burguera, Ali, and Brito 2017). There are 7 FDA approved anti-obesity drugs, most of which decrease appetite and only Orlistat decreases fat absorption and it's the only one that acts outside the brain. It has been suggested that a combination of antidiabetic and anti-obesity medication may be more effective for the treatment of both T2D and obesity (Burguera, Ali, and Brito 2017).

Despite the abundance of FDA approved drugs for both diabetes type 2 and obesity until now there is no effective drug available that can cure them. It is important to develop new approaches with new mechanism of action that not only improve the blood glucose control but also do not contribute to weight gain in patients that are suffering already from obesity (Esquivel and Lansang 2017; McFarlane 2009). The new treatments should target both metabolic diseases.

1.2 Protein Tyrosine Phosphatases (PTPs)

Protein phosphorylation and dephosphorylation are fundamental mechanisms for the control of cell growth, proliferation, differentiation and survival apoptosis (Soulsby and Bennett 2009). These reactions are catalyzed by the coordinated actions of protein tyrosine kinases (PTKs) and protein tyrosine phosphatases (PTPs), respectively. Abnormal activity of PTPs and PTKs can result into the development of many diseases like diabetes and cancer (He et al. 2005; Tamrakar, Maurya, and Rai 2014). Consequently, cellular pathways regulated by tyrosine phosphorylation offer a rich source of drug targets for developing novel therapeutics (S. Zhang and Zhang 2007).

Phosphatases are enzymes that catalyze dephosphorylation reactions. They can be divided based on their structure and substrate specificity into protein tyrosine phosphatases (PTPs) and

protein serine/threonine phosphatases (PSPs). There are more than hundred human PTPs that can be subdivided into four classes (Alonso et al. 2004). Classes I, II and III are cysteine-based PTPs and class IV are aspartate-based PTPs (Alonso et al. 2004; Tamrakar, Maurya, and Rai 2014).

Class I PTPs is the largest subfamily of cysteine-based PTPs and comprises two subfamilies, the "classical" and the "dual-specificity" PTPs (Barr 2010). The "classical" PTPs show a strictly substrate specificity for phosphotyrosine (pTyr) residues. They can be further classified into the intracellular PTPs and the transmembrane or receptor-like PTPs (Barr 2010; Tamrakar, Maurya, and Rai 2014). The most known receptor-like "classical" PTP is protein CD45 that is expressed on the surface of leucocytes. Some examples of intracellular PTPs are PTP1B, TCPTP, SHP2, STEP etc. In contrast, dual specificity PTPs (DUSPs) are cysteine-based PTPs with activity toward protein- and/or non-protein substrates. An example of DUSP with protein-specificity is the phosphothreonine (pThr)-/pTyr-specific MAPK phosphatases (MKPs). A DUSP with non-protein specificity is DUSP11, which is mRNA specific (Patterson et al. 2009).

Class II cysteine-based PTPs are the so-called "low molecular weight" PTPs (LMW-PTPs), with molecular weight of 15 to 18 kDa. They show specificity for pTyr substrates and have been found in numerous prokaryotes and eukaryotes. HCPTPA is an example of human LMW-PTP (Alonso et al. 2004).

Class III PTPs belong to the family of cell division control proteins (Cdc) and they are named Cdc25. They are acting by dephosphorylating cyclin-dependent kinases (Cdks) at their inhibitory, dually phosphorylated N-terminal Thr-Tyr motifs and subsequently activating them. There are three isoforms identified in humans: Cdc25A, B and C (Hobiger and Friedrich 2015; Alonso et al. 2004).

Class IV are aspartate-based PTPs, and as their name reveals they utilize aspartate-based catalysis (Moorhead, Trinkle-Mulcahy, and Ulke-Lemée 2007). They are a relatively new class of phosphatases, since they have only been noted in the last decade. It is clear that this is a much larger family of enzymes, which play important roles in development, sodium stress in yeast and nuclear morphology. RNA polymerase II C-terminal domain phosphatase is a member of this family (Moorhead et al. 2009).

From the above PTPs the phosphatase that has attracted special attention in recent years, because it is well-known to act as negative regulator in the insulin signaling pathway is protein

tyrosine phosphatase 1 B (PTP1B) (Goldstein et al. 2000). Therefore, it is a core subject of current pharmaceutical research as potential target for the treatment of type 2 diabetes and obesity.

1.3 PTP1B structural characteristics

Protein tyrosine phosphatase 1B (PTP1B) was the first intracellular PTP to be purified and characterized (Tamrakar, Maurya, and Rai 2014). PTP1B is a 50 kDa monomeric protein encoded by the PTPN1 gene and contains 435 amino acids (Feldhammer et al. 2013). The N-terminal domain (residues 1-298) includes the catalytic domain (PTP domain) which harbors 3 conserved motifs among PTPs: the phosphate binding loop (P-loop), the WPD loop and the Q loop. The P-loop (active site) of PTP1B is approximately 8 to 9 Å deep and is comprised of residues 214 to 221 (His-Cys-Ser-Ala-Gly-Ile-Gly-Arg), with Cys215 being responsible for the catalytic activity. The WPD loop (residues 179-181) is a highly flexible motif that defines if the protein is in "opened" or "closed" conformation and contains the residue Asp181 that plays a crucial role in the catalytic mechanism acting as a general acid. The Q-loop contains the residue 262 and is fundamental for the mechanism of the reaction catalysis. The C-terminal domain of PTP1B (residues 299-435) contains two proline rich motifs (residues 300-308 and 309-314), which have been reported to mediate binding to key SH3 domain-containing proteins, and a 35 amino acid hydrophobic tail (residues 400-435) that localizes the enzyme at the cytoplasmic face of the endoplasmic reticulum (ER) and plays a regulatory role by limiting the cellular space where PTP1B can exert its enzymatic activity (Feldhammer et al. 2013; Popov 2011; Jiang, Liang, and Guo 2012) (**Figure 1.1**).

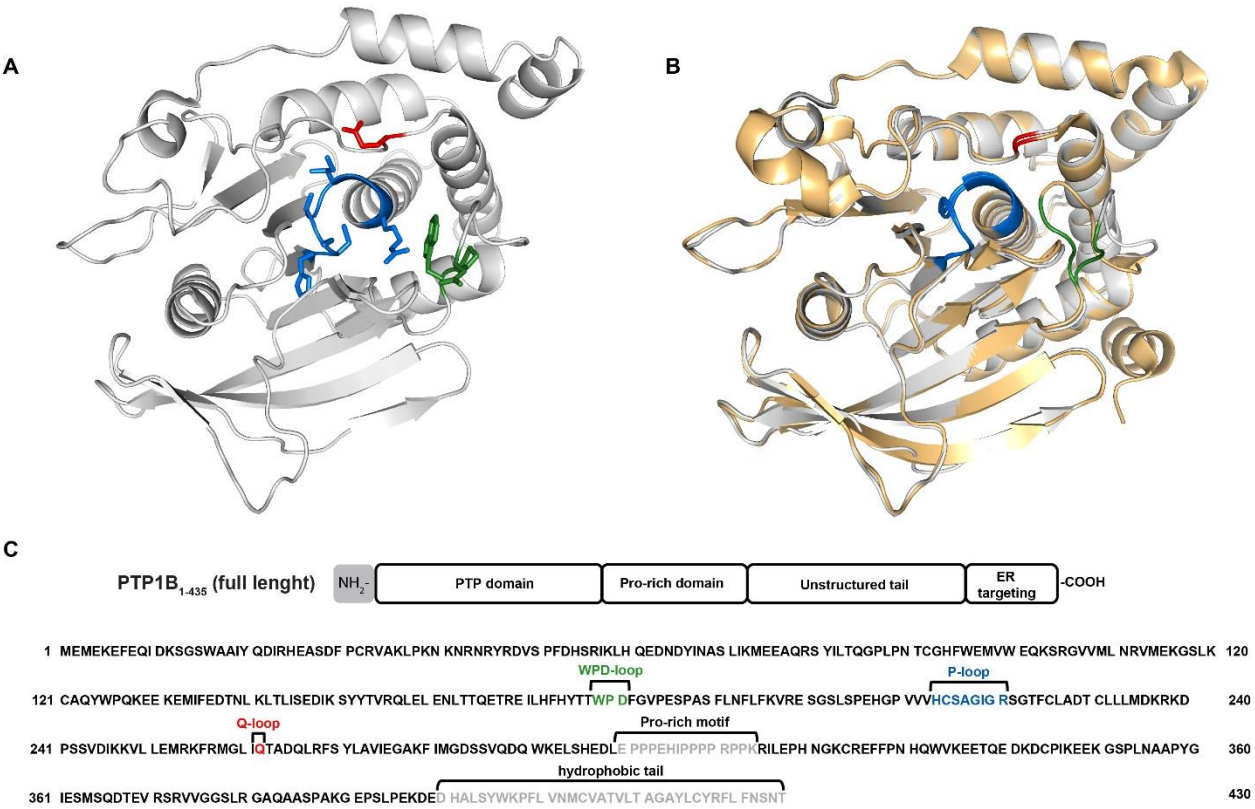

Figure 1.1 Structural characteristics of protein PTP1B.
(A) Illustration of the catalytic site characteristic loops, P-loop (blue), Q-loop (red) and WPD-loop (green). **(B)** Superimpose of the open (2HNP, grey) and the close (1WAX, gold) conformations of PTP1B, only the WPD-loop (green) undergoes a structural modification. **(C)** PTP1B domain organization and sequence with the characteristic structural motifs.

1.4 PTP1B reaction mechanism

The kinetic reaction catalyzed by PTPs can be described by a ping-pong mechanism (Z.-Y. Zhang 1998). The mechanism is characterized by a two-step catalytic process. In the first step, a nucleophilic attack on the substrate phosphate ester moiety by the catalytic cysteine of the P-loop results in the formation of a phosphoenzyme intermediate. The Asp181 residue of the WPD loop mediates the formation of the cysteine-phosphate intermediate donating a proton to the substrate leaving group. The second step of the reaction is carried out by the WPD loop. Upon substrate binding, the loop swings back over the catalytic pocket bringing the aspartate residue in proximity for catalysis. The last step of the reaction involves the glutamine residue of the Q loop and the aspartic acid of the WPD loop. Glu262 and Asp181 act together in order to hydrolyze the phosphoenzyme intermediate through the coordination of a water molecule in a general base reaction yielding the final products inorganic phosphate and the regenerated enzyme. The aspartic

acid in this loop functions as a general acid in the first step and as a general base catalyst in the second step (Brandão, Hengge, and Johnson 2010) (**Figure 1.2**).

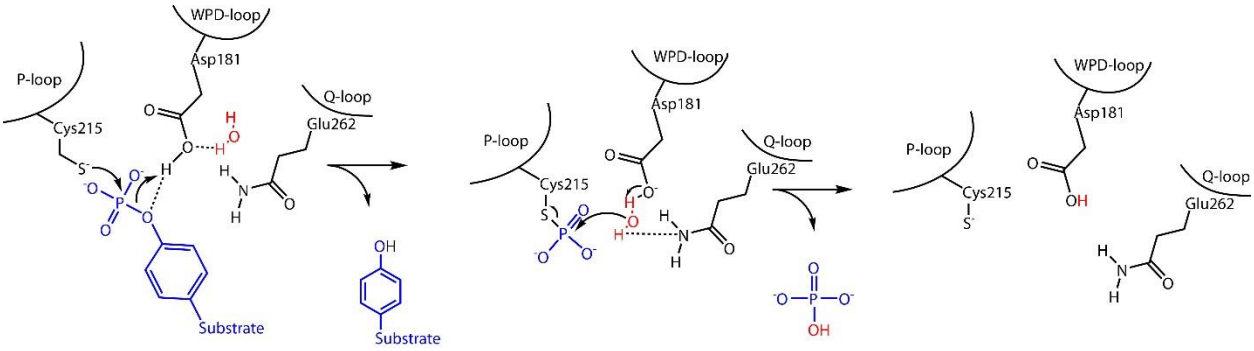

Figure 1.2 PTP1B reaction mechanism. Adapted from (Tautz and Sergienko 2013).

1.5 Role of PTP1B in insulin and leptin regulation

PTP1B is expressed ubiquitously in the classical insulin-targeted tissues such as liver, muscle and fat. Insulin is the hormone that maintains the glucose homeostasis. It has been reported that PTP1B plays a major role as regulator of insulin signaling, particularly in response to metabolic or inflammatory stresses (Tanti and Jager 2009; Powell 2006). PTP1B is also expressed in the brain and more specifically in the hypothalamus, where leptin a key hormone regulates energy intake and expenditure, including appetite/hunger, and a wide array of metabolic and regulatory processes (Feldhammer et al. 2013).

Insulin cascade starts upon binding of insulin on its receptor (insulin-receptor, IR) that activates the insulin-receptor substrate (IRS) through autophosphorylation. Activation of IRS induces the activation of phosphatidylinositol 3-kinase (PI3K) through binding to the p85 subunit and activating the catalytic p110 subunit. PI3K activation induces downstream effectors, such as protein kinase B (AKT), leading to translocation of glucose transporter 4 (GLUT4) to the plasma membrane and glucose uptake in muscle, and inactivation of glycogen-synthase kinase 3 (GSK3). PTP1B has been reported to terminate the insulin cascade by dephosphorylating the IR and the IRS (Johnson, Ermolieff, and Jirousek 2002). Thus, PTP1B act as a negative regulator of insulin action by dephosphorylating both IR and IRS1 (Goldstein et al. 2000) (**Figure 1.3**).

The leptin signaling pathway starts upon binding of leptin hormone to its receptor (ObR) that leads to phosphorylation of janus kinase 2 (JAK2), activating the JAK/signal transducer and activator of the transcription (STAT) pathway and possibly the PI3K pathway through less well-defined mechanisms. Activation of STAT3 through JAK2 phosphorylation induces translocation

of STAT3 to the nucleus. STAT3 induces gene responses that reduce transcription of the acetyl-coenzyme-A carboxylase (ACC), reducing malonyl CoA and fatty acid synthesis, while increasing fatty acid oxidation. STAT3 induces also SOCS3 (Suppressor of cytokine signaling 3) and POMC (pro-opiomelanocortin, anorexigenic neuropeptide, appetite-suppressor) expression, while repressing AgRP (agouti-related peptide, orexigenic neuropeptide, appetite-stimulant) (Y. Zhou and Rui 2013; Frühbeck 2006). In the leptin pathway (Johnson, Ermolieff, and Jirousek 2002) neuronal PTP1B dephosphorylates the leptin receptor associated JAK2, resulting in the down regulation of the leptin signaling (Cheng et al. 2002; de Chantemèle et al. 2009).

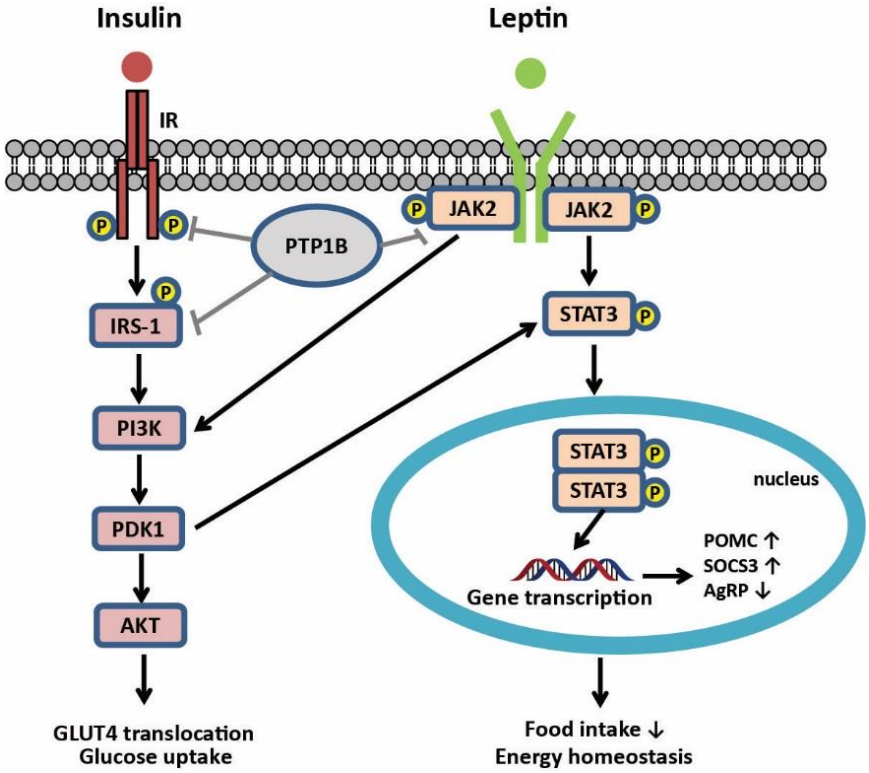

Figure 1.3 Role of PTP1B in insulin and leptin signaling pathways. Adapted from (Johnson, Ermolieff, and Jirousek 2002).

1.6 PTP1B as drug target

Overexpression or overactivation of PTP1B is associated with insulin and leptin resistance that consequently can lead to the development of metabolic disorders like diabetes, obesity and cancer (S. Zhang and Zhang 2007).

It has been shown that PTP1B KO mice appear healthy although they had slightly lower blood glucose levels when compared with the WT littermates. On a high-fat diet PTP1B KO and heterozygous mice had significantly lower triglyceride levels and showed an increased insulin

sensitivity and resistance to weight gain. This is unexpected because insulin is also an anabolic factor, and increased insulin sensitivity can result in increased weight gain (Klaman et al. 2000; Elchebly et al. 1999; Powell 2006). However, PTP1B is a negative regulator of leptin signaling as well. Thus, the resistance to diet-induced obesity observed in PTP1B KO mice is likely to be associated with increased energy expenditure owing to enhanced leptin sensitivity (Cheng et al. 2002). Therefore, PTP1B is an attractive drug target for diabetes type 2 and obesity (Huijsduijnen et al. 2002).

1.7 PTP1B inhibitors for the treatment of T2D

Since its identification in 1989, there are over 250 manuscripts published on the development of PTP1B small molecule inhibitors. Specifically, a range of compounds from natural products to competitive and non-competitive inhibitors of PTP1B have been developed by both industry and academia (G. Liu et al. 2003; Huijsduijnen et al. 2002; Cho 2013; Dadke and Chernoff 2003; Tamrakar, Maurya, and Rai 2014). Some of these compounds exhibit IC_{50} values in the nM range, although none of them have been made it past phase II clinical trials (Barr 2010; S. Zhang and Zhang 2007). Instability, low selectivity and inability of certain charged compounds to penetrate cell membrane were some of the most serious problems (Eleftheriou 2016).

PTP1B inhibitors, synthetic or isolated from natural products, can be classified according to the binding site. The developed inhibitors until now can be divided into two main categories. Inhibitors that bind to the active site of the enzyme and allosteric inhibitors that bind to a non-catalytic site of the protein far from the active site.

1.7.1 Active site inhibitors

The first synthetic and most studied inhibitors of PTP1B targeting the active site of the protein are phosphotyrosine (pTyr) mimetics (**Figure 1.4**). These molecules contain one or two aromatic rings bearing acidic groups, most commonly carboxylic and phosphate groups. They are highly negatively charged at physiological pH and possess polar groups that can form hydrogen bonds with the polar residues of the active site. Whereas Phe182 and Tyr46 that are surrounding the active site can be involved in hydrophobic $\pi \rightarrow \pi$ interactions that can stabilize the complex (Eleftheriou 2016). In general, small molecules that bind strictly to the active site (site A) should contain at least one acidic or hydrogen donor/acceptor moiety (**Figure 1.4**). Another known active site inhibitor of PTP1B is vanadate that has insulin like properties (Tamrakar, Maurya, and Rai

2014). Within the active site, vanadate forms a thiol-vanadyl ester linkage with the catalytic Cys215 (Popov 2011) (**Figure 1.4**). One major issue of these molecules is that they are not selective, since the active site of PTPs enzymes is highly conserved across the family, most PTPs have a close homolog that, if inhibited, would have adverse effects. TCPTP is the tyrosine phosphatase with the greatest similarity to PTP1B, sharing 72% sequence identity overall and 94% identity for the active site residues (**Figure 1.5**) (Barr 2010). This issue has been addressed by identifying of non-catalytic phosphate binding sites near the active site. A secondary binding site (site B) adjacent to the catalytic center in vicinity to residues Arg24, Ser28, Gln262 and Arg254 (**Figure 1.6 A, B**) and an aryl phosphate binding site (site C) facing Lys 41 (**Figure 1.6 C, D**) have been identified. Development of new inhibitors binding simultaneously to both site A and B or A and C has been proposed by scientists as the solution for achieving more effective and highly selectivity inhibitors, since more differences in amino acids between PTP1B and TCPTP are located in these areas. Examples of compounds binding to both sites are compounds containing difluoromethylene phosphate (DFMP) moieties also known as bidentate (**Figure 1.7**). The DFMP moieties were shown to occupy the A and C sites of PTP1B (Shen et al. 2001). The most potent compound of this category is compound 2 (K_i 2.4 nM and 10fold selectivity over TCPTP) that incorporates a nonhydrolyzable phosphonodifluoromethyl phenyl group (F2pmp) (Barr 2010) (**Figure 1.6** and **Figure 1.7**). This type of compounds should contain three hydrogen donor/acceptor moieties (Eleftheriou 2016). However, due to the high polarity, they are not cell permeable and have no cellular activity (Barr 2010). The problem of the restricted cell permeability was addressed by using a prodrug approach and by attaching to the compound a cell permeable peptide and a lipophilic fatty acid. In this way, once the compound enters the cytoplasm, the protecting groups are removed via cellular enzymes to regenerate the original phosphonate.

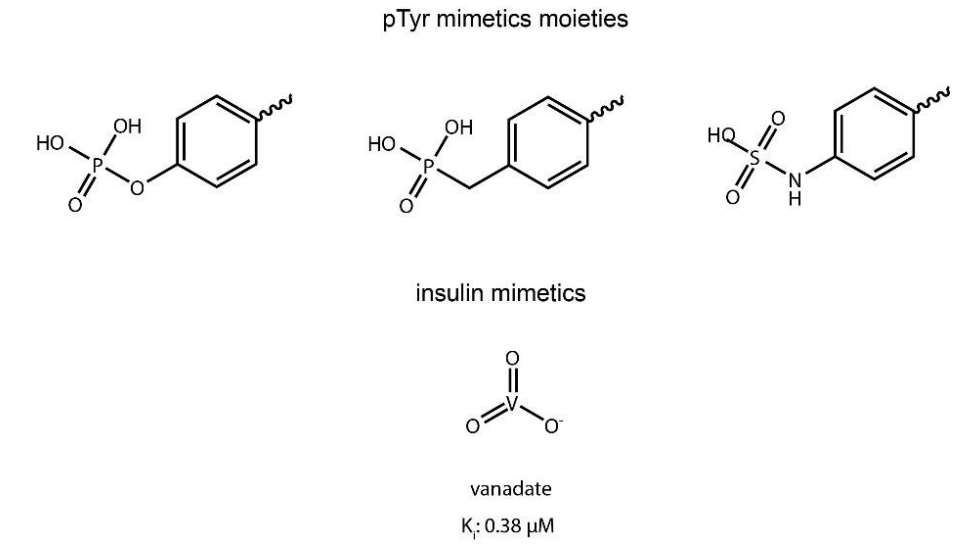

Figure 1.4 pTyr mimetics moieties and the active site inhibitor vanadate.

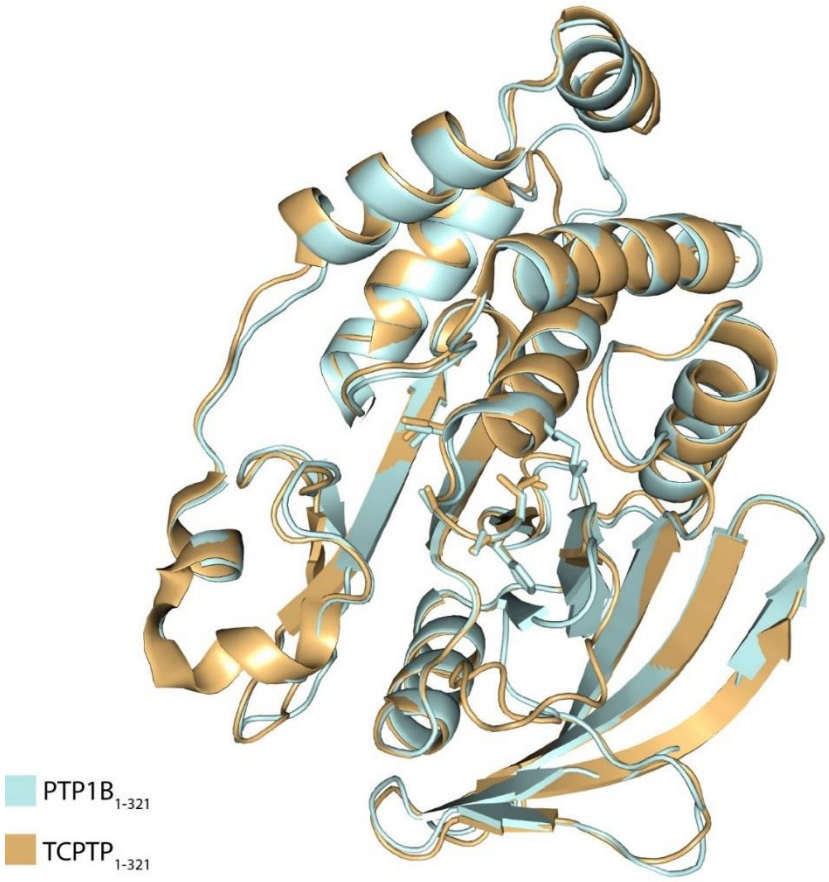

Figure 1.5 Superposition of the crystal structures of PTP1B (2HNP) and TCPTP (1L8K) catalytic domains. The two proteins are highly homologous.

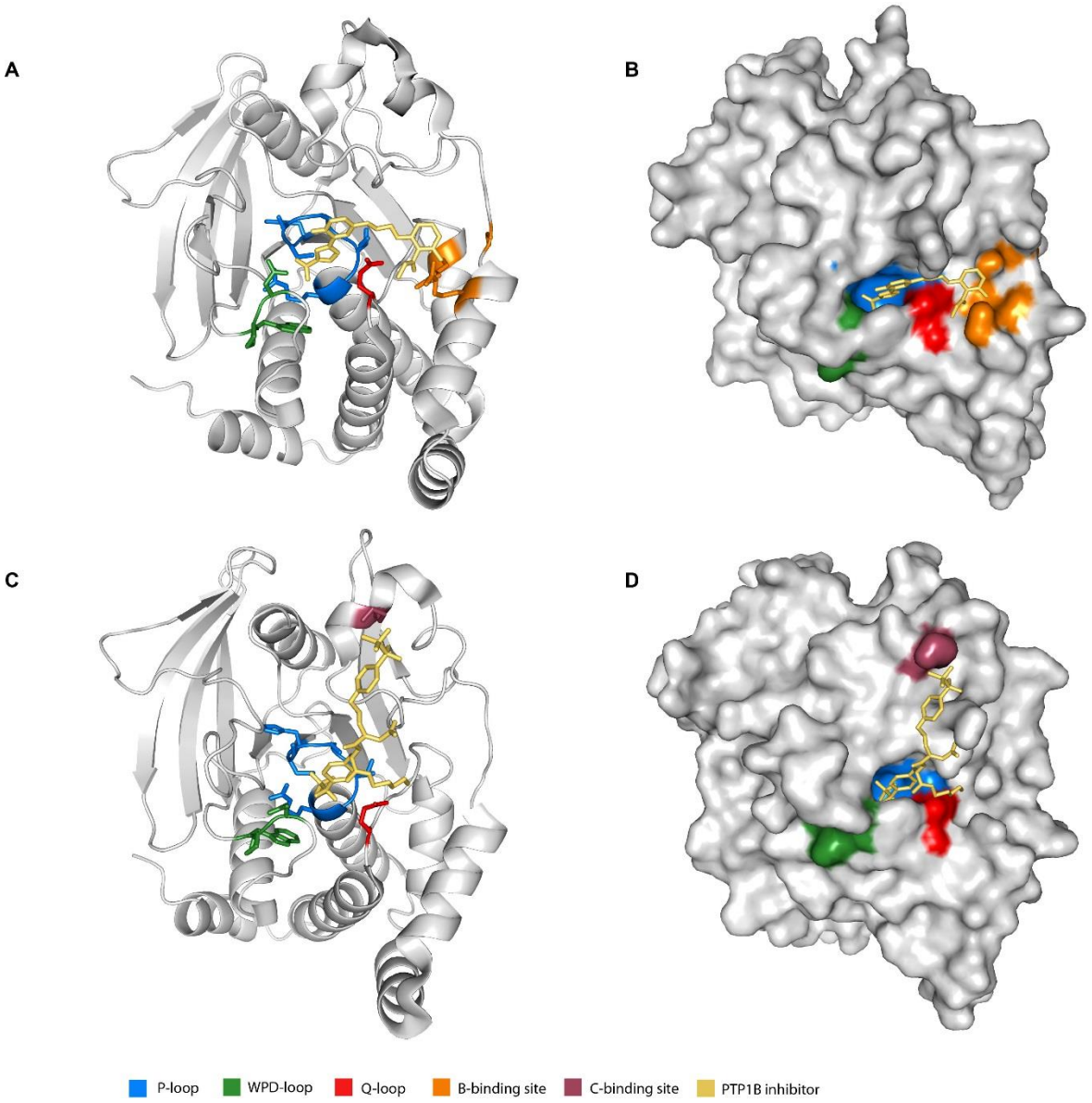

Figure 1.6 Structural characteristics of the secondary binding sites.
(A) Cartoon and **(B)** surface illustration of a pTyr mimetic compound binding into both the active site and the secondary B-binding site (pdb:1Q1M). **(C)** Cartoon and **(D)** surface illustration of compound 2 binding in both the active site and the secondary C-binding site (pdb:1PXH).

Thiadiazolidinone (TZD) and isothiazolidinone (IZD) are improved versions of pTyr mimetics that have modest cell permeability and significant inhibitory cellular activity (**Figure 1.7**). Compound 3 was synthesized by Novartis with an improved inhibitory potency (IC_{50} 126 nM against PTP1B) utilizing the TZD moiety without selectivity or bioavailability data (Cho 2013). Compound 4 was produced by several pharmaceutical companies (Novartis, AstraZeneca, Vertex and Incyte) and has significant cellular activity. IZDs, developed by Incyte, contain only one

delocalized negative charge in contrast to the highly charged phosphonate and carboxylate containing inhibitors, thereby providing improved membrane permeability. A series of more potent compounds have been reported but only minimal selectivity over TCPTP was observed (Barr 2010).

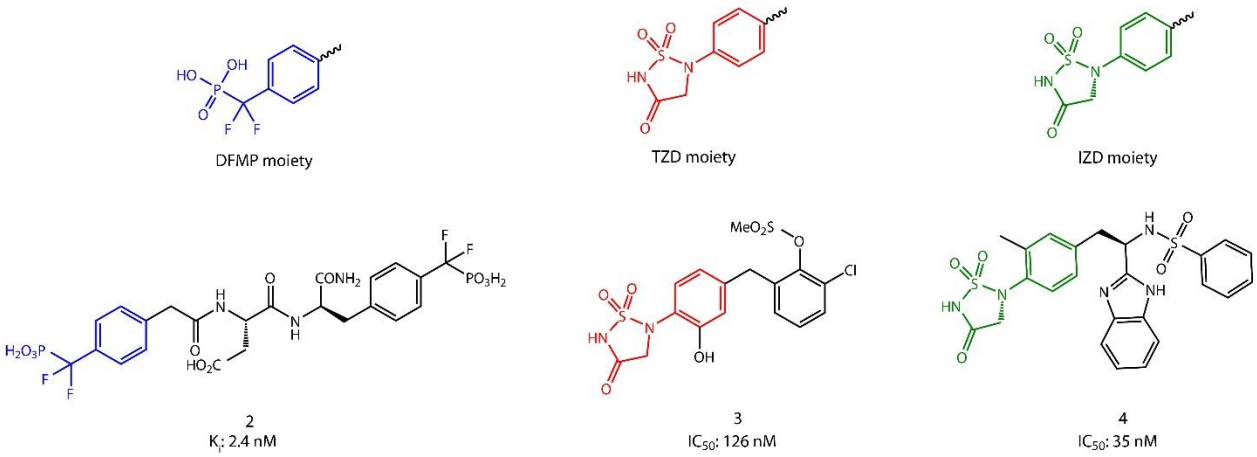

Figure 1.7 Active site inhibitors of the characteristic classes of DFMP, TZD and IZD compounds.

Using NMR-based methods together with X-ray fragment-based lead discovery, Abbott laboratories identified compounds that occupy both the active site and the secondary non-catalytic site. By linking the fragments, they developed compounds with Ki value in nM range and up to 4-fold selectivity over TCPTP (**Figure 1.8** compounds 5 and 6).

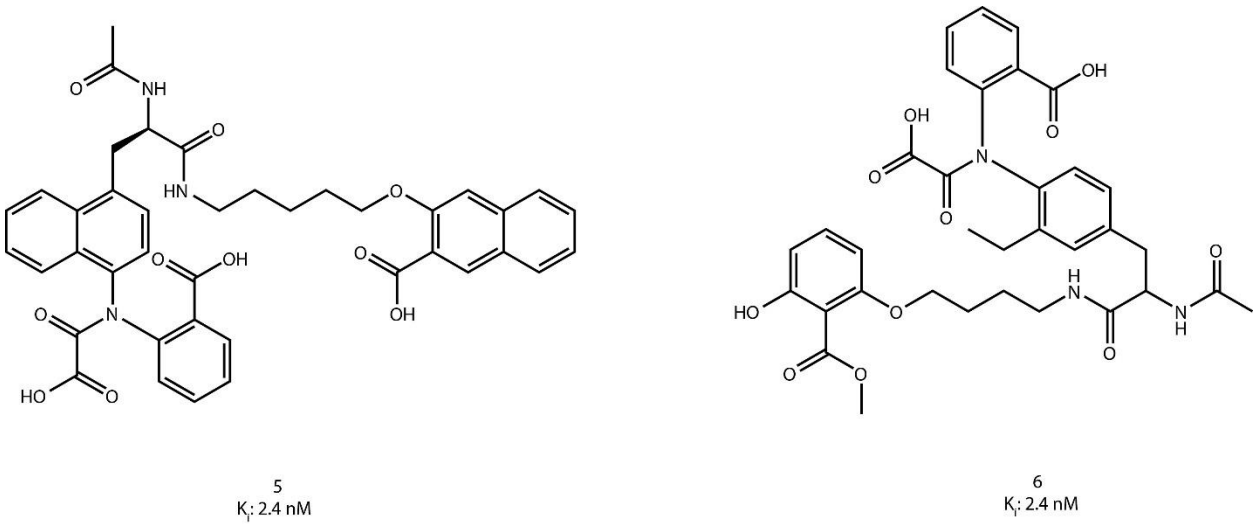

Figure 1.8 Examples of inhibitors synthesized based on structure-based drug design methods.

Wyeth-Ayerst Research used a high-throughput screening *in vitro* assay to identify benzofuran, benzothiophene and oxazole derivatives as potent PTP1B inhibitors, with IC_{50} values

in the range of 20-50 nM, one example is the compound 7 in **Figure 1.9**. Ertiprotafib was a similar compound that was the first PTP1B inhibitor that progressed to clinical trials phase II before being discontinued owing to unsatisfactory efficacy and side effects (**Figure 1.9**) (Erbe et al. 2005; Barr 2010). Wyeth has synthesized a series of thiophene compounds (**Figure 1.10)**, leading to the identification of some highly potent compounds with K_i 0.68 nM (compound 8). Although these compounds were actively transported into membranes, overcoming the cell permeability problems, they were not selective over TCPTP protein. A promising thiazole methyl amino acetate compound (compound 9) with 0.2 μM K_i value, 42-fold selectivity over TCPTP and good cell activity was developed but phase I clinical trials were discontinued for undisclosed reasons (Barr 2010).

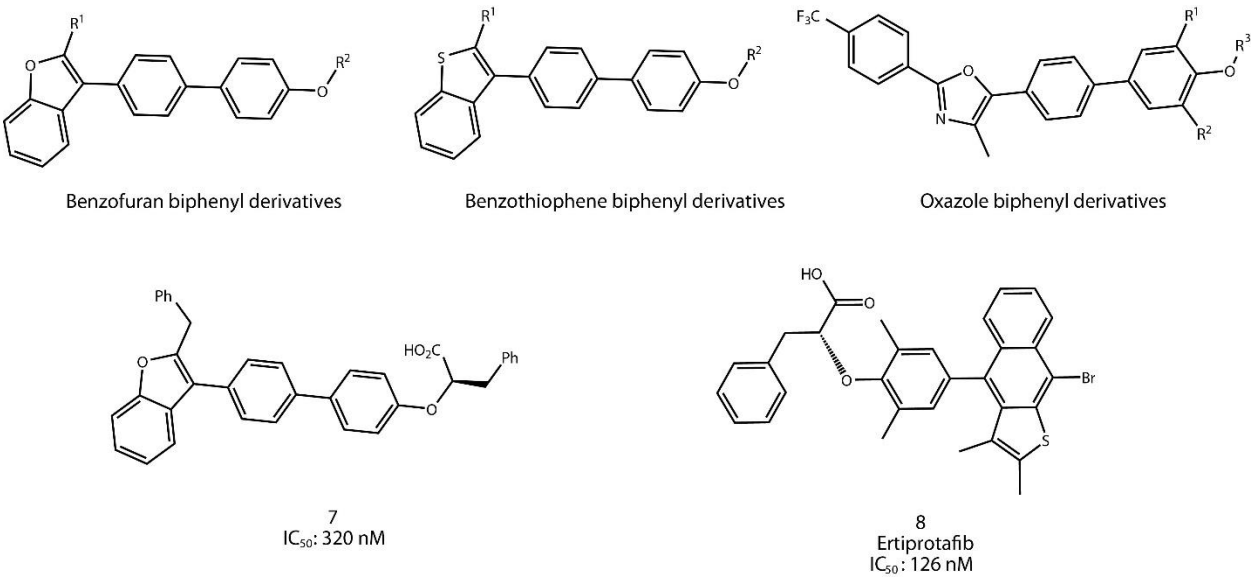

Figure 1.9 Active site inhibitors, benzofuran, benzothiophene and oxazole derivatives.

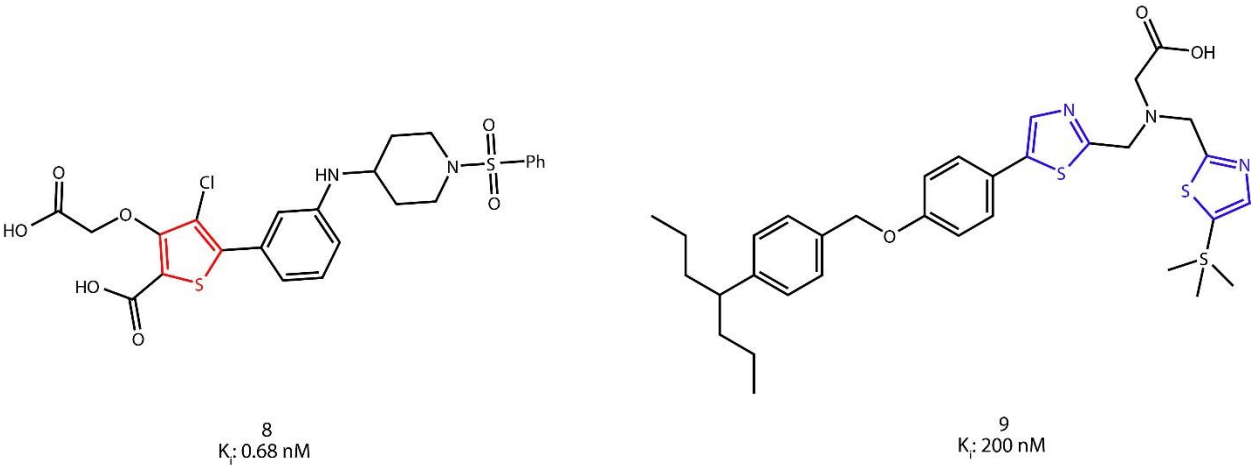

Figure 1.10 Active site thiophene and thiazole inhibitors.

Natural compounds inhibiting PTP1B in the active site were also identified. Kuwanons are flavonoids isolated from the plant *Morus bombycis* that were found to exhibit inhibitory activity with IC_{50} values ranging from 4.3 to 13.8 μM. Using a kinetics analysis was found that kuwanons inhibited PTP1B in a mixed-type manner, indicating that they might bind at both the active site and an additional binding site (site B or C) of the PTP1B (**Figure 1.11**) (Hoang et al. 2009). Naringenin, another flavonoid, and its glycosylated derivatives, prunin, naringin, and narirutin (**Figure 1.11**) were found to have antidiabetic properties. Among naringenin and its glycosylated derivatives, the most potent inhibitor of PTP1B was found to be prunin with an IC_{50} value of 17.5 μM. Narirutin and naringin were weaker inhibitors with IC_{50} values of 56.5 μM and 91.8 μM, respectively. Naringenin itself was the weakest inhibitor of PTP1B with an IC_{50} value of 130.1 μM. Molecular docking studies revealed that prunin had lower binding energy and higher binding affinity than glycosides with higher numbers of H-bonds, suggesting that prunin is the best binder to the PTP1B active site cavity. In addition, prunin significantly enhanced glucose uptake in a dose-dependent manner in insulin-resistant HepG2 cells (Jung et al. 2017).

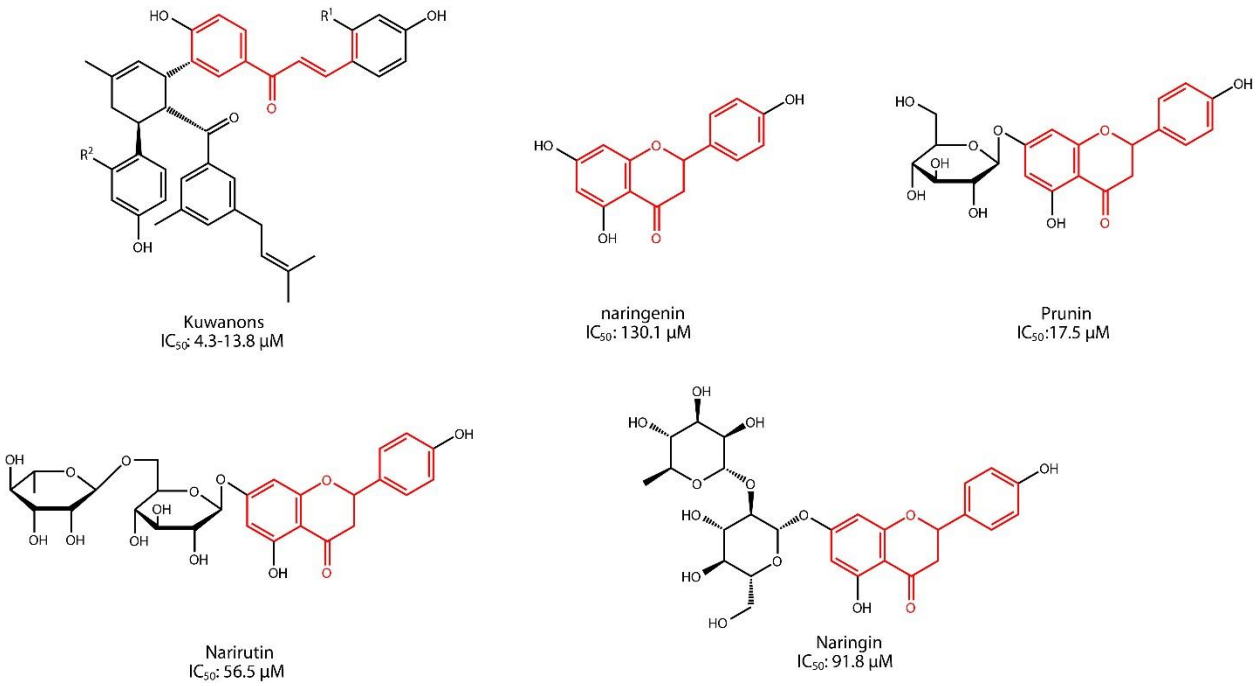

Figure 1.11 Active site inhibitors, flavonoids.

Moronic, morolic, oleanolic and ursolic acids are triterpenic acids isolated from the plant *Phoradendron reichenbachianum* found to inhibit PTP1B with around 13.2 μM, 9.1 μM, 9.5 μM and 2.3 μM IC_{50} values, respectively (**Figure 1.12**). Docking studies suggested that triterpenic

acids bind potentially in a binding pocket next to the catalytic site (site B) (Ramírez-Espinosa et al. 2011). Eleven derivatives of oleanolic acid were designed based on four approaches: a) prodrug approach in order to increase the bioavailability of the inhibitors, b) design of drugs with the capability of interacting with both the active and allosteric sites of the protein, c) design of inhibitors with better selectivity over other PTPs and d) evaluation of the degree with which inhibitor prevents or treats obesity and its complications. *In vitro* studies showed that almost all the derivatives have similar inhibitory activity with the parent compound and *in silico* data revealed that they bind in the same pocket (site B) as oleanolic acid (Ramírez-Espinosa et al. 2011). Bardoxolone methyl is the only derivative of oleanolic acid that has been tested in clinical trials (**Figure 1.12**). It successfully passed the Phase II trials (Pergola, Raskin, et al. 2011; Pergola, Krauth, et al. 2011) but not the Phase III trials due to a higher incidence of cardiovascular events (de Zeeuw et al. 2013).

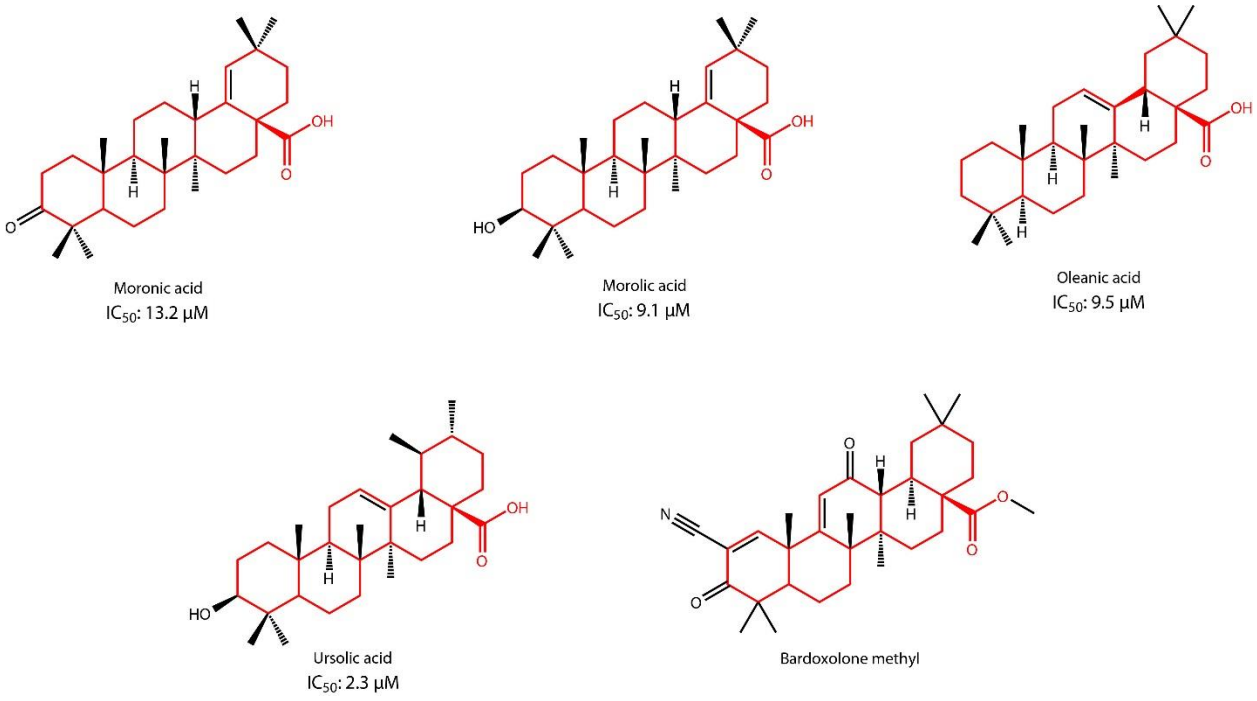

Figure 1.12 Triterpenic acids binding to both the active site and the secondary binding site B.

Berberine and papaverine (**Figure 1.13**) are alkaloids with anti-inflammatory properties that demonstrate insulin-mimicry effects on both adipocytes and myocytes and anti-hyperglycemic activities. Berberine inhibits competitively PTP1B *in vitro* with K_i 91.3 nM, while papaverine exhibited a potent *in vitro* inhibitory effect of IC_{50} 1.20 μM. In docking experiments, both

compounds were found to fit within the binding pocket of PTP1B with a low binding energy (C. Chen, Zhang, and Huang 2010; Bustanji et al. 2006; Bustanji, Taha, Al-masri, et al. 2009).

Fucosterol (**Figure 1.13**) is a sterol isolated from *Ecklonia stolonifera* that exerted potent and efficacious anti-diabetic effects by inhibiting PTP1B and activating IRS-1 and PI3K/AKT signaling pathways in insulin-resistant HepG2 cells (Jung et al. 2016). It has been reported that it inhibits PTP1B in a non-competitive manner with an IC_{50} value of 60.15 μM (Jung et al. 2013). Docking simulation analysis showed that fucosterol binds in the active site of the protein forming a specific hydrogen bond with a Glu101-interacting oxygen atom group and the fucosterol hydroxyl group (Jung et al. 2016).

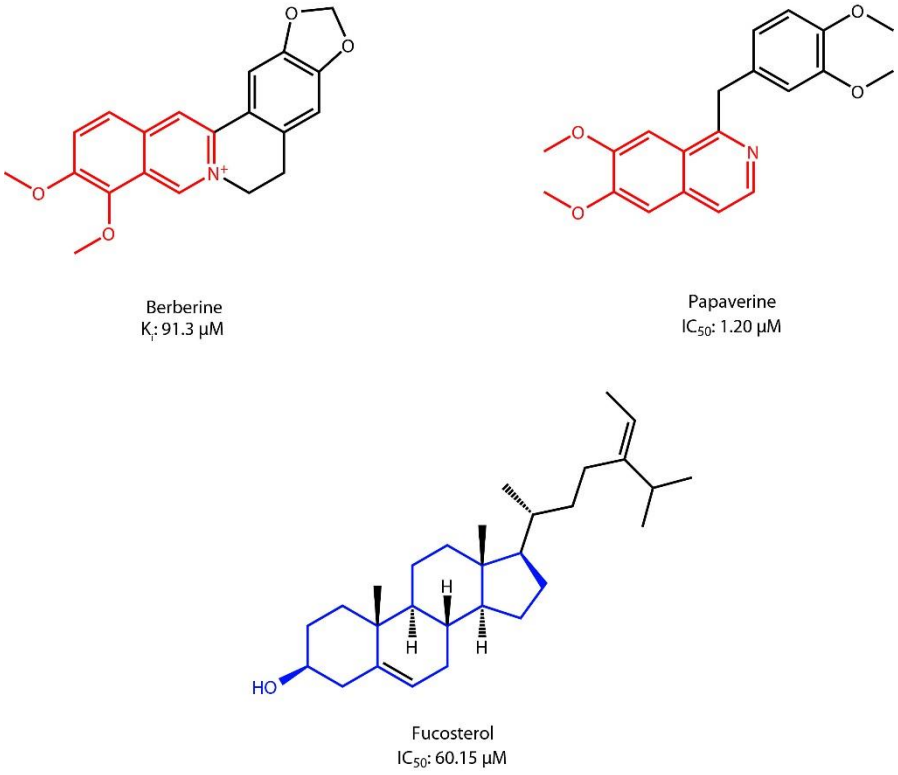

Figure 1.13 Active site, alkaloids (top) and sterol (bottom) inhibitors.

Despite the great effort in developing PTP1B active site inhibitors with increased cell permeability and selectivity toward other phosphatases, however, no compound was able to pass clinical trials. The strategies followed included mainly the discovery of secondary binding sites, adjacent to the active site that will improve selectivity potency. In addition, these secondary binding sites contain hydrophobic residues that contributed to the development of more hydrophobic compounds and subsequently more cell permeable. However, very few compounds

were both selective and cell permeable and those with both properties didn't progress to clinical trials phase II. Natural products were also identified to inhibit PTP1B selectively. The indication that they bind to the active site of the protein is based on kinetic and *in silico* studies, there are no structural data supporting this indication. Nevertheless, alternatives approaches were necessary to be developed in order to deal with these issues.

1.7.2 Allosteric inhibitors

An alternative approach to address the selectivity problem is by using allosteric inhibitors to target non-conserved regions of the protein that are far from the active site. The last years there is an increase interest around the development of this kind of inhibitors. First, Weismann and colleagues at Sunesis Pharmaceuticals developed an allosteric inhibitor (compound 10) with IC_{50} value of 8 μM and 5-fold selectivity over TCPTP (**Figure 1.14)** (Wiesmann et al. 2004). The crystal structure of the complex revealed that the compound binds at a site 20 Å away from the catalytic center, at the intersection of helices α3 (residues 191-201), α6 (residues 256-282), and α7 (residues 285-296), and prevents catalytic activity by blocking the WPD loop (**Figure 1.15**). Cell-based assay showed that the compound enhances insulin receptor phosphorylation and displayed several-fold selectivity over TCPTP and other PTPs.

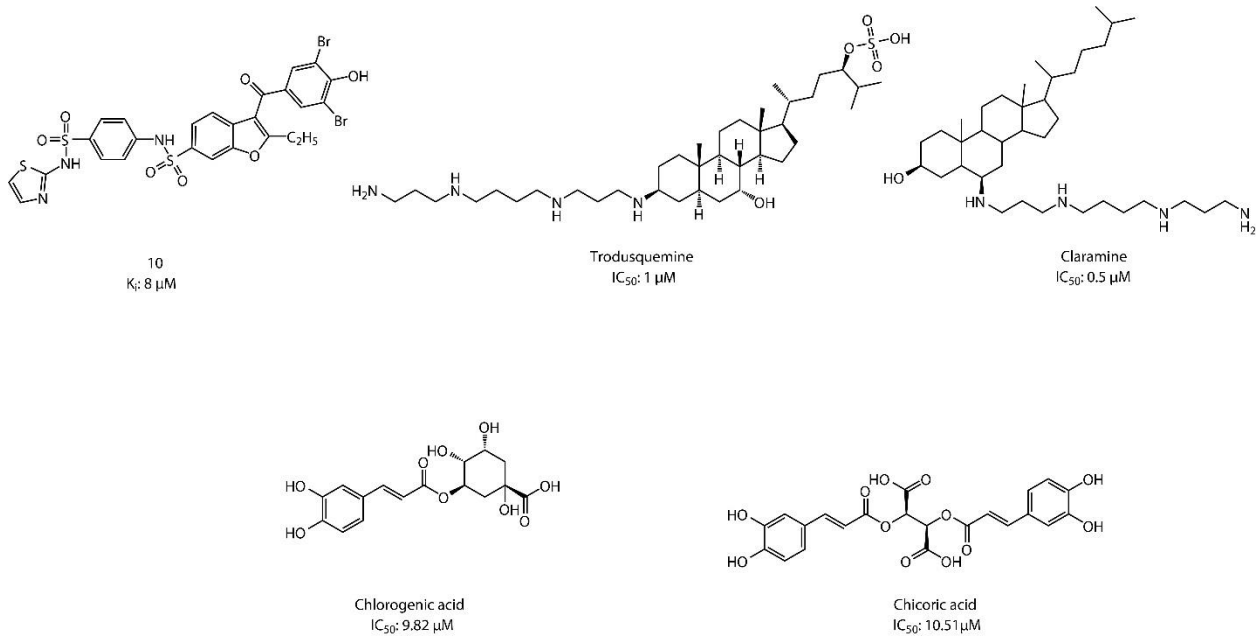

Figure 1.14 Allosteric inhibitors of PTP1B.

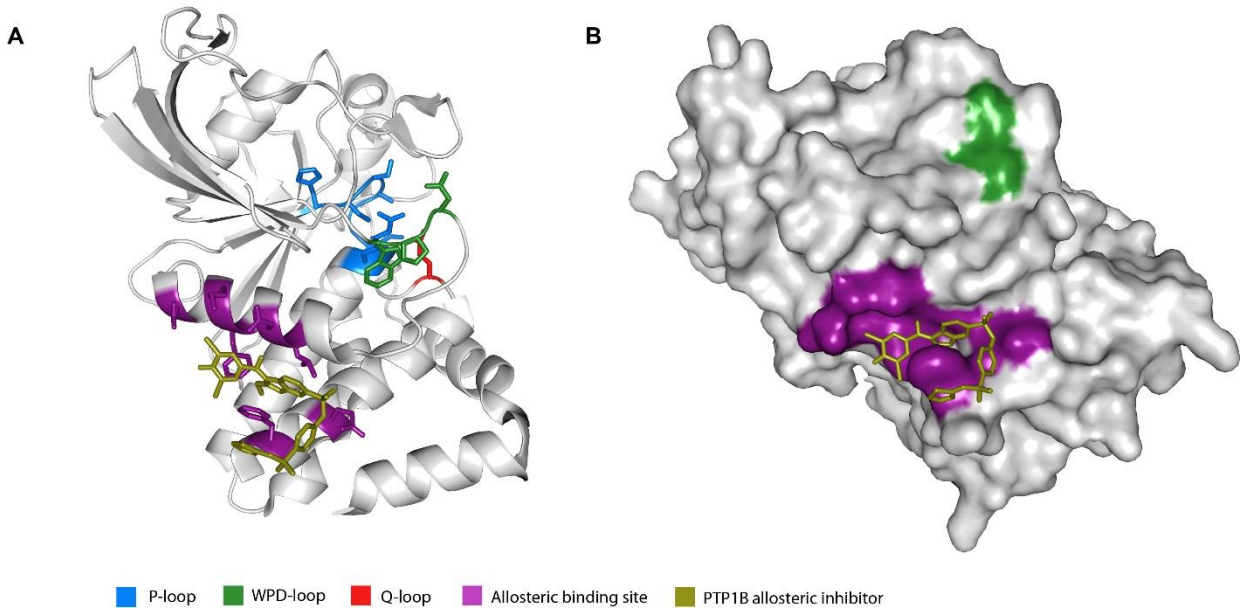

Figure 1.15 Structural characteristics of the allosteric binding site of compound 10 (A) represented as cartoon and (B) as surface. (pdb:1T4J).

Ganaera Corporation has reported that the natural compound trodusquemine (**Figure 1.14**) is another allosteric inhibitor of PTP1B with appetite-suppressant and antidiabetic properties. Trodusquemine is an aminosterol metabolite of cholesterol that was originally isolated from the liver of the dogfish shark. *In vitro* data shown that is a non-competitive inhibitor with IC_{50} of 1 μM and 200-fold selective over TCPTP. Mice model experiments verified that trodusquemine causes rapid and reversible weight loss in high fat diet-induced obese mice (Lantz et al. 2010). Tonks and colleagues demonstrated that the compound binds to two sites within PTP1B, one near the catalytic domain and another more preferable to the disordered C-terminal part of the full-length form of PTP1B, revealing a novel mechanism of PTP1B allosteric inhibition (Krishnan et al. 2014). Trodusquemine progressed to clinical trials phase II before being discontinued for unknown reasons. However, now is in clinical trials phase II against breast cancer (Krishnan et al. 2014). Claramine (**Figure 1.14**) is a synthesized derivative of trodusquemine that lacks the sulfate present in trodusquemine (Qin et al. 2015). It has also strong insulin-mimetic action in neuronal cells and rapidly restored glycemic control and insulin sensitivity in diabetic mice, while in addition suppresses food intake causing weight loss in mice. Like trodusquemine, it displayed selective inhibition of PTP1B with an IC_{50} of 0.5 μM but had no effect on TCPTP activity. The binding mode of claramine on PTP1B is still unclear. However, it can be expected that claramine

acts as an allosteric inhibitor of PTP1B, taking into account that has similar inhibitory activity to trodusquemine (Qin et al. 2015).

Chlorogenic and cichoric acid (**Figure 1.14**) are two caffeoyl derivatives that are reported to be non-competitive inhibitors of PTP1B with IC_{50} values of 9.82 μM and 10.51 μM respectively. Baskaran et al. using a molecular dynamic approach have shown that both compounds bind to the allosteric site of PTP1B previously described by Weismann et al. (Wiesmann et al. 2004). Both compounds interact with the helices α3, α6 and α7, which block the flexibility of the WPD loop (Baskaran et al. 2012). However, Loria's group recently showed using a combination of steady-state inhibition kinetics, solution NMR experiments, and Molecular Dynamics simulations that cichoric acid is a competitive inhibitor with K_i 1.4 mM (determined by kinetic assay) and K_d 1.6 mM (determined by NMR) that binds in the active site of PTP1B. Chorogenic acid, while a non-competitive inhibitor (K_i 8.2 mM, determined by kinetic assay and K_d 1.5 mM, determined by NMR), binds in the second aryl phosphate binding site, rather than the predicted benzofuran binding pocket (Lipchock et al. 2017).

1.7.3 Others compounds

There are plenty more PTP1B inhibitors isolated from natural resources that has been found to exhibit promising *in vivo* activities and selectivity profiles. The categories of the natural compounds identified as PTP1B inhibitors are flavonoids, bromophenols, phenolic acids, coumarins, lignans, sesquiterpenes, diterpenes, triterpenes, sesterterpenes and steroids. For most of these natural compounds inhibitors, SAR studies are missing that will be very useful for the development of new more potent drug-like PTP1B inhibitors. Many of the natural PTP1B inhibitors possess fascinating molecular architectures, potent activity, and better PTP1B selectivity that can be developed as antidiabetic drugs or at least promising drug candidates in the future (Jiang, Liang, and Guo 2012).

Another approach to inhibit PTP1B developed by ISIS Pharmaceuticals is to use Antisense-based oligonucleotides (ASOs) that bind selectively to PTP1B mRNA reducing its protein expression. ASO has been shown to decrease PTP1B mRNA expression levels in liver and adipose tissue (but not skeletal muscle) by about 50% and to produce significant glucose-lowering effects in hyperglycemic, insulin-resistant ob/ob and db/db mice (Swarbrick et al. 2009). This approach

shows improved selectivity toward PTP1B compared to the small molecule inhibitors discussed earlier. PTP1B-directed ASO was and is currently in phase II clinical trials (Cho 2013).

1.8 TCPTP

T-cell PTP (TCPTP) is ubiquitously expressed in all tissues and cell types at all stages of development. There are two forms of TCPTP that derive from the alternative splicing, a 48 kDa form that localizes the protein to the ER via a hydrophobic C-terminal tail, and a 45 kDa form that lacks the hydrophobic C-terminus and is targeted to the nucleus by a bipartite nuclear localization sequence (Iversen et al. 2002).

TCPTP is the most homologous phosphatase to PTP1B, sharing a 74% sequence identity in the catalytic domain and 94% identity for the active site residues (**Figure 1.5**) (Andersen et al. 2004). Thus, the two proteins have many common structural characteristics. It contains the characteristic binding motifs for PTPs that are identical to PTP1B: the P-loop, residues 215-223 (His-Cys-Ser-Ala-Gly-Ile-Gly-Arg), with Cys216 being responsible for the catalytic activity, the WPD loop (residues 180-182) and the Q-loop (residue 260) (**Figure 1.16**). The two proteins catalytic domains only differ on two areas. The first area which is directly accessible from the active site pocket contains the residues (PTP1B residues in bold) His32/**Cys 32**, Glu41/**Lys39**, Tyr54/**Phe52**. The second area is consisted of the residues Gln19/**Ala17**, Lue23/**Gln21** and Pro262/**Ala264,** which are directly accessible when the WPD loop is in the open conformation, while residue Phe183/**Phe182** is accessible when is in a closed conformation (Iversen et al. 2002).

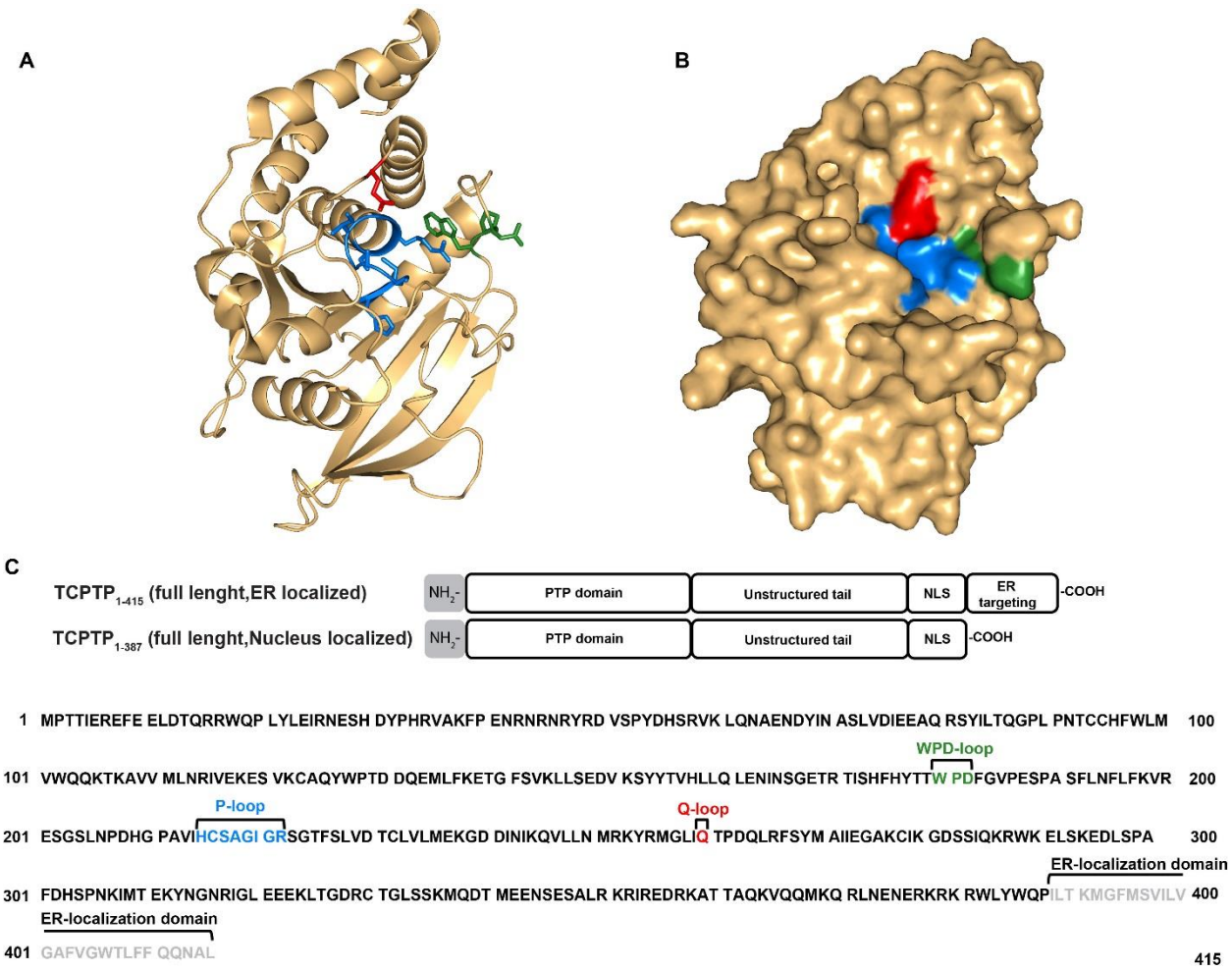

Figure 1.16 Structural characteristics of protein TCPTP (1L8K).
(A) Illustration as cartoon and **(B)** surface of the catalytic site characteristic loops, P-loop (blue), Q-loop (red) and WPD-loop (green). **(C)** TCPTP domain organization and sequence with the characteristic structural motifs.

Although according to *in vivo* observations, the two phosphatases share a high homology, it has been reported that they recognize different substrates and they exhibit different biological functions (Flint et al. 1997). This might be attributed to the slightly different structural characteristics mentioned above, to different subcellular localization or distinct tissue distribution (Tiganis and Bennett 2007) and to the different C-terminal region of the proteins. For example PTP1B recognizes JAK2 as substrate, but not JAK1 and JAK3, whereas TCPTP recognizes JAK1 and JAK3 but not JAK2 (Simoncic et al. 2002; Myers et al. 2001). Another example is the dephosphorylation of the c-Src C-terminal Y529 by the protein PTP1B, while TCPTP dephosphorylates the c-Src Y418 (van Vliet et al. 2005).

In contrast to PTP1B KO mice that show increased insulin sensitivity and resistance to diet-induced obesity, TCPTP KO mice die at 3-5 weeks of age from severe anemia, hematopoietic

defects and the development of progressive systemic inflammatory disease, revealing that TCPTP plays a significant role in both hematopoiesis and immune function (You-Ten et al. 1997).

TCPTP is involved in both leptin and insulin signaling pathways (**Figure 1.17**). In insulin signaling TCPTP dephosphorylates the insulin receptor (IR) (Galic et al. 2003). Thus, PTP1B and TCPTP can act in concert to control the intensity and the duration of IR activation (Tiganis 2013). In the leptin cascade, TCPTP is expressed in the POMC and AgRP neurons and dephosphorylates nuclear STAT3, preventing its translocation to the nucleus where it mediates effects on gene expression. Therefore, PTP1B and TCPTP act together to attenuate leptin JAK2/STAT3 signaling (Z.-Y. Zhang, Dodd, and Tiganis 2015). TCPTP can also regulate hematopoietic development and cytokine response (Wiede et al. 2011; Heinonen et al. 2004).

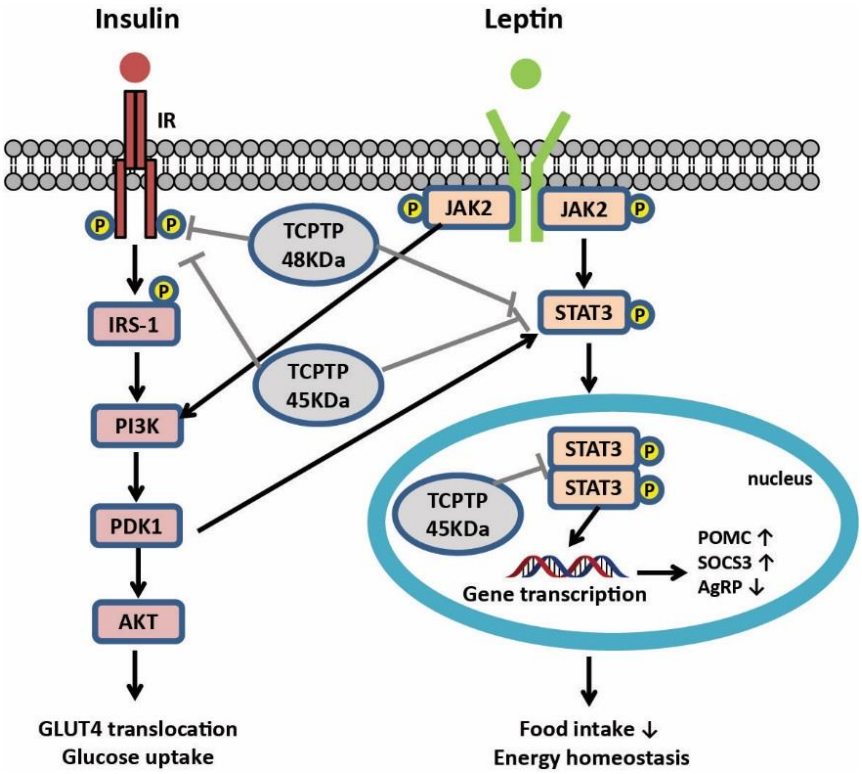

Figure 1.17 Role of TCPTP protein in insulin and leptin signaling. Adapted from (Johnson, Ermolieff, and Jirousek 2002).

2. Introduction II: NMR Spectroscopy

Structural Biology refers to the study of the molecular structure and dynamics of biological macromolecules (proteins and nucleic acids). Structural biology can help us to understand how the function of a protein is affected by changes upon binding of another macromolecule or a small ligand.

Structure-based drug design can contribute in different stages of drug development to direct the process or optimize existing compounds. It is based on knowledge of the drug-target complex three-dimensional structure and on the knowledge of the type of interactions between them. The methods that structural biologist use to determine their structures X-ray diffraction, NMR, electron microscopy, other spectroscopies and biophysical methods, protein expression, bio-physical and bio-organic chemistry, computer science and bioengineering. In this study the main technique used for determination of protein-ligand interactions is NMR spectroscopy and is described in detail in this chapter.

2.1 NMR Spectroscopy

Nuclear Magnetic Resonance (NMR) spectroscopy is one of the most advanced and most important spectroscopic methods in imaging molecules not only for Organic Chemistry, but also for material scientists and biochemists. NMR is the only tool that provides three-dimensional information of molecules both in solution and solid state.

NMR can be used not only for the determination of the three-dimensional (3D) structure, but it also provides information about the dynamics of the biomolecule under study. Uniform isotope labeling of molecules with ^{15}N, ^{13}C, and ^{2}H allows the study of large biomolecules, such as proteins and nucleic acids, up to molecular weight of approximately 40 kDa for the 3D structure determination and up to 1 MDa for other studies (Foster, McElroy, and Amero 2007).

2.1.1 NMR Spectroscopy Principles

Nuclear Magnetic Resonance spectra are derived from stimulated magnetic atomic nuclei, which are under the influence of a strong homogeneous magnetic field. The frequency of the electromagnetic radiation, which provokes these stimulations, is located in the area of the radiofrequencies ($3x\ 10^8 – 3\ x\ 10^6$ Hz or 1-100 m).

Atomic nuclei are charged and they have the intrinsic property to spin on an axis, creating a magnetic dipole. The angular momentum of the nucleus is characterized by a spin quantum number (I). There are three different basic groups of nuclei: 1) Nuclei with an even atomic and mass number (i.e. ^{12}C, ^{16}O, ^{32}S), have a spin quantum number equal to 0 and thus they don't have any magnetic properties and they don't give NMR spectra. 2) Nuclei with odd mass number and odd or even atomic number (i.e. ^{1}H, ^{13}C, ^{19}F), have a fraction spin quantum number. 3) Nuclei with even mass number and odd atomic number (i.e. ^{2}H, ^{15}N) have non-zero integer spin quantum number. In general, nuclei with spin quantum number $I \neq 0$ - can be considered as microscopic magnets which have the potential to interact with an external magnetic field.

In the absence of an external magnetic field, the orientation of the nucleus is random. However, this orientation ceases to be random and acquires a specific direction as soon as the nucleus is under the influence of a strong homogeneous magnetic field. The possible orientations of a nucleus with spin I are 2I + 1. In particular, the proton nucleus ^{1}H, which has spin I = 1/2, has two spin orientations in a magnetic field B_o, the lower energy parallel orientation that aligns with the outer field, I = + ½ (α) and the higher-energy anti-parallel I = -½ (β) which is the excited state and opposes the field. However, the rotational axis of the spinning nucleus cannot be oriented exactly parallel or anti-parallel to the applied field, but precesses in a circular motion called Larmor precession and is described by a Larmor frequency (ν_o) given by the Equation 1.

$$\nu_o = -\gamma B_0/2\pi \qquad \text{Eq. 1}$$

where B_o is the strength of the external magnetic field, and γ is the gyromagnetic ratio that relates the magnetic moment μ and the spin number I for any specific nucleus:

$$\gamma = 2\pi\mu/hI \qquad \text{Eq. 2}$$

where h is the Planck's constant.

As it is already mentioned, every orientation has specific non-equal energy. The difference in energy (ΔE) between the two states is very small and it depends on the strength of the external magnetic field (Eq. 3)

$$\Delta E = h\nu_o = \frac{h\gamma B_0}{2\pi} = 2\mu B_0 \qquad \text{Eq. 3}$$

The active nuclei will be distributed to the various spin states available. The signal intensity depends on the population difference between the two energy levels. Since the energy difference between the two states is relatively small, energy from thermal collisions is able to place many nuclei into higher energy states. The distribution of populations among the energy levels is given by the Boltzmann equation (Eq. 4):

$$\frac{N_\alpha}{N_\beta} = 1 - \frac{h\gamma B_0}{kT} \qquad \text{Eq. 4}$$

where N_α *and* N_β is the number of spins in the α and β state, respectively, k is the Boltzmann constant and T is the temperature.

There is a very small excess of nuclei found in the basic state N_α (magnetic moments that are aligned with the field) compare to the excited state N_β (magnetic moments that are opposed with the field). The opposing magnetic moments cancelling each other, and the remaining net population difference creates a bulk magnetization. The magnetization can be represented by a vector, called M_o in the direction of the applied external magnetic field B_o (z axis). The nuclei are still precessing around the applied field at the Larmor frequency. A radio frequency pulse (rf) is applied, in order to perturb these magnetic moments away from the equilibrium. This rf pulse induces the vector to tilt away from the z axis by an angle θ, rotating around the z-axis tracing a cone. The torque generated on the magnetization, in presence of an external field leads to the motion law described by the Bloch equation (Eq. 5).

$$\frac{dM(t)}{dt} = M(t) \times \gamma B(t) \qquad \text{Eq. 5}$$

where M(t) is the bulk magnetization, B(t) is the magnetic field strength.

Net magnetization in the z axis (z magnetization) is the result of the unequal population in the two spin states. It is not directly measurable because the net vector is stationary. On the other hand, the net magnetization in the x-y axis is called coherence and is the result of the temporary organization of each spin as they rotate around the cone. The coherence is measurable since it is

rotating creating the free induction decay (FID), which is recorded. The rf pulse is a magnetic field that converts the z magnetization into coherence. Following the pulse, the nuclei return to the thermal equilibrium and the NMR signal will decay due to relaxation effects.

Each chemically distinct nucleus of one molecule resonates at a slightly different but detectable frequency of the applied field, based on the chemical environment. The exact location of a signal in a NMR spectrum is called chemical shift. Differences in chemical shifts are due to local magnetic fields, which are generated by electrons that "protect" the nuclei from the external magnetic field. The nucleus thus undergoes the so-called electron protection that is as great as the electron density around the nucleus. The chemical shift δ (ppm) is given by the equation 6 (Eq. 6):

$$\delta_{ppm} = \frac{\nu - \nu_{TMS}}{\nu_{TMS}} \times 10^6 \qquad \text{Eq. 6}$$

where ν is the absolute resonance frequency of the measured sample and ν_{TMS} is the absolute resonance frequency of the measured reference sample tetramethylsilane (TMS), which is used in order to calibrate the chemical shifts and thus to be able to compare the chemical shifts derived from different instruments.

The complexity (duplication of observed signals) of one-dimension (1D) nuclear magnetic resonance spectra (1D NMR) led to the application of multidimensional NMR spectra that contributed significantly to the study of complicated molecules. Undoubtedly, this contribution is a result of the enormous progress in equipment technology and the evolution of the methodology of multidimensional NMR spectroscopy in recent years (Keeler 2005; Jacobsen 2007).

2.1.2 Product operator formalism

Simple NMR experiments can be explained with the vector formalism as it was described above. However, the vector model fails when applied towards coupled spin systems. In order to explain coherence transfer, product operators were introduced. Product operators utilize simple math to describe complex quantum mechanics of multi-pulse NMR experiments, observing the effects of pulses (rotation about the B_1 vector) and delays (rotation about the z axis, known as evolution) on the spin system.

The components of the magnetization along the x, y and z axis can be represented by the spin angular momentum operators I_x, I_y, and I_z, respectively. Thus, the density operator, σ, which

represents the state of the spin system, can be described as a sum of different amounts of these three operators at any given time (Eq. 7)

$$\sigma(t) = a(t)I_x + b(t)I_y + c(t)I_z \qquad \text{Eq. 7}$$

The amounts of the three operators will vary with time during pulses and delays. At equilibrium, where there is only z-magnetization, the density operator is equal to $\sigma_{eq} = I_z$. So I_z is the equilibrium state, I_y is the spin state immediately following a 90° pulse on the –x axis, and following a 90° pulse on the y axis the I_z spin state will rotate into the I_x state.

These simple product operators precess in the x-y plane at a frequency that corresponds to the chemical shift frequency in hertz. The chemical shift frequency can be represented as the angular velocity Ω ($\Omega = 2\pi\Delta\nu$).

$$I_x \xrightarrow{\Omega t I_z} = I_x \cos \Omega t + I_y \sin \Omega t \qquad \text{Eq. 8}$$

$$I_y \xrightarrow{\Omega t I_z} = I_y \cos \Omega t - I_x \sin \Omega t$$

$$I_z \xrightarrow{\Omega t I_z} = I_z \qquad \text{(no precession for the z magnetization)}$$

Product operators are also able to describe the spin system of two different kinds of nuclei. In this case the symbols I and S are used to represent the two nuclei. For example, in case of a ^{1}H-^{13}C system, the ^{1}H is represented as I and ^{13}C as S and there are three possible simple spins for each nucleus, I_x, I_y, I_z and S_x, S_y, S_z respectively. The spin states can be mixed, forming 16 products operators:

I_z, S_z	z magnetization
I_x, I_y, S_x, S_y	in-phase magnetization in the x-y plane
$2I_xS_z$, $2I_yS_z$, $2S_xI_z$, $2\ S_yI_z$	anti-phase magnetization in the x-y plane
$2I_xS_y$, $2I_yS_x$, $2I_xS_x$, $2I_yS_y$	zero and double quantum coherence (not observable)
$2I_zS_z$	longitudinal spin order (intermediate state in coherence transfer)
1	identity operator (represents the spin population that cancel each other)

The operators for two spins evolve under offsets and pulses in the same way as for single spin. The rotations have to be applied separately to each spin and the rotation of each spin does

not affect the other. Evolution under the influence of J coupling alone results in refocusing of the anti-phase magnetization, while the in-phase magnetization evolves into anti-phase.

The product operators and chemical shift and J-coupling evolution in time can be used to describe any combination of rf pulses and delays, giving a prediction the spectrum at the end of the sequence. This set a base for understanding 1D and 2D experiments (Keeler 2005; Jacobsen 2007).

2.1.3 Relaxation

Relaxation is the process in which after to a short rf pulse application, the excited magnetic state returns to its equilibrium distribution. Mainly three aspects contribute to relaxation in solution: dipole-dipole interactions, chemical shift anisotropy (CSA) and quadrupolar couplings (for nuclei with $I > 1/2$). There are two types of relaxation. The spin-Lattice or T_1 relaxation, also known as longitudinal relaxation, and the Spin-Spin or T_2 relaxation, also known as transverse relaxation. T_1 relaxation corresponds to the process by which the magnetization vector returns to equilibrium along the axis of the static applied magnetic field, the z-axis. T_2 relaxation describes the loss of phase coherence among nuclei. T_2 is less than or equal to T_1 (R = relaxation rate, $R2 = 1/T_2$, $R2 \geq R1$), since return of magnetization to the z-direction inherently causes decay of the x-y coherence (Keeler 2005; Jacobsen 2007).

2.1.4 NMR experiments for backbone protein assignment

NMR can be used to map the binding site of small molecules or the binding surface of a protein to another biomolecule. To reach to this result, it is necessary to perform a series of different complicated NMR experiments in order to get the assignment of the protein.

The one-dimensional proton (1D-^{1}H NMR) spectrum is the first source of information about the quality of a protein. It provides information about whether a protein is folded and therefore likely to be functional. In the spectrum of a well folded protein the peaks are sharp and narrow and the signal is well dispersed in the 1D spectrum, whereas if the protein is unfolded, the peaks are broad and the chemical shifts are not widely dispersed. The spectrum in the **Figure 2.1** is an example of a well folded protein, the peaks are sharp and the peak dispersion is ranging from a little over 10 ppm to -0.5 ppm (methyl region). However, a 1D-^{1}H NMR spectrum of a protein can be only used qualitatively and the reason is that each specific type of proton gives a specific chemical shift, depending on the proton's environment, leading to a great deal of overlap due to

protons with similar chemical shifts. As an example, all the amide protons signals will appear between 5 and 9 ppm and therefore there is high chance for overlap because many chemical shifts fall very close to each other. The situation worse up as protein molecular weight increases, as the complexity of the 1D-^{1}H NMR spectrum increases as well and consequently there will be more overlap. In addition to the overlap problem, the linewidth of a peak increases, as a result of the transverse relaxation T_2 reduction.

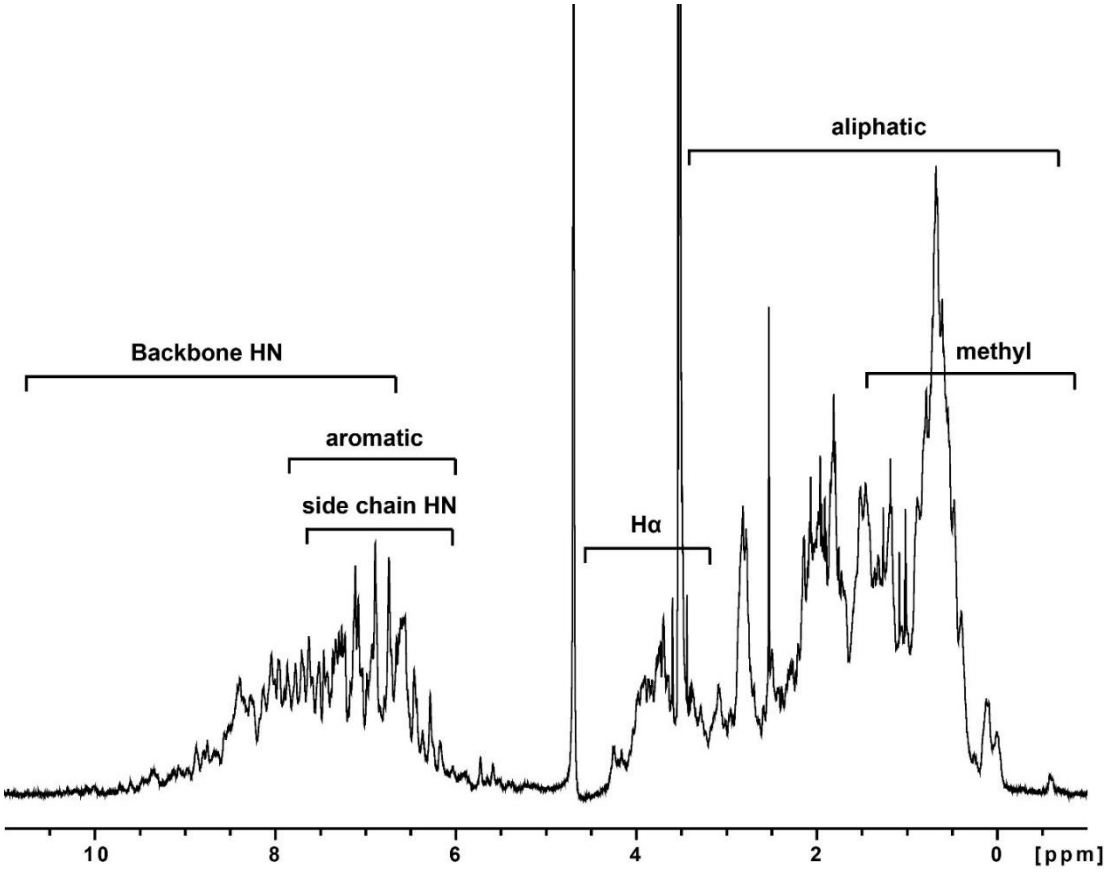

Figure 2.1 ^{1}H spectrum of PTP1B1-298. Proton chemical shift of specific groups.

For the structure determination of protein with mass up to 10 kDa proteins 2D homonulcear NMR experiments have been introduced. There are three homonuclear NMR spectra: COSY, TOCSY and NOESY. COSY (correlation spectroscopy) is the simplest experiment that describes ^{1}H-^{1}H correlations which are two (^{2}J) or three (^{3}J) bonds apart. For example, the crosspeak between the H^{N} with the $H^{C\alpha}$ protons is derived from the ^{3}J coupling constant between them. TOCSY (total correlation spectroscopy) is an extension of the COSY experiment, in which magnetization is dispersed over a complete spin system of coupled protons of an amino acid via multiple J-coupling. It correlates all protons of a spin system and therefore a characteristic pattern

of signals results for each protein residue can be identified. However, some amino acids have identical spin systems and therefore identical signal patterns. NOESY (nuclear Overhauser and exchange spectroscopy) is the simplest NOE experiment that correlates two protons that are close to each other, normally a signal is observed when the distance is smaller than 5 Å. Signals are observed not only for the protons of the residues that are close in the amino acid sequence but are also observed for those that are distant but close in space due to the tertiary structure of the protein. However, 2D homonulcear NMR experiments are limited by the protein size as it's already mentioned.

Many advances have been done in order to overcome the size limit of protein NMR, which is a result of the complexity problem and the linewidth problem (due to T_2 decrease). The complexity problem is dealt with by isotope labeling with NMR visible isotopes as ^{15}N and ^{13}C and by the use of multidimensional experiments, while the linewidth problem can be dealt with deuteration.

Expression of protein in cells can be carried out with uniformly labeled ^{15}N-ammonium chloride and ^{13}C-glucose at high enrichment as the only source of nitrogen and carbon respectively. The labeling of a protein enables the recording of 2D-NMR. The most standard and significant heteronuclear 2D-NMR experiment is a 2D proton-nitrogen correlation spectrum as the ^{1}H-^{15}N HSQC (Heteronuclear Single Quantum Coherence), which shows all the correlations between ^{1}H and ^{15}N that are in direct coupling with each other (^{1}J). These are mainly backbone amides, but this spectrum can contain crosspeaks from the side chains of Trp, Asn and Gln. In principle, the side chain of Arg and Lys are also visible, but the nitrogen chemical shift is outside of the recorded region and thus the peaks are folded (appear as negative peaks). The ^{1}H-^{15}N HSQC spectrum is considered as the fingerprint of the protein, since each crosspeak corresponds to a unique backbone amide and it's unique for each protein.

In order to assign every backbone amide of the protein sequence in a ^{1}H-^{15}N HSQC spectrum, triple-resonance experiments (3D NMR) were introduced that rely on double labeled protein samples (^{15}N and ^{13}C). The information which is obtained from these experiments includes among others, sequence specific chemical shift assignments and chemical shift deviators as indicators of secondary structure (positive for α-helixes and negative for β-sheets). The most basic 3D NMR backbone experiments are HNCACB and HN(CO)CACB. In these experiments, the magnetization is transferred from the backbone amide to the Cα and Cβ. The third dimension of

the spectrum contains the ^{13}C chemical shift of the Cα and the Cβ resonances of a given residue (i) and of the previous residue (i-1) in the sequence for the HNCACB experiment. Whereas, in the HN(CO)CACB experiment the carbon dimension contains only the Cα and the Cβ resonances of the previous residue (i-1) (**Figure 2.2**). Thus, the strip of a backbone amide N-H contains two sets of Cα and Cβ for HNCACB and one set for HN(CO)CACB. However, for bigger proteins the quality of these spectra is not sufficient to be able to get the full assignment. In this case is useful to combine with other 3D NMR spectra like HNCA, HN(CO)CA, HNCO and HN(CA)CO.

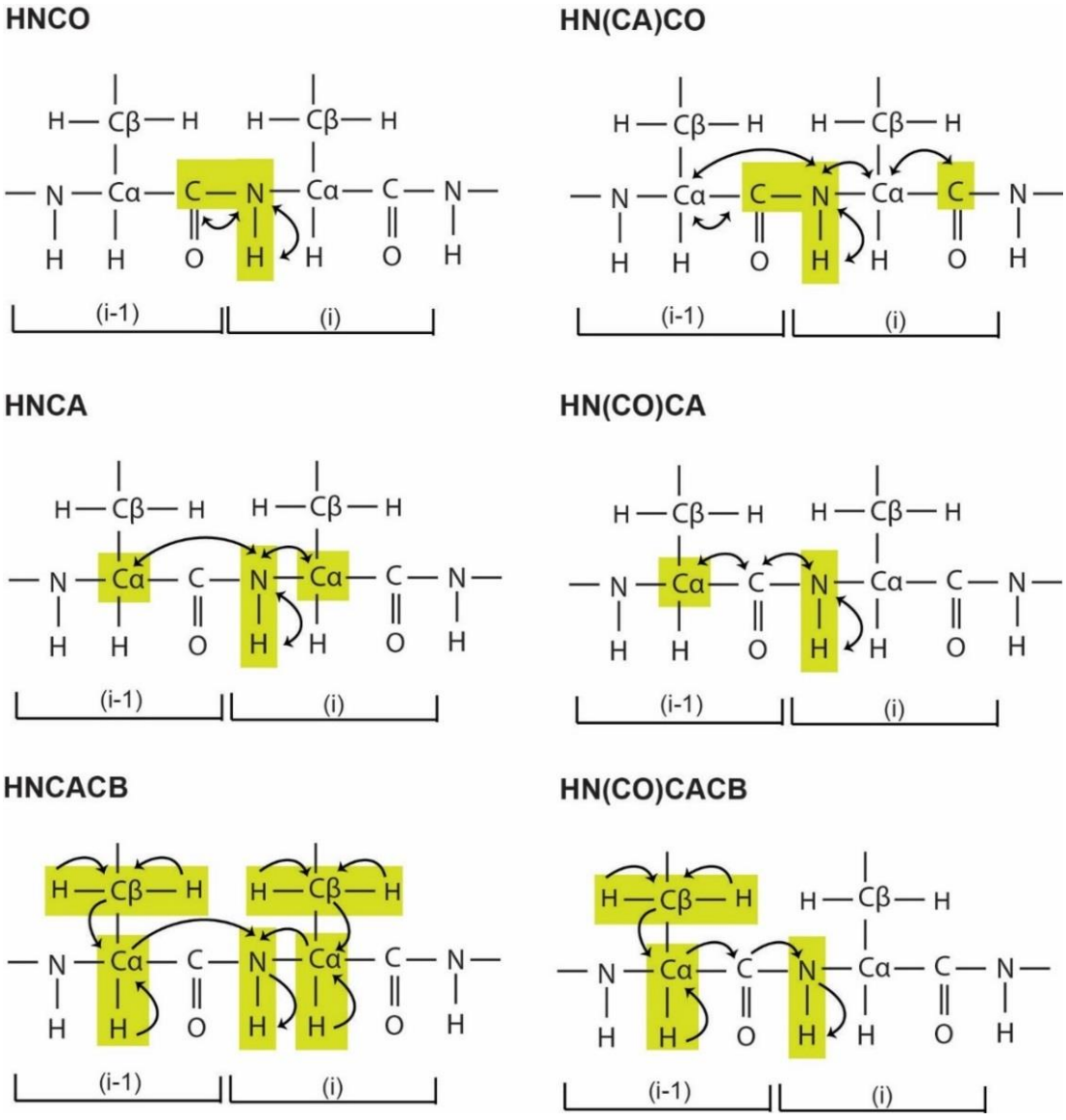

Figure 2.2 Schematic representation of the assignment steps.

As previously mentioned, the linewidth problem is due to short T_2. In large molecules, the dipole-dipole interaction is one the main reasons that shortens T_2. A way to reduce this interaction is by replacing the ^1H with ^2H (deuterium, D). That can be explained from the magnet strength (γ) of the deuterium, which is seven times smaller than that of proton, so the dipole-dipole interaction is smaller. Another technique used for improvement of the linewidth in the large protein spectrum is the replacement of the ^1H-^{15}N HSQC with the 2D ^1H-^{15}N TROSY (Transverse Relaxation Optimized Spectroscopy). The ^1H-^{15}N TROSY gives the same correlations as ^1H-^{15}N HSQC but it reduces the relaxation effects, by cancelling the dipole-dipole relaxation by CSA relaxation to get an effectively much longer T_2 value. Since the HSQC is the basis of all the 3D experiments, all these 3D experiments can be converted to TROSY versions.

A good strategy to start assigning a ^1H-^{15}N HSQC (or ^1H-^{15}N TROSY) protein spectrum is by looking for residues with characteristic Cα and Cβ chemical shifts, that differ to those of the other amino acids (**Figure 2.3**). Examples of these residues are Glycine, Alanine, Serine and Threonine. Glycine contains only a Cα chemical shift that appears at approximately 45 ppm, while alanine has a characteristic Cβ chemical shift that appears around 15-20 ppm. Threonine and serine have a characteristic Cβ chemical shift that appears between 65-70 ppm (Jacobsen 2007).

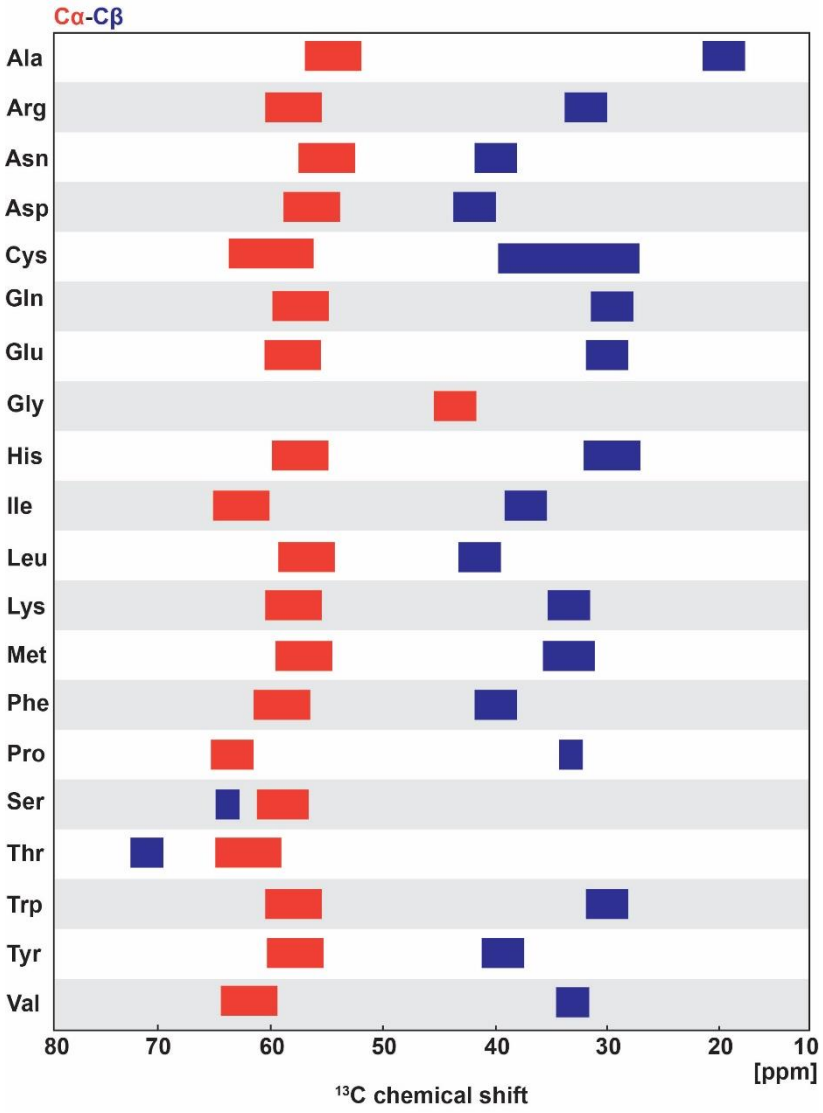

Figure 2.3 Characteristic chemical shifts of Cα and Cβ of the amino acids.
(Based on BMRB data bank http://www.bmrb.wisc.edu/ref_info/statsel.htm)

2.2 NMR approaches in SBDD

NMR is a very important biophysical method used widely in the structure-based drug design, since it detects and reveals protein-ligand interactions with a large range of affinities (nM to mM). NMR approaches used in SBDD can be subdivided into two classes, ligand-based and protein-based NMR experiments, in which the NMR parameters of the protein and the ligand, respectively, are compared in their free and bound states.

2.2.1 Protein-based NMR methods

Protein-based methods rely on the observation of the protein resonances, and they can provide information about where on protein an interaction may occur and how is made. The most typical parameter and the easiest to follow is the chemical shift. Chemical shift changes of the protein resonances upon addition of a ligand identified to localize the ligand binding site. The most common protein-based NMR technique is the 2D ^{1}H-^{15}N HSQC of ^{15}N-labelled protein. In this spectrum the NH amides are observed that correspond to a specific residue; therefore it allows monitoring binding events following chemical shift perturbation (CSP). Subsequently, this methodology requires the 2D ^{1}H-^{15}N HSQC to be well-resolved for monitoring CS changes. This can be achieved using triple resonances approaches of triple labeled proteins (^{2}H, ^{15}N, ^{13}C). Chemical shift perturbation (CSP) data are obtained upon ligand titration and they can be calculated using the equation 9. A comparison of the ^{1}H-^{15}N HSQC in the absence and the presence of the ligand reveals binding events. These can be monitored by following the shifting residues (fast exchange regime) or decrease in intensity and maybe even disappearance (slow exchange regime). Perturbed residues are usually identified as those which exhibit changes beyond one or two standard deviations. If the protein structure is known, the binding site can be identified by mapping the perturbed residues onto the protein 3D structure.

$$\Delta\delta(NH) = \sqrt{(\Delta\delta^{1}H)^{2} + (\frac{\Delta\delta^{15}N}{5})^{2}} \qquad \text{Eq. 9}$$

Since CSP methodology is used to identify the binding site of small molecules, SAR (structure-activity relationship) by NMR was developed. It uses CSP data from a weak binder compound in order to optimize its affinity for a given protein site. Then adjacent sites identified in

the protein where another compound binds weakly and its affinity is optimized again. Then the best orientation of the bound molecules in the protein should be found in order to design properly a linkage that will maintain this orientation in the final compound. This technique therefore allows high-affinity ligand elaboration and reduces the laborious chemical synthesis necessary for such potency.

The CSP methodology can be used for screening ligands in a broad affinity range (low nM to high mM) and can be employed for the determination of K_D in the μM to mM range. A disadvantage of the method is the experimental time and the necessity of a complete resonance assignment of the protein. Subsequently, isotope labeling of the protein is also required. In addition, these methods are limited to proteins with low molecular masses (< 30 kDa) (Cala, Guillière, and Krimm 2014; Carlomagno 2005).

2.2.2 Ligand-based NMR methods

Ligand-based methods rely on the observation of the ligand resonances and they are usually used when the target (protein) is too large (> 100 kDa) or it aggregates in solution in high concentrations. They can provide information about the interactions between a protein-ligand complex, as well as relevant structural information. Monitoring ligand binding has some advantages, the most obvious being that there is no need of protein isotope labelling and collection and analysis of highly resolved 2D spectra of the protein. There is no upper limit to the size of the target and can be used as a throughput by cocktailing several ligands simultaneously. One disadvantage of these methods is the compound solubility in aqueous solutions that limits the ligand concentration (usually concentration higher than 200 μM is required). The most simple and fastest ligand-based NMR method is the T_2 filter technique. This technique lies in the difference in T_2 of different molecular size. Larger molecules (proteins) have short T_2 spin relaxation times and broader line-width. Small molecules have long T_2 and sharper line-width. These resonances from big molecules (broader peaks) can be filtered out by keeping the magnetization in the transverse plane for relatively short periods of time. This application has been widely used in the study of blood samples (Gebregiworgis and Powers 2012). STD approach and the WaterLOGSY method are most used ligand-based NMR experiments (Cala, Guillière, and Krimm 2014; Carlomagno 2005).

2.2.2.1 Saturation Transfer Difference (STD)

Saturation Transfer Difference is a simple, fast and reliable NMR experiment, which can be used to determine the binding of a ligand to a receptor protein, with an affinity range between 10^{-8} to 10^{-3} M. In addition, the individual groups of the compound that contribute to this binding interaction can be specifically determined. The principle of this experiment is based on the transfer of the saturation from the protein to the bound ligand, which by dissociation is moved into the solution where it is detected.

Low-power irradiation is applied to a ^{1}H NMR spectral region containing protein signals but no ligand signals. This irradiation spreads quickly throughout the protein, saturating the protein ^{1}H NMR signals. ^{1}H NMR signals from a ligand bound transiently to the protein become saturated and, upon dissociation, lead to a decrease of the intensity of the ^{1}H NMR signals measured from the pool of free ligand. The experiment is repeated with the irradiation pulse placed outside the spectral region of protein and ligand, which does not lead to saturation transfer to the ligand. The two resulting spectra are subtracted to give the difference spectrum (Viegas et al. 2011) (**Figure 2.4**).

It is necessary to use high ligand excess, usually the protein to ligand ratio ranges from 1:100 to 1:1000 for large proteins (larger than 80 kDa). Therefore, signal intensities are larger, making the STD experiment more sensitive, and the discrimination between directly interacting and nonbinding groups even within a single residue is easier. The protein concentration depends on the molecular weight of the macromolecule (the larger the protein, the lower its concentration) but usually ranges from 10^{-4} to 10^{-10} M. Typical saturation times are 1–2 s. It is not applicable for strong binders because the protein saturation spreads to many protons of the ligand, rendering observation of differential saturation effects difficult. However, high-affinity ligands ($< 10^{-8}$ M), can be detected by competition STD experiments, if a reference molecule with a moderate affinity (10^{-8} M$< KD < 10^{-3}$ M) is available (Mayer and Meyer 2001).

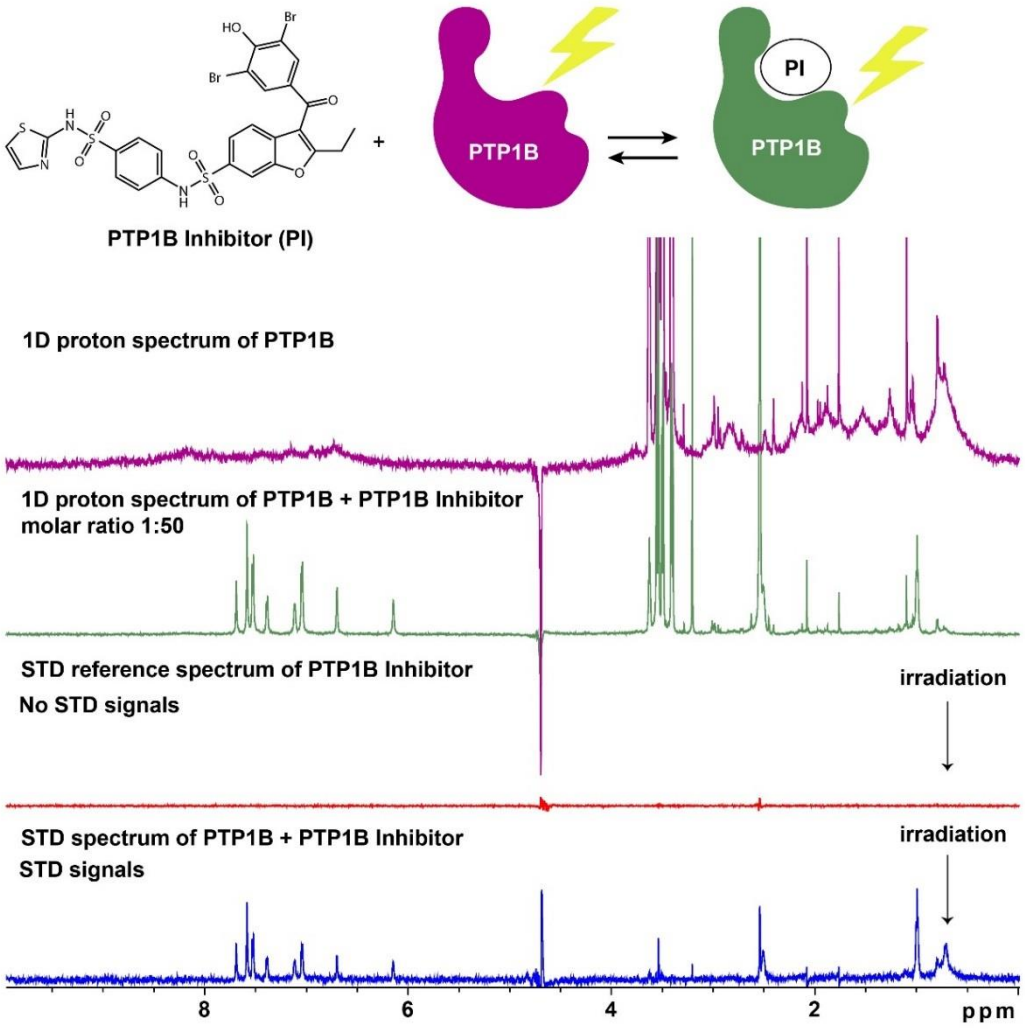

Figure 2.4 STD experiment example.

2.2.2.2 WaterLOGSY

WaterLOGSY (Water-Ligand Observed via Gradient SpectroscopY) is a widely applied 1D ligand-based technique for the detection of protein-ligand interactions. WaterLOGSY approach implies transfer of magnetization via intermolecular NOE and spin diffusion. The magnetization is transferred from the bulky water to the bound ligand via different mechanisms: direct transfer from water molecules immobilized in the protein binding site, with chemical exchange between excited water and protein exchangeable protons or from the water molecules found in the protein surface via the protein ligand complex.

In this experiment, the resonances of non-binding compounds appear with opposite sign and tend to be weaker than those of the interacting ligands, which enables easily discrimination of binders and non-binder. More specifically, the ligands interact with water via water-ligand-protein or protein-ligand complexes, whose rotational correlation times yield negative cross-relaxation rates and exhibit a negative NOE with water. By contrast, small molecules that only interact with bulk water (non-binders) will experience much faster tumbling, which leads into a positive NOE.

Similarly to the STD experiment, WaterLOGSY spectra are recorded with a low concentration of the protein. For small proteins (< 30 kDa), a concentration of 10^{-7} M is required, whereas 10^{-6} M is sufficient for larger proteins (> 60 kDa). By contrast with the STD experiment, a large protein to ligand ratio should be avoided, since the WaterLOGSY spectra reflect the free and the bound states of the ligand. The ratio should usually not exceed 1:100, with the ligand concentration ranging between 40-100 $\times 10^{-6}$ M. Usually, WaterLOGSY experiments should be preferred when ligands are not highly soluble, since they are more sensitive than STD experiments at low ligand concentrations. In WaterLOGSY method, long mixing times are used in order to take advantage of the spin diffusion process. In general, mixing times should range from 1 to 3 s. Temperature is another parameter that can affect the spin diffusion through the protein. Low temperature (15 ^{o}C) favors the spin diffusion. A drawback of the method, as with STD method, is its inability to detect strongly binding ligands with slow dissociation rates since the ligand is in high excess (Dalvit et al. 2001, 2000; Carlomagno 2005).

Scope of the thesis

Diabetes type 2 and obesity are two metabolic diseases that are closely associated. Although many therapeutic approaches have been developed for both diseases, however until now no effective drug can treat them effectively.

Protein Tyrosine Phosphatase 1B (PTP1B) is a negative regulator of both insulin and leptin signaling pathways, subsequently PTP1B is an attractive drug target for diabetes type 2 and obesity. A range of various compounds have been developed targeting PTP1B. However, the lack of cell permeability and low selectivity are two major obstacles in the development of efficient drugs for PTP1B.

The main objective of this project is the discovery of new scaffolds targeting PTP1B that can be used as potential antidiabetic and anti-obesity drug candidates. For this a structured-based drug discovery approach is employed. First, a small library is established with natural compounds that have been reported to have antidiabetic and/or anti-obesity properties. Structural information of protein inhibitor complexes is assessed using X-ray crystallography and/or NMR-spectroscopy. The inhibitory activity of those compounds will be tested using high-throughput assays for PTP inhibitors (pNPP and fluorescence assay). Best hits are validated by NMR spectroscopy by mapping their binding sites into the 3D structure of the PTP1B protein. In order to be able to map the binding site of the inhibitor, the backbone chemical shift assignment of protein construct is required. The selectivity of new compounds assessed comparing PTP1B and TCPTP. It has been shown that TCPTP regulates insulin signaling, by dephosphorylating insulin receptor. It also plays a role in the leptin signaling pathway, by dephosphorylating the STAT3 in nucleus and cytoplasm. Thus, identifying compounds that are inhibiting both PTP1B and TCPTP in the brain may prevent diet-induced obesity. The *in vivo* relevance of PTP1B binding and inhibition by the compounds will be tested in CLU-177 neuronal cell assay in collaboration with Paul Pflunger from IDO. The findings of this study can be used in the future for the design and optimization of a chemical structure with the goal of identifying a compound suitable for clinical testing, a drug candidate.

Compound celastrol is a triterpenoid that has been identified as a strong leptin sensitizer and therefore as a novel potent anti-obesity drug candidate. However, there is no molecular target that can explain its weight loss properties. Celastrol has structural similarities to trodusquemine, a

known inhibitor of PTP1B, while a recent inhibition study with triterpenoids showed inhibitory activity of celastrol towards several protein phosphatases including PTP1B. Therefore, in this thesis, I aim to assess whether celastrol induces weight loss via hypothalamic inhibition of PTP1B and TCPTP, thus leading to a resensitization to endogenous leptin. Using state-of- the-art NMR techniques and enzymatic assays, the inhibitory activity and the type of inhibition will be determined, as well as mapping of the binding site of the compound onto the 3D structure of PTP1B. In collaboration will be assesed whether celastrol mediates leptin resensitization via inhibition of hypothalamic PTP1B and TCPTP using mice genetically engineered.

3. Material and methods

3.1 Materials

3.1.1 List of materials

Cloning	
Material	**Reference**
Antarctic phosphatase	New England Biolabs (5000 U/mL, 0.2 mL)
Restriction enzyme Kpn I	New England Biolabs (10000 U/mL)
Restriction enzyme NcoI	New England Biolabs (10000 U/mL, 0.5 mL)
T4 DNA ligase	Thermo Fisher Scientific (5 U/µL, 0.2 mL)
Pfu polymerase	Thermo Fisher Scientific (2.5 U/µL)
dNTP Mix	Thermo Fisher Scientific
10x Pfu buffer + MgSO4	Thermo Fisher Scientific
10x NEB buffer 3.1.	New England Biolabs
100x BSA	New England Biolabs
T4 DNA Ligase Buffer	Thermo Fisher Scientific

Protein overexpression	
Material	**Reference**
LB medium (Lennox)	Carl Roth GmbH & Co. KG
Yeast extract	Thermo Fisher Scientific
tryptone	Sigma-Aldrich Chemie GmbH
NaCl	Merck KGaA
NaOH	Merck KGaA
Na_2HPO_4	Carl Roth GmbH & Co. KG
KH_2PO_4	Carl Roth GmbH & Co. KG
Na_2PO_4	Merck KGaA
NH_4Cl	Carl Roth GmbH & Co. KG
Glucose	Merck KGaA
Glycerol (Rotipuran®)	Carl Roth GmbH & Co. KG
Lactose	Sigma-Aldrich Chemie GmbH
[^{12}C]D-d7-glucose	97% D, Sigma-Aldrich
[^{13}C]D-d7-glucose	99% ^{13}C, Sigma-Aldrich
^{2}H, ^{13}C Glucose	97% D, 99% ^{13}C, Sigma-Aldrich
$MgSO_4$	Carl Roth GmbH & Co. KG
$CaCl_2$	Carl Roth GmbH & Co. KG
Biotin	Carl Roth GmbH & Co. KG
Thiamin	Carl Roth GmbH & Co. KG
$^{15}NH_4Cl$	99% ^{15}N, Cortecnet
^{15}N-rich growth media Silantes	Silantes
^{13}C, ^{15}N-rich growth media Silantes	Silantes
D_2O	99.85% D Euriso-top
Chloramphenicol	SERVA Electrophoresis GmbH
Kanamycin	SERVA Electrophoresis GmbH
Ampicilin	SERVA Electrophoresis GmbH
Carbenicilin	SERVA Electrophoresis GmbH
IPTG	Carl Roth GmbH & Co. KG

Protein purification	
Material	**Reference**
MES	Carl Roth GmbH & Co. KG
EDTA	Carl Roth GmbH & Co. KG
DTT	SERVA Electrophoresis GmbH
KCl	Carl Roth GmbH & Co. KG
Tris-HCl	SERVA Electrophoresis GmbH
Imidazole	Carl Roth GmbH & Co. KG
β-Mercaptoethanol	Carl Roth GmbH & Co. KG
Guanidine	Merck KGaA
NaN3	Carl Roth GmbH & Co. KG
Ni (II) chloride hexahydrate	Sigma-Aldrich Chemie GmbH
Bradford solution	AppliChem GmbH
TEV protease	Produced by Arie Geerlof (1 mg/mL)
AEBSF	Sigma-Aldrich Chemie GmbH
Lysozyme from chicken egg white	SERVA Electrophoresis GmbH (2.5 g, min. 100000 U/mg)
cOmplete Tablets, Mini, EDTA-free	Roche Diagnostics
DNAse I	SERVA Electrophoresis GmbH (100 mg, min. 3000 Kunitz U/mg, 1 mg/mL stock in PBS)
Nonidet®P40 (NP40)	AppliChem GmbH

DNA and Protein detection and evaluation	
Material	**Reference**
Agarose (for DNA electrophoresis, research grade)	SERVA Electrophoresis GmbH
Ethidium bromide (aqueous solution 1% w/v)	SERVA Electrophoresis GmbH
TAE	Thermo Fisher Scientific
GeneRuler 1 kb Plus DNA Ladder	Thermo Fisher Scientific
Precision plus protein™unstained standards	Bio-Rad Laboratories
Dodecylsulfate-Na-salt, cryst., research grade (SDS)	SERVA Electrophoresis GmbH
Page blue protein staining solution	Thermo Fisher Scientific
Bromophenol blue	Carl Roth GmbH & Co. KG
Xylene cyanol	Carl Roth GmbH & Co. KG

NMR experiments	
Material	**Reference**
d11-Tris-HCl	Cortecnet
d10-DTT	Cortecnet

Crystallography	
Bis-Tris Propane	AppliChem GmbH
Magnesium acetate	Sigma-Aldrich Chemie GmbH
PEG 800	Sigma-Aldrich Chemie GmbH

Screening assays	
Material	**Reference**
Bis-Tris Propane	AppliChem GmbH
Phosphatase substrate (5 mg tablets)	Sigma-Aldrich Chemie GmbH
DiFMUP substrate	Life Technologies GmbH
H_2O_2	Sigma-Aldrich Chemie GmbH
SYPRO	Sigma-Aldrich Chemie GmbH

Compounds	
Material	**Reference**
Chlorogenic acid	Cayman Chemical Company 70930
18β-Glycyrrhetinic acid	Sigma-Aldrich Chemie GmbH G10105
18α -Glycyrrhetinic acid	Sigma-Aldrich Chemie GmbH G8503
Calcitriol	Cayman Chemical Company 71820
Corticosterone	Sigma-Aldrich Chemie GmbH C2505
Metformin	Sigma-Aldrich Chemie GmbH P150959
(4-aminoanilino) (oxo) acetic acid	Sigma-Aldrich Chemie GmbH PH010859
Celastrol	Dr. Paul Pfluger Helmholtz Zentrum Munich Neurobiology of Diabetes Research Unit
Celastrol	Cayman Chemical Company 70950
Withaferin A	Enzo Life Sciences
Diosgenin	Sigma-Aldrich Chemie GmbH D1634
Vitamin D2	Sigma-Aldrich Chemie GmbH 15406
Vitamin D3	VWR International GmbH
Calcifediol	EDQM Council of Europe C0166000
Ursolic acid	Calbiochem 672315
Estriol	Sigma-Aldrich Chemie GmbH E1253
PTP1B inhibitor 539741	Calbiochem 539741
Estrone	Sigma-Aldrich Chemie GmbH E9750
Trodusquemine	Dr. Brunel Jean Michel Centre de Recherche en Cancérologie de Marseille (CRCM) Laboratory of Integrative Structural & Chemical Biology (iSCB)
SIXB	Dr. Brunel Jean Michel Centre de Recherche en Cancérologie de Marseille (CRCM) Laboratory of Integrative Structural & Chemical Biology (iSCB)
NV673	Dr. Brunel Jean Michel Centre de Recherche en Cancérologie de Marseille (CRCM) Laboratory of Integrative Structural & Chemical Biology (iSCB)
Cholesterol	Sigma-Aldrich Chemie GmbH C8667
Cortisol	VWR International GmbH SAFSH4001
Cortisone	VWR International GmbH SAFSC2755
Hydrocortisone	VWR International GmbH SAFSH4001
25-Hydroxyvitamin D2	Santa Cruz Biotechnology sc-231277
Aldosterone	VWR International GmbH SAFSA9477
Asiatic acid	Sigma-Aldrich Chemie GmbH 546712
Testosterone	Sigma-Aldrich Chemie GmbH 86500
β-estradiol	Sigma-Aldrich Chemie GmbH E8875
17A-Ethynylestradiol	Sigma-Aldrich Chemie GmbH E4876
Oleanolic acid	Sigma-Aldrich Chemie GmbH O5504
Cholesterol Sulfate	BIOMOL GMBH cAY15106
β-estradiol 3-sulfate sodium salt	VWR International GmbH
Oleanolic acid	Sigma-Aldrich Chemie GmbH O5504
Cholesterol Sulfate	BIOMOL GMBH cAY15106
Pregnenolone sulfate sodium salt	VWR International GmbH SAFSP162
5-pregnen-3β-ol-20-one	Sigma-Aldrich Chemie GmbH P9129

Madecassic acid	Enzo Life Sciences GmbH LKT-M0114-M500
Dehydroepiandrosterone sulfate	BIOMOL GMBH cAY15873
Dehydroisoandrosterone	Sigma-Aldrich Chemie GmbH D4000
Ganoderic acid A	Cfm Oscar Tropitzsch 7500987
Ganoderic acid B	Cfm Oscar Tropitzsch 7500987

3.1.2 Instrumentation

Method	Name	Device	Producer
Cloning	MyCycler thermal cycler	PCR	Bio-RAD
	Thermomixer comfort	thermoshaker	Eppendorf AG
Protein expression	Eppendorf BioPhotometer plus	Photometer	Eppendorf AG
	Heraeus® Incubator (line B6)	Incubator	Thermo Fisher Scientific
	New Brunswick™ Innova® 44	Incubator shaker	Eppendorf AG
	ABJ 80-4M	Analytic scales	Kern & Sohn GmbH
	EG 620-3NM	Scales	Kern & Sohn GmbH
	Sorvall Evolution RC super-speed centrifuge	Superspeed centrifuge	Thermo Fisher Scientific
	SLC 6000	Rotor for 1 l bottles	Thermo Fisher Scientific
Protein purification	SS 34	Rotor for 50 mL tubes	Thermo Fisher Scientific
		Sonicator	
	Cellulose Acetate Membrane Filter	Membrane filter 0.2 and 0.45 µm	Sartorius AG
		Concentrator 10 kDa	
	Centrifuge 5810R	Benchtop centrifuge	Eppendorf AG
	Centrifuge 5424	Big benchtop centrifuge	Eppendorf AG
	ÄKTA purifier Box-900, pH/C-900, UV-900, P-900	Äkta chromatography system for protein purification	GE Healthcare Europe GmbH
	HiLoad 16/60 Superdex 75	Gel filtration chromatog-raphy column	GE Healthcare Europe GmbH
		Ion exchange chromatography column	
	Nanodrop	NanoDrop 2000 UV-Vis Spectrophotometer	Thermo Fisher Scientific
DNA and Protein detection and evaluation	Molecular Imager® Gel Doc™ XR+ Imaging System (with Image Lab Software)	Gel imager	Bio-Rad Laboratories
	Mini-PROTEAN Tera System	SDS-gel electrophoresis system	Bio-Rad Laboratories
	Mini-Sub® Cell GT Cell	Agarose gel electrophoresis system	Mini-Sub® Cell GT Cell
NMR experiments	NMR tubes	NMR tubes	Norell ®
	Shigemi tubes	Shigemi tubes	Shigemi ® Ca, LTD.

	Bruker AvanceIII 800 MHz	Spectrometer	Bruker
	Bruker AvanceIII 600 MHz	Spectrometer	Bruker
Screenings	EnVision®	Multilabel plate reader	PerkinElmer
	black polysterene 384 well-plates with flat bottom	Screening plates for Fluorescence assay	Corning
	96 well plate, half area transparent	Screening plates for colorimetric assay	Greiner bio-one
	384 well plate, flat bottom, black polyester	Screening plates for thermofluor	Corning
	Stratagene M x 3005P	Thermofluor device	Agilent Tech.
Crystallography	EasyXtal, X-seal crystal supports (10x15)	Plates	Qiagen Sciences

3.1.3 Cell strains

***E.coli* Strain**	**Genotype**
BL21 (DE3)	$F^–$ ompT gal dcm lon $hsdS_B(r_B^- m_B^-)$ λ(DE3 [lacI lacUV5-T7 gene 1 ind1 sam7 nin5])
Rosetta 2 (DE3)	F- ompT $hsdSB(r_B- m_B-)$ gal dcm (DE3) pRARE2 (CamR)
DH5a	$F^–$ *endA1 glnV44 thi-1 recA1 relA1 gyrA96 deoR nupG purB20* φ80d*lacZ*ΔM15 Δ(*lacZYA-argF*)U169, $hsdR17(r_K^– m_K^+)$, $λ^–$

3.1.4 Genes

Plasmid	**Vector**	**Insert**	**Resistance**	**Reference**
pT7-PTP1B	pT7	$PTP1B_{1-321}$	Ampicilin	Provided by Dr Ana Messias
PTPN1	pUCIDT	$PTP1B_{1-435}$	Kanamycin	Integrated DNA Technologies
$PTP1B_{1-298}$	pETM11	$PTP1B_{1-298}$	Kanamycin	This study
$PTP1B_{1-321}$	Z2NK	$PTP1B_{1-321}$	Kanamycin	This study
$PTP1B_{1-393}$	pETM11	$PTP1B_{1-393}$	Kanamycin	This study
PTPN2	pUCIDT	$TCPTP_{1-415}$	Kanamycin	Integrated DNA Technologies
$TCPTP_{1-296}$	pETM11	$TCPTP_{1-296}$	Kanamycin	This study
$TCPTP_{1-336}$	pETM11	$TCPTP_{1-336}$	Kanamycin	This study
SOCS3	pET-Duet	$SOCS3_{20-185}$	Kanamycin	Provided by Dr. Jeffrey J. Babon

3.1.5 Buffers and expression media protocols

Cloning	
Protocol	**Components**
PCR protocol	5 µl 10x Pfu buffer + MgSO4 0.5 µl Forward primer (100 pmol/ µl) 0.5 µl Reverse primer (100 pmol / µL) µl dNTP (10 mM) 0.5 µl Template gene (20 ng) 1 µl Pfu polymerase 0.05 U / µL 41.5 µl H_2O
Digestion protocol	40 µl extracted DNA 5 µl NEB buffer x10 0.5 µl BSA x100 2.5 µl NCOI enzyme 2.5 µl KPnI enzyme
Ligation protocol	2 µl LB buffer 10 ng Vector x3V Insert 1 µl ligase H_2O

Protein overexpression	
Protocol	**Components**
Lysogeny Broth (LB) (1L) medium	1% tryptone 0.5% yeast extract 0.5% NaCl
Superbroth (SB) (1L) medium	3.5% tryptone 2% yeast extract 0.5% NaCl 5 mM NaOH
^{15}N Labelled M9 minimal medium	100mL M9 salt solution (10x), 20mL 20% (w/v) glucose, 1mL 1M $MgSO_4$, 0.3mL 1M $CaCl_2$, 1mL biotin (1mg/mL), 1mL Thiamin (1mg/mL), 10mL trace elements solution (100x)
ZYM-5052 medium	958 mL ZY solution 20 mL 50 x M solution 20 mL 50 x 5052 solution 2 mL 1 M $MgSO_4$ 0.2 mL trace elements solution (1000x)
N-5052 medium	50 mL 20 x N solution 20 mL 50 x 5052 solution 2 mL 1 M $MgSO_4$ 1 mL trace elements solution (1000x)

M9 salt solution (10x)	75.2 g/L Na_2HPO_4-$2H_2O$ 30 g/L KH_2PO_4 5 g/L NaCl 5 g/L NH_4Cl
ZY solution	1% tryptone 0.5% yeast extract
50 x M solution	335 g/L Na_2HPO_4-$7H_2O$ 170 g/L KH_2PO_4 134 g/L NH_4Cl 35.5 g/L Na_2SO_4
50 x 5052	25% glycerol 2.5% glucose 10% a-lactose
20 x N	17.8 g/100 mL Na_2HPO_4-$2H_2O$ 13.6 g/100mL KH_2PO_4 5.36 g/100mL $^{15}NH_4Cl$ 1.42 g/100mL Na_2SO_4
Trace elements solution (100 x)	5 g/L EDTA 0.83 g/L $FeCl_3.6H_2O$ 84 mg/L $ZnCl_2$ 13 mg/L $CuCl_2.2H_2O$ 10 mg/L $CoCl_2.2H_2O$ 10 mg/L H_3BO_3 1.6 mg/L $MnCl_2.4H_2O$
Trace elements solution (1000 x)	2 mM CaCl2-2 H2O 2 mM MnCl2-4 H2O 2 mM ZnSO4-7 H2O 0.4 mM CoCl2-6 H2O 0.2 mM CuCl2-2 H2O 0.4 mM NiCl2-6 H2O 0.2 mM Na2MoO4-2 H2O 0.2 mM Na2SeO3 0.2 mM H3BO3
PBS Buffer	8 g/L NaCl 0.20 g/L KCl 1.44 g/L Na_2HPO_4-$2H_2O$ 0.24 g/L KH_2PO_4 pH 7.2

Protein purification	
Protocol	**Components**
Lysis Buffer **pT7-PTP1B**	30 mL Buffer A ion exchange 1 pill cOmplete Tablets, Mini, EDTA-free 10 µg/mL DNAse I 1 mg/mL Lysozyme 2.5 mM $MgSO_4$ 0.2 % NP-40
Buffer A ion exchange	100 mM MES pH 6.5 1 mM EDTA 1 mM DTT
Elution Buffer ion exchange	100 mM MES pH 6.5 1 mM EDTA 1 mM DTT 1 M NaCl
Lysis Buffer	30 mL Buffer A

PTP1B$_{1-298}$ **PTP1B$_{1-321}$**	1 pill cOmplete Tablets, Mini, EDTA-free 25 µg/mL DNAse I 0.1 mg/mL Lysozyme 2.5 mM $MgSO_4$ 0.2 % NP-40
Buffer A **All phosphatases apart from PTP1B$_{1-393}$**	50 mM Tris-HCl pH 8 300 mM NaCl 5 mM Imidazole 5 mM β-mercaptoethanol
Wash Buffer **All phosphatases apart from PTP1B$_{1-393}$**	50 mM Tris-HCl pH 8 1 M NaCl 10 mM Imidazole 5 mM β-mercaptoethanol
Elution Buffer **All phosphatases apart from PTP1B$_{1-393}$**	50 mM Tris-HCl pH 8 300 mM NaCl 300 mM Imidazole 5 mM β-mercaptoethanol
Lysis Buffer **PTP1B$_{1-393}$**	30 mL Buffer A 3 pill cOmplete Tablets, Mini, EDTA-free 25 µg/mL DNAse I 0.1 mg/mL Lysozyme 2.5 mM $MgSO_4$ 0.67 % NP-40
Buffer A **PTP1B$_{1-393}$**	50 mM Tris-HCl pH 8 300 mM NaCl 5 mM Imidazole 5 mM β-mercaptoethanol 1 pill/50 mL cOmplete Tablets, Mini, EDTA-free
Wash Buffer **PTP1B$_{1-393}$**	50 mM Tris-HCl pH 8 1 M NaCl 10 mM Imidazole 5 mM β-mercaptoethanol 1 pill/50 mL cOmplete Tablets, Mini, EDTA-free
Elution Buffer **PTP1B$_{1-393}$**	50 mM Tris-HCl pH 8 300 mM NaCl 300 mM Imidazole 5 mM β-mercaptoethanol 1 pill/50 mL cOmplete Tablets, Mini, EDTA-free
Lysis Buffer **Only TCPTPs**	50 mM Tris-HCl pH 8 2 pill cOmplete Tablets, Mini, EDTA-free 25 µg/mL DNAse I 1 mg/mL Lysozyme 2.5 mM $MgSO_4$ 0.5 % NP-40
Dialysis Buffer **PTP1Bs and TCPTPs**	50 mM Tris-HCl pH 8 300 mM NaCl 5 mM β-mercaptoethanol
Gel Filtration Buffer **PTP1Bs and TCPTPs**	50 mM Tris-HCl pH 7.5 150 mM NaCl 5 mM DTT 1 mM EDTA 0.02 % NaN_3
Lysis Buffer **SOCS3**	30 mL PBS buffer 1mM AEBSF 5 mM DTT

	0.5 mg/mL lysozyme 1 pill cOmplete Tablets, Mini, EDTA-free 3 µg/mL DNAse I
Guanidine Buffer A **SOCS3**	7 M guanidine HCl pH 8 10 mM Tris 100 mM Na_2HPO_4
Guanidine Buffer B **SOCS3**	7 M guanidine HCl pH 6.3 10 mM Tris 100 mM Na_2HPO_4
Guanidine Buffer C **SOCS3**	7 M guanidine HCl pH 4 10 mM Tris 100 mM Na_2HPO_4
Refolding Buffer **SOCS3**	20 mM Tris pH 8.5 2 mM β-mercaptoethanol
Gel Filtration Buffer **SOCS3**	20 mM Tris pH 7.5 150 mM NaCl 2 mM DTT

DNA and Protein detection and evaluation	
Protocol	**Components**
Agarose gel	0.4 mg agarose (0.8% w/v) in 50 mL TAE x1 1 µl EtBr (1 % w/v)
TAE buffer	Trizma base 48.4 g Glacial acetic acid 11.44 mL 1 L H_2O
6x SDS loading buffer	10 mM Tris-HCl 0.03 % Bromophenol blue 0.03 % Xylene cyanol 60 % glycerol 60 mM EDTA H_2O
4x SDS loading buffer	200 mM Tris-HCl 277 mM SDS 0.08 % Bromophenol blue 40 % glycerol 573 mM β-mercaptoethanol H_2O
10 x SDS Running Buffer	250 mM Tris 2 M glycin 34.7 mM SDS
12 % SDS gel	16 ml 1.5 M Tris-HCl pH 8.8 25.6 ml 30% Acrylamide 192 µM 10% Ammonium persulfate 38 µM 60% (v/v) TEMED 38 ml H_2O
15 % SDS gel	16 ml 1.5 M Tris-HCl pH 8.8 32 ml 30% Acrylamide 192 µM 10% Ammonium persulfate 38 µM 60% (v/v) TEMED 16 ml H_2O

5% stacking gel	0.5 M Tris-HCl pH 6.8 10% SDS 30% Acrylamide 10% Ammonium persulfate 60% (v/v) TEMED H_2O

NMR experiments and Crystallography	
Material	**Reference**
NMR buffer **PTP1Bs and TCPTPs**	50 mM d11-Tris pH 7.5 75 mM NaCl 5 mM d10-DTT
NMR buffer **SOCS3**	50 mM sodium phosphate pH 6.7 2 mM d10-DTT
Crystallization Buffers	100 mM Bis-Tris Propane pH 7.5 3 mM DTT 10-20% PEG 8000 175-250 mM $MgSO_4$

Screening assays	
Material	**Reference**
pNPP buffer	25 mM Bis-Tris Propane pH 7.5 50 mM NaCl 2.5 mM EDTA 2 mM DTT wi and w/o 10% NP40
DiFMUP buffer	25 mM Bis-Tris Propane pH 7.5 50 mM NaCl 2.5 mM EDTA 2 mM DTT

3.2 Methods

3.2.1 Cloning

The genes used in this study are shown in **Figure 3.1** and they were subcloned from full length protein in expressing vector or they were recloned to another more efficient vector for protein overexpression. After the design and ordering of the right primer (DNA oligonucleotides compliment to the region of interest in the target gene) the protocol which was followed for the cloning was the same in all cases. First step is the amplification of the gene of interest by PCR (**Table 3.1** and **Table 3.2**). Then the PCR product is isolated through agarose gel electrophoresis from which is extracted using commercially available kits for PCR. The pure PCR product and the expressing vector are digested using two restriction enzymes at 37 ^{o}C for 2 hours, to produce compatible stranded overhangs in both molecules (**Table 3.3**). The vector used in all cases for subcloning was the pETM11 vector which includes a 6 x His tag, a TEV protease recognition site and the NcoI and KpnI restriction enzyme recognition sites. The vector undergoes an additional dephosphorylion step after the digestion, incubating the vector with the Antarctic Phosphatase at 37 ^{o}C for 1 hour, to prevent from recircularization during the next step (**Table 3.4**). Both the digested DNA and vector are purified again with the same commercially available kits for PCR as before, following the corresponding protocol.

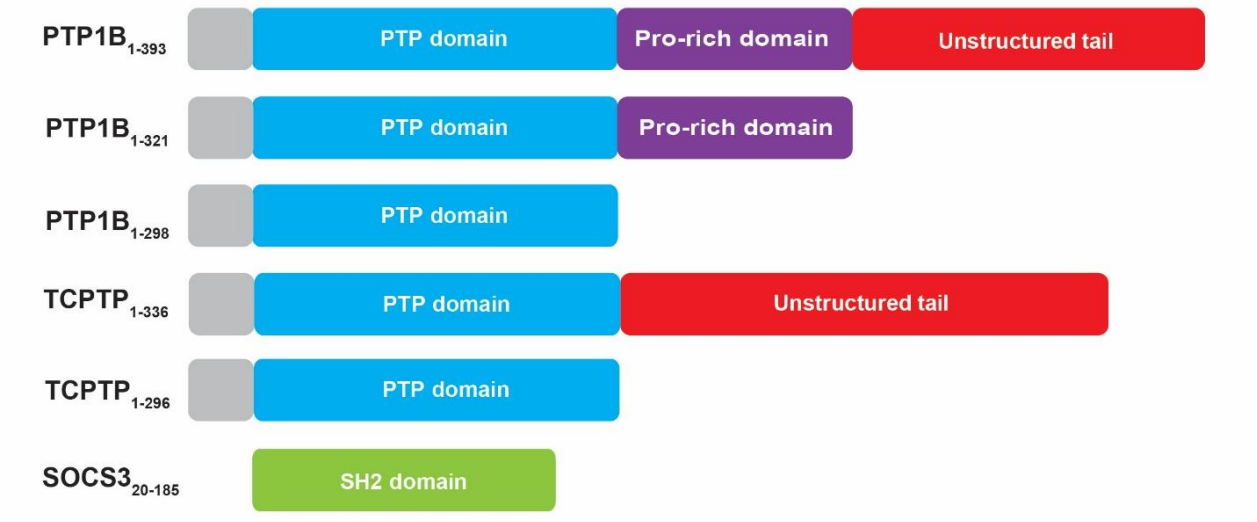

Figure 3.1 Constructs used in this study.

Table 3.1 PCR protocol: Sample preparation

Component	Volume[µL]
10 x Pfu buffer + $MgSO_4$	5 µL (10 x)
Forward Primer	0.5 µL (100 pmol/µL)
Reverse Primer	0.5 µL (100 pmol/µL)
dNTP	1 µL (10 mM)
Template gene	Calculated to be 20 ng final concentration
Pfu Polymerase	1 µL (2.5 U/µL)
H_2O	Calculated to have total volume 50 µL

Table 3.2 PCR protocol run

Phase	Temperature	Time
Denaturation	95 ºC	2 min
Amplification:		x 30 cycles
Denaturation	95 ºC	30 sec
Annealing	56 ºC	30 sec
Extension	72 ºC	2 min 30 sec
Extension	72 ºC	10 min
Cool down	4 ºC	∞

Table 3.3 Digestion protocol

Component	Volume[µL]
PCR product (gene)/ vector	40 µL
NEB (x10)	5 µL
Restriction enzyme NcoI	2.5 µL
Restriction enzyme KpnI	2.5 µL

Table 3.4 Dephoshorylation of the vector

Component	Volume[µL]
Digested vector sample	50 µL
NEB	2 µL
Antarctic Phosphatase	2 µL
H_2O	16 µL

The next step is the ligation of the insert into the vector. The molar ratio of insert to vector DNA was ranged from 2:1, 3:1 and 6:1. The reaction starts after the addition of 1 µL of ligase enzyme (1 U/µL), 2 µL ligase buffer (LB), calculated vector and insert volumes and water to final volume of 20 µL. The reaction is incubated at 16 ºC overnight. The equation used for the calculation of the right volumes of insert and vector is given in the Equation 10.

$$insert\ mass = a \times \frac{insert\ size}{vector\ size} \times vector\ mass \qquad \text{Eq. 10}$$

where α = 2, 3 or 6, *vector size*= 5200 bp, *vector mass*= 40 ng and *insert size* $PTP1B_{1\text{-}298}$= 937 bp, $PTP1B_{1\text{-}321}$= 966 bp, $PTP1B_{1\text{-}393}$= 1198 bp, $TCPTP_{1\text{-}296}$= 913 bp, $TCPTP_{1\text{-}336}$= 1033 bp

3.2.2 DNA purification by agarose gel electrophoresis

Agarose gel electrophoresis is a method of DNA analysis and separation based on the its size. For the agarose gel preparation, 0.4 g agarose (0.8%) were dissolved in 50 mL TAE x1 buffer in 250 mL glass flask and heated in a microwave oven until is totally dissolved. After the solution is cooled down, it is transferred to a 50 mL plastic falcon tube and 1 μL EtBr (1% v/v) is added. The solution is poured into a special gel tray with a well comb and after approximately 20 min the gel is completely solidified. Afterwards, 10 μL 6x SDS Loading buffer is added to 50 μL DNA sample (PCR product) before is loaded to the gel. The gel box is filled with TAE x 1 buffer until is covered. Then the DNA sample is loaded to the available lanes and one lane is used for the weight ladder (1 kb standard). The gel runs at 100 V for approximately 30 min. After the end of the run the DNA bound to ethidium bromide is detected under UV radiation and the desired molecular weight band is cut from the gel and purified as explained above.

3.2.3 Competent cells transformation

Transformation is the process of importing a recombinant vector from a reaction mixture or vector solution into competent cell strains. The ligation mixture from the cloning procedure is used to transform DH5α-cells (200 μL). The samples were kept on ice for 20 min. Then, the samples were transferred into a thermoshaker for 2 min at 42 ^{o}C, and returned back to the ice for 2 more minutes. Afterwards, 750 μL LB media is added under sterile conditions and the samples are placed for 30 min in a shaking thermoshaker at 37 ^{o}C. The cells are separated from the LB media upon centrifugation for 30 secs at 18407 x g, the supernatant is discarded apart from approximately 80 μL, which are used for resuspension of the cell pellets. The cells are plated on a LB agar plate and incubated overnight at 37 ^{o}C.

3.2.4 Mini-Preps and DNA sequencing

Mini-preps are used for the isolation and amplification of the plasmid DNA from a bacteria culture from a single colony. Thus, before the mini-prep, precultures were prepared with 10 mL

LB media, 10 μL kanamycin antibiotic (pETM11 vector contains a kanamycin resistance gene) and one colony from the transformation plate and each preculture was incubated at 37 ºC overnight.

Five mL of the preculture were centrifuged for 10 min at 3202 x g and the supernatant was discarded. To extract and purify the plasmid DNA, the mini-prep kit *NucleoSpin®Plasmid/Plasmid (No Lid)* was used and the protocol described in the instructions was followed.

Then, 20 μL of 30 ng/μL isolated DNA plasmid were sent for sequencing, performed by GATC Biotech. The primers used for the sequencing were the forward primer T7 (TAATACGACTCACTATAGGG) and the reverse pET-RP (CTAGTTATTGCTCAGCGG) primer.

3.2.5 Protein overexpression

All phosphatase proteins were expressed in Rosetta2 (DE3), while SOCS3 protein was expressed in BL21 (DE3) bacterial strains. Rosetta2 (DE3) strain is BL21 (DE3) derivative designed to enhance the expression of proteins that contain codons rarely used in *E. coli*. More specifically Rosetta2 (DE3) contains an additional plasmid pRARE coding AGG/AGA (arginine), CGG (arginine), AUA (isoleucine), CUA (leucine)CCC (proline), and GGA (glycine) tRNA codons (Fu, Lin, and Cen 2007). The plasmid of interest was transformed into competent *E. coli* cells, following the same protocol as previously described in the section 3.2.3, the only difference is that the Rosetta2 (DE3) cells are plated in agar plates with kanamycin and chloramphenicol antibiotic and the BL21 (DE3) cells are plated in agar plates containing only kanamycin antibiotic. In case of Rosetta 2 (DE3) is used an extra antibiotic because the additional plamid pRare also carries its own antibiotic (chloramphenicol). Transformed colonies were suspended in 20 mL LB media, containing the right antibiotic, for overnight growth at 37 ºC. The following day the preculture for all protein phosphatases was used to inoculate 1 L of autoinduction media ZYM-5052 supplemented with 100 μg/mL chloramphenicol and 100 μg/mL kanamycin, while for SOCS3 the preculture was added to 1 L. Superbroth medium supplemented with 100 μg/mL kanamycin. A large-scale culture for all phosphatases was incubated at 37 ºC until optical density at 600 nm (OD_{600}) reaches 1, after which it was cooled down to 20 ºC (PTP1Bs) or 15 ºC (TCPTPs). Next day, the cultures were harvested by centrifugation at 5000 x g for 30 min. SOCS3 cells were grown at 37 ºC till OD_{600} reached about 0.8-1.0, cells then were induced with 1 mM IPTG solution and were grown for 2 more hours at 37 ºC and then the culture was centrifuged at 5000 x g for 30

min to pellet the cells. The cell pellet was washed with PBS and transferred to a 50 mL Falcon tube, and then it was centrifuged for 60 min at 3202 x g and stored at -20 ^{o}C.

Different isotopically labeled protein phosphatases proteins were prepared for NMR studies. Uniformly ^{2}H (~70%), ^{13}C (99%), ^{15}N (99%)-labeled protein expression was performed at 37°C using M9 minimal medium containing $^{15}NH_4Cl$ (99% ^{15}N), [^{13}C]D-d7-glucose(2 g/L) (97% D, 99% ^{13}C,) supplemented with 0.012% (w/v) ^{13}C, ^{15}N-rich growth media Silantes in 70% D_2O (99.85% D). Uniformly ^{2}H (~70%), ^{15}N (99%)-labeled protein was expressed at 37°C using M9 minimal medium containing $^{15}NH_4Cl$, [^{12}C]D-d7-glucose(2 g/L) (97% D) and ^{15}N-rich growth media Silantes in 70% D_2O. A standard protocol (Sprangers 2014) of sequential precultures for better D_2O adaptation over a 3 days period was followed to increase the yield of protein expression in 70% D_2O. On the first day, a 25 mL preculture in LB medium was prepared and grown overnight at 37°C. The next day, three precultures of 50 mL M9 minimal medium in H_2O were inoculated with 0.5, 1.0 or 2.0 mL of the overnight LB preculture and grown at 37°C. Later on the same day, the preculture with OD_{600} closest to 0.6 was spun down for 10 min at 3202 x g. The cells were resuspended in 1 mL of M9 medium in 70% D_2O and used for the inoculation of 100 mL of M9 medium in 70% D_2O, such that the OD_{600} was 0.1-0.15. This small culture was left overnight at 37°C. The next day, this culture was added to 900 mL of M9 medium in 70% D_2O. All cultures in minimal media were induced at 0.8 OD_{600} with 1 mM of IPTG overnight at 20^{o}C.

For the preparation of uniformly SOCS3 ^{15}N (99%)- labeled protein, expression was performed in the same way as for the unlabeled protein, described above, but using M9 minimal medium containing $^{15}NH_4Cl$ for bacterial growth.

3.2.6 Protein purification

For the purification of all proteins, affinity chromatography purification protocol with nickel-bearing beads (Ni-NTA resin, QIAGEN) was used, since all proteins have a 6His-tag on their N-terminal. A final purification step was added in order to reach high levels of purity by size exclusion chromatography. Molecules are separated based on their hydrodynamic radius in a column containing the stationary phase, which is consisted of porous material. The smaller molecules are trapped transiently in the porous, while the bigger molecules pass through unaffected. Thus, smaller proteins have higher retention time in comparison to bigger protein.

$PTP1B_{1-298}$ and $PTP1B_{1-321}$ cell pellets were resuspended in buffer A (50 mM Tris-HCl pH 8, 300 mM NaCl, 5 mM imidazole and 5 mM mercaptoethanol) supplemented with 0.025 mg/mL DNAse I, 0.1 mg/mL Lysozyme, 2.5 mM $MgSO_4$ and 0.1% NP-40 (Nonidet P40) whilst $PTP1B_{1-393}$ resuspension buffer contained additionally 0.67% NP-40 and 3 pills/30 mL of protease inhibitor EDTA free (cOmplete Tablets, Mini EDTA free). TCPTP cell pellets were resuspended in lysis buffer containing 20 mM, Tris-HCl pH 8, 5 mM mercaptoethanol, 0.025 mg/mL DNAse I, 0.1 mg/mL Lysozyme, 2.5 mM $MgSO_4$, 0.5% NP-40 and 2 pills/30 mL of protease inhibitor EDTA free. Cells were lysed by sonication and the cell lysate was centrifuged at 60.000 x g for 30 min at 4°C. After filtration, His-tagged proteins in the supernatant were purified by IMAC (Immobilized Metal Affinity Chromatography). In short, the supernatant was applied to Ni-NTA resin (QIAGEN) previously equilibrated with 3 column volumes of buffer A. Bound protein was washed with 3 column volumes of buffer A and unspecific bound protein was washed away with 3 column volumes of Wash Buffer (50 mM Tris-HCl pH 8, 1 M NaCl, 5 mM Imidazole and 5mM mercaptoethanol). His-tagged protein was eluted using elution buffer (50 mM Tris-HCl pH 8, 300 mM NaCl, 300 mM Imidazole and 5 mM mercaptoethanol). For $PTP1B_{1-393}$ all buffers were supplemented with 1 pill of protease inhibitor EDTA-free per 50 mL buffer to avoid protein degradation. The affinity His-tag was removed from the protein by TEV (1:5 protein:TEV ratio) cleavage during dialysis into 50 mM Tris-HCl pH 8, 300 mM NaCl and 5 mM mercaptoethanol buffer overnight at 4°C. The cleaved tag and TEV protease were removed from the target protein using a second IMAC step in dialysis buffer. Finally, a size-exclusion chromatography (SEC) step in GF buffer (50 mM Tris-HCl pH 7.5, 150 mM NaCl, 1 mM EDTA and 5 mM Dithiothreitol (DTT)) using a Superdex 75 Hiload 16/60 column was performed. For $PTP1B_{1-393}$ and $TCPTP_{1-336}$ a second SEC step was performed to yield pure protein.

SOCS3 protein was purified in a slightly different way. The protein was purified under denaturating conditions of insoluble inclusion bodies. Cell pellets were resuspended in 30 mL PBS buffer (138 mM NaCl, 2.7 mM KCl, 1.5 mM KH_2PO_4, 8.1 mM Na_2HPO_4 pH 7.2) supplemented with 1 mM AEBSF (4-(2-aminoethyl)benzenesulfonyl fluoride hydrochloride), 0.025 mg/mL DNAse I, 0.5 mg/mL Lysozyme, 5 mM DTT and one pill/30 mL of protease inhibitor EDTA free. Cells were lysed by sonication and the cell lysate was centrifuged at 20.000 x g for 30 min at 4°C. After centrifugation, the supernatant was discarded and the cell pellet was resuspended in 50 mL guanidine buffer A (7 M guanidine pH 8, 10 mM Tris-HCl pH 8, 100 mM NaH_2PO_4) for at least

1 h at room temperature. Afterwards, the solubilized pellet was centrifuged again at 20.000 x g for 10 min at 4°C. After filtration the supernatant was applied to Ni-NTA resin previously equilibrated with 3 column volumes of guanidine buffer A. Bound protein was washed with 10 mL of guanidine buffer A, then the resin was washed with 10 mL of guanidine buffer B (7 M guanidine pH 6.3, 10 mM Tris-HCl pH 8, 100 mM NaH_2PO_4). His-tagged SOCS3 protein was eluted using 5 mL of guanidine buffer C (7 M guanidine pH 4, 10 mM Tris-HCl pH 8, 100 mM NaH_2PO_4). After the purification, the denaturated protein is refolded to its native state by sequential dialysis until guanidine is completely removed. The concentration of the eluted protein was adjusted to be approximately 5-10 mg and then it was mixed with 25 mL guanidine buffer A and 25 mL dialysis buffer (20 mM Tris-HCl pH 8.5, 2 mM mercaptoethanol). The solution was transferred into dialysis tubing with molecular weight cut-off of 3 kDa. The dialysis tubing was dialyzed against 2 L of dialysis buffer for 3 h at 4 ^oC. Then the dialysis buffer was replaced with fresh dialysis buffer and the dialysis was continued for another 3 h at 4 ^oC. After the last 3 h of dialysis, the dialysis buffer was again replaced with a fresh one and left overnight at 4 ^oC. Next day an additional dialysis step with fresh dialysis buffer took place for 2 h at 4 ^oC. Then, the solution was removed from the dialysis bag and it was concentrated in a 3 kDa centrifugal concentrator to final volume of 5 mL. The affinity His-tag was removed from the protein by TEV cleavage protease (1:5 protein : TEV ratio) overnight at 4 ^oC. After cleavage, the protein was separated from the free tag by IMAC, following the same protocol for $PTP1B_{1-298}$ described above. Finally, a size-exclusion chromatography (SEC) step in GF buffer (20 mM Tris pH 7.5, 150 mM NaCl, 2 mM DTT) was performed.

3.2.7 Protein Detection and Evaluation

3.2.7.1 SDS-PAGE gel and Coomassie Blue stain

SDS-PAGE (sodium dodecyl sulphate-polyacrylamide gel electrophoresis) (Laemmli 1970) is a common method used for the separation of proteins based on their molecular weight after the application of an electrical field. The protein sample is mixed with Laemmli buffer that contains SDS. SDS is an anionic detergent that along with a bit of boiling disrupts the tertiary structure of the protein. Laemmli buffer contains additionally DTT or β-mercaptoethanol in a high concentration to break down protein-protein disulphide bonds. In an applied electrical field, the negatively charged SDS-bound proteins will move toward the positive anode at a different rate

which depends on the molecular weight. The acrylamide gel contains two layers. The upper layer (stacking gel) includes the sample wells and ensures that all the proteins arrive at the running gel (lower layer) at the same time, so protein of the same molecular weight will migrate as tight bands. The lower layer (separating or running gel) is responsible for separating proteins by size. Once the protein are in the running gel, they are separated because protein with higher molecular weight are moving slower through the porous acrylamide gel than lower molecular weight protein. The size of the gel pores can be altered depending on the size of the proteins supposed to be separated by changing the acrylamide concentration. To detect the proteins on a gel, staining with protein specific dye, Coomassie Brilliant Blue dye, was performed. The dye develops colored complexes with the proteins that are as little as 0.5 μg/cm^2.

For each sample, 10 μL protein sample was mixed with 30 μL 4 x SDS loading buffer. The samples were heated at 95 ^{o}C for 5 min. Then the samples were loaded onto a right size pore SDS-PAGE gel. The first lane was always reserved for the protein standard marker. The gel box is filled with SDS running buffer until the electrode assembly, containing the gel, is covered. The gel runs at 110 V for approximately 30 min and then at 220 V until it runs to the end. After the end of the run, the gel was washed with water and heated to near-boiling temperature in a microwave, followed by cooling down under slow shaking for 3 min. The procedure was repeated three times. Then, to make the proteins visible, Coomassie Brilliant Blue dye was added to the gel, which was heated for few seconds. The gel was stained for around 30 min under slow shaking. At the end, the gel was washed thoroughly with water and was destained for 30 min.

3.2.7.2 Protein concentration determination

Protein concentration was always determined by using the NanoDrop 2000 UV-Vis Spectrophotometer. The method is based on the UV light absorption from aromatic residues. A drop of 1-3 μL from the protein sample is placed on the sensor of the device and the absorbance at 280 nm will be analyzed using molar extinction coefficients of 46410 M^{-1} cm^{-1} for $PTP1B_{1-298}$ and $PTP1B_{1-321}$, 53400 M^{-1} cm^{-1} for $PTP1B_{1-393}$, 50880 M^{-1} cm^{-1} for $TCPTP_{1-296}$, 52370 M^{-1} cm^{-1} for $TCPTP_{1-336}$ and 14440 M^{-1} cm^{-1} for $SOCS3_{20-185}$, according to the Lambert-Beer law giving as a result the final concentration of the protein. The molar extinction coefficients of each protein was calculated using the ProtParam tool on the ExPASy server (Gasteiger et al. 2005; Wilkins et al. 1999).

3.2.8 In vitro assays

3.2.8.1 Thermofluor screening

The Thermofluor assay (Ericsson et al. 2006) is a quick, temperature-based assay to assess the stability of proteins for biochemical and structural studies, measuring the temperature-induced melting points in different conditions. The unlabeled protein was tested in 92 different buffer conditions (**Table 3.5** pHs ranging between 4 to 9.5 and salt between 40mM to 400mM) and with 48 different additives using SYPRO orange dye (**Table 3.6**). All buffers were used at a final concentration of 40 mM and each well contains 20 µL of buffer with 2.5 µL 100x SYPRO orange dye and 2.5 µL of 10 mg/mL protein. In the additive screening, each well contains 15 µL of additive, 5 µL of the best buffer (5x) as determined from the buffer screening, 2.5 of 10 mg/mL µL protein and 2.5 µL 100x SYPRO orange dye. The concentrations described in the tables are final concentrations after mixing.

The Thermofluor assay can be used for ligand screening, using the same principle as for searching for optimization of conditions. 6 different compounds (Trodusquemine, SIXB, NV673, berberine, 4-aminoanilino (oxo) acetic acid, PTP1B inhibitor 539741) were tested in the optimum buffer conditions (Bis-Tris propane pH 7.5) in high and low salt concentration (400 and 80 mM NaCl).

Table 3.5 Thermofluor buffer screening plate

	1	2	3	4	5	6	7	8	9	10	11	12
A	Acetate 4.0 40 NaCl	Acetate 4.5 40 NaCl	Citrate 5.0 40 NaCl	Citrate 5.4 40 NaCl	MES 6.0 40 NaCl	MES 6.5 40 NaCl	Cacodylate 5.0 40 NaCl	Cacodylate 5.5 40 NaCl	Phosphate 6.0 40 NaCl	Phosphate 6.5 40 NaCl	Phosphate 7.0 40 NaCl	Bis-Tris Propane 7.0 40 NaCl
B	Acetate 4.0 80 NaCl	Acetate 4.5 80 NaCl	Citrate 5.0 80 NaCl	Citrate 5.4 80 NaCl	MES 6.0 80 NaCl	MES 6.5 80 NaCl	Cacodylate 5.0 80 NaCl	Cacodylate 5.5 80 NaCl	Phosphate 6.0 80 NaCl	Phosphate 6.5 80 NaCl	Phosphate 7.0 80 NaCl	Bis-Tris Propane 7.0 80 NaCl
C	Acetate 4.0 200 NaCl	Acetate 4.5 200 NaCl	Citrate 5.0 200 NaCl	Citrate 5.4 200 NaCl	MES 6.0 200 NaCl	MES 6.5 200 NaCl	Cacodylate 5.0 200 NaCl	Cacodylate 5.5 200 NaCl	Phosphate 6.0 200 NaCl	Phosphate 6.5 200 NaCl	Phosphate 7.0 200 NaCl	Bis-Tris Propane 7.0 200 NaCl
D	Acetate 4.0 400 NaCl	Acetate 4.5 400 NaCl	Citrate 5.0 400 NaCl	Citrate 5.4 400 NaCl	MES 6.0 400 NaCl	MES 6.5 400 NaCl	Cacodylate 5.0 400 NaCl	Cacodylate 5.5 400 NaCl	Phosphate 6.0 400 NaCl	Phosphate 6.5 400 NaCl	Phosphate 7.0 400 NaCl	Bis-Tris Propane 7.0 400 NaCl
E	HEPES 7.0 40 NaCl	HEPES 7.5 40 NaCl	TRIS 8.0 40 NaCl	TRIS 8.5 40 NaCl	CAPSO 9.0 40 NaCl	CAPSO 9.5 40 NaCl	Imidazole 7.0 40 NaCl	Imidazole 7.5 40 NaCl	Bicine 8.0 40 NaCl	Bicine 8.5 40 NaCl	Glycine 9.0 40 NaCl	Glycine 9.5 40 NaCl
F	HEPES 7.0 80 NaCl	HEPES 7.5 80 NaCl	TRIS 8.0 80 NaCl	TRIS 8.5 80 NaCl	CAPSO 9.0 80 NaCl	CAPSO 9.5 80 NaCl	Imidazole 7.0 80 NaCl	Imidazole 7.5 80 NaCl	Bicine 8.0 80 NaCl	Bicine 8.5 80 NaCl	Glycine 9.0 80 NaCl	Glycine 9.5 80 NaCl
G	HEPES 7.0 200 NaCl	HEPES 7.5 200 NaCl	TRIS 8.0 200 NaCl	TRIS 8.5 200 NaCl	CAPSO 9.0 200 NaCl	CAPSO 9.5 200 NaCl	Imidazole 7.0 200 NaCl	Imidazole 7.5 200 NaCl	Bicine 8.0 200 NaCl	Bicine 8.5 200 NaCl	Glycine 9.0 200 NaCl	Glycine 9.5 200 NaCl
H	HEPES 7.0 400 NaCl	HEPES 7.5 400 NaCl	TRIS 8.0 400 NaCl	TRIS 8.5 400 NaCl	CAPSO 9.0 400 NaCl	CAPSO 9.5 400 NaCl	Imidazole 7.0 400 NaCl	Imidazole 7.5 400 NaCl	Bicine 8.0 400 NaCl	Bicine 8.5 400 NaCl	Glycine 9.0 400 NaCl	Glycine 9.5 400 NaCl

Table 3.6 Thermofluor additive screening plate

	1	2	3	4	5	6
A	450 mM NaCl	60 mM KCl	60 mM imidazole 7.5	60 mM AmSO4	100 mM AmCl	60 mM LiCl
B	6 mM CaCl2	6 mM MgCl2	3 mM NiSO4	3 mM ZnCl2	30 mM NaI	30 mM NaBr
C	3% glycerol	6% glycerol	9% glycerol	12% glycerol	3% MPD	6% MPD
D	18 mM Lysine	18 mM Arginine	18 mM Serine	18 mM Proline	18 mM Alanine	18 mM Glycine
E	3% Glucose	3% Fructose	3% Sucrose	3% Mannitol	18 mM Methionine	18 mM Cysteine
F	3 mM ATP + 3 mM MgCl2	3 mM ADP + 3 mM MgCl2	3 mM GTP + 3 mM MgCl2	3 mM CTP + 3 mM MgCl2	3 mM UTP + 3 mM MgCl2	3 mM NADH + 3 mM MgCl2
G	3 mM Spermidine	3 mM Spermine	6 mM EDTA 7.5	6 mM EGTA 7.0	10 mM Urea	3 mM Adenine
H	3 mM TCEP	3% PEG400	2% DMSO	1% DDMAD	2 mM NDSB201	Water

3.2.8.2 Crystallization

Protein crystals are very important for solving protein structures. The regular shapes of crystals reflects the special properties of the atoms and molecules which comprise them. Within a crystal, these atoms and molecules are arranged in very regular repeating patterns on a grid and this enables us to use the technique of crystallography to explore the three dimensional arrangement of the atoms within them.

Under specific conditions proteins can adopt higher ordered structures, forming protein crystals, this process is called crystallization. In order to obtain crystals, highly pure and homogeneous protein samples are required. Apart from the purity there are more factors that affect the crystallization of a protein sample, such as pH, concentration of the protein, precipitant, temperature and additives. There are several methods of protein crystallization. The method used for the protein crystallization in this study was the vapor diffusion method by hanging drop. In this method, the crystallization drop is set by mixing the protein with the crystallization buffer and then the drop is equilibrated against a reservoir solution of the crystallization buffer. As the drop and reservoir equilibrate, the precipitant and protein concentrations increase in the drop leading to the supersaturation of the protein and subsequently into the crystal formation (McPherson 2009).

Once the crystals grow, they need to be taken out from the drops to be placed into an X-ray beam. To protect the crystals from radiation damage, caused by high intensity X-rays, they are usually frozen at a temperature of liquid nitrogen and X-ray data are collected at these temperatures (cryo-temperature). X-rays pass through the crystal and a diffraction pattern is released due to the electron cloud surrounding the atoms around the crystal. The diffraction pattern allows the 3D

reconstruction of the electron density map via which the structure of the protein is solved (Parker 2003).

Molecular replacement (Evans and McCoy 2008) is a method of solving crystal structures when a suitable homologous model is available. It provides a solution of the crystallographic phase problem, by providing initial estimates of the phases of the new structure from a previously known protein structure. It is usually successful in cases with high sequence identity (>40 %) between the target protein and its homologue.

After a screening in the crystallization conditions (**Table 3.7**), PTP1B protein crystals were obtained. Protein and reservoir were mixed in different ratios. PTP1B protein was co-crystallized with different compounds or crystals of the free protein were soaked with a solution of the compound. More specifically, PTP1B crystals were soaked with 11 compounds from the compound library in a ratio of 1:3 (1mM compound). Co-crystallization with Trodusquemine and two of its derivatives in a ratio of 1:2 (606 μM) at the same conditions was performed. Diffraction data on 40 crystals were tested at the ESRF Grenoble using the ID23-1 beamline.

Table 3.7 Crystallization screening conditions plate

	1	2	3	4	5
A	70 µL BIS-TRIS prop pH:7.5	70 µL BIS-TRIS prop pH:7.5	70 µL BIS-TRIS prop pH:7.5	70 µL BIS-TRIS prop pH:7.5	70 µL BIS-TRIS prop pH:7.5
	122.5 µL Mg acetate	122.5 µL Mg acetate	122.5 µL Mg acetate	122.5 µL Mg acetate	122.5 µL Mg acetate
	0 µL PEG 8000	70 µL PEG 8000	140 µL PEG 8000	120 µL PEG 8000	280 µL PEG 8000
	507.5 µL H2O	437.5 µL H2O	367.5 µL H2O	297.5 µL H2O	227.5 µL H2O
B	70 µL BIS-TRIS prop pH:7.5	70 µL BIS-TRIS prop pH:7.5	70 µL BIS-TRIS prop pH:7.5	70 µL BIS-TRIS prop pH:7.5	70 BIS-TRIS prop pH:7.5
	147 µL Mg acetate	147 µL Mg acetate	147 µL Mg acetate	147 µL Mg acetate	147 µL Mg acetate
	0 µL PEG 3350	70 µL PEG 8000	140 µL PEG 3350	210 µL PEG 8000	280 µL PEG 3350
	483 µL H2O	413 µL H2O	343 µL H2O	273 µL H2O	280 µL H2O
C	70 µL BIS-TRIS prop pH:7.5	70 µL BIS-TRIS prop pH:7.5	70 µL BIS-TRIS prop pH:7.5	70 µL BIS-TRIS prop pH:7.5	70 µL BIS-TRIS prop pH:7.5
	175 µL Mg acetate	175 µL Mg acetate	175 µL Mg acetate	175 µL Mg acetate	175 µL Mg acetate
	0 µL PEG 3350	70 µL PEG 3350	140 µL PEG 8000	210 µL PEG 6000	280 µL PEG 6000
	455 µL H2O	385 µL H2O	315 µL H2O	245 µL H2O	175 µL H2O

A Co-crystallization screening for compounds trodusquemine, SIXB and NV673 was performed at Max Planck crystallography platform. Seven different screenings [Inhouse screenings Crystal platform Magic 1 and 2 (MA1, MA2) (Max Planck Crystallization Facility), Qiagen PEGs (NPG), Qiagen JCSG+ (JSG), Qiagen Classics (NCS) and Qiagen PACT (PAC) (QIAGEN screenings), Hampton research Index (IND) (Hampton research Index)] of 95 different co-crystallization conditions each were tested. The ratio between the compound and the protein was 1:5 (1.5 mM compound). Twenty of the most promising crystals, which show different morphology than the one of the native protein, were frozen. This could indicate binding of the compound to the protein. Those crystals were tested again in ESRF Grenoble

A last screening with the 15 best conditions from the previous two screenings was performed. Co-crystallization of compounds Trodusquemine and SIXB and soaking of the free protein with the same compounds were tested. For co-crystallization 5 (1.5 mM) and 15 (5 mM) times more compounds concentration than protein was used. In case of soaking 3 (1 mM) and 15 (5 mM) times more compound was tried.

The diffraction data were analyzed with molecular replacement in order to get the first model of the protein with the ligand using the structure of a homologous protein as model. All the structures were built in Coot (Emsley and Cowtan 2004) model building software and the model was further refined in Refmac from the CCP4 suite (Winn, Murshudov, and Papiz 2003).

3.2.8.3 Activity assay screenings

3.2.8.3.1 pNPP phosphatase assay

The pNPP phosphatase assay (Peters et al. 2003) is a simple colorimetric assay to measure inhibition of phosphatases. It's a fast method, which requires very small amounts of protein and compound. p-Nitrophenyl phosphate (pNPP) is a chromogenic substrate for most phosphatases. The principle of this method is based on the dephosphorylation reaction of pNPP yielding p-Nitrophenol (pNPH), which is converted in an intense yellow soluble product (p-Nitrophenylene anion pNP) under alkaline conditions, and can be conveniently measured at 405 nm on a spectrophotometer (**Figure 3.2**). The IC_{50} values can be estimated from the analysis of the data derived from this assay, using different concentrations of inhibitor.

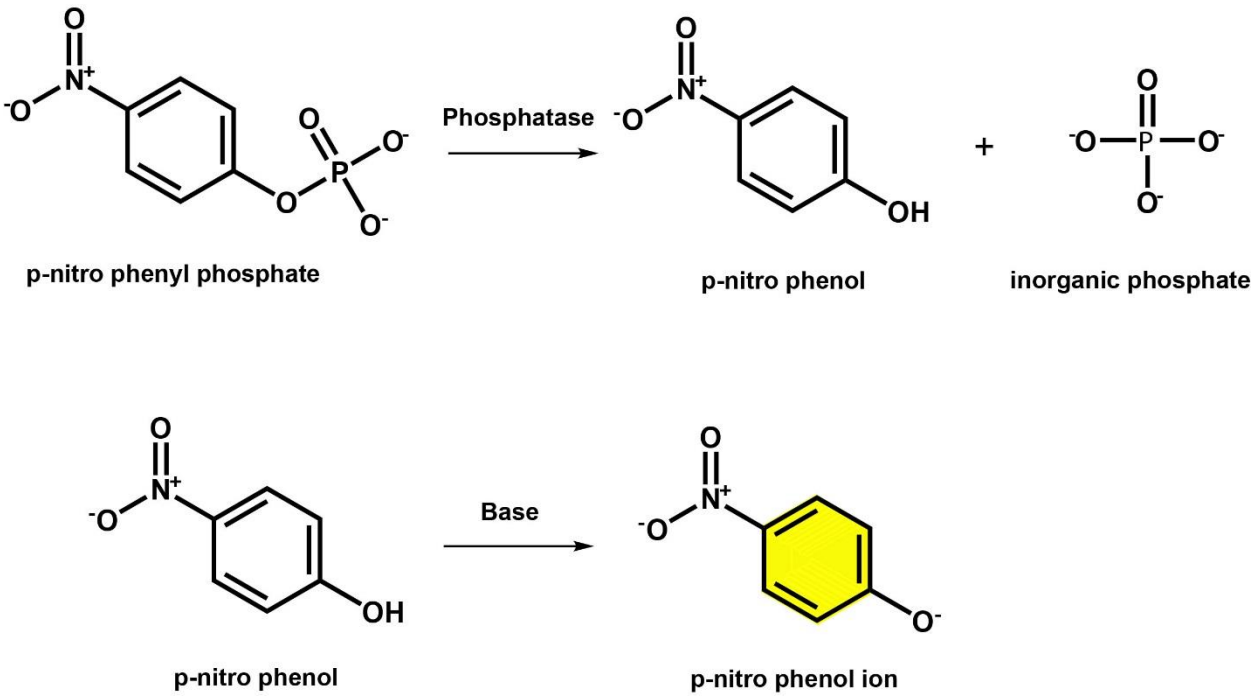

Figure 3.2 pNPP phosphatase assay principle.

In the beginning, protein and substrate concentration conditions that should be used for the assay were optimized. A dilution series of pNPP (0.1-10 mM) was prepared and mixed in a 96-well plate with a dilution series of the enzyme (10-120 nM in presence of NP-40 and 30-150 nM in absence of NP-40) in a total volume of 80 µL. The buffer conditions used were 25mM Bis-Tris-Propane pH 7.5, 50mM NaCl, 2.5mM EDTA, 0% or 0.025% NP-40, 2mM DTT. Detergent NP-40 prevents protein and compound aggregation, unspecific binding and protein binding to the walls of the plate. The kinetic constants K_m and k_{cat} were estimated. Then the effect of the solvents, in which our compounds are dissolved, was investigated on the K_m by using different percentages ranging from 0-10%. Changes of absorbance at 405 nm over time were measured with an EnVision® reader at 37 °C. The kinetic constants K_m and k_{cat} were determined as Endpoints, terminating the reaction after approximately 5 min incubation of the protein with the substrate by addition of 10 µL highly concentrated NaOH solution. The lowest enzyme concentration that shows detectable Michaelis-Menten curves was chosen for the inhibition screening and the corresponding K_m giving the concentration of the substrate at which the reaction rate is half-maximum. The kinetic constants K_m and k_{cat} and V_{max} were determined using the Michaelis-Menten equation in GraphPad Prism program 5.03 (GraphPad Software, Inc. La Jolla, CA, USA).

Using the same method, an inhibition screening for the determination of the IC_{50} values could be performed. The concentration of the enzyme and the substrate used was determined as previously described and was always kept constant, while the inhibitor concentration varied (ranging from 0.5-500 μM). The experiment was set it up by mixing the inhibitor with the protein solution and the reaction started after the addition of the pNPP substrate. The reaction performed in the same buffer conditions in presence and absence of NP-40 detergent and was monitored with the same system. The analysis of the inhibition screening data were performed using the nonlinear regression GraphPad Prism equation log(inhibitor) versus response –Variable slope (four parameters) and the IC_{50} of potential inhibitor was calculated. IC_{50} values were defined as the concentration of the inhibitor that caused a 50% decrease in the phosphatase activity.

3.2.8.3.2 DiFMUP phosphatase assay

For the IC_{50} determination of colorful inhibitors, for which the pNPP assay could not be used, a fluorescence assay (Welte et al. 2005) with DiFMUP as substrate was used. Experiments were performed in triplicate in black polystyrene 384-well plates with flat bottom at 37°C. The fluorescence excitation was measured at 358 nm and fluorescence emission at 455 nm and was monitored continuously for 10 min using a PerkinElmer EnVision multilabel plate reader. The protein concentration was optimized for maximum sensitivity and linearity using minimal protein concentration. In short, each protein was prediluted in reaction buffer (25 mM Bis-Tris propane pH 7.5, 50 mM NaCl, 2 mM EDTA and with or without 2 μM DTT) to three different concentrations in a final volume of 45 μL. Reactions were initiated by adding 5 μL of DiFMUP to the reaction mixture to yield final concentrations of 2-100 μM. Enzyme kinetic parameters were determined using the Michaelis-Menten equation in GraphPad Prism program.

For IC_{50} determination, 1 nM purified PTP1B or TCPTP protein was incubated 10 min with celastrol in fifteen concentrations ranging from 0 to 500 μM in reaction buffer (25 mM Bis-Tris propane pH 7.5, 50 mM NaCl, 2mM EDTA and with or without 2 μM DTT) in total volume of 45 μL. The reaction was started by adding 5 μL of substrate buffer containing DiFMUP to a final concentration equivalent to the protein construct K_m for DiFMUP. IC_{50} values were determined using the equation fitting log(inhibitor) vs. response from nonlinear regression analysis in the GraphPad Prism program. Compounds tested with this assay were celastrol and AOAC (4'-aminoxanilic acid).

In case of the compounds celastrol the reversibility of the inhibition could also be checked by this assay incubating 1 nM full length protein with 80 μM celastrol, or with DMSO in reaction buffer for 10 min. The reaction was started by addition of 5 μM DiFMUP and was monitored continuously for 40 min. Further addition of DiFMUP or DiFMUP and H_2O_2 was used in order to test that the inhibition is reversible. H_2O_2 was used as a negative control (Salmeen et al. 2003).

3.2.8.4 NMR Spectroscopy

All protein samples were exchanged by sequential concentration/dilution steps into NMR buffer. All 1D, 2D and 3D spectra were recorded at 20 ºC on Bruker AvanceIII 600 MHz and Bruker AvanceIII 800 MHz spectrometers equipped with a cryogenic QCI-probehead (^{1}H, ^{31}P, ^{13}C, ^{15}N) equipped with Z-gradients.

First 1D-^{1}H spectra and 2D ^{1}H,^{15}N TROSY spectra were recorded in order to judge whether our constructs are folded or not. Initial buffer conditions used for NMR (25mM Tris-HCl pH 7.5, 75mM NaCl, 5 mM DTT, 0.01% NaN_3, 0.5 mM EDTA) were very similar to those described by Meier and collaborators (25 mM Tris-HCl pH 7.5, 10 mM DTT, 0.02% sodium azide, 50 mM NaCl) (Meier et al. 2002). Then, the best buffer conditions found through thermofluor screening wereused, in which PTP1B has found to have a maximum stability at pH 7.5 and high salt (450 mM NaCl). However high-ionic strengths are not suitable for cryo-NMR probes, therefore 75 mM of NaCl was used instead. The final NMR buffer conditions chosen for all the NMR experiment was 50 mM fully deuterated d11-Tris-HCl pH 7.5, 75 mM NaCl, and 5 mM d10-DTT and 10% D_2O, unless otherwise stated. In order to optimize the quality of the ^{15}N-PTP1B spectra, that is to maximize resolution signal to noise, several 1D and 2D spectra of ^{15}N-PTP1B at different temperatures were recorded. Better spectra were obtained at 20 ºC, and protein precipitation and aggregation were observed at higher temperatures (20 ºC and 25 ºC).

3.2.8.4.1 Backbone Assignments

Backbone chemical shift assignments of $PTP1B_{1-298}$ were obtained using TROSY versions of standard triple resonance HNCACB, HNCA, HN(CO)CA, HN(CA)CO, HNCO experiments on a 420 μM sample of random fractional (~70%) deuterated, ^{13}C, ^{15}N labeled $PTP1B_{1-298}$ based on the assignment of a similar construct ($PTP1B_{1-303}$) reported previously (Krishnan et al. 2014). Backbone chemical shift assignments of $TCPTP_{1-296}$ were obtained using TROSY versions of standard triple resonance HNCACB, HN(CO)CACB, HNCA, HN(CO)CA, HN(CA)CO, HNCO

experiments on a 400 μM sample of random fractional (~70%) deuterated, ^{13}C, ^{15}N labeled $TCPTP_{1-296}$. All spectra were recorded on Bruker 800 MHz spectrometer at 293K (20 ^{o}C). All datasets were processed using NMRPipe software (Delaglio et al. 1995) and analyzed with CCPN analysis 2.4.2 (Skinner et al. 2016).

3.2.8.4.2 NMR screenings

Two different approaches can be used to follow protein ligand interactions by NMR Spectroscopy. First by looking at the protein (target) spectrum and observing the changes in chemical shifts upon ligand titration. Second, recording the recording the spectra of a sample of ligand and follow changes upon addition of small amounts of protein. In the first approach, the most common technique used is ^{1}H, ^{15}N correlation HSQC spectrum (or TROSY experiments for bigger proteins), in which chemical shift changes due to ligand interaction can be easily followed. The use of ^{15}N-labeled proteins is necessary in relatively high amounts, but prior to this experiment a total or partial assignment of the protein should be done in order to be able to define which residues are involved in the interaction. In the ligand based approach, ligand spectra are recorded with very small amounts of nonlabelled protein and in peak intensities and shifts, diffusion or saturation transfer can be used to obtain information about the binding process. In this study TROSY experiments were used for the first approach, while simple 1D spectra and STD experiments were used in the case of the ligand based NMR screening.

3.2.8.4.3 Ligand-based NMR screenings

A simple 1D NMR approach was followed for the detection of interactions between ligands and proteins. This method was used only for the phosphatases and for a specific number of compounds from our compound library. For each protein phosphatase construct four-titration points were recorded with 32k time domain and 128 scans by adding protein to final concentrations of 0, 10, 20 and 30 μM to a 100 μM of compound solution in 50 mM fully deuterated d11-Tris-HCl pH 7.5, 75 mM NaCl, and 5 mM d10-DTT and 10% D_2O.

Another technique used to study ligand binding to our protein was STD-NMR spectroscopy (Viegas et al. 2011). STD-NMR experiments were performed with 46 compounds from our library and $PTP1B_{1-321}$ protein. Compounds celastrol and AOAC were tested with $PTP1B_{1-298}$, $PTP1B_{1-396}$, $TCPTP_{1-296}$ and $TCPTP_{1-336}$ as well. All STD experiments were recorded with 800 number of scans at 20 ^{o}C in Bruker 800 MHz, with saturation time (d3) 1 second (d2=0.5 s and d1=1.5 s), 43 dB, using an interleaved pulse program with off-resonance irradiation at -5 ppm and on-resonance

irradiation varying each time depending on the compound chemical shifts. Ten μM unlabeled protein in NMR buffer in 10% D_2O (NS 64, 800 MHz) was added to a 500 μM compound solution. Reference STD experiment were performed without the protein, using the same irradiation regions. In case of celastrol, competition experiments were recorded in the same way adding $PTP1B_{1-298}$ protein to a mixture of 500 μM celastrol and 500 μM of AOAC.

3.2.8.4.4 Protein-based NMR screening

In order to confirm the binding and map the binding site of the most promising compounds onto the protein structure, binding experiments of compounds to PTP1B, TCPTP and SOCS3 constructs were performed. In all experiments 100 μM ^{2}H (~70%), ^{15}N (99%) $PTP1B_{1-298}$, ^{2}H (~70%) ^{15}N (99%) $TCPTP_{1-336}$ protein was used in NMR buffer or ^{15}N (99%) $SOCS3_{20-185}$ protein in a 50 mM phosphate buffer (pH 6.7, 10% D_2O) was used. Fifty mM compound were added to the protein sample to a final concentration of 500 μM and the changes were monitoring by ^{1}H, ^{15}N TROSY experiments for the phosphatases and by ^{1}H, ^{15}N HSQC experiments for the SOCS3 protein. All experiments were recorded in Bruker 800 MHz for the protein phospahatases and in Bruker 600 MHz for the protein SOCS3 with 2048 k (ω2) x 128 (ω1) time domain points and 64 scans. A reference experiment was always recorded under the same conditions where the compound was replaced by an addition of the same volume of DMSO-d_6. The compounds tested with this approach in order to map their binding site were Trodusquemine, 18β-glycyrrthetinic acid, cholesterol sulfate, celastrol and dihydrocelastrol.

The chemical shift perturbations (CSP) for each amide group were calculated by using the following formula:

$$\Delta\delta(NH) = \sqrt{(\Delta\delta^{1}H)^{2} + (\frac{\Delta\delta^{15}N}{5})^{2}} \qquad \text{Eq. 9}$$

3.2.8.5 MALDI-TOF

In order to confirm if the compound celastrol binds covalently to $PTP1B_{1-298}$, mass spectrometry experiments were performed. Twenty μL of 2 mg/mL protein was incubated with and without celastrol (ratio 1:5) in NMR buffer containing DTT and without containing DTT, for 30 minutes. A MALDI-TOF mass spectrum was then obtained from a Bruker Ultraflex TOF/TOF using a P10 size Millipore Zip Tip C4 in a Cyano-4-Hydroxy-Cinnamic acid matrix (CHCA, MW189.04 Da).

3.2.8.6 Chemical synthesis of dihydrocelastrol

The compound dihydrocelastrol was synthesized as previously described by Klaic and colleagues (Klaić et al. 2011) using as starting material celastrol. In details, in a 5mL round flask 5 mg celastrol (0.011 mmol) were dissolved in approximately 1 mL MeOH and 4.2 mg (0.11 mmol) of $NaBH_4$ were added to the solution. The mixture immediately turned from orange to a clear solution. After 10 min of stirring in room temperature the reaction was quenched with 0.1 M HCl and the precipitants were extracted with 5 mL $CHCl_3$ and 10 mL H_2O in a 20 mL extraction flask. The aqueous layer was washed with CHCl3 3 times and the organic layer (the one at the bottom) was collected and dried with Na_2SO_4 for a short period to prevent reoxidation of the product to celastrol. The Na_2SO_4 was removed from the organic layer by simple filtration. The solvent was removed in a Buchi Rotavapor R-200 with "V" assembly under vacuum. The purity of the compound was tested by HPLC-UV/MS and by NMR. Dihydrocelastrol was found to be 97% pure whith 3% celastrol, most probably as reoxidation product.

3.2.8.7 HPLC-MS analysis

HPLC-MS was used for testing the purity of the synthesized compound and for checking rapidly the product formation of different reactions. In that, 500 μM celastrol in NMR buffer with and without DTT was lyophilized and then dissolved in MeOH at a final concentration of 1 mg/mL. Five more samples of celastrol, celastrol with a mixture of GSH/GSSG (ratio 10:10:1), celastrol with DTT (ratio 1:1), celastrol with d10-DTT (ratio 1:1) and celastrol with TCEP were prepared in MeOH in a final concentration of 1 mg/mL.

HPLC-UV/MS analysis was performed on a Dionex UltiMate 3000 HPLC system coupled with a Thermo Finnigan LCQ ultrafleet mass spectrometer, using following method: Waters X-Bridge C18 (4.6 x 30 mm, 3.5 mm) column; gradient: 5 to 95% of acetonitrile + 0.1% formic acid v/v in water + 0.1% formic acid v/v over 5 min period; flow rate: 1.1 mL/min; UV detection at 214 and 280 nm.

3.2.9 SwitchSENSE

The switchSENSE technology (Langer et al. 2013)on the DRX instrument (Dynamic Biosensors GmbH, Martinsried, Germany) was used to determine the kinetic and affinity parameters (k_{on}, k_{off}, K_D) of $PTP1B_{1-298}$ and celastrol interaction. $PTP1B_{1-298}$ was immobilized on the switchSENSE chip (MPC-48-2-Y1-S) biosensor surface. More specifically, $PTP1B_{1-298}$ was

covalently coupled to single-stranded 48mer DNA complementary in sequence to the single-stranded DNA functionalized on the biosensor surface using amine chemistry (Amine coupling kit CK-NH2-1-B48). The PTP1B-DNA conjugate was hybridized to the covalently immobilized single stranded surface DNA. Immobilized protein was used as the ligand, while celastrol was injected as the analyte in the solution. All experiments were carried out in PE40 buffer (10 mM Na_2HPO_4/NaH_2PO_4, pH 7.4, 40 mM NaCl, 50 µM EGTA, 50 µM EDTA, 0.05 % Tween20) using the fluorescence proximity sensing (FPS) mode. Celastrol was injected at increasing concentrations up to 100 µM under a constant flow of 100 µl/min. During the dissociation phase, the flow channel was rinsed with running buffer at a flow rate of 100 µl/min. The dissociation kinetics were only recorded for the three highest concentration steps. The biosensor surface was regenerated and functionalized with fresh PTP1B-DNA conjugate for each association-dissociation measurement cycle. All used consumables were obtained from Dynamic Biosensors GmbH, Martinsried, Germany. Data analysis was performed by switchANALYSIS software (Dynamic Biosensors GmbH, Martinsried, Germany) using a mono exponential global fit model.

3.2.10 Cell assay

A cell assay on CLU-177 neuronal cells (adult mouse hypothalamic cell line mHypoA-a/12 CLU177 lysate) was used to test the effect of hit compounds on insulin and leptin sensitivity. CLU177 hypothalamic cells were cultured in DMEM supplemented with 10% fetal bovine serum (FBS) and antibiotics (penicillin 100 IU/mL and streptomycin 100 µg/mL) at 37ºC. Several passagings in 10 mm plates were performed to reach a sufficient number of cells for splitting. In each passaging, 80-90% confluent cells were trypsinized with 1mL trypsin for 5min at 37ºC, transferred to a 15 mL Falcon and centrifuged for 5 min at 11000 x g. Cells were well resuspended with 3 mL medium and 10 µL of the cell suspension were loaded in a special counting slide, which was inserted into the slide slot of Automated Cell Counter (TC20^{TM} Bio-Rad). Cells were split in new 10 mm plates to reach seeding density of 0.2 x 10^6 cells/mL per plate if a new passaging was necessary, or in six-well plates to reach seeding density of 0.15 x 10^6 cells/mL per well. Plates were placed at 37ºC for 24h incubation. CLU177 cells were cultured in 6-well plates until they reached 80-90% confluency, followed by serum-starvation for 6 hours and then incubated with or without Celastrol for 40 min at indicated doses (0.3, 1, 3, 10, 30 µM). Control cells were treated with or without 3 different stimulus: insulin (100 ng/mL; Humolog Pen, Eli Lily, Indianapolis, IN,

USA), leptin (10 ng/mL; R & D system, Minneapolis, MN, USA) and growth hormone (30 μg/mL, 85 μg/mL, 200 μg/mL) for 10 min prior to harvest.

RIPA buffer containing protease and phosphatase inhibitor cocktail (Thermo Fisher Scientific Inc., Rockford, IL, USA) and 1 mM phenyl-methane-sulfonyl fluorid (PMSF) was used for the extraction of protein. A Trans Blot Turbo transfer apparatus (Biorad, Hercules, CA, USA) transferred proteins from the gel to nitrocellulose membranes. Membranes were incubated with anti-ß-Actin (rabbit polyclonal, 1:20000, Cat #4970), anti-pSTAT3^{T705} (rabbit polyclonal, 1:2500, Cat #9145), anti-STAT3 (mouse monoclonal, 1:2500, Cat #9139), anti-pSTAT5, anti-STAT5, anti-pAKT^{S473} (rabbit polyclonal, 1:1000, Cat #4058), anti-AKT (mouse polyclonal, 1:1000, Cat #2920), anti-pJAK2$^{T1007/1008}$ (rabbit polyclonal, 1:1000, Cat #3771) anti-pERK1/2$^{T202/Y204}$ (rabbit polyclonal IgG, 1:1000, sc-16982-R), anti-ERK1/2 (rabbit polyclonal IgG, 1:1000)

All antibodies were purchased form Cell Signaling Technology (Cell Signaling, Danvers, MA, USA). Membranes were detected on a LiCor Odyseey instrument (Lincoln, NE, USA) using ECL (Biorad, Hercules, California, USA), and densitometric quantifications were performed using internal LiCor Odyssey software.

3.3 *In silico* studies with HADDOCK

The High Ambiguity Driven protein-protein DOCKing (HADDOCK) web server was used to dock celastrol on PTP1B (Dominguez, Boelens, and Bonvin 2003). The Easy interface was used for docking analysis. In this method, active and passive residues are defined. Active residues are the ones in which shift changes are larger than 2σ standard deviation and subsequently are found in the interface and in addition are on the surface. HADDOCK also defines passive residues, which are surface residues or residues close to the active site that have a smaller shift change than the active residues. For this run a crystal structure of the open conformation of the protein was used (pdb ID: 2HNP) and a pdb file of the compound was produced using the PRODRG Server.

4. Results I: Challenges and solutions for recombinant PTPs protein expression, purification and evaluation

4.1 Constructs

Three different constructs of human PTP1B were cloned (**Figure 4.1**) corresponding to the catalytic domain (amino acids 1-298), an extended catalytic domain including the C-terminal Pro-rich region (amino acids 1-321) and a longer construct without the ER localization region (amino acids 1-393).

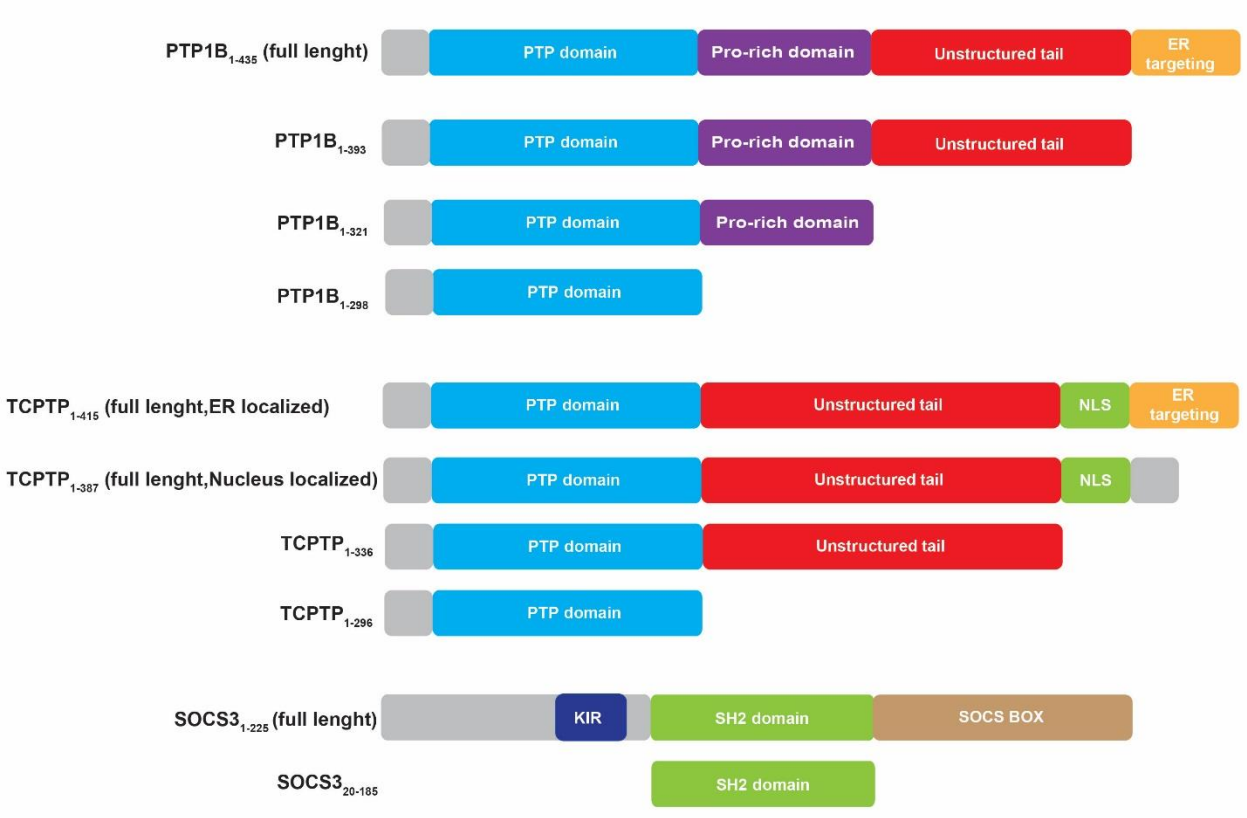

Figure 4.1 PTP1B and TCPTP Constructs.

Initially, I attempted to express and purify a PTP1B$_{1-321}$ construct in pT7 vector, which is ampicillin resistant. Overexpression of the protein in minimal medium containing ^{2}H, ^{15}N and ^{13}C isotopes was always resulting in very low amounts of purified protein. The reason why the expression of triple labeled protein was not successful might be because of the antibiotic ampicillin (Sivashanmugam et al. 2009). Beta-lactamase is secreted by the bacteria and is expressed from the

plasmid-borne*bla* gene. The resulting build-up of extracellular beta-lactamase can inactivate the ampicillin in the culture medium, removing the selective pressure. This means that a possibly very large portion of the cells in a liquid medium culture no longer have the plasmid, giving poor yielding protein expression.

The incapability of sufficient triple labeled protein production for NMR experiments led us to the decision of recloning our construct into pETM expressing vectors, which are modified pET (Stier, EMBL). pET vectors were chosen due to their capability of recombinant production of any target in *E. coli* cells. They contain: 1) the lacI gene encoding the lac repressor, 2) the T7 promoter that is compatible only with T7 RNA polymerase, 3) the f1 origin of replication and 4) the desired antibiotic resistance gene. All pET vectors express the target protein fused with poly-histidine tail in the N-terminal end of the protein. $PTP1B_{1-321}$ plasmid was recloned into Z2NK vector, which is pETM modified kanamycin resistant vector and has a poly-histidine tail fused in the N-terminal end of the protein and an additional Z-tag that increases the solubility of the protein.

Since the C-terminus is disordered and it's not really visible in the crystal structure, a new shorter construct (1-298) was prepared in pETM-11 vector, which contains N-His tag, kanamycin resistance and a TEV cleavage site.

The full length $PTP1B_{1-435}$ was also cloned but could not be successfully expressed, due to ER (endoplasmic reticulum) targeting domain that makes the protein very unstable. For this reason it was decided to produce a smaller construct, $PTP1B_{1-393}$, in which the ER targeting domain of the protein is excluded from the construct (it was successfully recloned by a master student, Stefanie Schmidt (Schmidt 2016)).

For human TCPTP, two different constructs (**Figure 4.1**) were cloned corresponding to the catalytic domain (amino acids 1-296) and a long construct without the ER and NLS localization sequences (amino acids 1-336). Both TCPTP constructs were prepared in pETM11 vectors, which contain N-His tag, kanamycin resistance and a TEV cleavage site. TCPTPs construct were cloned the same master student, Stefanie Schmidt (Schmidt 2016).

The reason for the preparation of the different size constructs was the investigation of the role of the C-terminus in the activity of the protein.

In this study, in addition to the PTP1B and TCPTP constructs, $SOCS3_{20-185}$ construct (**Figure 4.1**) in pET-Duet vector was also used. It was kindly provided by the professor Jeffrey J. Babon from the University of Melbourne in Australia.

4.2 Protein expression and purification

For all protein constructs, the conditions of overexpression in bacterial hosts to produce larger amounts of unlabeled and labeled material were optimized by screening different strains and media. All produced protein constructs are folded as confirmed by NMR spectroscopy, since the chemical shifts are widely dispersed. As an example is given the NMR spectrum of $PTP1B_{1-298}$ **(Figure 4.2)**.

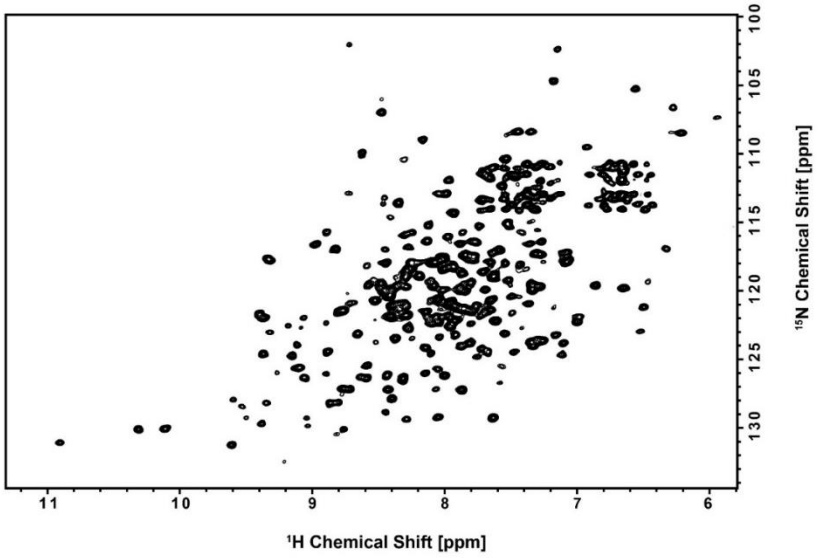

Figure 4.2 ^{1}H. ^{15}N TROSY of well folded $PTP1B_{1-298}$.

4.2.1 Strain selection

Two different bacterial strains, Rosetta2(DE3) and BL21(DE3), were tested for protein phosphatase overexpression in rich media (Lysogeny Broth Lennox (LB) and ZYM-5052 (Studier 2005)) and in minimal media (M9 and N-5052). It was observed that better overexpression, in terms of total amounts of soluble protein was observed using the Rosetta2(DE3) strain. BL21(DE3) cells were used for SOCS3 protein overexpression in SB medium, following a standard protocol from Babon's lab (Liau, Laktyushin, and Babon 2017).

4.2.2 Medium selection for unlabeled protein production

For unlabeled phosphatase protein expression two different media were used, LB and ZYM, at 20 and 37 °C. More protein in the supernatant fraction was obtained with the ZYM medium at 37 °C.

The ZYM medium was therefore selected for protein overexpression. Yields of the final unlabeled proteins were 60 mg $PTP1B_{1-298}$, 50 mg $PTP1B_{1-321}$, 28 mg $PTP1B_{1-393}$, 44 mg $TCPTP_{1-296}$ and 20 mg $TCPTP_{1-336}$ per liter of ZYM-5052 cell culture.

$SOCS3_{20-185}$ unlabeled protein was produced for testing the expression protocol giving a yield of 25 mg per liter of SB medium.

4.2.3 Isotope labeled protein ($^{2}H/^{15}N/^{13}C$)

In order to optimize triple isotope labeling for the phosphatases, initial tests were made only with ^{15}N media. Two different media, M9 and auto induction N-5052 medium, were tested. Both media have controlled sources of nitrogen and carbon, allowing in this way the uniform labeling of protein for NMR studies, which demand NMR visible isotopes (^{15}N and ^{13}C). At the beginning, both media gave poor level of expression. Therefore, the media were supplemented with 1% ^{15}N-Silantes rich medium, and overexpression tested at different temperatures of induction (20 ^{o}C/37 ^{o}C) that can affect the inclusion bodies formation. Additionally, different percentages of detergent NP-40 (1%/ 5%) were used in the lysis buffer in order to solubilize the protein to the maximum. Best results were obtained in N-5052 medium when the temperature of induction was 20 ^{o}C and using 1% NP-40 in the lysis buffer. For SOCS3 protein M9 medium was used following the standard ^{15}N labeled protocol described by (Babon et al. 2005), giving a yield of 8mg per liter of M9 medium.

Double labeled, ^{15}N, ^{2}H(~70%) PTP1B proteins were expressed in N-5052 auto induction medium supplemented with 10% ^{2}H,^{15}N-Silantes in 70% D_2O. Yields of the final labeled proteins were 30 mg ^{2}H(70%), ^{15}N $PTP1B_{1-298}$ and 20 mg ^{2}H(70%), ^{15}N $PTP1B_{1-321}$, 14 mg ^{2}H(70%) $PTP1B_{1-393}$. Deuteration 70% can improve the resolution and the sensitivity of the NMR spectra.

^{15}N, ^{2}H(~70%) TCPTP proteins were expressed in M9 minimal medium supplemented with 10% ^{2}H,^{15}N-Silantes in 70% D_2O. Yields of the final labeled proteins were 15 mg ^{2}H(70%), ^{15}N $TCPTP_{1-296}$ and 10 mg ^{2}H(70%), ^{15}N $TCPTP_{1-336}$ per liter of M9 cell culture

Triple labeled ^{2}H(70%), ^{13}C, ^{15}N $PTP1B_{1-298}$ and ^{2}H(70%), ^{13}C, ^{15}N $TCPTP_{1-296}$ were expressed in M9 minimal medium supplemented by 10% ^{2}H,^{15}N-Silantes following a standard protocol of sequential precultures, as described in the material and method part. Yields of the final labeled protein were 15 mg ^{2}H(70%), ^{13}C, ^{15}N $PTP1B_{1-298}$ and 10mg ^{2}H(70%), ^{13}C, ^{15}N $TCPTP_{1-296}$ per liter of M9 cell culture.

4.2.4 Protein purification

All proteins were purified following the same protocol **Figure 4.3**. After cell lysis and clarification of the supernatant, an affinity chromatography purification protocol with Ni-NTA beads was used, since all proteins have a His-tag on their N-terminal. This was followed by an overnight TEV cleavage in order to remove the His-tag and solubilization tag when present. Then a second IMAC purification step using Ni-NTA column was performed in same way as in the first case, to remove uncleaved protein and impurities. A final purification step was added in order to reach high levels of purity by size exclusion chromatography. For SOCS3 protein a first inclusion bodies purification protocol was followed before the Ni-NTA column as described in details in the methods part. The characteristic retention time of each protein in the size exclusion chromatography is shown in the **Figure 4.4**. The retention time for A) $PTP1B_{1-298}$ is 60 min, B) $PTP1B_{1-321}$ is 58 min, C) $PTP1B_{1-393}$ is 55 min, D) $TCPTP_{1-296}$ is 60 min, E) $TCPTP_{1-336}$ is 55 min and F) $SOCS3_{20-185}$ is 68min.

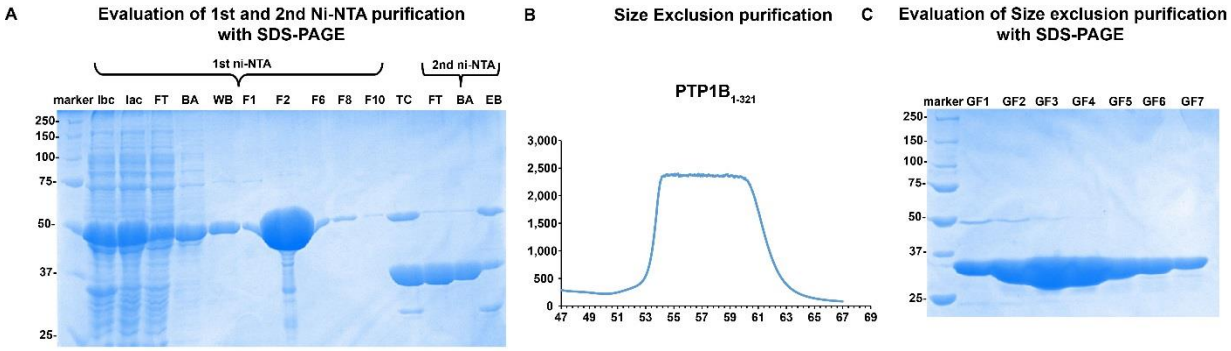

Figure 4.3 Protein purification protocol for $PTP1B_{1-321}$.
(A) SDS PAGE evaluation of the 1st and the 2nd Nickel column purifications (lbc: lysate before centrifugation, lab: lysate before centrifugation, FT: flow through, BA: Buffer A, WB: wash buffer, F1-10: elution fractions 1-10, TC: TEV cleavage, EB: elution buffer). (B) Size exclusion chromatography step. (C) SDS PAGE evaluation of the size exclusion chromatography (GF1-7: Gel filtration fractions 1-7).

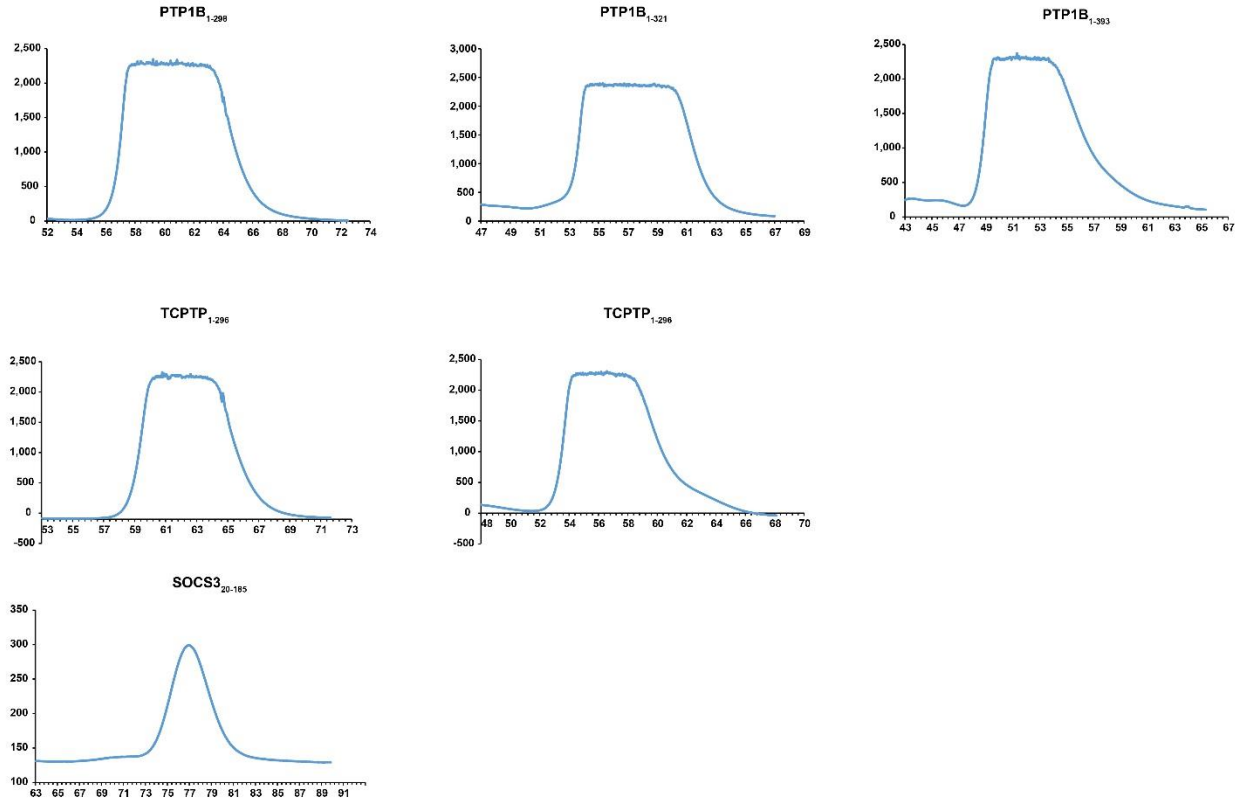

Figure 4.4 GF chromatograms of all protein constructs.

4.3 *In vitro* assays

4.3.1 Thermofluor screening of PTP1B$_{1\text{-}321}$

Thermofluor assay was used in order to find the best buffer conditions in which the protein PTP1B is most stable. Highest melting point temperatures (**Figure 4.5**) were found for Bis-Tris-propane pH 7.5 and in high salt (450 mM), indicating that PTP1B$_{1\text{-}321}$ is most stable in these conditions.

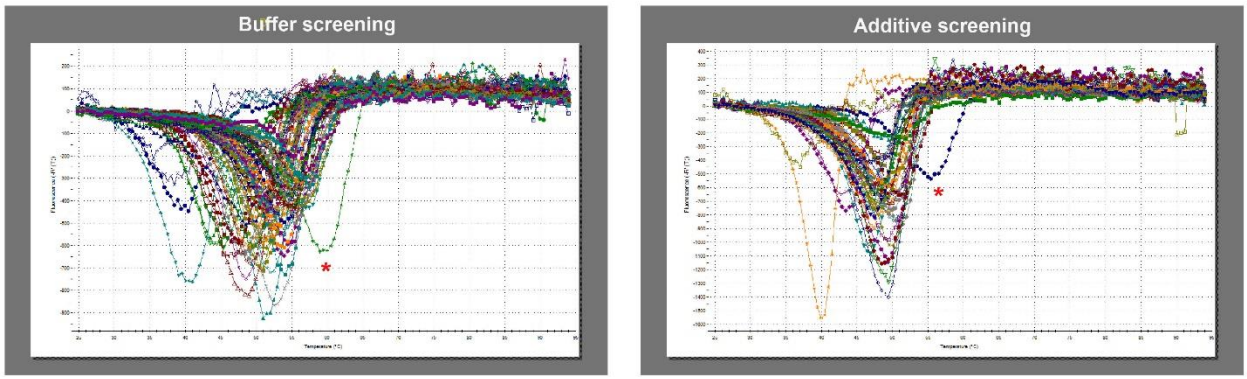

Figure 4.5 Thermofluor screening for the optimal buffer (left) and additive (right) conditions of the protein stability.

4.3.2 Protein NMR spectroscopy

Our constructs are well folded as judged from the dispersion of the resonances on 1D-^{1}H spectra and 2D ^{1}H,^{15}N TROSY spectra. Our initial buffer conditions for NMR (25mM Tris-HCl pH7.5, 75mM NaCl, 5 mM DTT, 0.01% NaN_3, 0.5 mM EDTA) are very similar to those described by Meier and collaborators (25 mM Tris-HCl pH 7.5, 10 mM DTT, 0.02% sodium azide, 50 mM NaCl) (Meier et al. 2002). The Thermofluor assay revealed that PTP1B has a maximum stability at pH 7.5 and high salt (450 mM NaCl), however high-ionic strengths are not suitable for cryo-NMR probes, because it leads to reduce of sensitivity and therefore the signal-to-noise (S/N) (Jacobsen 2007). In order to optimize the quality of the ^{15}N-PTP1B spectra, that is to maximize resolution and S/N, several 1D and 2D spectra of ^{15}N-PTP1B at different temperatures were recorded. Improved spectra were obtained at 293K, and protein precipitation and aggregation were observed at higher temperatures (298K and 303K). ^{1}H,^{15}N TROSY showed better resolution and for some peaks also better S/N than the corresponding ^{1}H,^{15}N HSQC, but partial deuteration was necessary. The ^{1}H,^{15}N TROSY of the ^{2}H(~70%), ^{15}N PTP1B compared with the correspondent one of the ^{15}N PTP1B, showed better resolution (**Figure 4.6**).

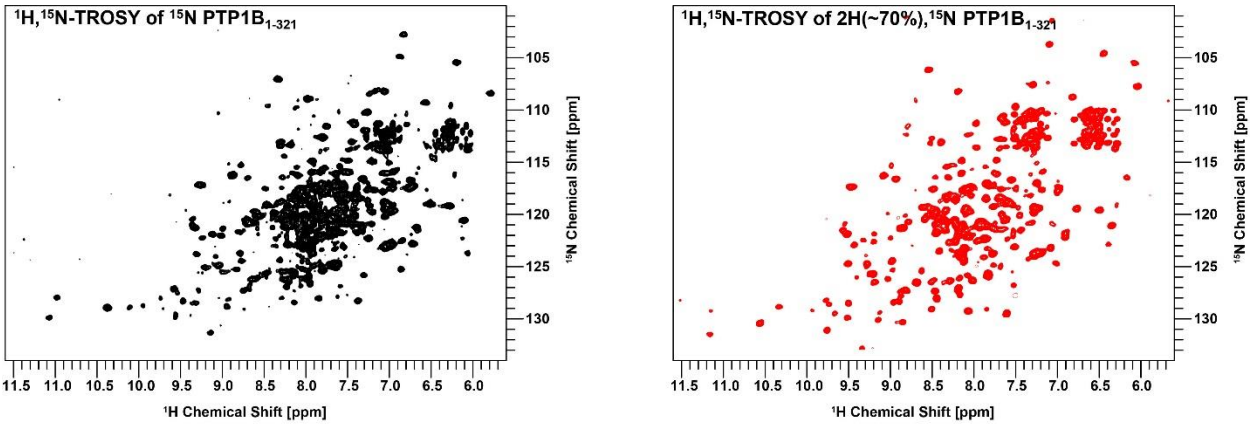

Figure 4.6 Comparison of the TROSY spectra of deuterated (red) and non-deuterated (black) PTP1B$_{1-321}$. ^{1}H,^{15}N TROSY of a 100 µM ^{15}N-PTP1B (black) and ^{15}N, ^{2}H(~70%)-PTP1B (red) sample in 25 mM Tris.HCl pH= 7.5, 75 mM NaCl, 0.5 mM EDTA, 5 mM DTT, 0.01% NaN_3 (~10% D_2O) recorded at 20 ºC (800 MHz).

Triple labeled PTP1B$_{1-298}$ was used for recording all necessary backbone assignment NMR spectra (^{15}N-TROSY, HNCACB, HNCA, HN(CO)CA, HNCO and HN(CA)CO) (Sattler, Schleucher, and Griesinger 1999). This construct was chosen for assignment because there were in the literature assignments of similar constructs that could be useful (BMRB ID: 5474) (Meier et al. 2002). With the help of an already known assignment of another construct (BMRB ID: 19223) by Tonks (Krishnan et al. 2014) 75% of the backbone amides (**Figure 4.7**) were successfully assigned. A ^{15}N-TROSY and a HNCACB were recorded as well at exactly the same conditions as those that Tonks used. Though the two spectra overlay better, there are still shifts all over the spectrum because the constructs are slightly different (Our construct includes residues 1-298, while Tonks construct includes residues: 1-303).

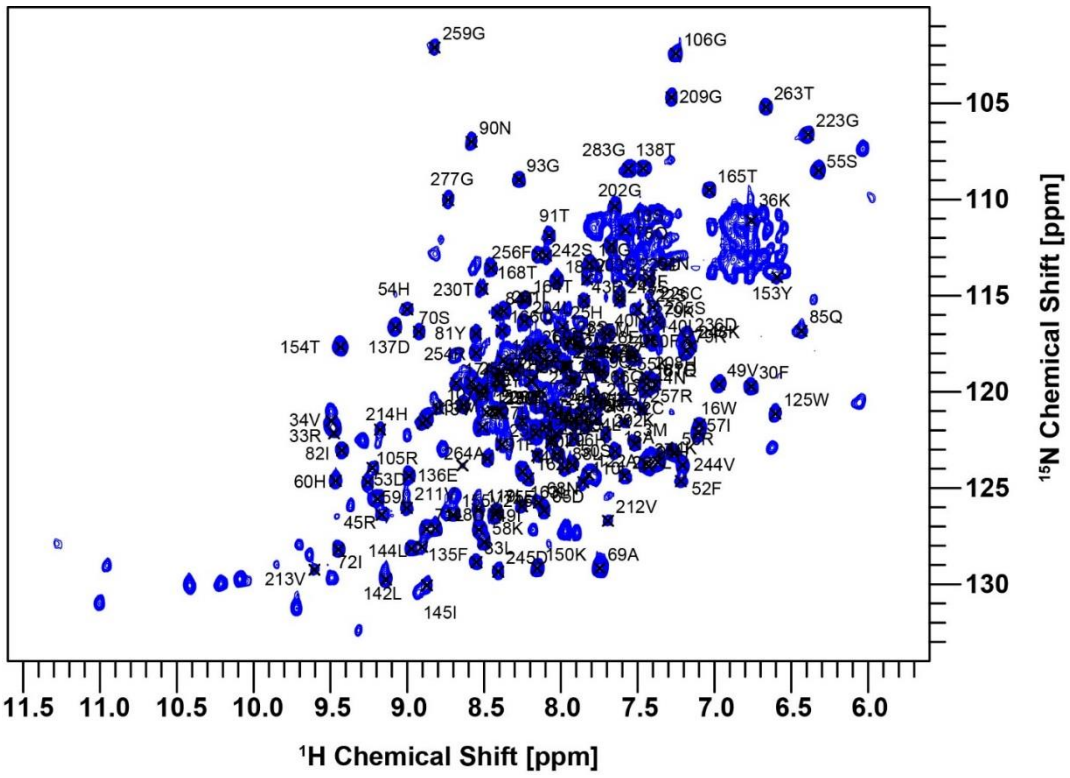

Figure 4.7 Assignment of the PTP1B$_{1-298}$ TROSY spectrum.

Assignment spectra for triple labeled TCPTP$_{1-296}$ were recorder as in case of PTP1B$_{1-298}$ (^{15}N-TROSY, HNCACB, HNCA, HN(CO)CA, HNCO, HN(CA)CO and HN(CO)CACB). These spectra are in the process of being analyzed.

Protein backbone assignments are necessary in order to be used for mapping the binding site of relevant compounds from our library.

4.3.3 Phosphatase activity assay

In the beginning, using the pNPP assay, the protein and substrate concentration conditions that should be used for the assay were optimized by determining the k_{cat} for each protein phosphatase construct. The buffer conditions were 25 mM Bis-Tris-Propane pH 7.5, 50 mM NaCl, 2.5 mM EDTA, 0.025% NP-40, 2 mM DTT. The lowest protein concentration at which the saturation curve is easily detectable was in all cases 30 nM. The kinetic constant K_m for pNPP, was estimated to be approximately 0.20 mM, 0.34 mM, 0.57 mM, 0.47 mM and 0.34 mM for PTP1B$_{1-298}$, PTP1B$_{1-321}$, PTP1B$_{1-393}$, TCPTP$_{1-296}$ and TCPTP$_{1-336}$ respectively (**Table 4.1**).

However, when the compound inhibition screening was performed, it was observed that the detergent NP-40, which is used to prevent compound aggregation and non-specific binding of

the protein to the well plate walls, affects the binding of the compounds to the protein by giving, in general, a higher IC_{50}. For this reason, the assay repeated without detergent in the buffer conditions. The kinetic constants were calculated again when there is no NP-40 in the buffer conditions, the K_m was found to be 0.38 mM, 0.30 mM, 0.49 mM, 0.41 mM, 0.36 mM for $PTP1B_{1-298}$, $PTP1B_{1-321}$, $PTP1B_{1-393}$, $TCPTP_{1-296}$ and $TCPTP_{1-336}$ respectively **Table 4.1**. In this case the protein concentration used was 80 nM, almost three times higher than the one used when detergent is present in the buffer conditions. A possible explanation for this effect could be that the enzyme is more active when NP-40 is present (Feng and Shoichet 2006). The k_{cat} values were calculated by running endpoint measurements and are shown in the **Table 4.2**. For $PTP1B_{1-321}$ the kinetic constant values were compared with the literature and it was found that they agree well with those of Peters and collaborators (Peters et al. 2003).

Table 4.1 K_m constant calculated for the different constructs.

Protein	K_m (mM) with NP-40	K_m (mM) without NP-40
$PTP1B_{1-298}$	0.20	0.38
$PTP1B_{1-321}$	0.34	0.30
$PTP1B_{1-393}$	0.57	0.49
$TCPTP_{1-296}$	0.47	0.41
$TCPTP_{1-336}$	0.34	0.36

Table 4.2 k_{cat} constant calculated for the different constructs.

Protein	k_{cat} (s^{-1}) with NP-40 (30 nM PTP1B/ 20nM TCPTP)	k_{cat} (s^{-1}) without NP-40 (80 nM PTP1B/ 60 nM TCPTP)
$PTP1B_{1-298}$	1.65	1.55
$PTP1B_{1-321}$	1.00	1.02
$PTP1B_{1-393}$	3.20	2.18
$TCPTP_{1-296}$	1.42	1.36
$TCPTP_{1-336}$	2.56	2.31

From the K_m reported in the **Table 4.1**, it was concluded that in case of PTP1B constructs, the bigger the protein is the worse the affinity for the substrate is, since the K_m increases for bigger constructs. In case of TCPTP, it was observed the opposite effect, the bigger the protein the better the affinity for the substrate, since the K_m decreases. The k_{cat} in **Table 4.2** show that both PTP1B and TCPTP longest constructs are more active than the shorter ones. From these results it is obvious that the C-terminal part of the protein plays a role in the activity of the protein.

Then the effect of the solvents, in which our compounds are dissolved, was investigated on the K_m (**Figure 4.78**). It was found out that 5% of each solvent doesn't cause any significant change to the K_m (**Table 4.3**).

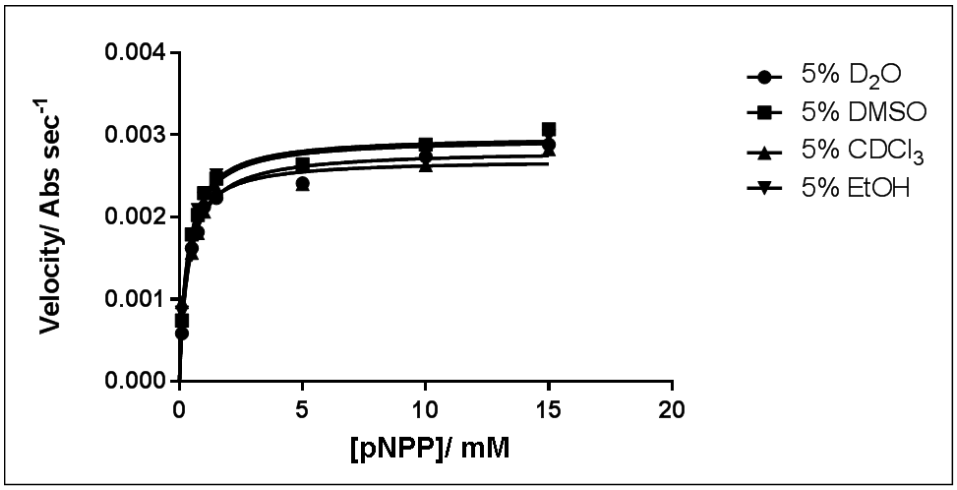

Figure 4.8 The effect of the organic solvent.

Table 4.3 Effect of 5% of organic solvent on the kinetic constants.

	5% D_2O	**5% DMSO**	**5% $CDCl_3$**	**5% EtOH**
k_{cat} **/1/s**	10.41	11.07	10.00	10.96
V_{max} **/Abs/s**	0.0028 ± 0.001	0.0030 ± 0.0002	0.0027 ± 0.0001	0.0030 ± 0.0001
K_m **/mM**	0.38 ± 0.03	0.33 ± 0.03	0.26 ± 0.04	0.34 ± 0.04

.

5. Results II: Novel scaffolds modulating potently PTP1B and TCPTP activity

5.1 Compound Library

Our in-house build compound library is composed of commercially available compounds that have been described in the literature as potential inhibitors of our target proteins or with anti-diabetic and anti-obesity properties. These compounds are mainly natural compounds found in the plants or in living organisms and they have been isolated from different extracts or synthesized chemically. Only three compounds from our library were synthesized and provided by our collaborator Dr. Jean-Michel Brunel from the Centre de Recherche en Cancérologie de Marseille (Trodusquemine, claramine and NV673). Our compounds were separated into three different classes : A. triterpenoids (10 compounds), B. Steroids (25 compounds) and C. Others (15 compounds) (**Figure 5.1**).

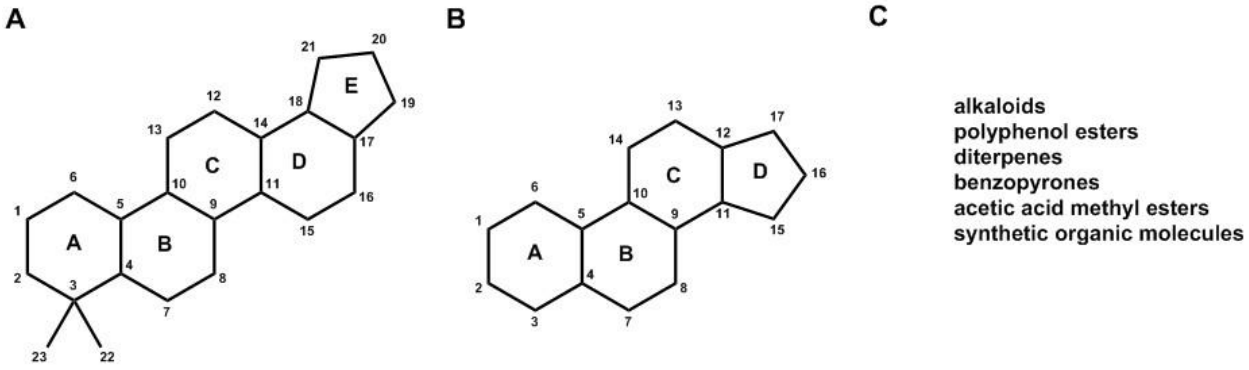

Figure 5.1 Compound scaffolds.

Almost all the compounds were tested for their ability to inhibit PTP1B and TCPTP by using the pNPP activity assay screening and ligand-based NMR screening experiments. The best and more interesting compounds, showing inhibition activity, were screened by the protein-based NMR screening in order to map their binding site into the protein structure by calculating the chemical shift perturbations (CSPs). The most promising compounds were furtherly tested in relevant cell line or mouse models. Compound squalamine could not be dissolved in any solvent and therefore it was not possible to be studied. Binding studies of compound celastrol will be described in a separate chapter with more details later.

5.1.1 Triterpenoids

Compounds 18β-glycyrrhetinic acid, 18α-glycyrrhetinic acid, ursolic acid, asiatic acid, oleanolic acid, madecassic acid, celastrol, gymnemagenin, ganoderic acid A and ganoderic acid B (**Figure 5.2**) are all triterpenoids.

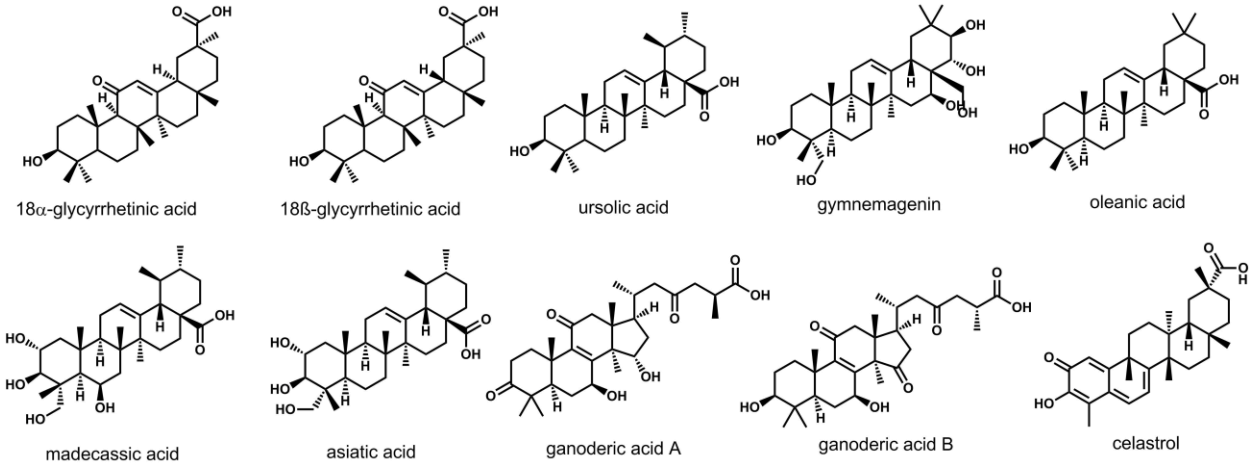

Figure 5.2 Triterpenoids compounds tested in this research.

18β-glycyrrhetinic acid, 18α-glycyrrhetinic acid, ursolic acid, gymnemagenin and PTP1B Inhibitor 539741 (Wiesmann et al. 2004), which is a known inhibitor of PTP1B protein (IC_{50}= 4-8μM) were tested by 1D ligand-based screening NMR. **Figure 5.3** shows 1D-^{1}H spectra of the five compounds in the absence (black) and in the presence of unlabeled PTP1B (red). PTP1B Inhibitor 539741 was used as a positive control. After the addition of small amount of protein 5μM (red) shifts and lower intensity peaks were observed in comparison with the spectrum of the free compound 100 μM (black), indicating binding. Lower intensity was clearly observed for compound 18β-glycyrrhetinic acid and for compounds gymnemagenin and ursolic acid, though the effect is very weak. On the other hand, compound 18α-glycyrrhetinic acid does not seem to be affected from the protein addition, indicating that it does not bind to the protein.

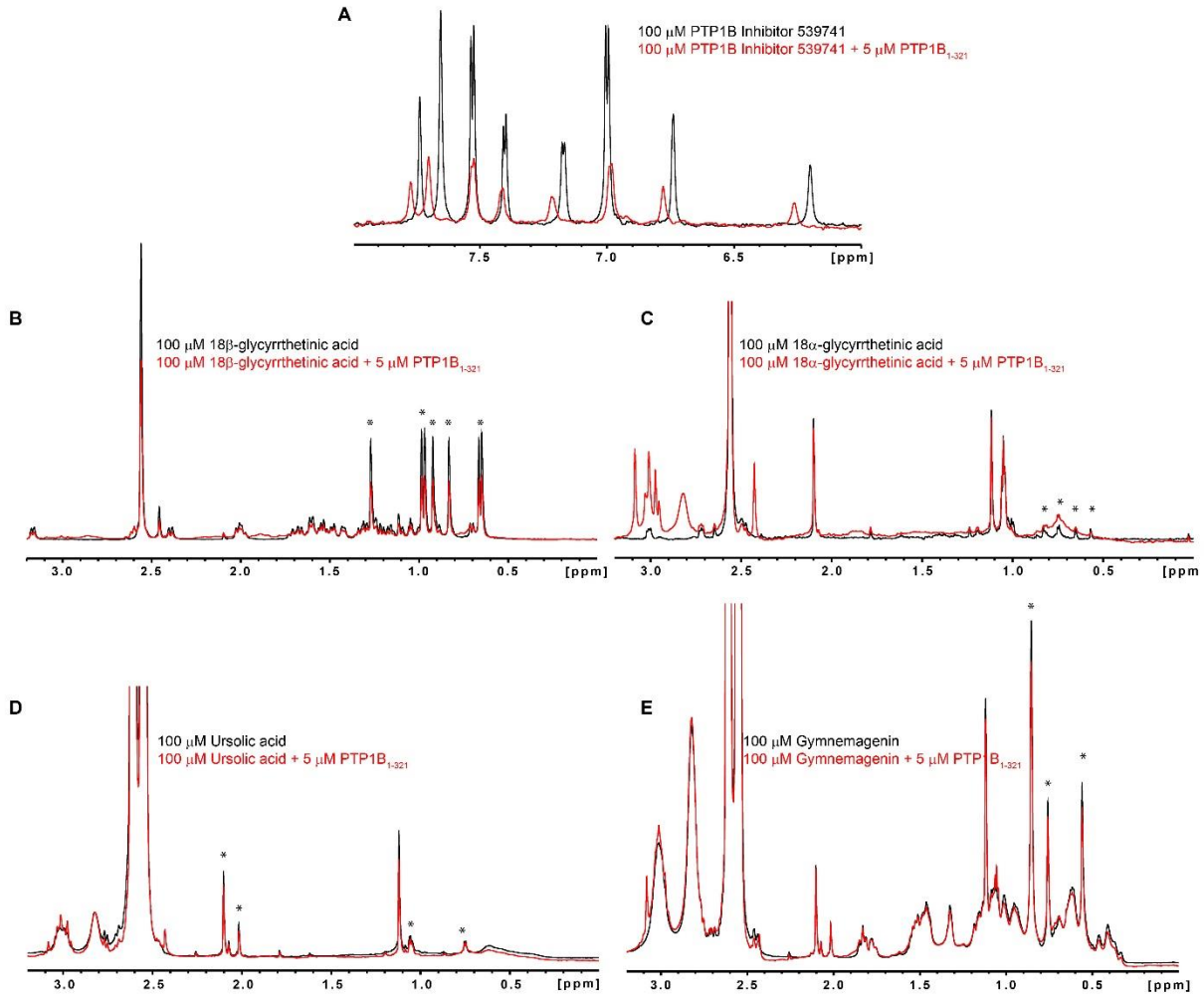

Figure 5.3 1D screening of triterpenoids.
1D screening of compounds **(A)** PTP1B inhibitor 539741, **(B)** 18β-glycyrrhetinic acid, **(C)** 18α-glycyrrhetinic acid, **(D)** ursolic acid and **(E)** gymnemagenin. On black color, it's shown the free compound spectrum and on red color, it's shown the spectrum of the compound after the addition of 5 μM $PTP1B_{1-321}$. Compound peaks are indicated with stars.

Seven out of nine compounds were next screened by STD NMR (**Table 5.1**). STD spectra showing peaks coming from the compounds, give an evidence of binding to the protein. PTP1B inhibitor 539741 was used as a positive control in that case as well (**Figure 5.4 A**). 18β-glycyrrhetinic acid (**Figure 5.4 B**) and gymnemagenin showed STD signals, confirming that they bind to the protein. STD signals are observed in case of asiatic acid, oleanolic acid and madecassic acid as well, indicating that they are binding to the protein. Only 18α-glycyrrthetinic (**Figure 5.4 C**) clearly does not show STD signals, confirming that it doesn't bind to the protein. For ursolic acid was not easy to answer if it binds to the protein due to precipitation that didn't allow us to run

a STD spectrum. Compound 18β-glycyrrhetinic acid was also tested with $TCPTP_{1-336}$ construct, giving STD signals (**Figure 5.4 D**).

Table 5.1 STD results from the triterpenoid compounds tested with this method.

Compound	STD signals with $PTP1B_{1-321}$	STD signals with $TCPTP_{1-336}$
18β-glycyrrhetinic acid	✓	✓
18α-glycyrrhetinic acid	x	not tested
gymnemagenin	✓	not tested
asiatic acid	✓	not tested
oleanolic acid	✓	not tested
madecassic acid	✓	not tested
ursolic acid	precipitated	not tested

✓: STDs signals
X: No STDs signals

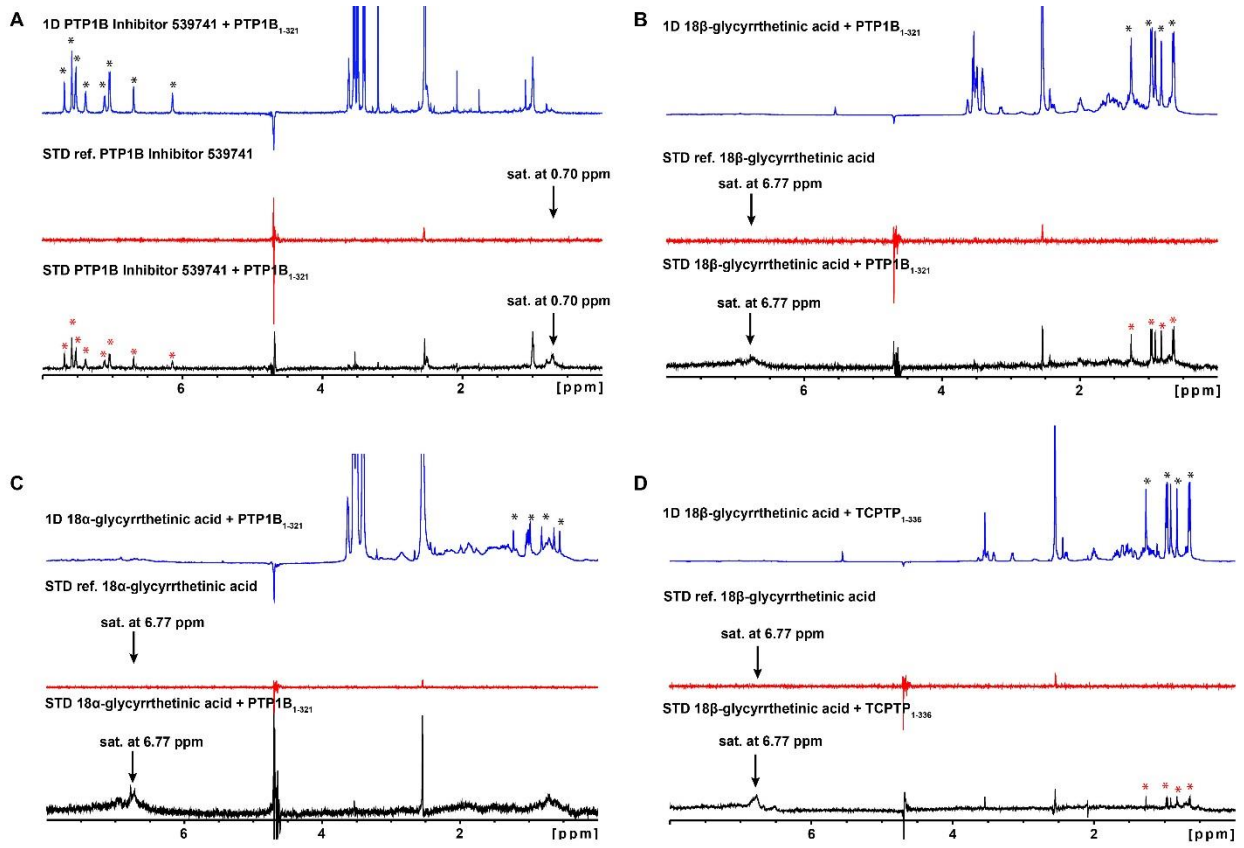

Figure 5.4 STD spectra of triterpenoids.
STD spectra of **(A)** PTP1B inhibitor 539741 (positive control)**, (B)** 18β-glycyrrhetinic acid with $PTP1B_{1-321}$, **(C)** 18α-glycyrrhetinic acid with $PTP1B_{1-321}$ and **(D)** 18β-glycyrrhetinic acid with $TCPTP_{1-336}$. Compound peaks are indicated with stars, red stars are indicating positive STD signals.

In order to further characterize our inhibitors, a secondary assay was used to confirm their inhibitory activity, that is, if they can inhibit phosphatase activity. For this purpose the pNPP phosphatase assay was used to measure inhibition of PTP1B and TCPTP constructs.

After optimization of the conditions for the assay, inhibitory activity tests could be run and the IC_{50} of our compounds can be determined keeping the substrate at K_m concentration (**Table 4.1** section 4.3.3). All compounds were tested in buffer conditions with and without NP-40 detergent. Results are shown in the **Table 5.2** and the graphs of the best compounds are shown in the **Figure 5.5**. PTP1B inhibitor 539741 was tested in order to be compared with the literature (Peters et al. 2003), as a control. Best inhibitory activity was found for compound ursolic acid that inhibits both PTP1Bs and TCPTPs constructs with similar inhibition values ($PTP1B_{1-393}$ 6.8 μM and $TCPTP_{1-336}$ 6.3 μM). It inhibits stronger the longer constructs in both cases. Second best inhibitory activity is shown by compound oleanolic acid that also inhibits both proteins but it is twelve times more selective for PTP1B ($PTP1B_{1-393}$ 12.8 μM and $TCPTP_{1-336}$ 86.3 μM). Asiatic acid is the next best inhibitor, which is interesting because it inhibits PTP1B, while it activates TCPTP ($PTP1B_{1-393}$ 128 μM and $TCPTP_{1-336}$ 8.5 μM). Then 18β-glycyrrhetinic acid is following, inhibiting only PTP1B with relatively high IC_{50} values ($PTP1B_{1-393}$ 255 μM). It is very interesting that its stereoisomer, 18α-glycyrrhetinic acid, doesn't inhibit PTP1B but only TCPTP ($TCPTP_{1-336}$ 158.2 μM) though they only differ in the stereochemistry of one proton, which is apparently enough to affect their selectivity towards the two phosphatases. Madecassic acid also inhibits only PTP1B constructs in high micromolar range ($PTP1B_{1-298}$ 262 μM and $PTP1B_{1-321}$ 238 μM). The compounds ganoderic acid A and ganoderic acid B do not show any inhibitory activity against the two proteins.

Table 5.2 Results from the activity assay for all triterpenoids against all protein constructs.

Protein / compound	$PTP1B_{1-298}$		$PTP1B_{1-321}$		$PTP1B_{1-393}$		$TCPTP_{1-296}$		$TCPTP_{1-336}$	
	w/ NP-40 (μM)	w/o NP-40 (μM)	w/ NP-40 (μM)	w/o NP-40 (μM)	w/ NP-40 (μM)	w/o NP-40 (μM)	w/ NP-40 (μM)	w/o NP-40 (μM)	w/ NP-40 (μM)	w/o NP-40 (μM)
PTP1B inhibitor 539741	39	26.5	46.9	15.4	50.7	16.3	216.6	141.4	164.6	73.13
18β-glycyrrhetinic acid	148	127	161	200.3	255	Amb	-	Amb	-	Amb
18α-glycyrrhetinic acid	-	-	-	-	-	-	-	125.8	-	158.2
Madecassic acid	259	262	4400	238	-	-	-	-	-	-
Gymnemagin	-	-	-	234						
Oleanolic acid	Amb	18.7	120	7.8	-	12.8	-	24.2	-	86.3
Asiatic acid	Amb	133	-	135.8	-	128	Amb up	11.3 (act)	Amb	9.5 (act)
Ursolic acid	Amb	14.9	Amb	7.6	Amb	6.8	-	20.9	-	6.3
Ganoderic acid A	-	-	-	-						
Ganoderic acid B	-	-	-	-						

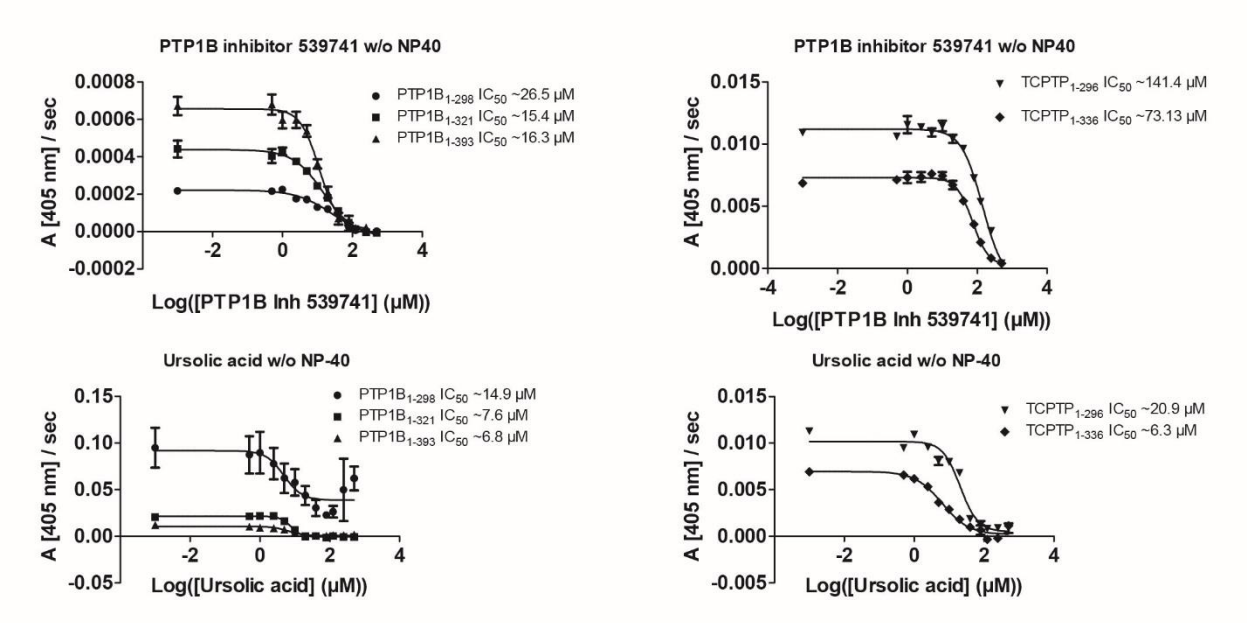

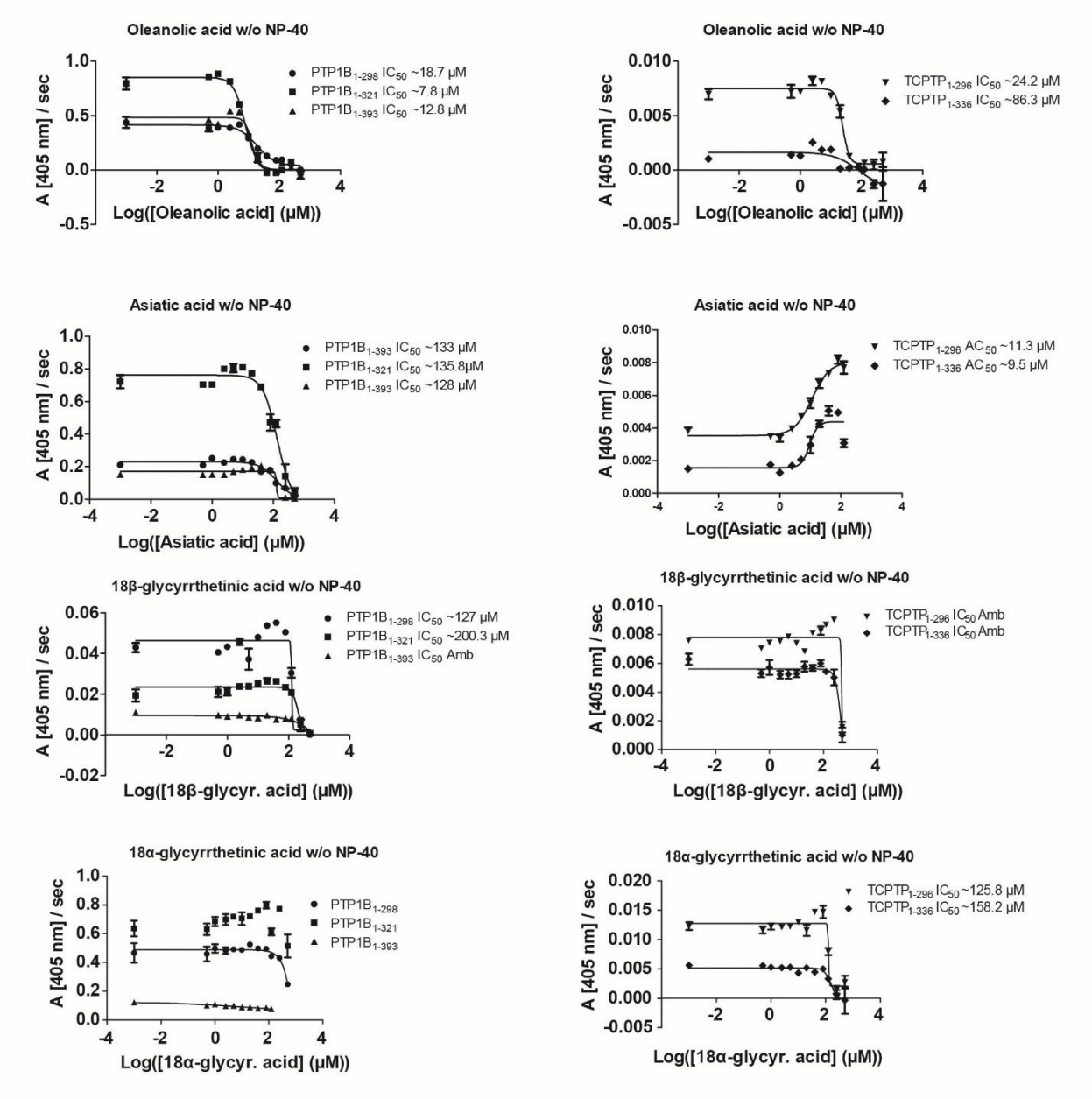

Figure 5.5 Activity assay results of the best triterpenoid compounds.

Our results indicate that the less decorated compound, which is ursolic acid, is the one that inhibits the protein in a low micromolar range. Furtherly, the hydroxyl group at C2 position, an alkyl substitution of C18 in R conformation and a carboxyl or an ether group substitution at C17 position in S conformation are important for the activity in case of triterpenes **Figure 5.6**.

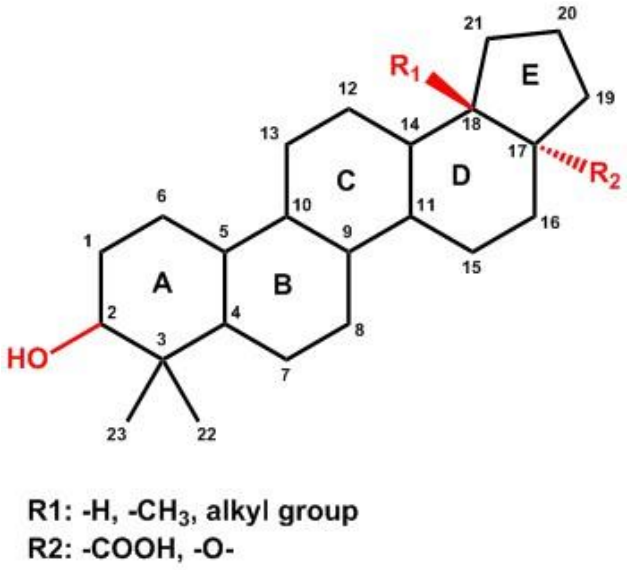

Figure 5.6 Important groups in the triterpenoid structure for the binding to the protein.

Compound 18β-glycyrrhetinic acid was then tested with the protein-based screening in order to follow the chemical shift perturbations upon binding and map the binding site in the PTP1B structure. It's clear that there are shifts and also many peaks disappear, while some other peaks appear. Unfortunately, there are peaks that are affected and are not assigned yet (**Figure 5.7**).

CSPs were calculated and the residues that are involved in the binding were identified. As it is already mentioned, there are many peaks that disappear, from those only Val212, Cys226, Leu234, Met258 are assigned. There are peaks that shift from which eleven are assigned, Glu2, Glu7, Ser28, Phe30, Arg45, Gln85, Asp229, Leu233, Arg268, Gly277 and Ser286 (**Figure 5.8 A**). In **Figure 5.8 B**, the residues that were perturbed upon the compound addition, are mapped on the crystal structure of PTP1B (1WAX), the binding site of 18β-glycyrrhetinic acid is not close to the active site, indicating that it's an allosteric inhibitor.

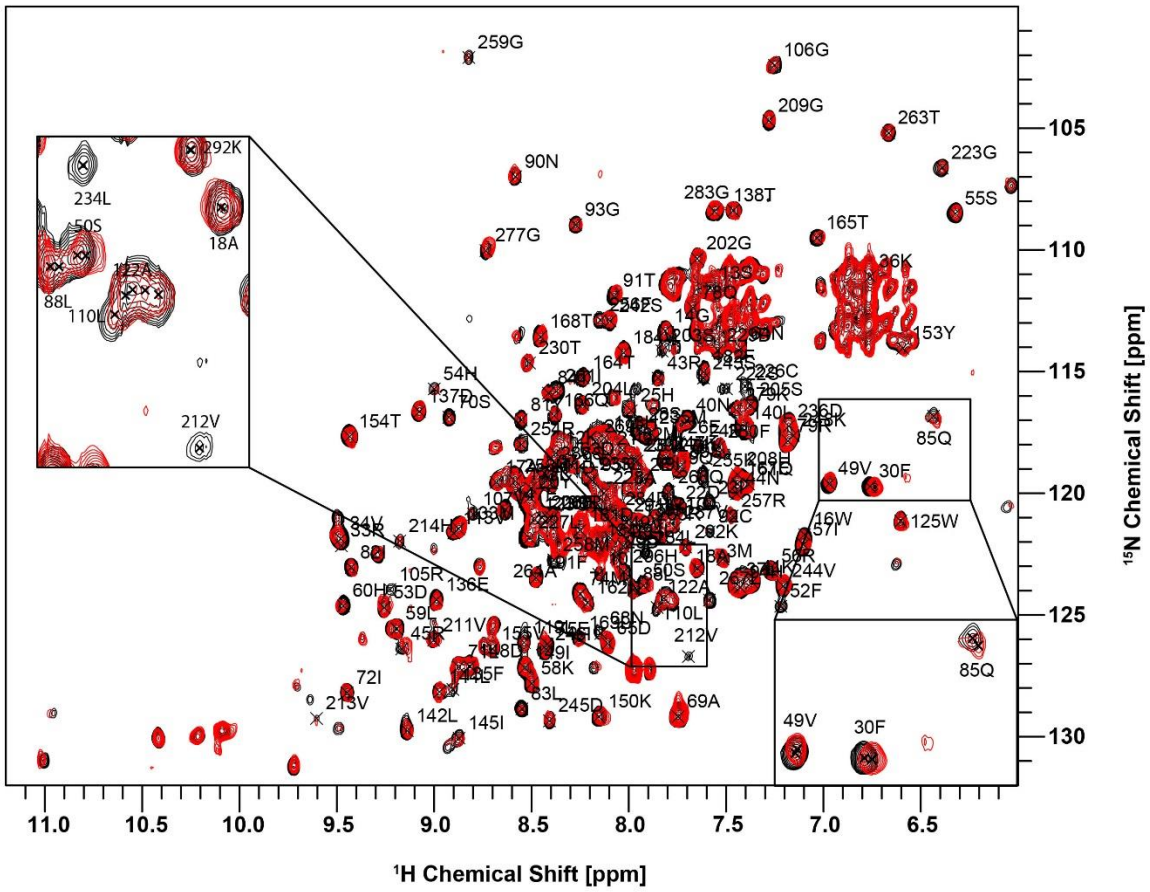

Figure 5.7 Superposition of 2D $^{1}H,^{15}N$ correlation spectra of 100 µM PTP1B$_{1-298}$ recorded without (black) and with 500 µM 18β-glycyrrhetinic acid (red) (800 MHz, 20 ºC, 16 scans).

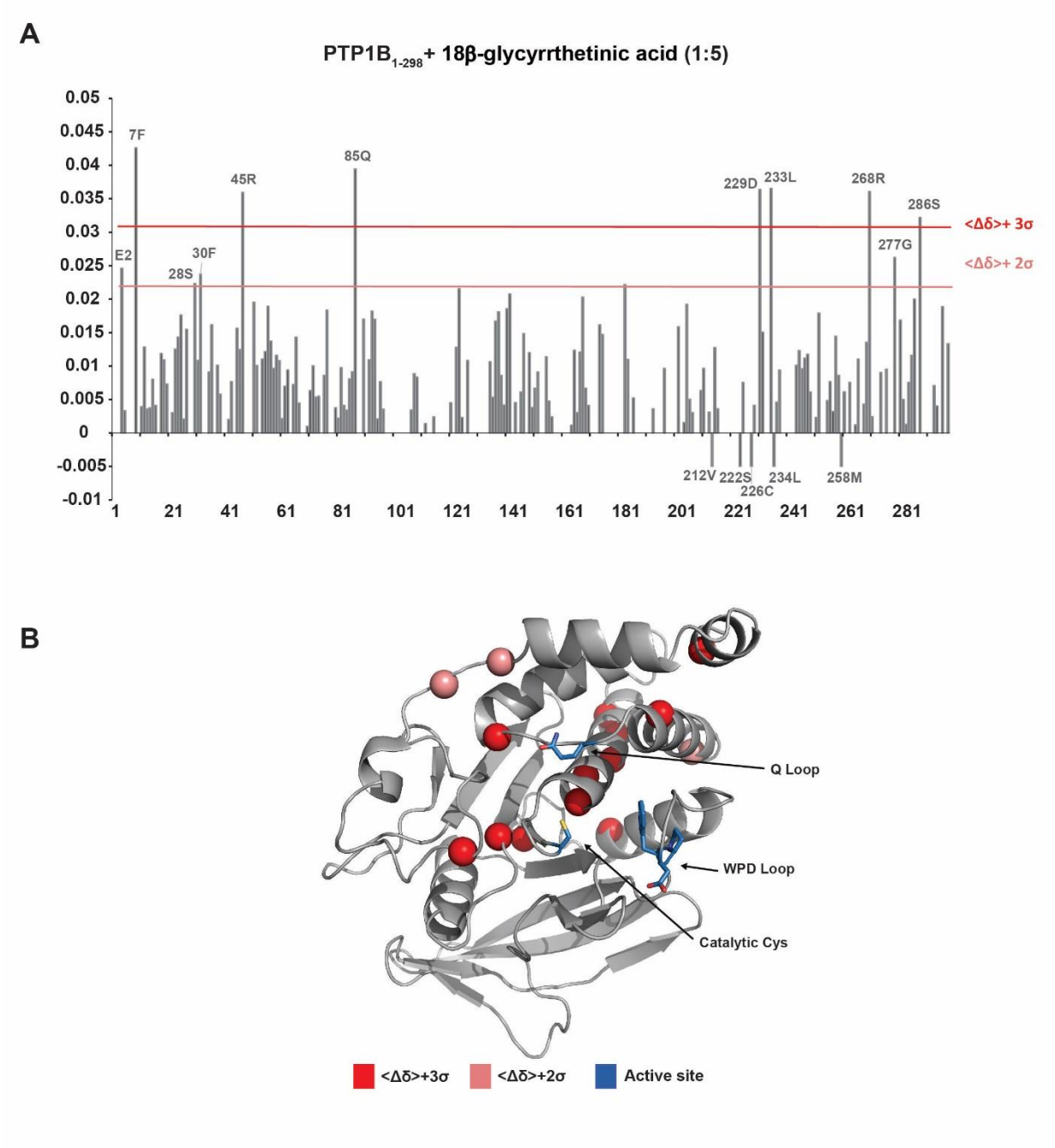

Figure 5.8 Chemical shift perturbations of compound 18β-glycyrrhetinic acid.
(A) Chemical shift perturbations (CSP, Δδ) observed upon 18β-glycyrrhetinic acid binding to $PTP1B_{1-298}$. Colored lines indicate 2 and 3 σ standard deviation from the mean <Δδ>. **(B)** Mapping of the spectral changes upon titration of 18β-glycyrrhetinic acid onto the structure of PTP1B (1WAX). NMR signals of amide groups in $PTP1B_{1-298}$ that experience CSPs above 2 and 3 standard deviations (SDs) from the mean <Δδ> are represented as spheres and colored salmon and red, respectively. Standard deviation 3 σ includes also the residues that undergo severe line broadening.

5.1.2 Steroids, Sterols and Secosteroids

This group is consisted of the compounds hydrocortisone (cortisol), cortisone, testosterone, β-estradiol, β-estradiol 3-sulfate sodium salt, aldosterone, cholesterol, cholesterol sulfate, dehydroisoandrosterone crystalline, dehydroepiandrosterone sulfate, pregnenolone, pregnenolone sulfate sodium salt, squalamine, trodusquemine, claramine (SIXB), NV673, diosgenin, stigmasterol, fucosterol, cycloastragenol, IPI-926, cyclopamin, vitamin D2, vitamin D3 and whithaferin A (**Figure 5.9**).

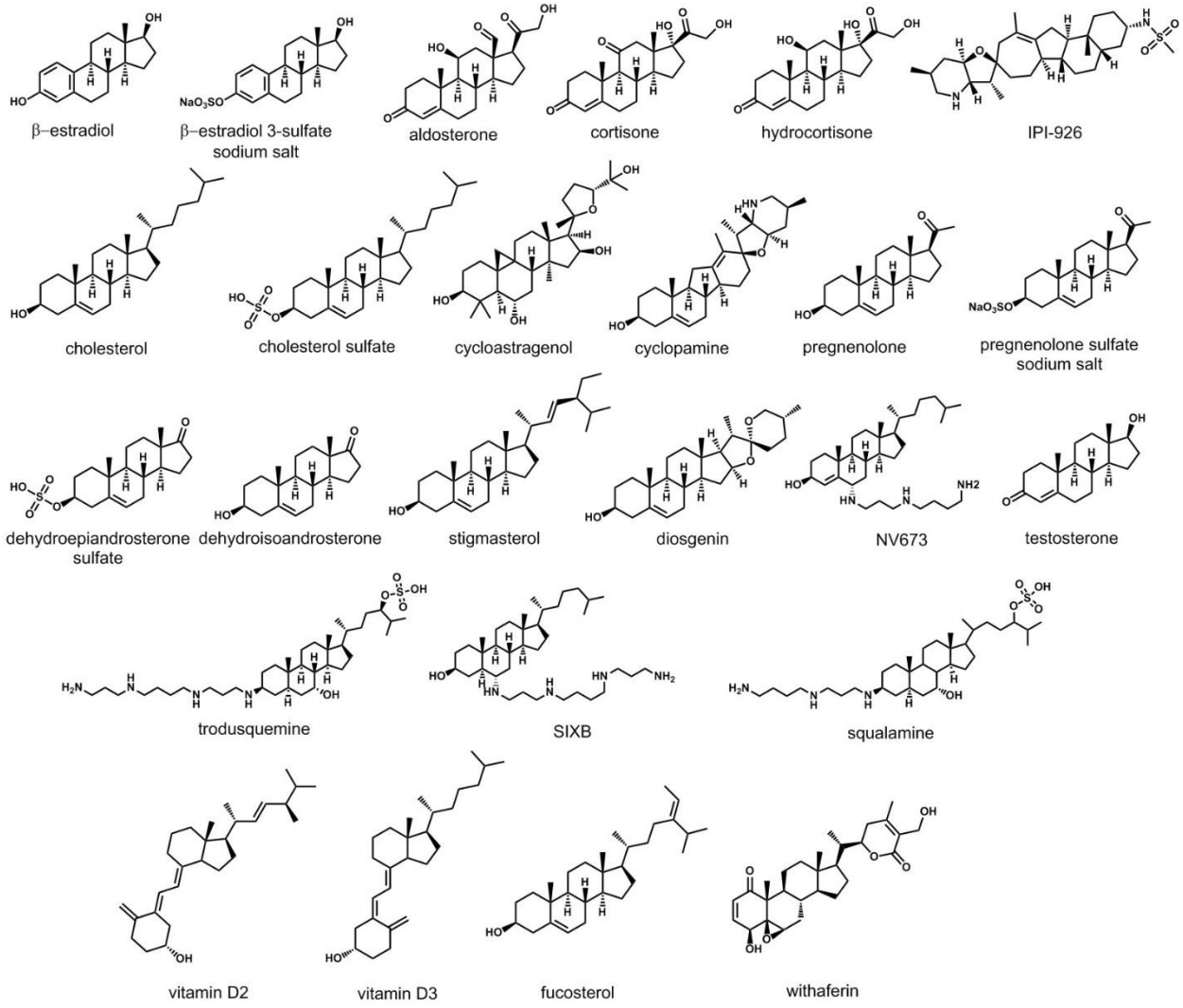

Figure 5.9 Structure of steroid compounds used in this research.

Trodusquemine, SIXB, NV673, diosgenin and stigmasterol were tested by 1D ligand-based screening NMR. In **Figure 5.10** are shown the 1D-^{1}H spectra of the three first compounds in the absence (black) and in the presence of unlabeled PTP1B (red). After the addition of small amount

of protein 5μM (red) shifts and lower intensity peaks were observed in comparison with the spectrum of the free compound 100 μM (black), indicating binding for compounds trodusquemine and its derivatives. Diosgenin and stigmasterol are not well solubilized in the NMR buffer, thus is not easy to define if they interact with the protein.

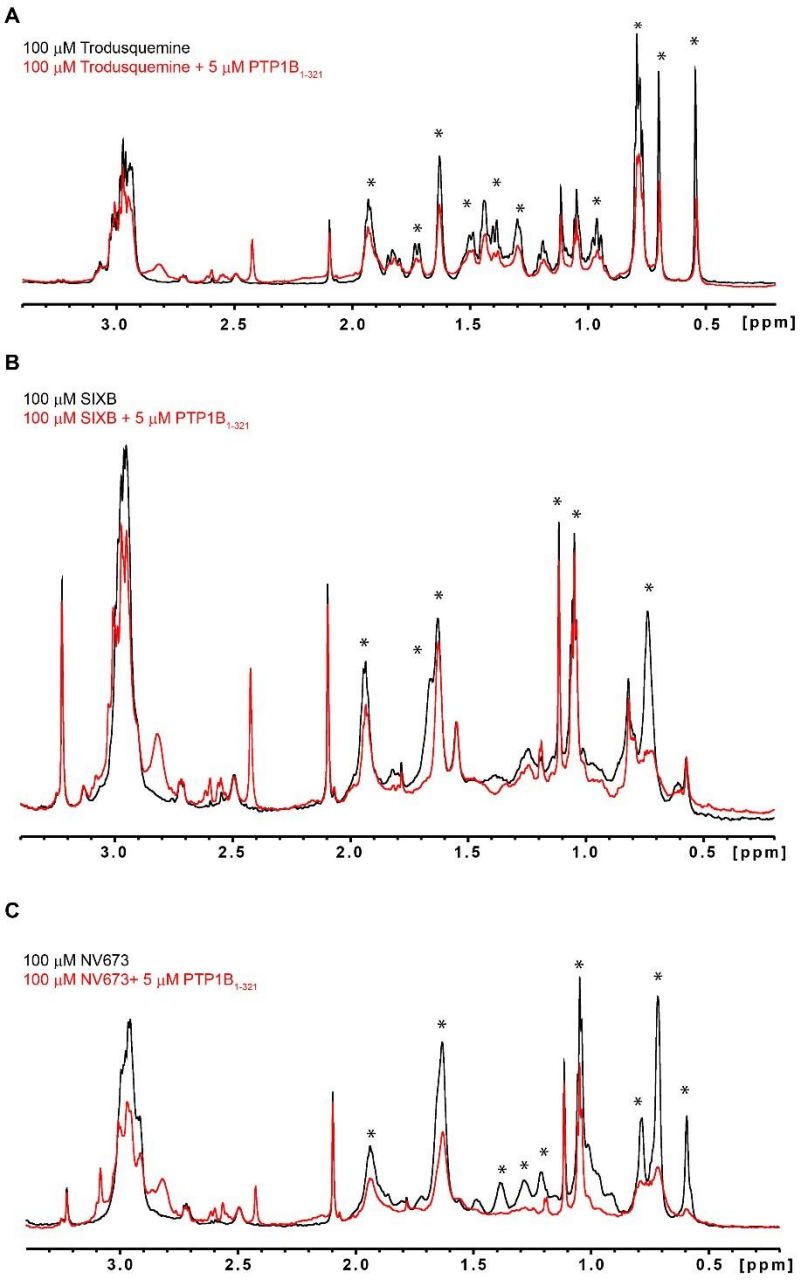

Figure 5.10 1D screening of sterols.
1D screening of compounds **(A)** Trodusquemine, **(B)** SIXB and **(C)** NV673. On black color, it's shown the free compound spectrum and on red color, it's shown the spectrum of the compound after the addition of 5 μM $PTP1B_{1-321}$. Compound peaks are indicated with stars.

The ability of 19 out of 25 compounds to bind to the $PTP1B_{1-298}$ and two compounds to bind to $TCPTP_{1-336}$ was further tested by STD NMR experiments (**Table 5.3**). Hydrocortisone, cortisone, dehydroepiandrosterone sulfate, β-estradiol 3-sulfate, pregnenolone sulfate, cholesterol sulfate, cycloastragenol, trodusquemine and claramine gave STD signals, indicating binding to the PTP1B protein. Examples are given in the **Figure 5.11**. Compounds pregnenolone, β-estradiol, cholesterol, dehydroisoandrosterone, diosgenin, stigmasterol and fucosterol showed precipitation issues making difficult to determine if they bind to the protein. In principle, since their sulfate analogues, which are better soluble under the NMR buffer conditions, show binding to the protein, one would expect that the non-sulfate compounds should bind to the protein too. Aldosterone, testosterone and NV673 should be repeated since the experiment was not properly set up. Compounds withaferin A, cyclopamine, IPI-926, vitamin D2 and vitamin D3 were not tested with this method. Compounds trodusquemine and claramine give no STD signals when they were tested with TCPTP construct, indicating that they don't bind to the protein, showing a selectivity towards PTP1B (**Figure 5.11**).

Table 5.3 Results of the STD experiment for the steroid compounds.

Compound	STD signals with $PTP1B_{1-321}$	STD signals with $TCPTP_{1-336}$
Hydrocortisone	✓	not tested
Cortisone	✓	not tested
Testosterone	Must be repeated	not tested
β-estradiol	Precipitated	not tested
β-estradiol 3-sulfate	✓	not tested
Cholesterol	Precipitated	not tested
Cholesterol sulfate	✓	not tested
Aldosterone	Must be repeated	not tested
dehydroisoandrosterone crystalline	Precipitated	not tested
dehydroepiandrosterone sulfate	✓	not tested
pregnenolone	Precipitated	not tested
pregnenolone sulfate	✓	not tested
Trodusquemine	✓	x
SIXB	✓	x
NV673	Must be repeated	not tested
Diosgenin	Precipitated	not tested
fucosterol	Precipitated	not tested
stigmasterol	Precipitated	not tested
cycloastragenol	✓	not tested

✓: STDs signals
X: No STDs signals

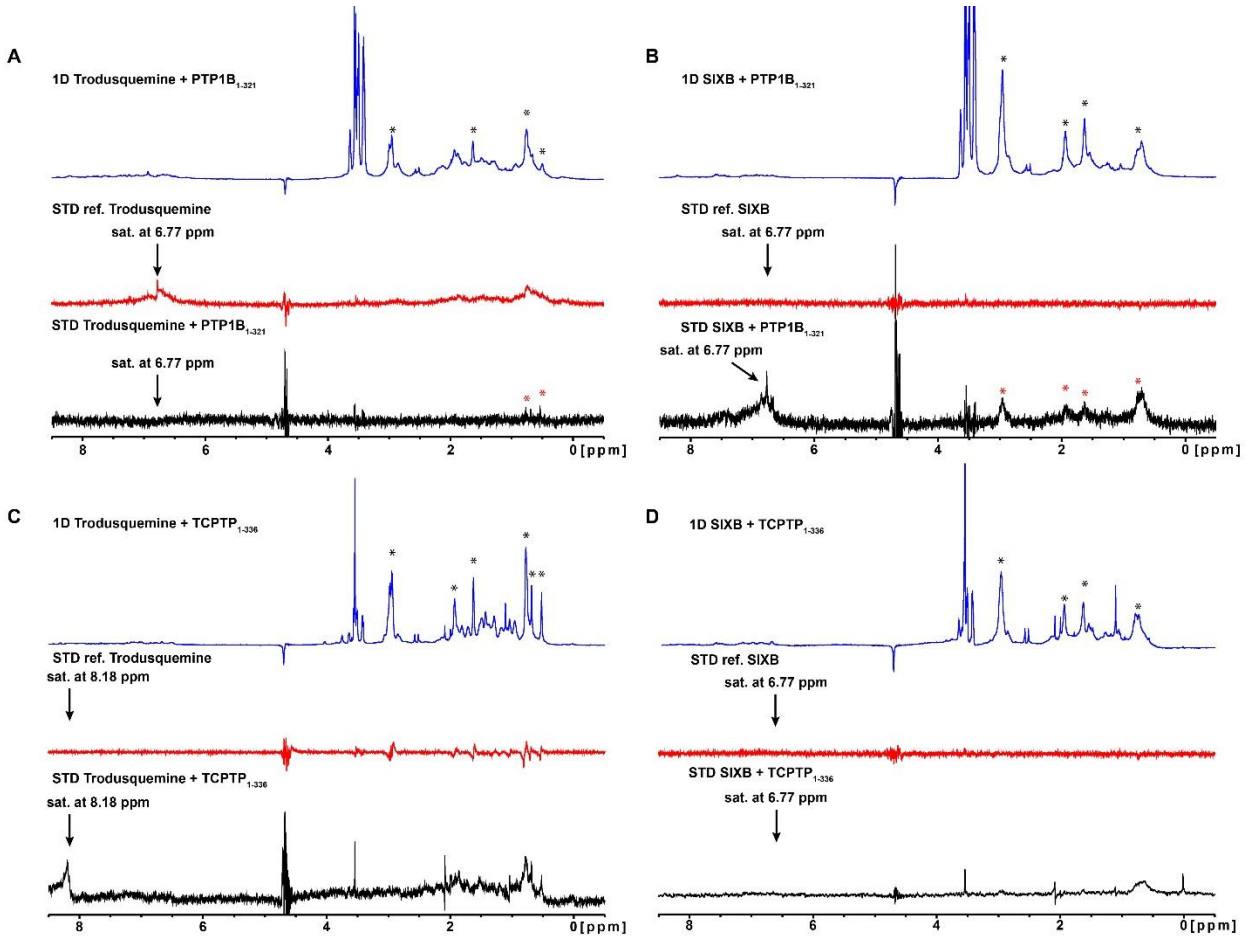

Figure 5.11 STD spectra of sterols.
STD spectra of **(A)** Trodusquemine and **(B)** SIXB with PTP1B$_{1-321}$**, (C)** Trodusquemine and **(D)** SIXB with TCPTP$_{1-336}$. Compound peaks are indicated with stars, red stars are indicating positive STD signals.

The inhibitory ability of the compounds was tested using the pNPP activity assay. As before, all compounds were tested in buffer conditions with and without NP-40 detergent. Results are shown in the **Table 5.4** and the graphs of the best and most interesting compounds are shown in **Figure 5.12**. Here it can be seen that the best inhibitor of this group of compounds is cholesterol sulfate that inhibits in low micromolar range both phosphatases (PTP1B$_{1-298}$ 8.6 µM, PTP1B$_{1-321}$ 0.52 µM, PTP1B$_{1-393}$ 1.6 µM and TCPTP$_{1-296}$ 2.3 µM, TCPTP$_{1-336}$ 1.3 µM). Again, the longer constructs are inhibited strongly, showing that in that case the C-terminal of the proteins plays an important role in the activity of the protein. However, the IC$_{50}$ value does not differ significantly between the two proteins, indicating that the compound is not selective towards the two proteins. It is interesting that the non-sulfated cholesterol does not inhibit the phosphatases but seems to activate them. PTP1B$_{1-298}$ construct is activated by cholesterol with an AC$_{50}$ of 6.8 µM and

$PTP1B_{1-321}$ construct with an AC_{50} of 4.3 μM, while for both TCPTP constructs shows an activation trend. One explanation can be the solubility issues that cholesterol addressed in previous experiments too. The second best inhibitory compound is SIXB. It inhibits both PTP1B ($PTP1B_{1-298}$ 9.5 μM, $PTP1B_{1-321}$ 3.7 μM, $PTP1B_{1-393}$ 20 μM) and TCPTP ($TCPTP_{1-296}$ 16.1 μM, $TCPTP_{1-336}$ 22.3 μM), but only PTP1B in very low micromolar range, revealing that is approximately two to seven times more selective for PTP1B. The third best inhibitory ligand is trodusquemine. Trodusquemine is the parent compound of SIXB and its inhibitory ability was tested only against PTP1B constructs. It inhibits better the longer constructs ($PTP1B_{1-298}$ 130.3 μM, $PTP1B_{1-321}$ 3 μM, $PTP1B_{1-393}$ 2.1 μM), confirming that the binding site is in the C-terminal part of the compound as Tonks claims in his paper (Krishnan et al. 2014). However, clearly our data show binding of trodusquemine to the shorter construct as well, this observation contrast Tonks findings. The fourth best compound is diosgenin, inhibiting PTP1B constructs more strongly than TCPTPs. It has an IC_{50} of 11.5 μM for the $PTP1B_{1-321}$ construct in comparison to 95 μM and 112 μM for $PTP1B_{1-298}$ and $PTP1B_{1-393}$ respectively, indicating that most probably the compound interacts with the residues 299-321 and that the C-terminal part of the $PTP1B_{1-393}$ construct affects those residues increasing the IC_{50} value of the compound. Pregnenolone also inhibits both PTP1B and TCPTP with 7 and 3-fold stronger, respectively, for the longer constructs. The IC_{50} values towards the two proteins are similar ($PTP1B_{1-321}$ 220 μM, $PTP1B_{1-393}$ 30.3 μM and $TCPTP_{1-296}$ 195 μM, $TCPTP_{1-336}$ 57.5 μM), indicating that the compound is not selective between the two proteins. Very interesting is the case of the vitamin D2 and vitamin D3. Both vitamins inhibit PTP1B, while activate TCPTP protein. The remaining compounds either inhibit the two proteins in high micromolar to low milimolar range or they don't show any inhibitory effect.

Table 5.4 Results from the activity assay for all steroids against protein constructs.

Protein / compound	$PTP1B_{1-298}$		$PTP1B_{1-321}$		$PTP1B_{1-393}$		$TCPT_{1-296}$		$TCPT_{1-336}$	
	w/ NP-40 (μM)	w/o NP-40 (μM)	w/ NP-40 (μM)	w/o NP-40 (μM)	w/ NP-40 (μM)	w/o NP-40 (μM)	w/ NP-40 (μM)	w/o NP-40 (μM)	w/ NP-40 (μM)	w/o NP-40 (μM)
Hydrocortisone			Amb	Amb	Amb	4131	72.3 (act)	Amb	Amb	Amb
Cortisone			Amb	164.4	-	154.5	25.1	31.6 (act)	Amb	Amb
Testosterone			Amb	Amb						
β-estradiol			Amb	64.4	Amb	Amb	Amb	226.3	Amb	-
β-estradiol 3-sulfate	194.8	622.1	Amb	Amb	Amb	131.1	Amb	109	Amb	906.8
Cholesterol		6.8 (act)	191 (act)	4.3 (act)	Amb	Amb (act)	up	Amb up	Amb up	Amb (act)
Cholesterol sulfate	20.4	8.6	51.9	0.52	105.9	1.6	277.1	2.3	200	1.3
Aldosterone			-	-						
dehydroisoandrosterone crystalline			Amb	Amb						
dehydroepiandrosterone sulfate			Amb	Amb						
pregnenolone	Amb	Amb	Amb	220	Amb	30.3	Amb	195	Amb	57.5
pregnenolone sulfate	Amb	15000	Amb	133.4	388.2	Amb	Amb (act)	Amb (act)	-	Amb (act)
Trodusquemine	131.4	130.3	81.6	3	Amb	2.1	-	-	-	-
SIXB	25.5	9.5	11.7	3.7	166.2	20	16.1	Amb	-	22.3
Diosgenin	Amb	95.4	201.6	11.6	Amb	115	Amb	322.5	Amb	Amb
Stigmasterol	-	-	-	-						
Vitamin D2			Amb	118	-	186.9	3.9	4.4 (act)	-	6 (act)
Vitamin D3			-	-	-	160.8	-	11 (act)	-	7.7 (act)
Withaferin A					Amb	Amb			Amb	Amb

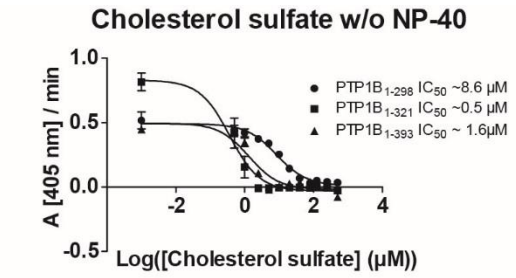
Cholesterol sulfate w/o NP-40
A [405 nm] / min
Log([Cholesterol sulfate] (μM))
PTP1B1-298 IC50 ~8.6 μM
PTP1B1-321 IC50 ~0.5 μM
PTP1B1-393 IC50 ~ 1.6μM

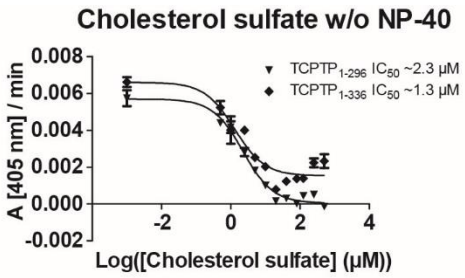
Cholesterol sulfate w/o NP-40
A [405 nm] / min
Log([Cholesterol sulfate] (μM))
TCPTP1-296 IC50 ~2.3 μM
TCPTP1-336 IC50 ~1.3 μM

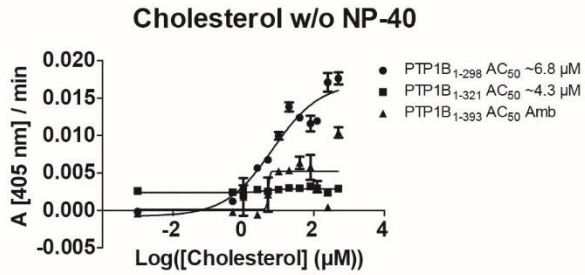
Cholesterol w/o NP-40
A [405 nm] / min
Log([Cholesterol] (μM))
PTP1B1-298 AC50 ~6.8 μM
PTP1B1-321 AC50 ~4.3 μM
PTP1B1-393 AC50 Amb

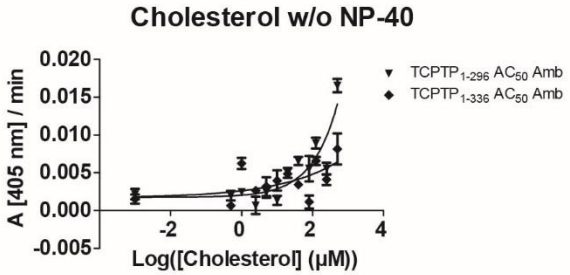
Cholesterol w/o NP-40
A [405 nm] / min
Log([Cholesterol] (μM))
TCPTP1-296 AC50 Amb
TCPTP1-336 AC50 Amb

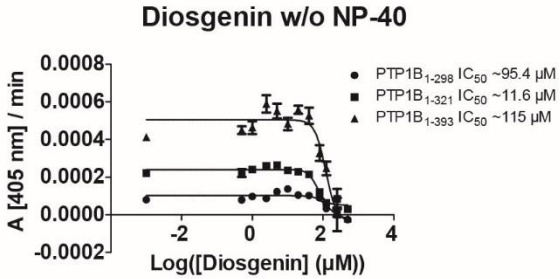
Diosgenin w/o NP-40
A [405 nm] / min
Log([Diosgenin] (μM))
PTP1B1-298 IC50 ~95.4 μM
PTP1B1-321 IC50 ~11.6 μM
PTP1B1-393 IC50 ~115 μM

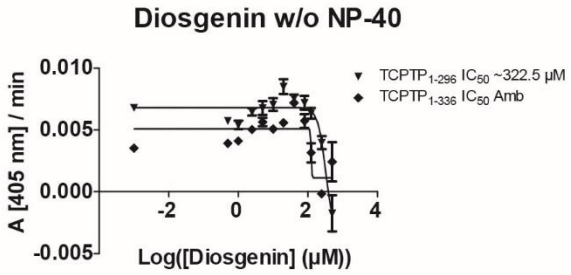
Diosgenin w/o NP-40
A [405 nm] / min
Log([Diosgenin] (μM))
TCPTP1-296 IC50 ~322.5 μM
TCPTP1-336 IC50 Amb

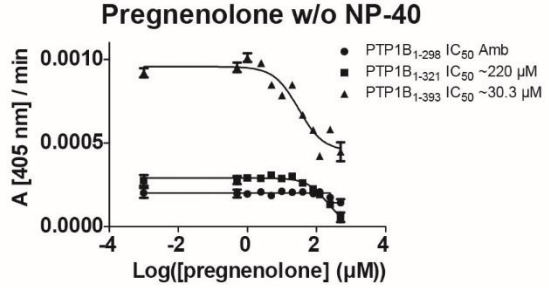
Pregnenolone w/o NP-40
A [405 nm] / min
Log([pregnenolone] (μM))
PTP1B1-298 IC50 Amb
PTP1B1-321 IC50 ~220 μM
PTP1B1-393 IC50 ~30.3 μM

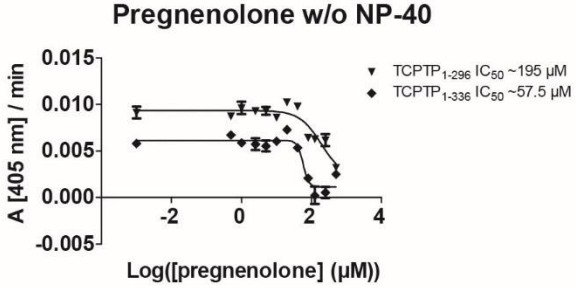
Pregnenolone w/o NP-40
A [405 nm] / min
Log([pregnenolone] (μM))
TCPTP1-296 IC50 ~195 μM
TCPTP1-336 IC50 ~57.5 μM

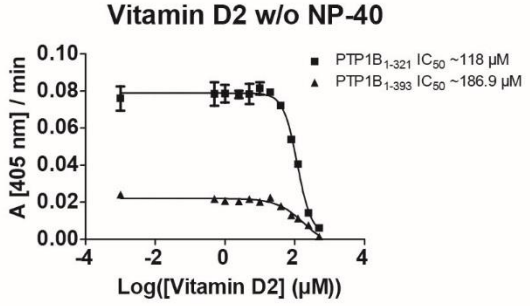
Vitamin D2 w/o NP-40
A [405 nm] / min
Log([Vitamin D2] (μM))
PTP1B1-321 IC50 ~118 μM
PTP1B1-393 IC50 ~186.9 μM

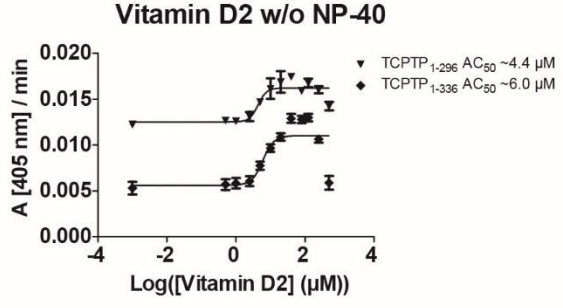
Vitamin D2 w/o NP-40
A [405 nm] / min
Log([Vitamin D2] (μM))
TCPTP1-296 AC50 ~4.4 μM
TCPTP1-336 AC50 ~6.0 μM

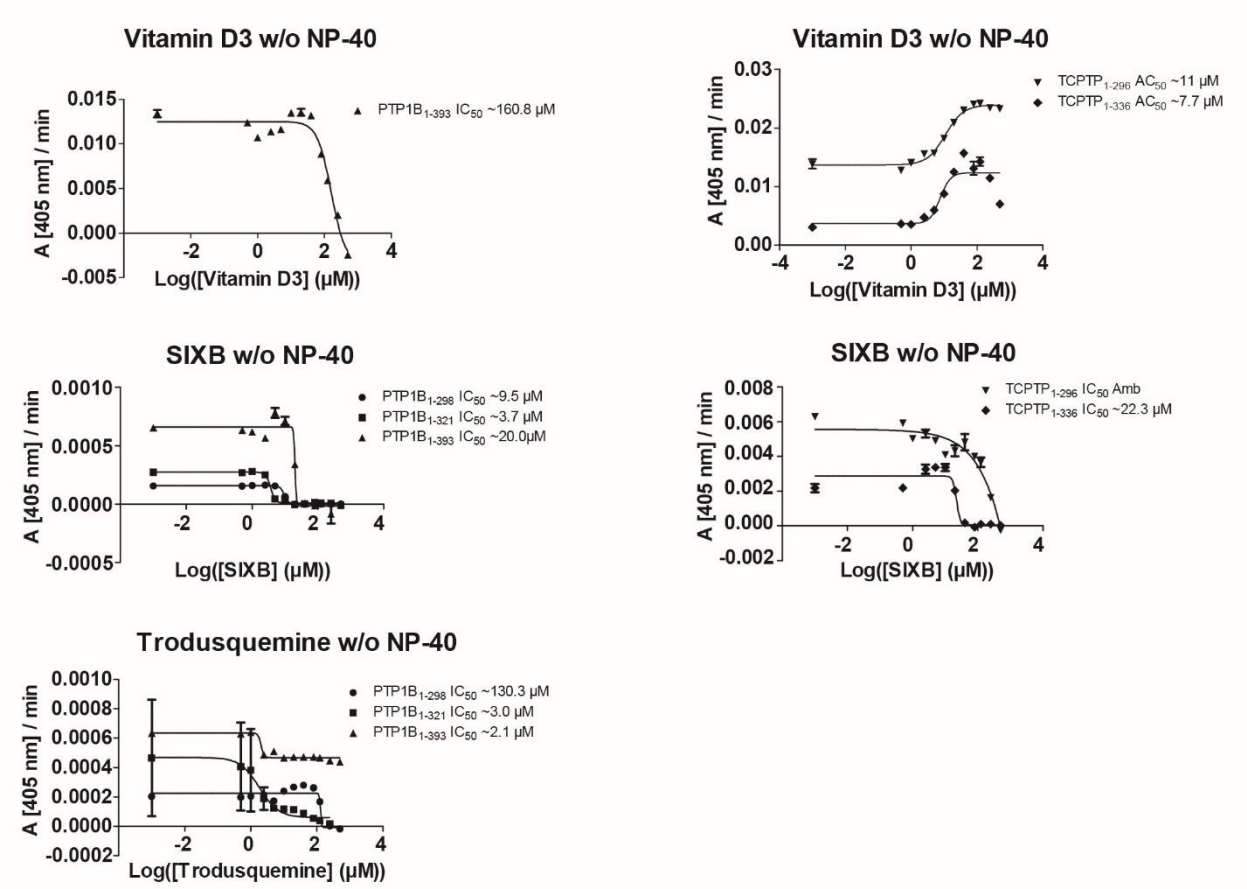

Figure 5.12 Activity assay results of the best steroid compounds.

Briefly, in case of steroids important groups are a hydroxyl group at C2 position, a methyl group substitution at C12 in R conformation and a hydroxyl or a ketone or an alkyl substitution at C17 position in S conformation **Figure 5.13**.

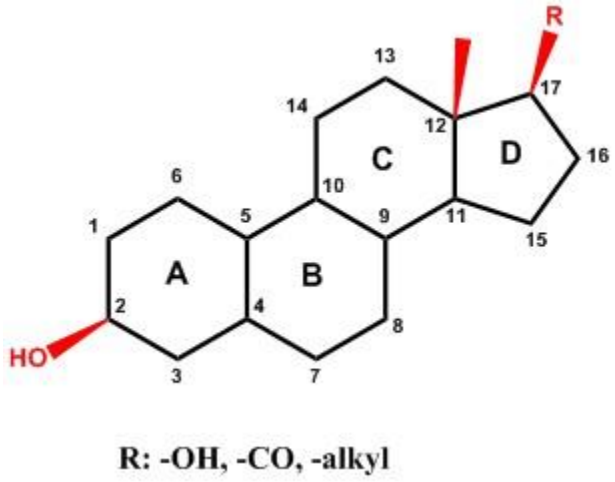

Figure 5.13 Important groups in the steroids structure for the binding to the protein.

Compounds trodusquemine and cholesterol sulfate were also tested with the protein-based screening in order to map the binding site into the PTP1B 3D structure. Titration NMR spectra of each compound are shown in **Figure 5.14** and **Figure 5.15** respectively. In both cases there are shifts and many peaks disappear, while others appear. Effects in the tryptophan side chain region are also seen.

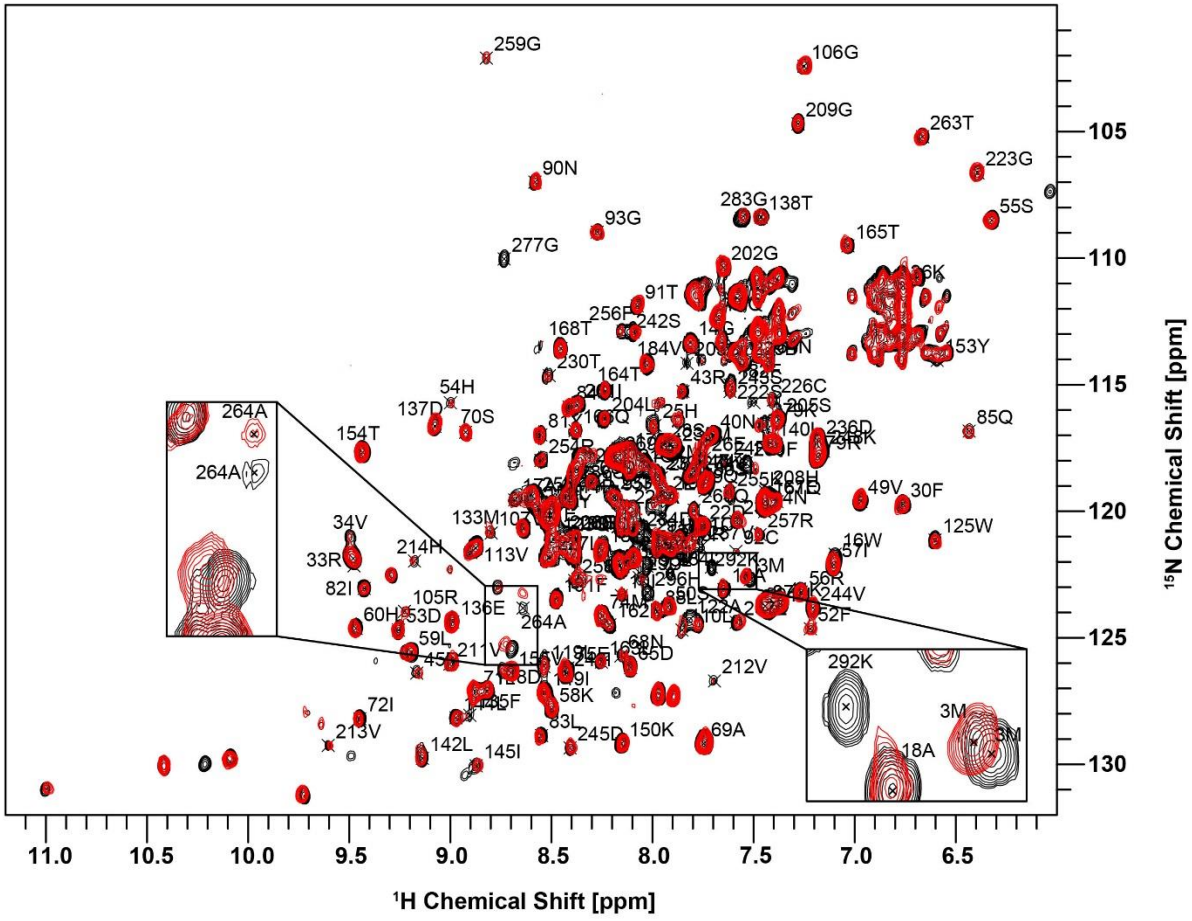

Figure 5.14 Superposition of 2D $^{1}H,^{15}N$ correlation spectra of 100 µM $PTP1B_{1-298}$ recorded without (black) and with 500 µM trodusquemine (red) (800 MHz, 20 ºC, 16 scans).

The amino acids at trodusquemine binding site are Met3, Asn64, Glu75, Tyr153, Ser222, Leu234, Met235, Ala264, Gly277, Lys279, Asp284 and Lys292. Very importantly these residues are close to the Q loop (**Figure 5.16**). This indicates that the compound is an allosteric binder.

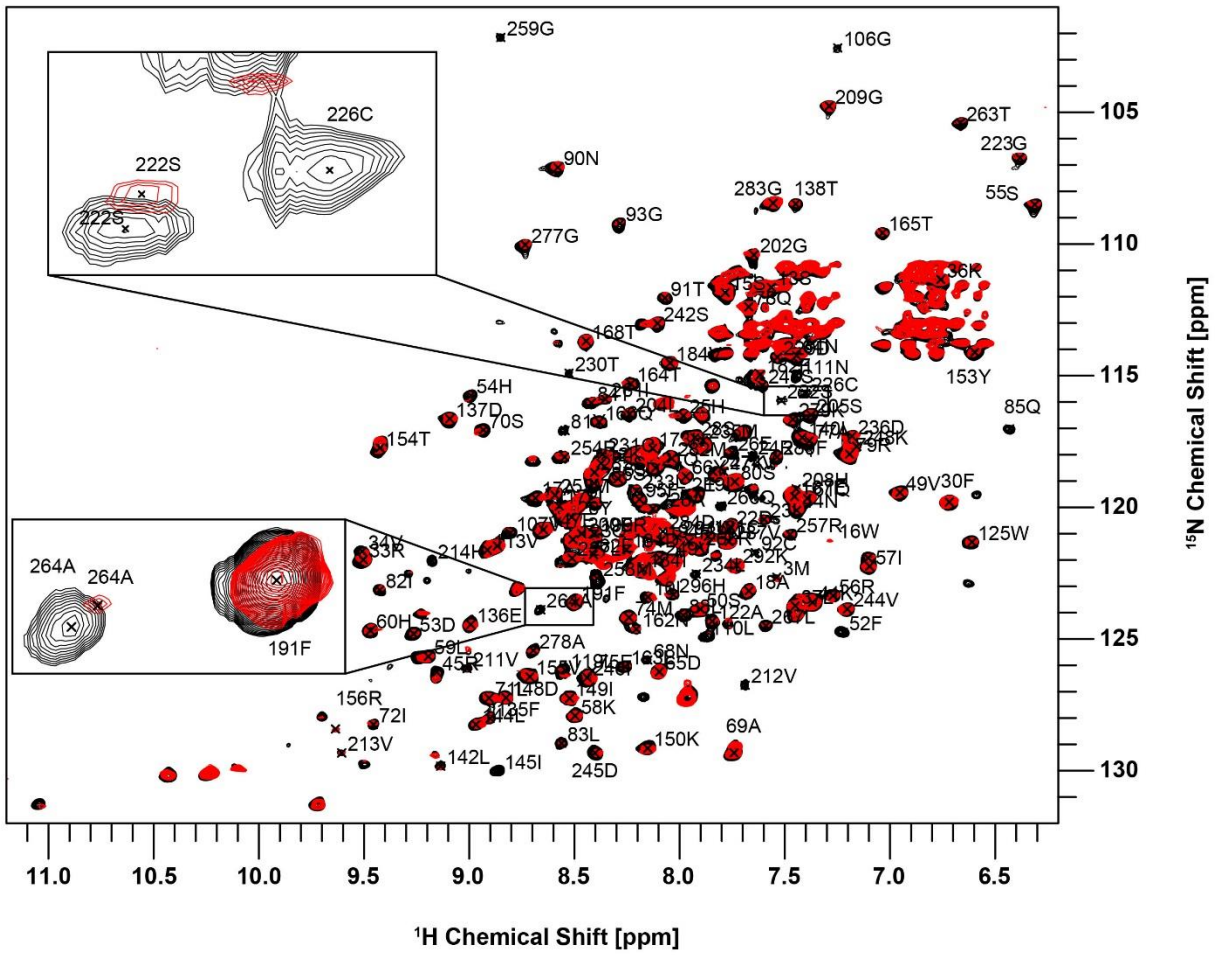

Figure 5.15 Superposition of 2D $^{1}H,^{15}N$ correlation spectra of 100 µM $PTP1B_{1-298}$ recorded without (black) and with 500 µM Cholesterol sulfate (red) (800 MHz, 20 °C, 16 scans).

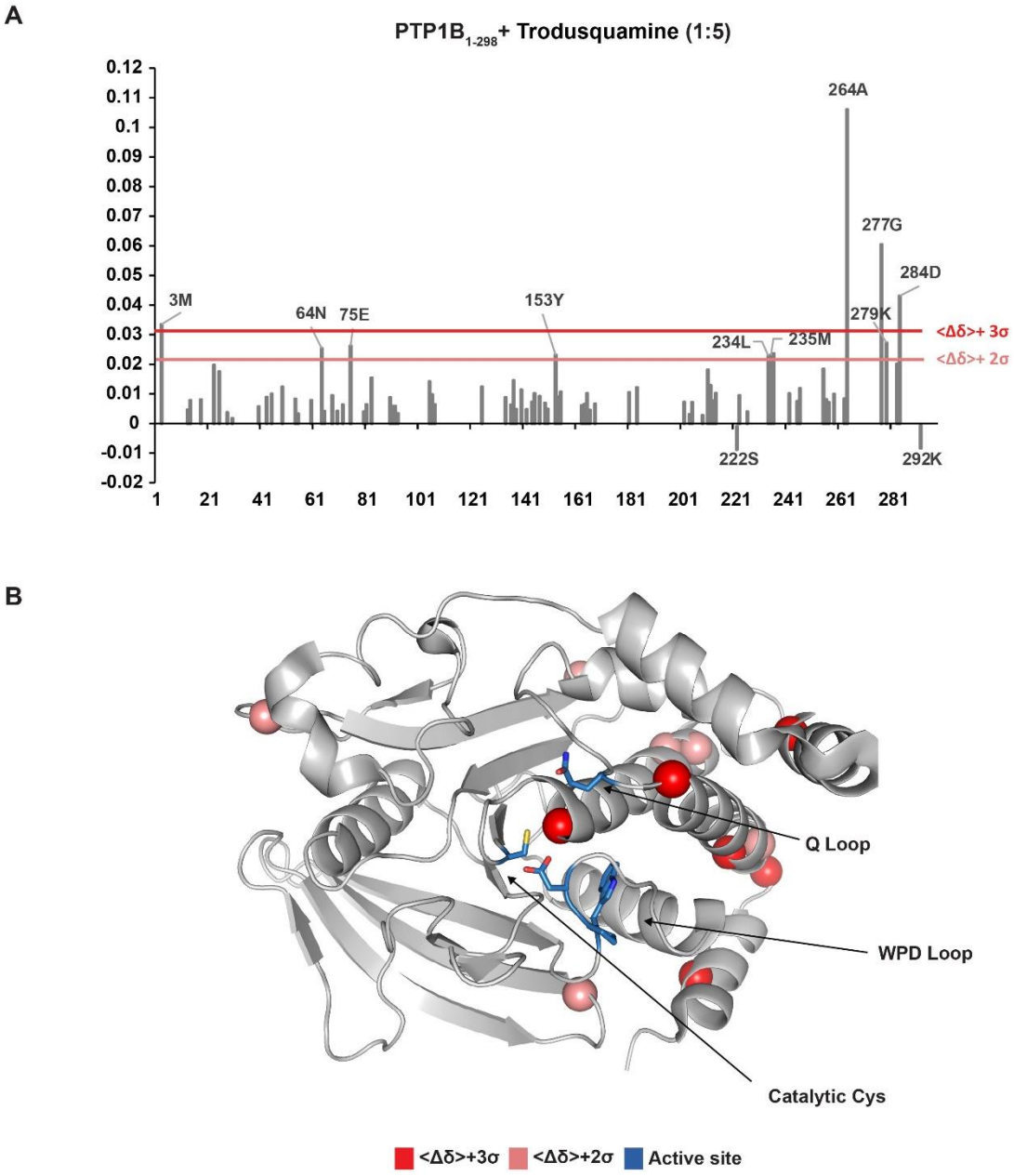

Figure 5.16 Chemical shift perturbations of compound Trodusquemine.
(A) Chemical shift perturbations (CSP, Δδ) observed upon trodusquemine binding to $PTP1B_{1-298}$. Colored lines indicate 2 and 3 σ standard deviation from the mean <Δδ>. **(B)** Mapping of the spectral changes upon titration of trodusquemine onto the structure of PTP1B (1WAX). NMR signals of amide groups in $PTP1B_{1-298}$ that experience CSPs above 2 and 3 standard deviations (SDs) from the mean <Δδ> are represented as spheres and colored salmon and red, respectively. Standard deviation 3 σ includes also the residues that undergo severe line broadening.

Concerning cholesterol sulfate, since it inhibits both phosphatases in low micro molar range, it would be expected that it binds to the active site of the protein. The CSPs were calculated

and the binding side on PTP1B was mapped. Most of the residues that are involved in the binding are located around the catalytic site (**Figure 5.17**).

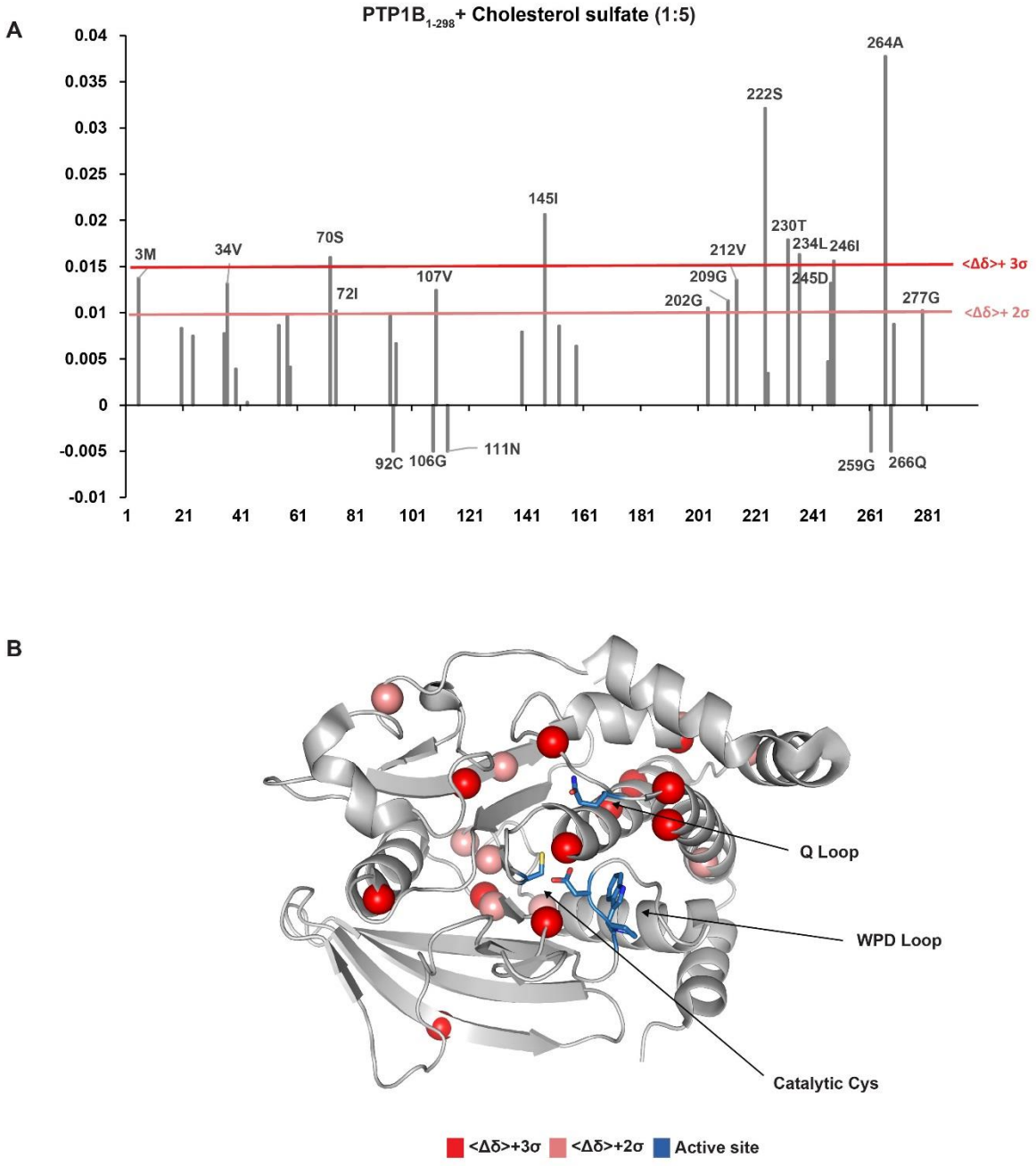

Figure 5.17 Chemical shift perturbations of compound cholesterol sulfate.
(A) Chemical shift perturbations (CSP, Δδ) observed upon cholesterol sulfate binding to $PTP1B_{1-298}$. Colored lines indicate 2 and 3 σ standard deviation from the mean <Δδ>. **(B)** Mapping of the spectral changes upon titration of cholesterol sulfate onto the structure of PTP1B (1WAX). NMR signals of amide groups in $PTP1B_{1-298}$ that experience CSPs above 2 and 3 standard deviations (SDs) from the mean <Δδ> are represented as spheres and colored salmon and red, respectively. Standard deviation 3 σ includes also the residues that undergo severe line broadening.

5.1.3 Other compounds

In this group have been classified the compounds not belonging to the other classes, chlorogenic acid, berberine, papaverine, protopanaxadiol, metformin, steviol, trigonelline, forskolin, coumarin, methyltetracosanoate, 4-aminoanilino(oxo)acetic acid (AOAC), PTP1B inhibitor 539741, Protein Tyrosine Phosphatase Inhibitor III (PTP inhibitor III), HePTP Inhibitor, SHP1/2 PTPase Inhibitor (**Figure 5.18**).

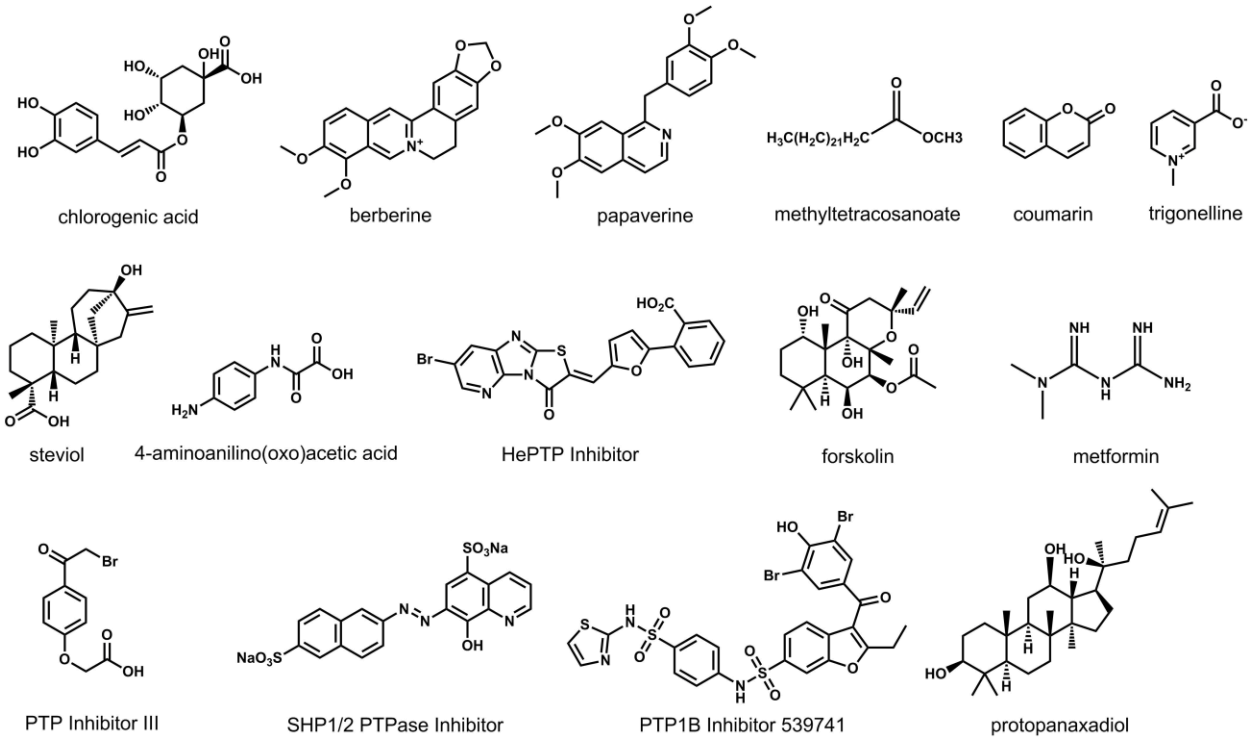

Figure 5.18 Structure of compounds beloning to C class.

Eleven of these compounds (papaverine, steviol, berberine, HePTP Inhibitor, SHP1/2 PTPase inhibitor, coumarin, trigonelline, forskolin, protopanaxadiol PTP1B inhibitor 539741 and metformin) were tested by 1D ligand-based screening NMR (**Figure 5.19)**. In this figure, the shifts or the changes in the peak intensity of compounds in the 1D-^{1}H spectra before (black) and after the addition of unlabelled PTP1B (red) indicate binding to the protein. PTP1B inhibitor 539741 (**Figure 5.3**), papaverine, steviol, berberine and HePTP Inhibitor showed interaction with the protein. SHP1/2 PTPase inhibitor, coumarin, trigonelline, metformin and forskolin did not show interaction with the protein since no difference in the compound spectrum is observed after the addition of the protein. Protopanaxadiol is not well solubilized in the NMR buffer, thus is not easy to define if they are interacting with the protein.

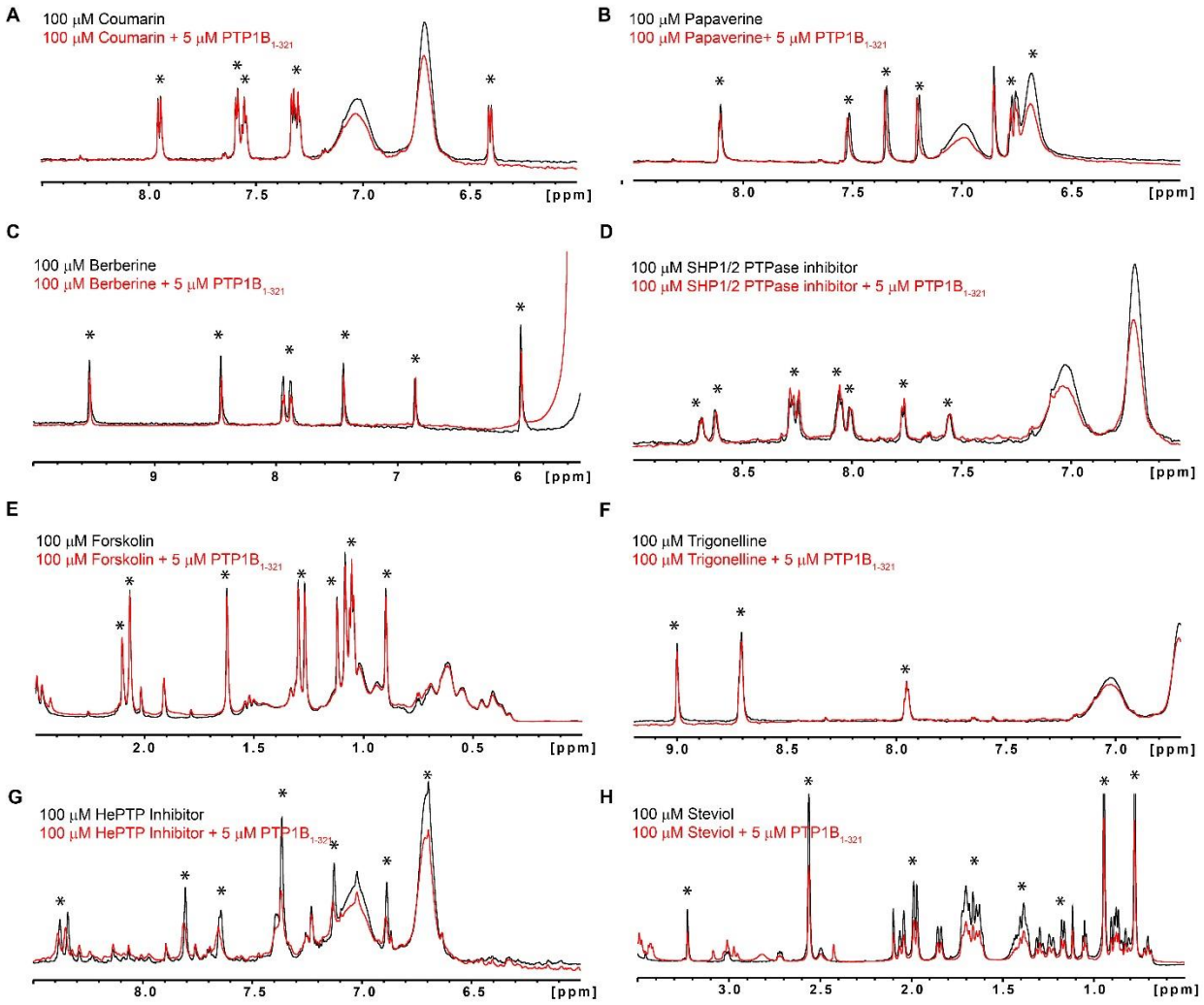

Figure 5.19 1D screening of compounds belonging to C group.
1D screening of compounds **(A)** Coumarin, **(B)** papaverine, **(C)** berberine, **(D)** SHP1/2 PTPase inhibitor, **(E)** forskolin, **(F)** trigonelline, **(G)** HePTP inhibitor and **(H)** steviol. On black color, it's shown the free compound spectrum and on red color, its shown the spectrum of the compound after the addition of 5 μM $PTP1B_{1-321}$. Compound peaks are indicated with stars..

The ability of all the compounds to bind the protein were furtherly tested by STD NMR experiments (**Table 5.5**). Compounds berberine, papaverine, AOAC and HePTP Inhibitor showed STD signals (examples are shown in **Figure 5.20**), indicating binding to PTP1B protein which is consistent with the 1D experiment. Compounds chlorogenic acid, methyltetracosanoate, SHP1/2 PTPase inhibitor and PTP inhibitor III did not show STD signals and therefore they don't bind to the protein. Compounds protopanaxadiol, steviol, coumarin, trigonelline and forksolin due to

precipitation issues was not easy to clarify if they bind or not to the protein. For metformin was not very clear if it gives STD signals.

Table 5.5 Results of the STD experiment of the compounds tested.

Compound	STD signals with $PTP1B_{1-321}$
Chlorogenic acid	x
Berberine	✓
Papaverine	✓
Metformin	not clear
AOAC	✓
Methyltetracosanoate	x
PTP Inhibitor III	x
HePTP Inhibitor	✓
SHP1/2 PTPase inhibitor	x
Trigonelline	Precipitated
Forskolin	Precipitated
Coumarin	Precipitated
steviol	Precipitated
protopanaxadiol	Precipitated
PTP1B inhibitor 539741	✓
✓: STDs signals X: No STDs signals	

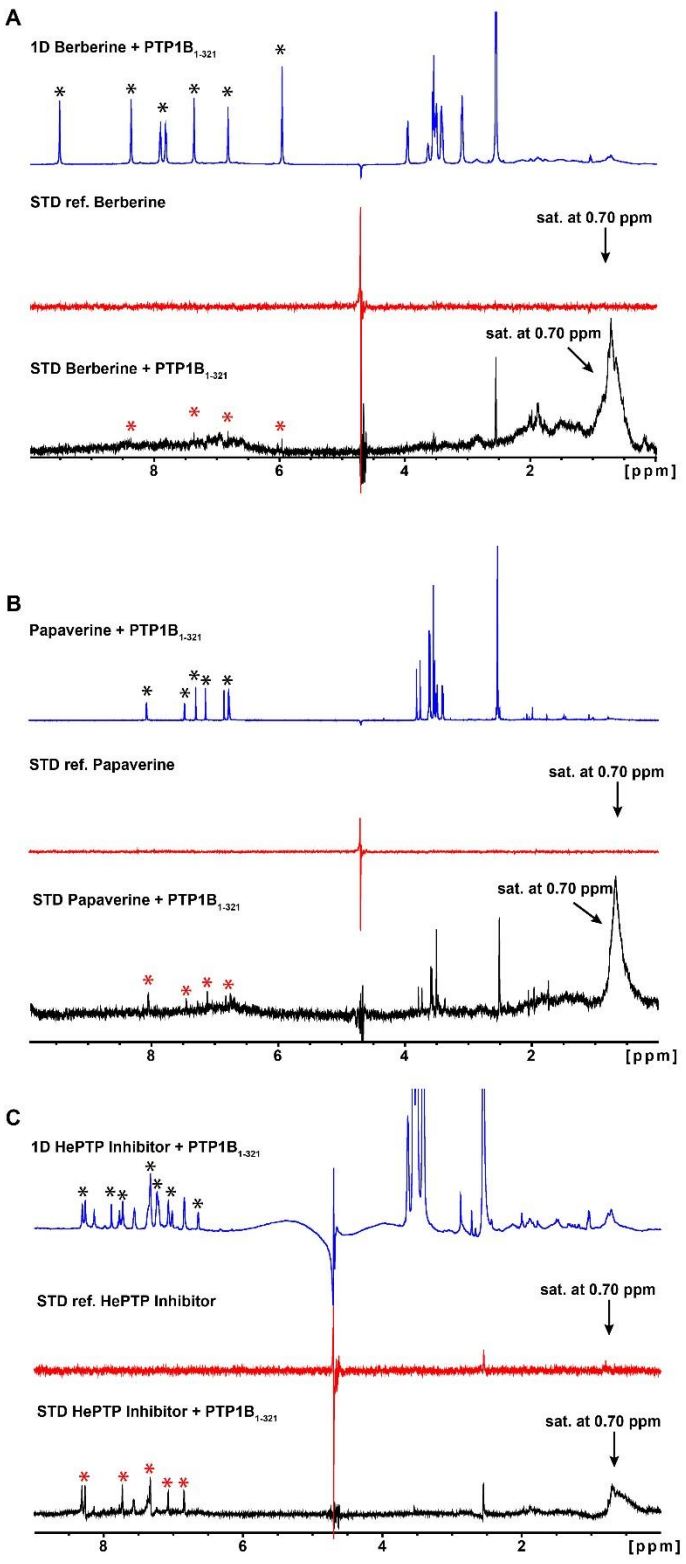

Figure 5.20 STD spectra of compounds belonging to group C.
STD spectra of **(A)** berberine, **(B)** papaverine and **(C)** HePTP inhibitor with $PTP1B_{1-321}$. Compound peaks are indicated with stars, red stars are indicating positive STD signals.

The pNPP assay was used in order to determine if the compounds apart from binding to the proteins also inhibit them. Compounds papaverine, steviol, trigonelline, coumarin, metformin, forskolin and protopanaxadiol were tested against $PTP1B_{1-298}$ and $PTP1B_{1-321}$ constructs, while metformin was tested against all the phosphatases constructs (**Table 5.6**). Although, it has been shown by NMR that most of these compounds bind to the PTP1B protein none of them inhibits strongly any of the two proteins. Most of them showed a trend of inhibition or activation of the activity of the protein (compounds papaverine and trigonelline, **Figure 5.21**). Chlorogenic acid and berberine are bright yellow compounds while AOAC has a light brown color and therefore they cannot be tested with this assay since their color can affect the measurement.

Table 5.6 Activity assay results for all compounds of group C against all protein constructs.

Protein / compound	$PTP1B_{1-298}$		$PTP1B_{1-321}$		$PTP1B_{1-393}$		$TCPT_{1-296}$		$TCPT_{1-336}$	
	w/ NP-40 (μM)	**w/o NP-40 (μM)**	**w/ NP-40 (μM)**	**w/o NP-40 (μM)**	**w/ NP-40 (μM)**	**w/o NP-40 (μM)**	**w/ NP-40 (μM)**	**w/o NP-40 (μM)**	**w/ NP-40 (μM)**	**w/o NP-40 (μM)**
Papaverine	Amb	2.4 (act)	Amb	33.1 (act)						
Steviol	Amb	Amb	Amb	Amb						
Trigonelline	Amb	Amb	65.9 (act)	75.9 (act)						
Coumarin	Amb	Amb	Amb	Amb						
Metformin	Amb	Amb	Amb	Amb	Amb	Amb	Amb	Amb	Amb	Amb
Forskolin	-	-	Amb	254.3						
Protopanaxadiol	Amb	Amb	Amb	Amb						

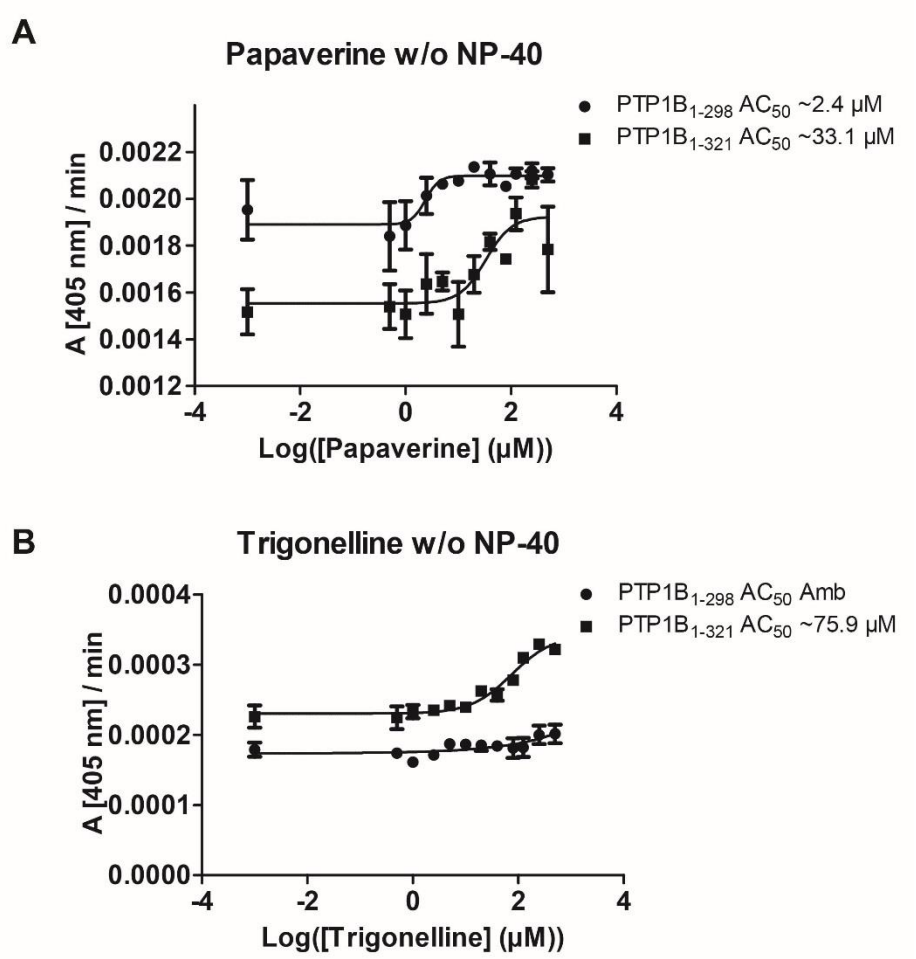

Figure 5.21 Activity assay graphs of compounds papaverine (A) and trigonelline (B).

5.2 Thermofluor screening

Thermofluor screening can also be used in order to screen for compound binding to proteins. Twenty-five different compounds (Class A: compounds 18β-glycyrrhetinic acid, 18α-glycyrrhetinic acid, ursolic acid and gymnemagenin, Class B: compounds trodusquemine, claramine (SIXB), NV673, diosgenin, stigmasterol and fucosterol, all compounds (15) of the Class C) were tested in the optimum buffer conditions, Bis-Tris propane pH 7.5, in high and low salt concentration, 400 and 80 mM NaCl. An increase of the initial fluorescence in the presence of the tested compounds was observed, indicating possible interference with the dye (**Figure 5.22 left**). For the tested compounds, a decrease of the melting point of the protein was always observed (**Figure 5.22 right**). Decrease in the melting point is also an indication of binding. The compounds may find hydrophobic sites in the native state or additional hydrophobic surfaces formed upon

protein unfolding. If a ligand binds stronger to the unfolded state of the protein, then such ligand will exhibit a destabilizing effect on the protein rather than stabilizing it (Cimmperman and Matulis 2011). In **Figure 5.23** is showing the assay with the compound Trodusquemine which has been suggested to be an inhibitor of PTP1B. However, the tested compounds probably aggregate with the dye, so further confirmation with other techniques is necessary.

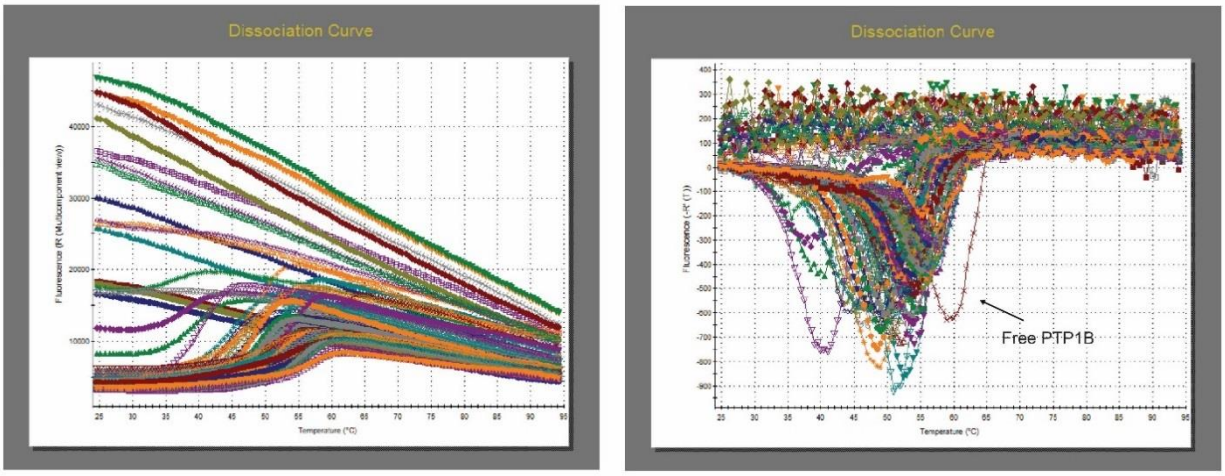

Figure 5.22 Thermofluor dissociation curves of the tested compounds in the optimized buffer conditions. Dissociation curve plot as **(left)** Fluorescence R versus temperature and **(right)** Fluorescence -R'(T) versus temperature

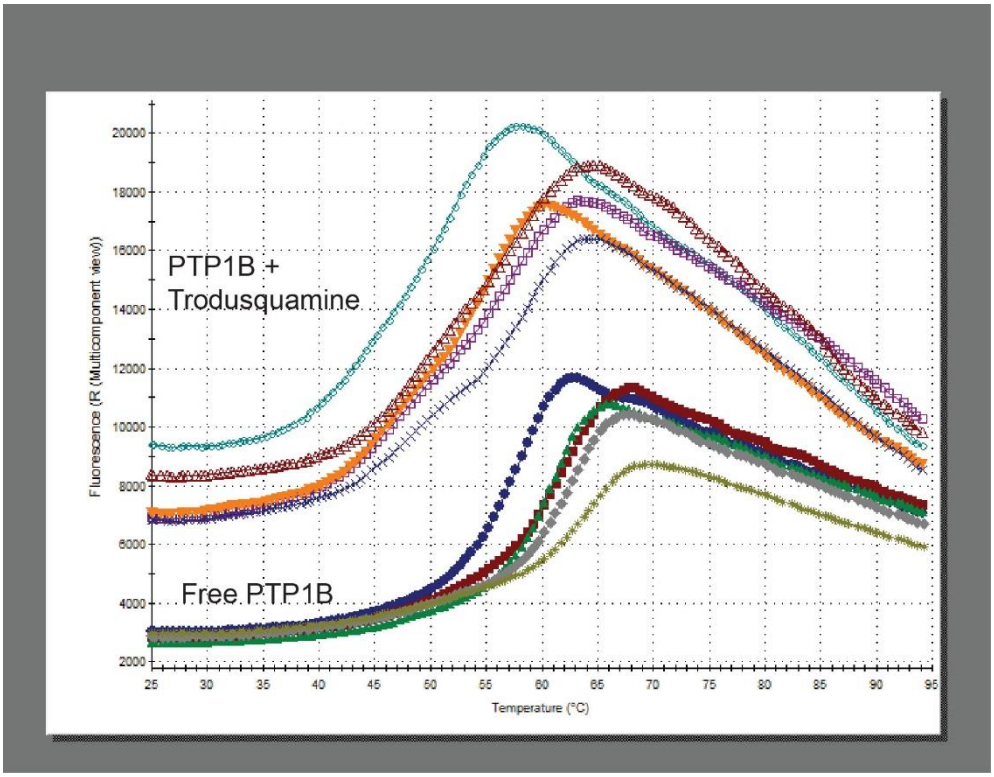

Figure 5.23 Thermofluor assay dissociation curves of compound Trodusquemine.

5.3 Crystallization of PTP1B$_{1-321}$ with compounds

In the beginning a screening in the crystallization conditions of PTP1B$_{1-321}$ was performed (Pedersen et al. 2004). Crystals were developed in four different conditions. The best conditions were observed when protein and reservoir solution (1:2) were mixed, while the reservoir solution contained 70 mM Bis-Tris Propane pH 7.5, 3 mM DTT, 0-10% PEG 8000, 122.5-147 mM Magnesium acetate. Hexagonal crystals appear after 2 days at 4 ^{o}C (**Figure 5.24).** Co-crystallization trials of the protein with different compounds and soaking of crystals of the free protein with a solution of the compound were performed. Forty diffraction data with resolution between 1.8-2.3 Å, collected in ESRF (Grenoble) were analyzed, but no ligand was found to be bound to the protein. For this reason, another co-crystallization screening in Max Planck crystallography platform was tested, as described in section 3.2.8.2. In this screening only Trodusquemine, SIXB and NV673 were tested and crystals with different morphology from those of the native protein appeared in NPG, PAC and IND screenings (**Figure 5.25**). Diffraction data on the crystals were again obtained at the ESRF with resolution between1.95-3 Å. However, no ligand density was found this time too after analysis of the diffraction data.

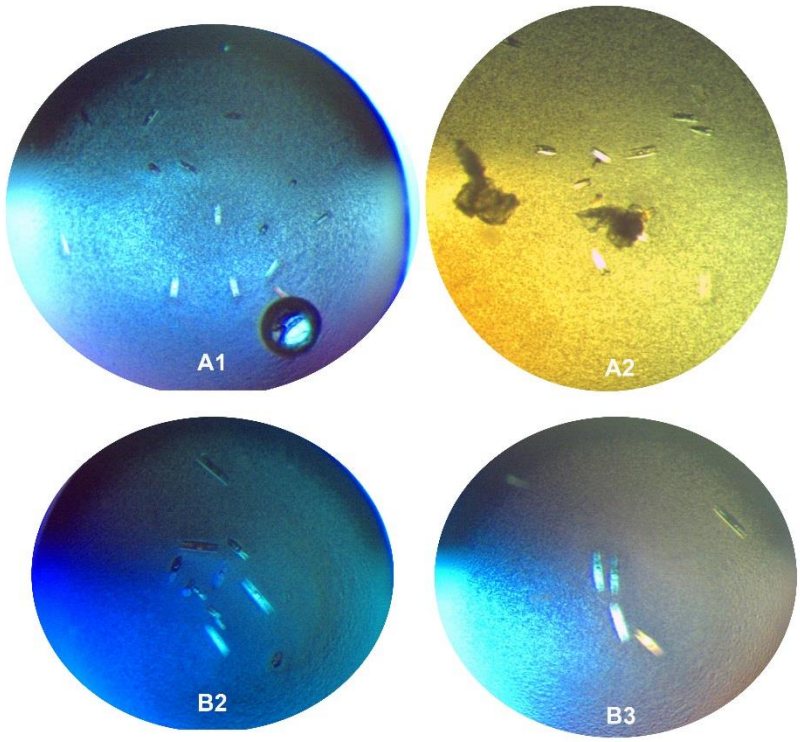

Figure 5.24 Crystal growth of free PTP1B$_{1-321}$. Conditions refer to Table 3.7.

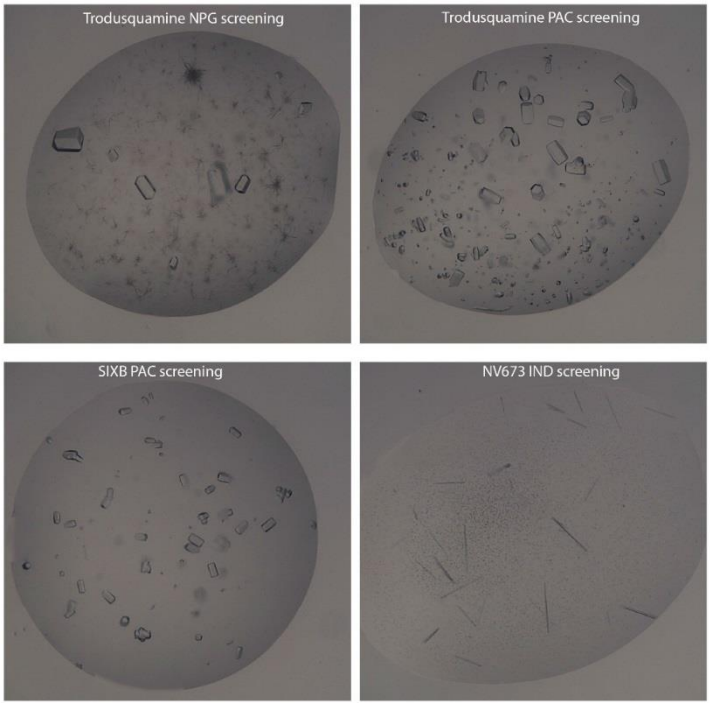

Figure 5.25 Cocrystallization of PTP1B$_{1\text{-}321}$ with 4 compounds using the Max Planck screening.

In total, diffraction data were collected at ESRF for 52 crystal datasets and analyzed (**Table 5.7**). However, no ligand density was found in any of them. Furthermore, in the density map of the crystals, the density after the amino acid 282 was not visible (**Figure 5.26**). That can be attributed to the non-aromatic nature of the compounds that makes it difficult to be crystallized. Exception is the case of a known allosteric inhibitor of PTP1B, PTP1B inhibitor 539741 that has been crystallized before (Wiesmann et al. 2004). In this case the density of the compound bound to the protein was visible, around residue Phe280 as was expected.

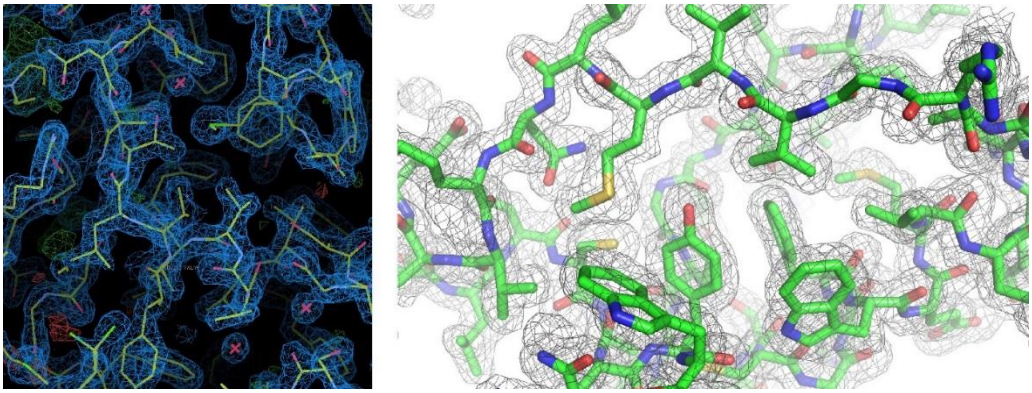

Figure 5.26 Protein crystal density after diffraction data analysis, no ligand density was found.
Density of the crystal structure of the protein exported from **(left)** Coot and **(right)** pymol software.

Table 5.7 Crystal datasets

No dataset	Compound	Type of crystallization method	Days of crystal growth	Crystallization conditions	Compound concetration (mM)	Morphology of crystal	Resolution (Å)	Space group
1	Trodusquemine	cocrystallization	1 day	C3 (Table 3.7)	0.606 (x2)	Rod	1.8	P3121
2	Trodusquemine	cocrystallization	1 day	C3 (Table 3.7)	0.606 (x2)	Rod	1.7	P3121
3	NV673	cocrystallization	1 day	C3 (Table 3.7)	0.606 (x2)	Rod	2.4	P3121
4	NV673	cocrystallization	1 day	C3 (Table 3.7)	0.606 (x2)	Rod	2.3	P3121
5	Trodusquemine	soaking	5 hours	C4 (Table 3.7)	1 (x3)	Rod	1.9	P3121
6	Trodusquemine	soaking	5 hours	C4 (Table 3.7)	1 (x3)	Rod	1.8	P3121
7	NV673	soaking	5 hours	C4 (Table 3.7)	1 (x3)	Rod	1.8	P3121
8	NV673	soaking	5 hours	C4 (Table 3.7)	1 (x3)	Rod	1.7	P3121
9	SIXB	soaking	5 hours	C4 (Table 3.7)	1 (x3)	Rod	2.1	P3121
10	SIXB	soaking	5 hours	C4 (Table 3.7)	1 (x3)	Rod	1.7	P3121
11	Berberine	soaking	3 hours	C4 (Table 3.7)	1 (x3)	Rod	2.1	P3121
12	Berberine	soaking	3 hours	C4 (Table 3.7)	1 (x3)	Rod	1.8	P3121
13	Chlorogenic acid	soaking	3 hours	C4 (Table 3.7)	1 (x3)	Rod	2.05	P3121
14	Chlorogenic acid	soaking	3 hours	C4 (Table 3.7)	1 (x3)	Rod	2	P3121
15	18β-glycyrrthetinic acid	soaking	4 hours	C4 (Table 3.7)	1 (x3)	Rod	1.8	P3121
16	Trodusquemine	cocrystallization	6 days	B2 (Table 3.7)	0.606 (x2)	Rod	2.4	P3121
17	Trodusquemine	cocrystallization	6 days	B2 (Table 3.7)	0.606 (x2)	Rod	2.2	P3121
18	NV673	cocrystallization	6 days	C4 (Table 3.7)	0.606 (x2)	Rod	1.9	P3121
19	NV673	cocrystallization	6 days	C4 (Table 3.7)	0.606 (x2)	Rod	1.9	P3121
20	NV673	cocrystallization	6 days	C4 (Table 3.7)	0.606 (x2)	Rod	1.9	P3121
21	NV673	cocrystallization	6 days	C4 (Table 3.7)	0.606 (x2)	Rod	2	P3121
22	NV673	soaking	2 days	C4 (Table 3.7)	1 (x3)	Rod	2.6	P3121
23	NV673	soaking	2 days	C4 (Table 3.7)	1 (x3)	Rod	1.9	P3121
24	Berberine	soaking	2 days	C4 (Table 3.7)	1 (x3)	Rod	2.6	P3121
25	Chlorogenic acid	soaking	2 days	C4 (Table 3.7)	1 (x3)	Rod	1.9	P3121

26	Chlorogenic acid	soaking	2 days	C4 (Table 3.7)	1 (x3)	Rod	1.78	P3121
27	18β-glycyrrthetinic acid	soaking	2 days	C4 (Table 3.7)	1 (x3)	Rod	1.8	P3121
28	Metformin	soaking	1 day	C4 (Table 3.7)	1 (x3)	Rod	2.2	P3121
29	Metformin	soaking	1 day	C4 (Table 3.7)	1 (x3)	Rod	1.88	P3121
30	Trigonelline	soaking	1 day	C4 (Table 3.7)	1 (x3)	Rod	1.9	P3121
31	Trigoneline	soaking	1 day	C4 (Table 3.7)	1 (x3)	Rod	1.78	P3121
32	papaverine	soaking	1 day	A4 (Table 3.7)	1 (x3)	Rod	1.9	P3121
33	methyltetracosanoate	soaking	1 day	A4 (Table 3.7)	1 (x3)	Rod	3	P3121
34	methyltetracosanoate	soaking	1 day	A4 (Table 3.7)	1 (x3)	Rod	2.04	P3121
35	stigmasterol	soaking	1 day	A4 (Table 3.7)	1 (x3)	Rod	1.71	P3121
36	stigmasterol	soaking	1 day	A4 (Table 3.7)	1 (x3)	Rod	1.8	P3121
37	Trodusquemine	cocrystallization	1 month	PAC C11	0.606 (x2)	box like	2.71	P3221
38	Trodusquemine	cocrystallization	1 month	PAC C11	0.606 (x2)	box like	3	P3221
39	Trodusquemine	cocrystallization	1 month	PAC C11	0.606 (x2)	box like	3.1	P3221
40	SIXB	cocrystallization	1 month	PAC C11	1.5 (x5)	box like	1.95	P3221
41	SIXB	cocrystallization	1 month	PAC C11	1.5 (x5)	box like	2.6	P3221
42	SIXB	cocrystallization	1 month	IND G10	1.5 (x5)	rod	2.5	P3121
43	Trodusquemine	cocrystallization	1 month	NPG G11	1.5 (x5)	rod	3	P3121
44	NV673	cocrystallization	1 month	IND G11	1.5 (x5)	needle	2.5	P212121
45	SIXB	cocrystallization	1 month	PAC C11	1.5 (x5)	box like	2.1	P3221
46	Trodusquemine	soaking	3 days	C4 (Table 3.7)	1 (x3)	Rod	2.1	P3121
47	Trodusquemine	soaking	3 days	C4 (Table 3.7)	5 (x16)	Rod	2	P3121
48	Trodusquemine	soaking	1 day	B5 (Table 3.7)	1 (x3)	Rod	2.1	P3121
49	Trodusquemine	soaking	1 day	B5 (Table 3.7)	5 (x16)	Rod	2.6	P3121
50	SIXB	soaking	3 days	C4 (Table 3.7)	1 (x3)	Rod	1.9	P3121
51	SIXB	soaking	3 days	C4 (Table 3.7)	5 (x16)	Rod	2	P3121
52	PTP1B inhibitor 539741	soaking	1 day	B5 (Table 3.7)	1 (x3)	Rod	2.1	P3121

5.4 Cell assay

The insulin receptor contains two α (IRα) and two β (IRβ) subunits. The IRα carry the insulin binding regions, while the IRβ has intrinsic tyrosine kinase activity. Upon binding of insulin, IRβ phosphorylates tyrosyl residues of its own protein and of signaling molecules that elicit its downstream effects, including the insulin receptor substrate (IRS), PI3K and a key serine-threonine kinase AKT. Phosphorylated and activated AKT then increases peripheral glucose uptake by increasing the number of GLUT4 transporters at the cell surface membrane (Vogt and Brüning 2013).

Signal transducer and activator of transcription 3 (STAT3) mediates the expression of a variety of genes in response to cell stimuli, and thus plays a key role in many cellular processes such as cell growth and apoptosis. This protein is activated through phosphorylation of tyrosine 705, in response to various cytokines and growth factors including the hormone leptin (Buettner et al. 2006).

CLU-177 neuronal cells (Adult Mouse Hypothalamus Cell Line) were used for this assay. For the analysis of the results western blots were performed. A daily protocol, described in the methods part, was followed from cell culturing until the development of the western blot.

Initially, confluent neuronal CLU-177 cells were serum starved for 6 hours and then incubated with or without compound for 30 min in three different doses (1μM, 10μM and 100μM). Control cells were treated with or without insulin (100nM) and leptin (10nM) for 10 min prior to harvest (Figure 5.27). Equal amounts of protein were separated by SDS-PAGE and phosphorylated proteins were detected by immunoblot analysis.

From this experiment was found out that the best dose to work with is 10μM, since 100μM is too high and it seems to be harmful for the cells (most probably toxic).

Figure 5.27 Immunoblot analysis of the compound dose screening

The best compounds resulting from the screenings described above, were then tested with a cellular assay in collaboration with Paul Pflunger.

After determining that 10 μM is the best dose to be used for the assay, a daily protocol was followed from cell culturing until the development of the western blot. In total six compounds were tested from our library: oleanolic acid, 18β-glycyrrhetinic acid, cholesterol sulfate, which are 3 of our best hits, claramine, trodusquemine and PTP1B inhibitor 539741, which are previously described as PTP1B inhibitor compounds. Proteins p-AKT (**Figure 5.28**) and p-STAT3 were detected.

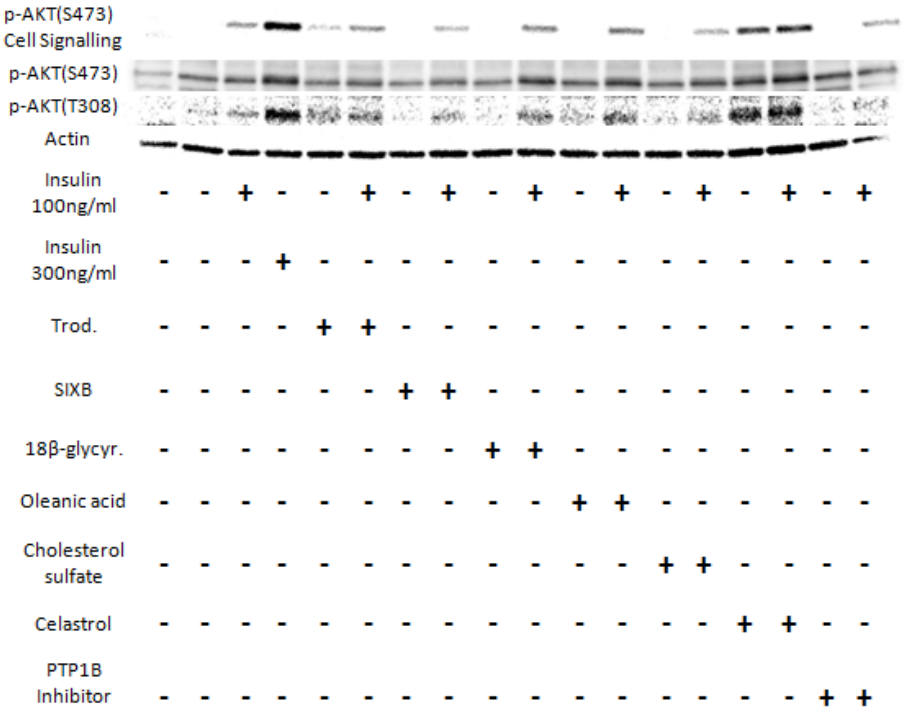

Figure 5.28 Immunoblot analysis of the phosphorylated AKT proteins.

Quantification analysis of the results from p-AKT(S473) from Cell Signaling Inc. is shown in the **Figure 5.29**. Apart from trodusquemine, celastrol and cholesterol sulfate, all the other compounds show no insulin pathway activation when they are not treated with insulin (red line). That might be because of the selectivity of the antibody. As it can be seen from the immunoblot analysis in **Figure 5.28**, when the same samples are blocked with another antibody (p-AKT(S473) from Santa Cruz and p-AKT(T308) from Cell Signaling Inc.) they activate phosphorylation of AKT. On the other hand, in almost all cases, compounds elicited insulin pathway activation, when the cells where treated with insulin (green line). p-STAT3 was not able to be detected, most probably because there is not sufficient protein expression.

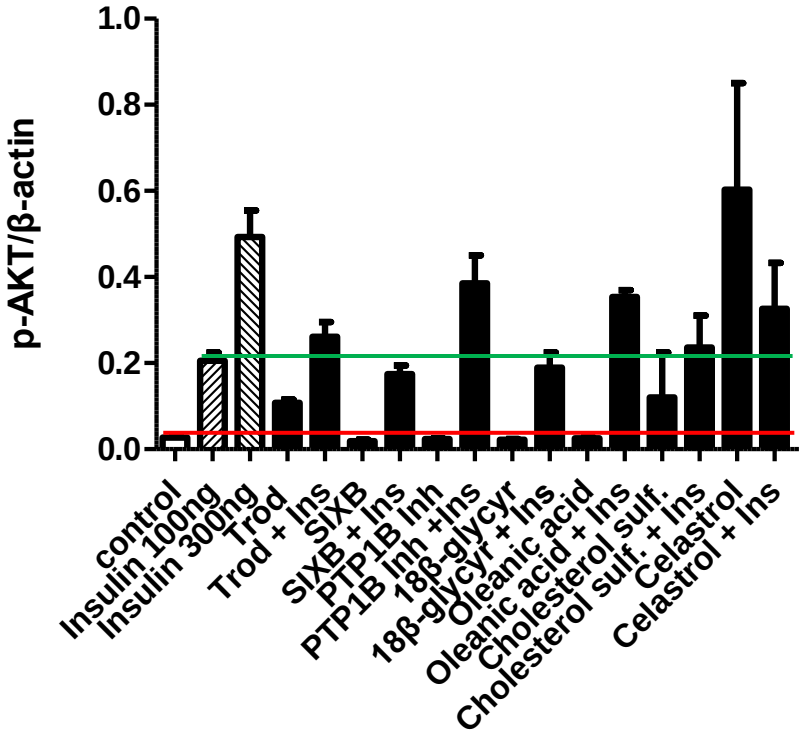

Figure 5.29 Quantification of the immunoblot analysis for p-AKT(S473) from Cell Signaling. Red line indicates comparison with the control with cell treated without insulin. Green line indicates comparison with the control treated with 100 ng of insulin with the corresponding cells. Experiment was repeated 3 times.

Compounds 18β-glycyrrhetinic acid, oleanolic acid, PTP1B inhibitor 539741 and cholesterol sulfate stimulate mostly insulin sensitivity.

The ability of another seven compounds to enhance the phosphorylation levels of insulin signaling components was confirmed by using the same assay. The compounds tested were diosgenin, usrolic acid, β-estradiol, 18α-glycyrrhetinic acid, cortisol, metformin and asiatic acid (**Figure 5.30**). Quantification analysis of the results from p-AKT(S473) from Cell Signaling Inc. is shown in the **Figure 5.31**. Metformin, asiatic acid, disogenin and cortisol stimulate insulin sensitivity the most.

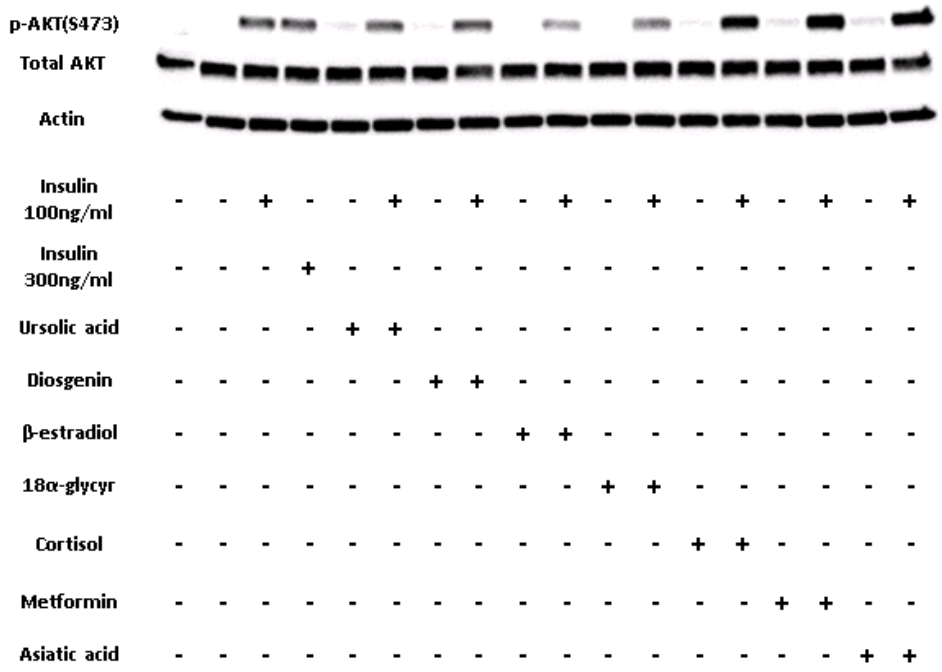

Figure 5.30 Immunoblot analysis of the phosphorylated AKT protein.

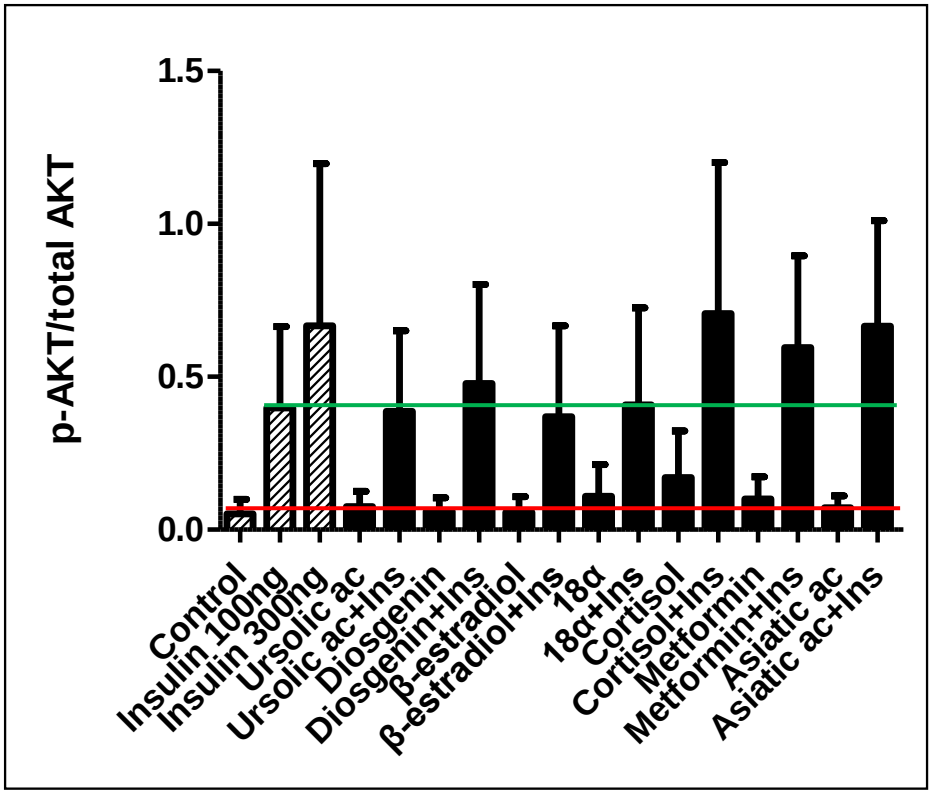

Figure 5.31 Quantification for the immunoblot analysis for p-AKT(S473) from Cell Signaling. Red line indicates comparison with the control with cell treated without insulin. Green line indicates comparison with the control treated with 100 ng of insulin with the corresponding cells. Experiment was repeated 3 times.

6. Results III: Celastrol reverses obesity by inhibiting PTP1B and TCPTP

Celastrol is a triterpenoid isolated from Thunder God Vine, that has been described in the literature as an antiobesity molecule (J. Liu et al. 2015a) but for which the physiological molecular targets responsible for the weight-lowering effect were not known. Here is investigated if celastrol can bind and inhibit PTP1B and TCPTP.

6.1 Activity assay with celastrol

Initially, the pNPP enzyme colorimetric assay was used for the detection of the inhibitory ability of celastrol. However, celastrol has an orange color which might interfere with the assay. For this reason, another enzyme kinetic assay was used, using as a substrate a fluorogenic compound, 6,8-difluoro-4-methylumbiliferyl phosphate (DiFMUP). Initially, the kinetic parameters were determined and then the IC_{50} values of celastrol for all constructs of both proteins were evaluated in a buffer with reducing agent (**Figure 6.1**). Celastrol inhibits PTP1B and TCPTP constructs with low micromolar IC_{50} values. Using the same assay, the type of inhibition was determined and it was shown that celastrol is a non-competitive inhibitor for both phosphatases, since the K_m does not change and the V_{max} decreases.

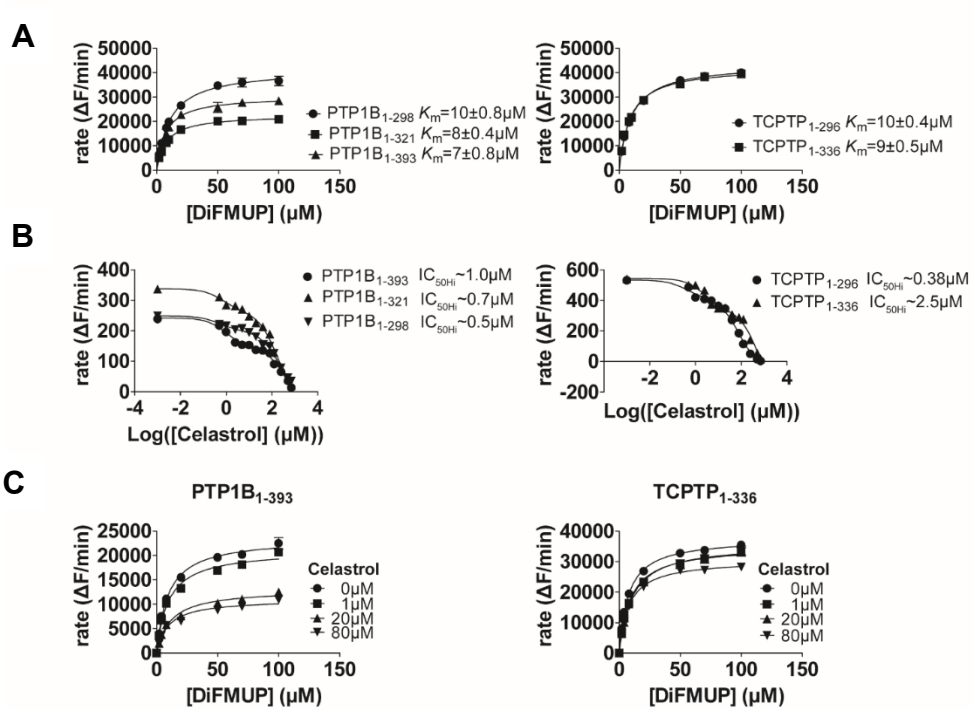

Figure 6.1 Kinetic studies with celastrol on PTP1B and TCPTP constructs in a buffer with reducing agent. **(A)** The kinetic constant K_m for the hydrolysis of DiFMUP for all PTP1B (left) and TCPTP (right) constructs were calculated plotting the initial velocities against substrate concentration and fitted with Michaelis-Menten equation. **(B)** Inhibition curves of PTP1B (left) and TCPTP (right) constructs in the presence of celastrol using DiFMUP as a substrate. Biphasic fitting from nonlinear regression analysis was used to obtain IC_{50} values. $PTP1B_{1-298}$ IC_{50Hi}: ~ 0.5 μM IC_{50Lo}: ~213.6 μM, $PTP1B_{1-321}$ IC_{50Hi}: ~0.7 μM IC_{50Lo}: ~185.3 μM, $PTP1B_{1-393}$ IC_{50Hi}: ~1.0 μM IC_{50Lo}: ~466.5 μM, $TCPTP_{1-296}$ IC_{50Hi}: ~0.38 μM IC_{50Lo}: ~81.8 μM, $TCPTP_{1-336}$ IC_{50Hi}: ~2.5 μM IC_{50Lo}: ~737.6 μM. **(C)** $PTP1B_{1-393}$ (left) and $TCPTP_{1-336}$ (right) were incubated with different amount of substrate DiFMUP (0-100 μM) in the absence and presence of celastrol at three different concentrations. Data were fitted with Michaelis-Menten equation. Buffer conditions, 25 mM Bis-Tris propane pH 7.5, 50 mM NaCl, 2 mM EDTA, 2 μM DTT.

6.2 Mapping of the celastrol binding site by NMR Spectroscopy

NMR Spectroscopy experiments were used to confirm binding of celastrol to both PTP1B and TCPTP. First, 1D spectra of the celastrol were recorded in the presence of increasing amounts of phosphatase (**Figure 6.2**). With the addition of increasing amounts of protein, the intensities of the NMR signals of the compound are reduced, indicating an interaction with the protein. Then STD NMR experiments for both proteins were recorded, to further confirm celastrol binding to the proteins (**Figure 6.3 A, B**). After that an additional competitive STD NMR experiment was run with celastrol and 4'-aminoanilino oxo-acetic acid (AOAC), which is very similar to a known PTP1B active site inhibitor (4-(aminomethyl)phenyl amino oxo-acetic acid) (IC_{50}:86 μM, (Hartshorn et al. 2005)) although less potent ($PTP1B_{1-393}$ IC_{50}=910 μM; $TCPTP_{1-336}$ IC_{50}=478 μM). Either starting with celastrol or with AOAC, addition of the other compound, did not lead to

reduction on the intensity of the signals of the first compound with both compounds showing signals simultaneously (**Figure 6.3 C**). This indicates that both compounds can simultaneously bind to the protein and do not compete with each other.

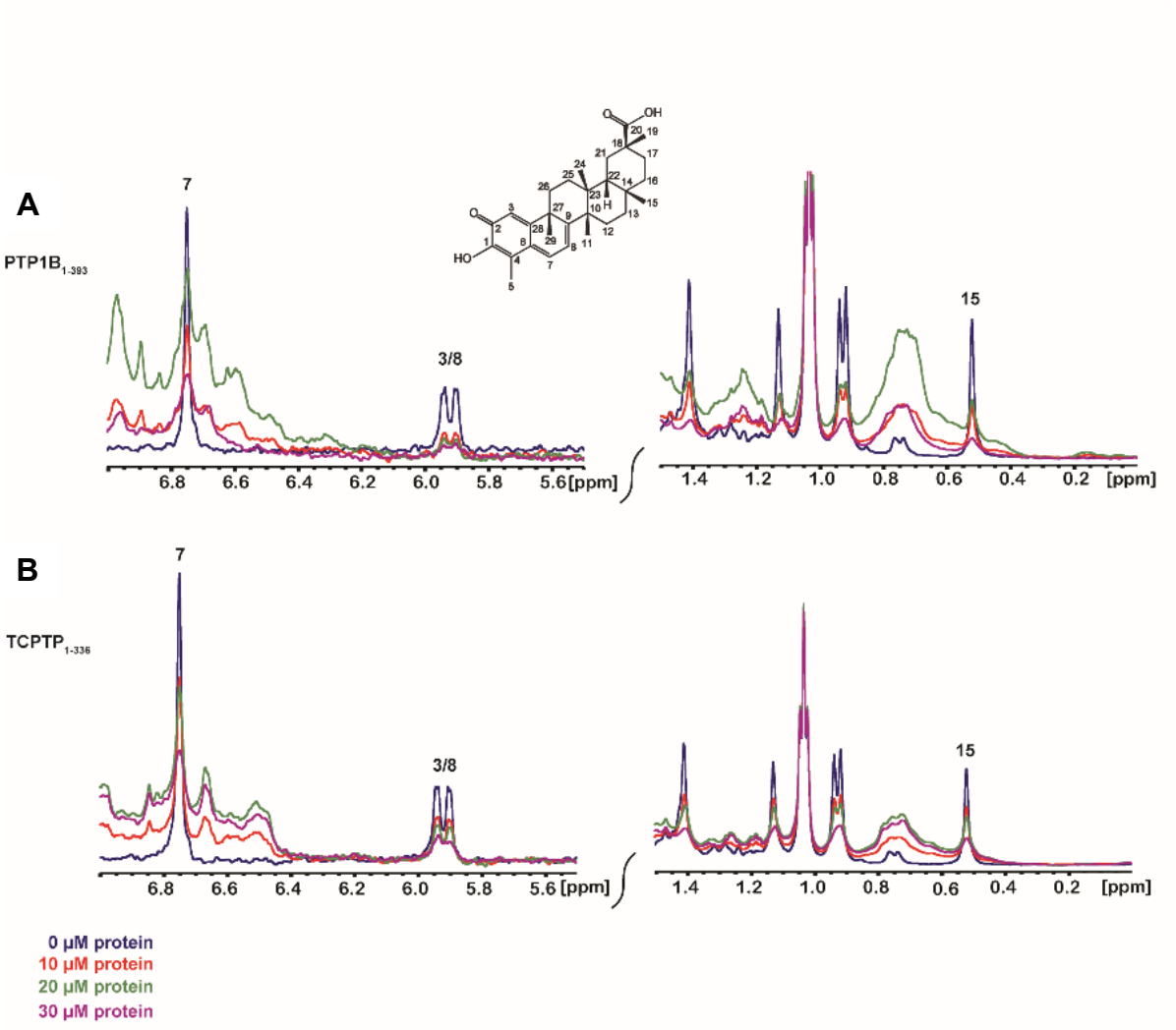

Figure 6.2 1D screening of celastrol with PTP1B and TCPTP.
(A) Celastrol was titrated with $PTP1B_{1-393}$ and **(B)** with $TCPTP_{1-336}$ in three different concentrations 0 µM (blue), 10 µM (eed), 20µM (Green), and 30 µM (purple) in 50 mM d11-Tris pH 7.5, 75 mM NaCl, 5 mM d10-DTT. Differences in the intensity of celastrol peaks are observed both in the aromatic (left spectra) and in the aliphatic region of the spectra (right) (600 MHz, 20 ^{o}C, 128 scans).

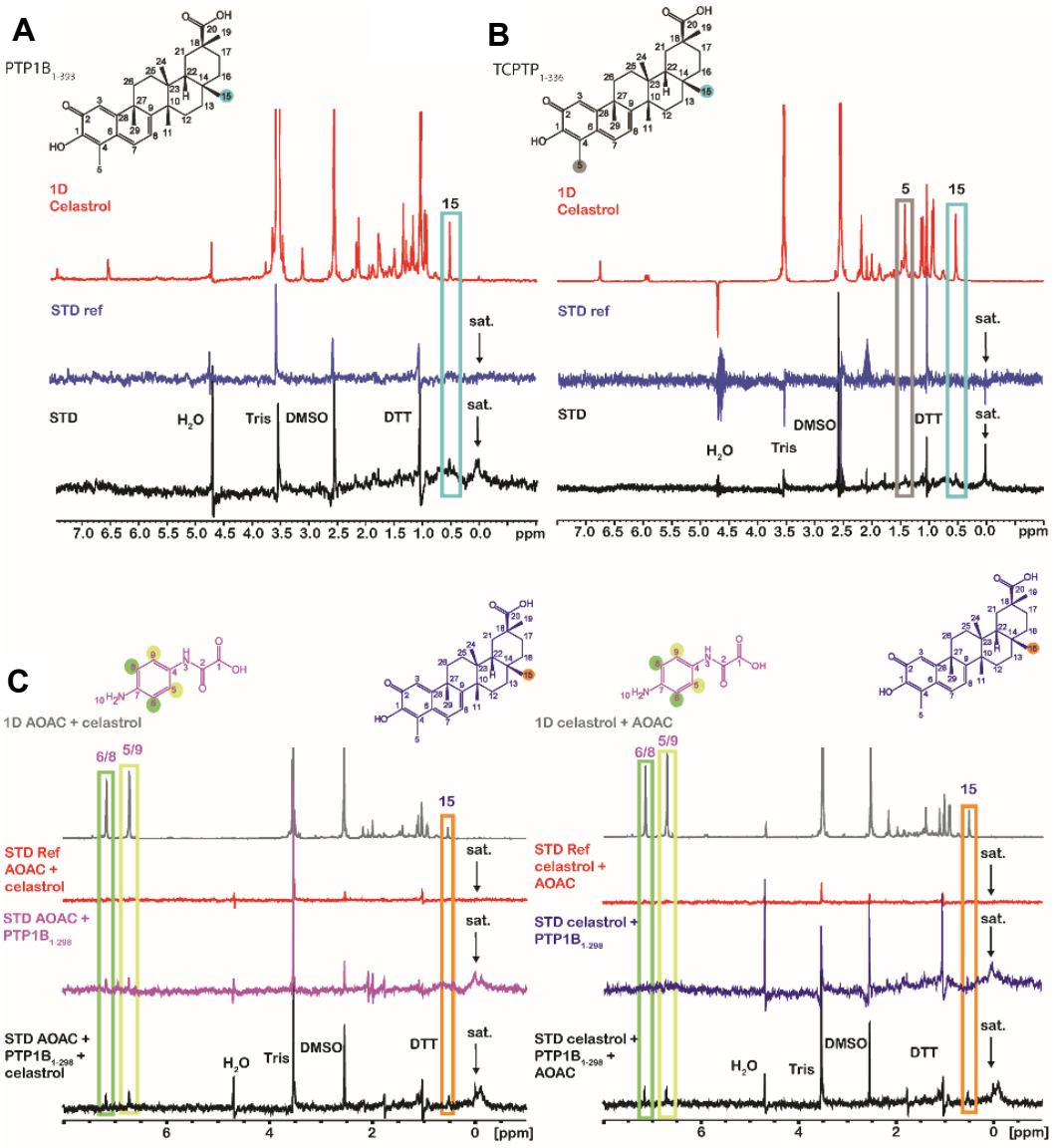

Figure 6.3 STD studies with celastrol.
The red spectrum in both **(A)** and **(B)** corresponds to the 1D spectrum of 500 µM celastrol in NMR buffer, 50 mM d11-Tris pH 7.5, 75 mM NaCl, 5 mM d10-DTT (800 MHz, 20 ºC, 128 scans). Some celastrol peaks are assigned in the spectrum. The blue spectrum in both **(A)** and **(B)** corresponds to the reference STD spectrum of celastrol in NMR buffer. In the black spectra, STD signals from celastrol indicate binding to **(A)** $PTP1B_{1-393}$ (10 µM) and **(B)** $TCPTP_{1-336}$ (10 µM), the numbers denote the celastrol protons for which STD signals are seen. **(C)** Competition STD NMR experiments were performed adding celastrol and AOAC in a different order. On the left, celastrol was added after AOAC, while on the right AOAC was added after celastrol. The grey spectra correspond to the 1D spectrum of 500 µM celastrol and 500 µM AOAC in NMR buffer (800 MHz, 20 ºC, 128 scans), peaks corresponding to each compound are shown. Red spectra correspond to the reference STD spectra of the 2 compounds in NMR buffer. In the pink spectrum (left) STD signals from AOAC are seen, whilst in the blue spectrum (right) STD signals from celastrol are seen. This indicates that both compounds individually bind to the protein. Addition of the second compound (celastrol, left; AOAC, right) leads to additional STD signals but does not lead to a decrease of the STD signals from the first compound (black spectra), indicating that the compounds are noncompetitive. In all STD experiments, the arrow indicates the irradiation region (0.05 ppm) (800 MHz, 20 ºC, 800 scans).

Then 2D $^{1}H,^{15}N$ TROSY NMR experiments were recorded to map the binding site of celastrol onto the structure of PTP1B. For many PTP1B amide resonances chemical shift perturbations (CSP) were observed as well as line-broadening (**Figure 6.4 A**). The CSPs were mapped onto the crystal structure of $PTP1B_{1-321}$ (**Figure 6.4 B**) and indicate that celastrol binds in the vicinity of the active site. A similar experiment was performed for $TCPTP_{1-336}$, and also reveals chemical shift perturbations and line broadening upon addition of celastrol (**Figure 6.5**), thus confirming a similar binding to TCPTP, but the binding site could not yet be mapped.

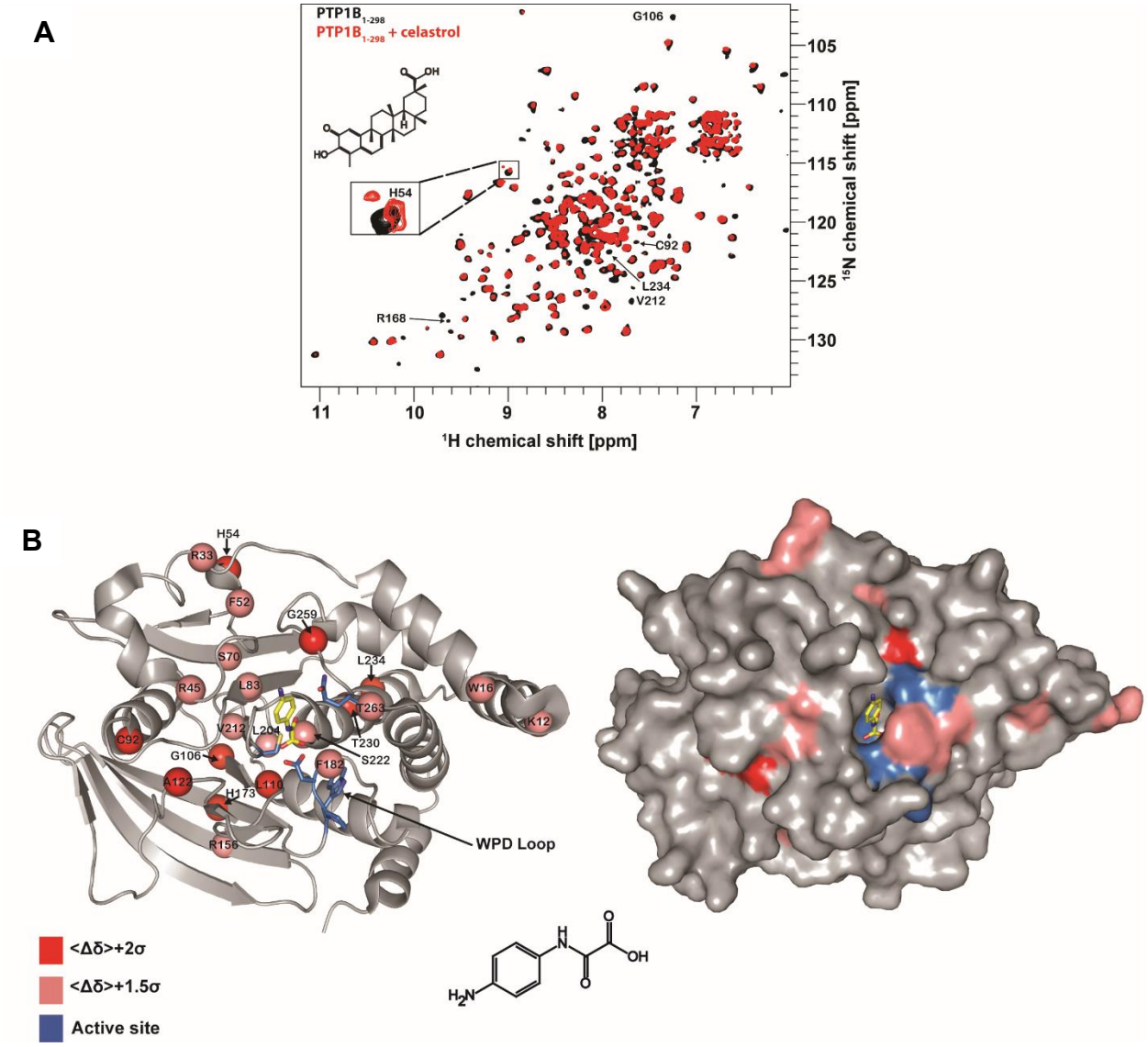

Figure 6.4 Mapping the binding site of celastrol onto PTP1B structure.
(A) Overlay of the 2D $^{1}H,^{15}N$ TROSY spectra of $PTP1B_{1-298}$ (100µM) without (black) and with (red) celastrol (500µM) in in 50 mM d11-Tris pH 7.5, 75 mM NaCl, 5 mM d10-DTT. Insert: zoom of regions where chemical shift perturbations and line broadening are observed. **(B)** Mapping of the PTP1B backbone amides which shift or disappear upon addition of celastrol to $PTP1B_{1-298}$ calculated from the CSPs (Fig. 8). Colored residues indicate 1.5 and 2 s.d. from the mean <Δδ>.

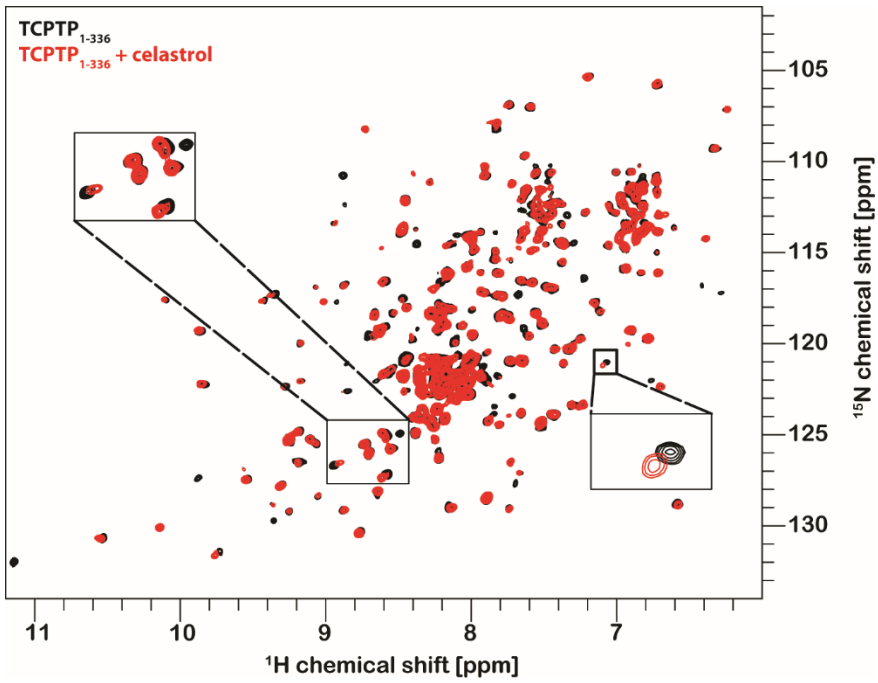

Figure 6.5. Overlay of the 2D $^{1}H,^{15}N$ TROSY spectra of 100µM $TCPTP_{1-336}$ without (black) and with (red) 500µM celastrol in in 50 mM d11-Tris pH 7.5, 75 mM NaCl, 5 mM d10-DTT. Insert: zoom in regions where chemical shifts perturbation and line broadening is observed.

6.3 *In silico* studies with Haddock

The program HADDOCK was used to dock celastrol on PTP1B (Dominguez, Boelens, and Bonvin 2003). For this run a crystal structure of the open conformation of the protein was used (pdb ID: 2HNP) and a pdb file of the compound was produced using the PRODRG Server, the best score gives the cluster with the compound bound in the active site (**Figure 6.6**). This result was unexpected, since the residues affected from the binding of the compound to the protein are around the active site but not in the active site. In combination to the kinetic studies, showed that the compound is non-competitive, these results cannot be trusted.

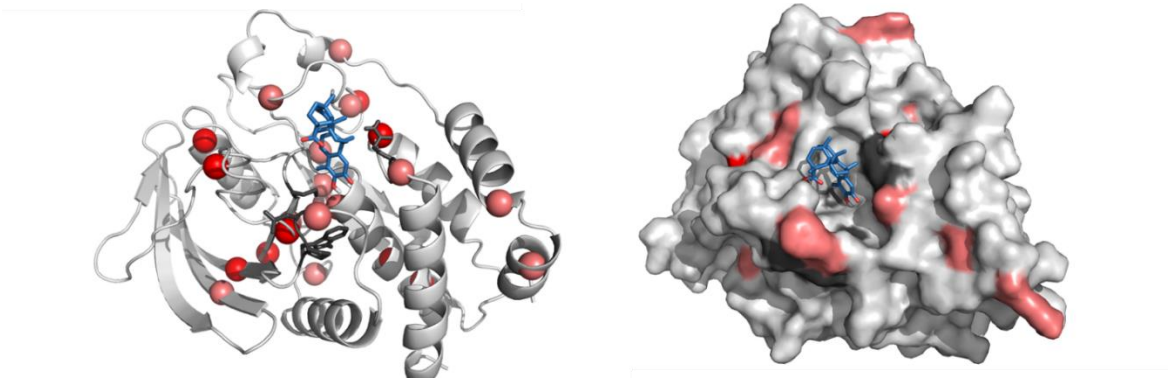

Figure 6.6 3D Structural representation of the best score cluster from HADDOCK.
On left side, a cartoon representation is shown, while on the right a surface representation is shown.

6.4 Cell assay with celastrol

Initially, a dose response experiment with celastrol was performed to find out which is the less harmful dose for the cells. It was found that 1 μM is the best dose. For the analysis of the results, western blots were performed (**Figure 6.7**). The experiment was performed like before, confluent neuronal CLU-177 cells were serum starved for 6 hour and then incubated with or without celastrol. Control cells were treated with or without insulin (100ng/mL), leptin (10ng/mL) and growth factor (200 ng/mL, 85 ng/mL, 30 ng/mL) for 10 min prior to harvest. Equal amounts of protein were separated by SDS-PAGE and phosphorylated proteins were detected by immunoblot analysis. protein p-AKT was detected, which is a component of insulin signaling pathway, p-STAT3, p-STAT5 and p-JAK2, which are involved in leptin signaling and p-ERK1/2, which is part of growth hormone pathway (**Figure 6.8 and Figure 6.9**). It was observed that celastrol enhances significantly AKT phosphorylation. p-STAT3 protein was not possible to be detected, most probably because there is not sufficient protein expression. For protein p-STAT5 and p-JAK2 was not observed any significant influence from celastrol, but most probably because of the short time of the cell incubation with the stimulus and the compound. Finally, for p-ERK1/2 no effect from celastrol treatment was seen, meaning that celastrol is not affecting the growth hormone pathway.

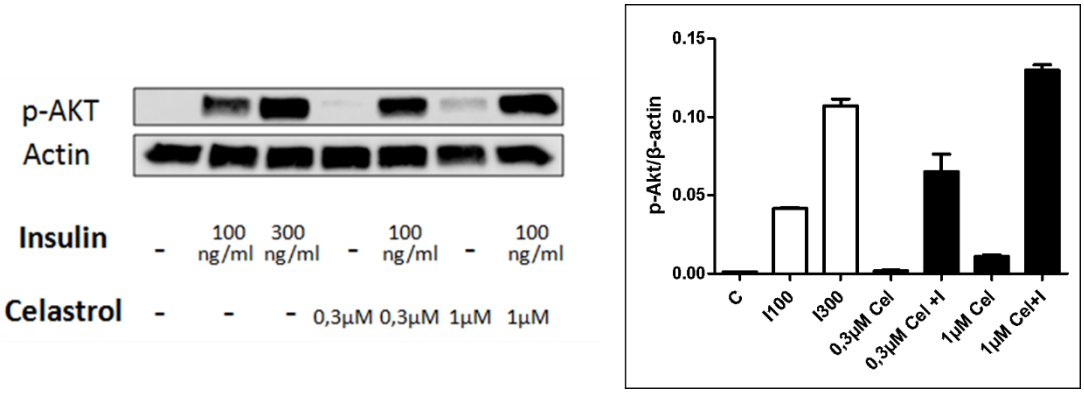

Figure 6.7 p-AKT immunoblot analysis.
Immunoblot analysis of the phosphorylated proteins **(left)** and quantification **(right)** of the immunoblot analysis for p-AKT(S473) from Cell Signaling. Experiment was repeated 3 times.

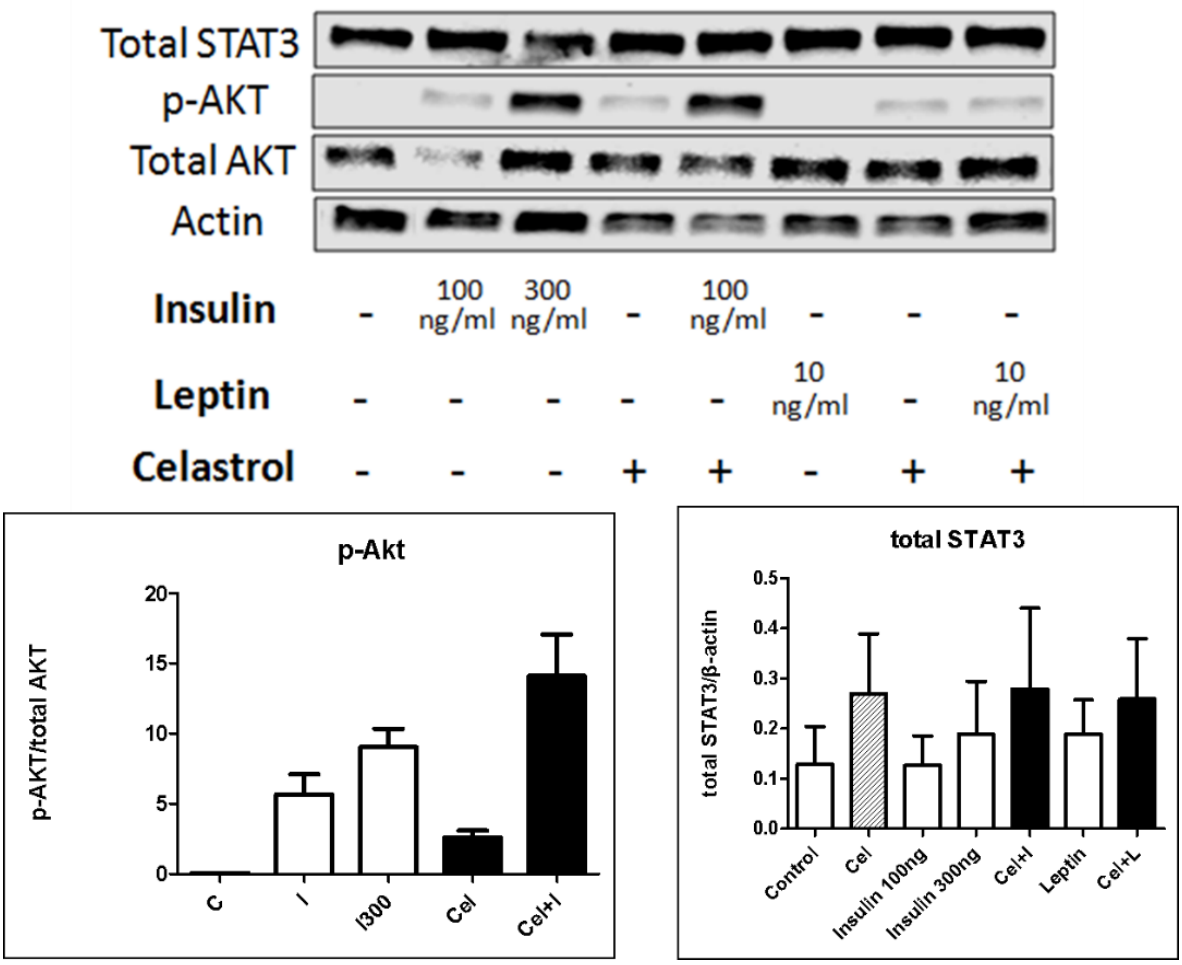

Figure 6.8 Immunoblot analysis of the AKT and STAT3 proteins.
Immunoblot analysis of the phosphorylated proteins **(top)** and quantification of the immunoblot analysis for p-AKT(S473) from Cell Signaling **(left bottom)** and for total STAT3 **(right bottom)**. Experiments were repeated 3 times.

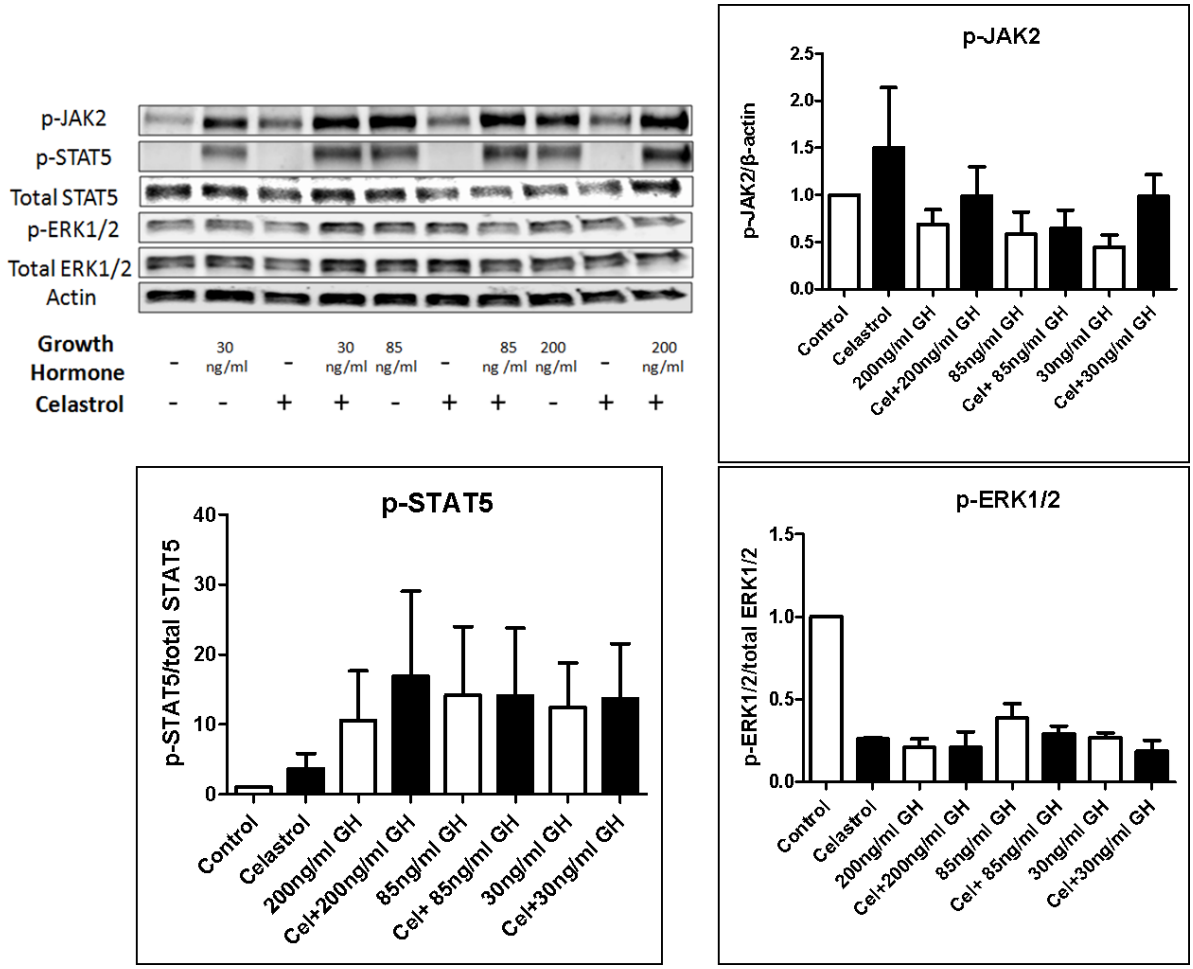

Figure 6.9 Immunoblot analysis of JAK2, STAT5 and ERK1/2 proteins.
Immunoblot analysis of the phosphorylated proteins **(top left)** and quantification of the immunoblot analysis for p-JAK2 **(right top)**, for p-STAT5 **(left bottom)** and for p-ERK1/2 **(right bottom)**. Experiments were repeated 3 times.

6.5 Withaferin A

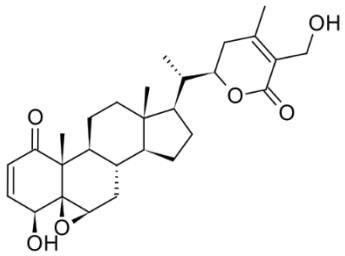

Withaferin is a steroidal lactone with a wide range of pharmacological activities that has similar mRNA expression profile to that of celastrol. Recently it has been revealed that withaferin A has strong antidiabetic properties (Lee et al. 2016). Initially, withaferin A was tested with the activity assay. The inhibition of this compound to PTP1B is very weak (milimolar range) and even weaker for TCPTP (**Figure 6.10**). Experiment will be repeated with fresh protein.

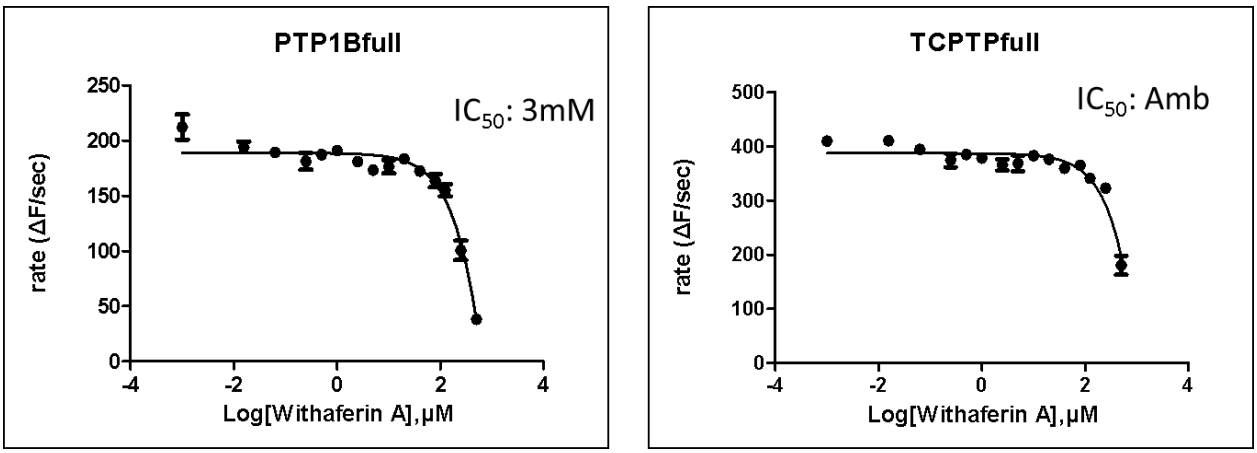

Figure 6.10 Fluorescence curves for withaferin A for PTP1B$_{1-396}$ (left) and TCPTP$_{1-336}$ (right).

6.6 Celastrol reactivity

Celastrol is known to undergo Michael addition with biological sulfur nucleophiles (Klaić et al. 2011). Because of that the reactivity of celastrol under different buffer conditions was investigated. By running 1D NMR experiments (**Figure 6.11**) was found that celastrol in presence of the reducing agent DTT in the NMR buffer conditions (100 mM d11-Tris-HCl pH 7.5, 75mM NaCl, 5 mM d10-DTT) changes from dark orange to completely discolored, suggesting that it undergoes structural rearrangement. Our first hypothesis was that celastrol was reduced to dihydrocelastrol (**Figure 6.12**) under these conditions. For this reason the compound dihydrocelastrol was synthesized as previously described by Klaic and colleagues (Klaić et al. 2011) using as starting material celastrol (**Figure 6.12)**. The purity of the compound was tested by LC-MS and by NMR and it was found to be 97% pure while 3% was celastrol, most probably as reoxidation product.

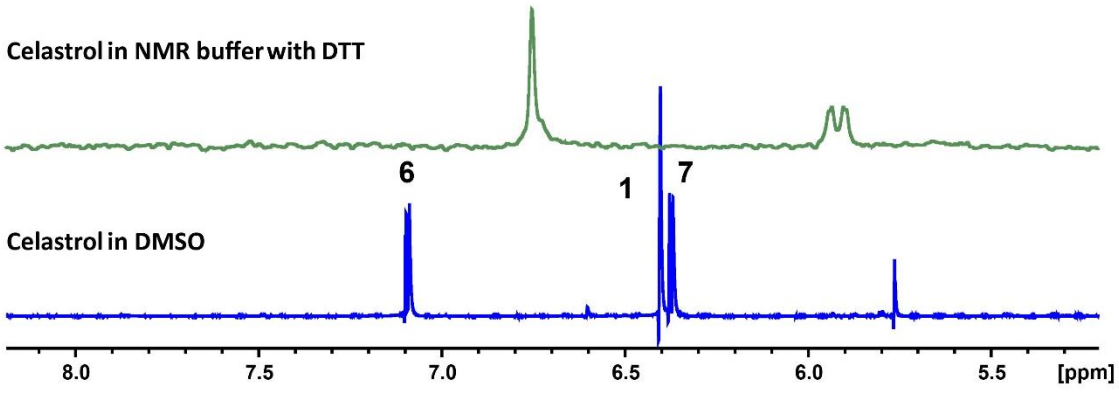

Figure 6.11 Celastrol in presence of DTT undergoes structural changes.

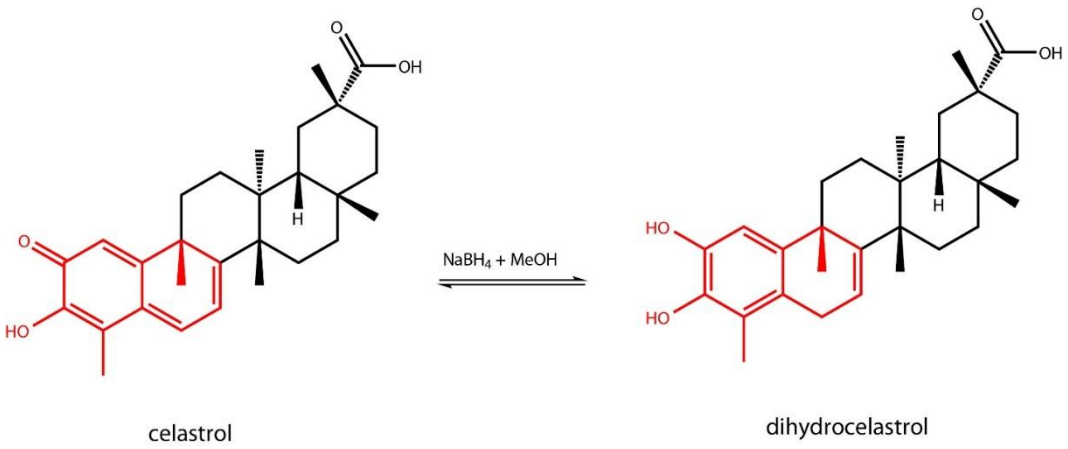

Figure 6.12 Reduction reaction of celastrol to dihydrocelastrol.

By running a 2D ^{1}H-^{15}N TROSY of $PTP1B_{1-298}$ with dihydrocelastrol was tested whether the compound induces the same chemical shifts on the protein spectra as celastrol in the same NMR buffer conditions. In the **Figure 6.13** is shown the 2D ^{1}H-^{15}N TROSY spectrum, where some chemical shift perturbations and line broadening are observed but not as dramatic as in case of celastrol under the same conditions, indicating that either: 1) the product of celastrol with DTT might differ from dihydrocelastrol or 2) that both the left (highlighted with red color) and the right (highlighted with black color) parts of celastrol are important for the binding to PTP1B (**Figure 6.12**).

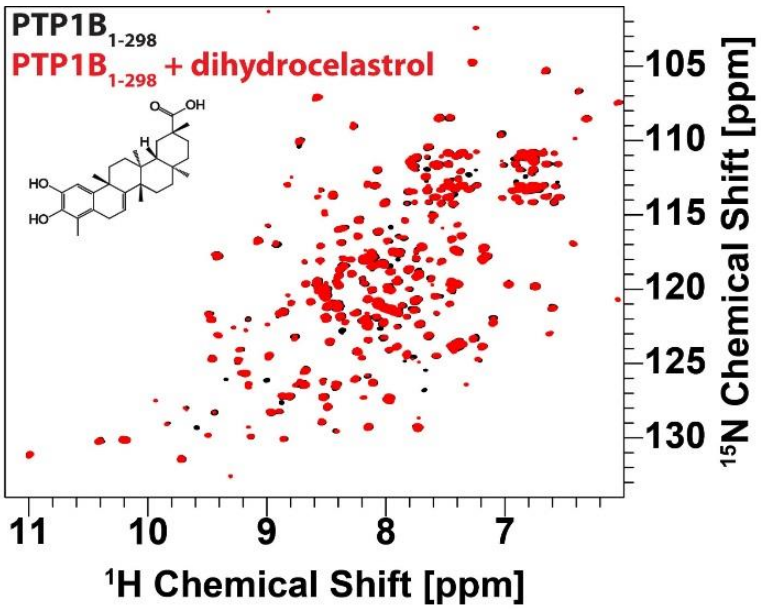

Figure 6.13 Superposition of 2D ^{1}H-^{15}N correlation spectra of 100 µM $PTP1B_{1-298}$ recorded without (black) and with 500 µM dihydrocelastrol (red) in 100mM d11-Tris-HCl buffer pH 7.5, 75 mM NaCl, 5 mM d10-DTT (800 MHz, 20 ºC, 16 scans)

DiFMUP assay was also used in order to determine the inhibitory ability of a dihydrocelastrol against $PTP1B_{1-393}$ and $TCPTP_{1-336}$. It was found that the compound inhibits both compounds in milimolar range in comparison to low micromolar in case of celastrol (**Figure 6.14**).

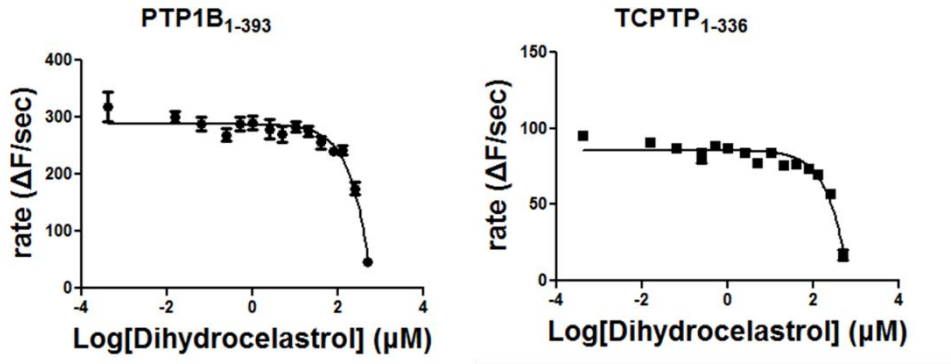

Figure 6.14 Activity assay results for dihydrocelastrol.
Inhibition curves of PTP1B **(left)** and TCPTP **(right)** in the presence of dihydrocelastrol using DiFMUP as a substrate. The fitting is ambiguous. (Buffer conditions: 25 mM Bis-Tris propane pH 7.5, 50 mM NaCl, 2 mM EDTA, 2 mM DTT)

Comparison of the 1D spectrum of the dihydrocelastrol with celastrol under different buffer conditions revealed that the product of celastrol with DTT is not dihydrocelastrol (**Figure 6.15**). Celastrol in DMSO-d6 (Figure 4, blue spectrum) and in NMR buffer without DTT (**Figure 6.15**, red spectrum) give the same pattern of peaks corresponding to the aromatic part of the compound. On the other hand, celastrol in NMR buffer in presence of DTT (**Figure 6.15**, green spectrum) shows a different pattern of peak arrangement, indicating that celastrol interacts with DTT. The corresponding spectra of dihydrocelastrol (**Figure 6.15**, purple, yellow, orange spectra) indicate that the compound is not affected from the presence of DTT and that it differs from the celastrol product with DTT. They differ mostly in the peak, which in the case of dihydrocelastrol is a doublet attributed to proton 7, whereas in celastrol with DTT (**Figure 6.15**, green spectrum) appears as a doublet of the doublet or as two doublets.

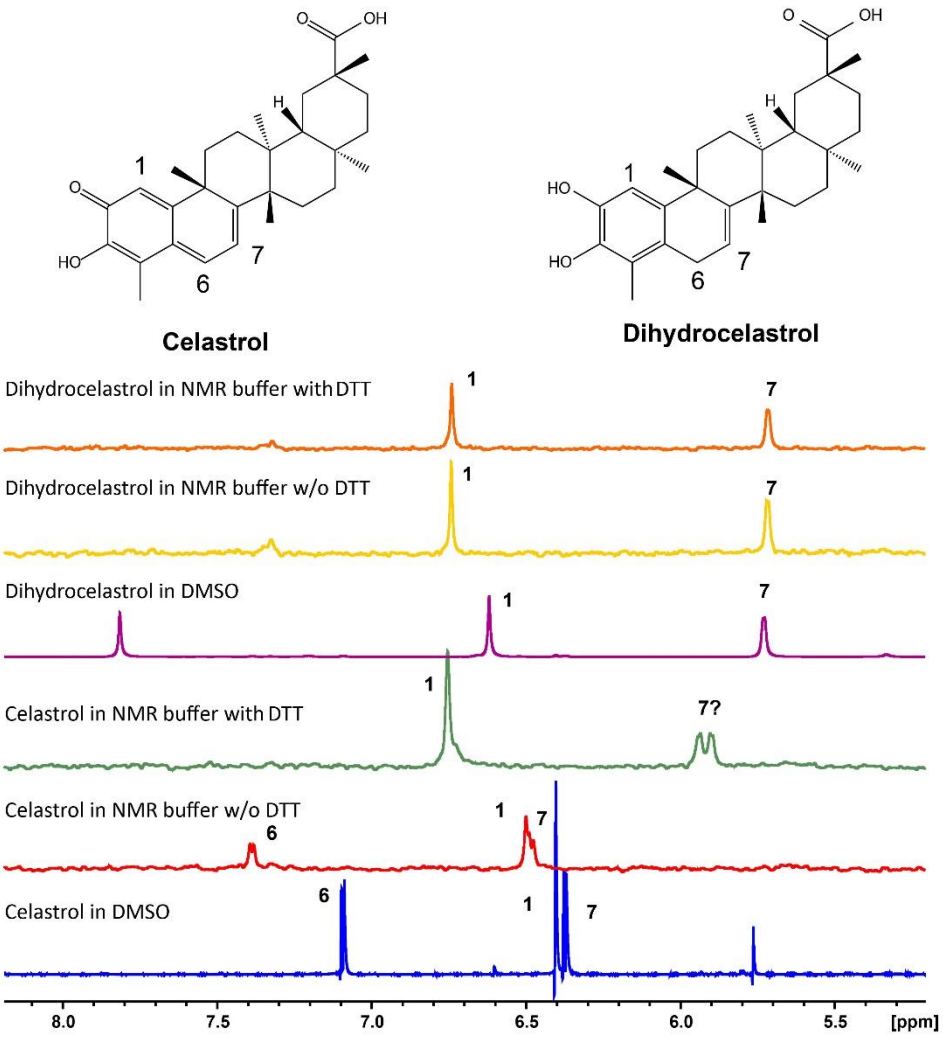

Figure 6.15 Comparison of the 1D spectra of celastrol and dihydrocelastrol under different conditions. Superposition of proton 1D spectra of celastrol (blue, red, green) and dihydrocelastrol (purple, yellow, orange) under different buffer conditions.

In an attempt to identify exactly the product of celastrol with DTT, ^{1}H-^{13}C HSQC and HMBC NMR experiments were run (**Figure 6.16**). The assignment could not be unambiguously completed. So far it was concluded that the peak at around 6 ppm marked as 7? (**Figure 6.16**, green spectrum) is the superposition of two doublets, because there are two resonances in the HSQC. Further, it was concluded that there is more than one product in the sample, one of those is the complex of celastrol with DTT. This is evident from the characteristic crosspeak in the HMBC spectrum of the DTT peaks with celastrol peaks. One more observation is that the same peak in DMSO looks like two triplets instead of two doublets as they were shown in NMR buffer with

DTT. A possible explanation could be that the complex of celastrol with DTT is more stable in DMSO and therefore detectable in NMR.

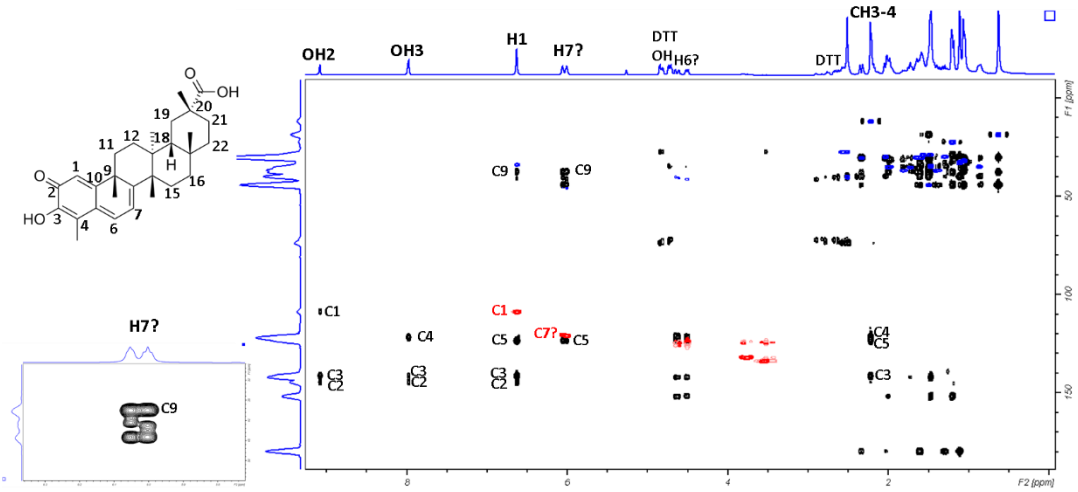

Figure 6.16 Superposiiton of ^{1}H-^{13}C HMBC (black), ^{1}H-^{13}C HSQC aromatic (red) and HSQC aliphatic (blue) of 15 mM celastrol with 15 mM DTT in DMSO-d6 (500 MHz, 20 ºC, HMBC ns:160 HSQC aromatic ns:60 HSQC aliphatic ns:60)

HPLC-MS was performed as a last experiment in order to find out if the complex of celastrol with DTT is formed. Celastrol has been tested with a mixture of glutathione/glutathione disulfide (GSH/GSSG) in a ratio of 1:10, which corresponds to the physiological ratio in the blood plasma (Aquilano, Baldelli, and Ciriolo 2014), in order to figure out what is happening when celastrol enters the human body. Another reducing agent, TCEP, was tested in order to be used as an alternative in case that it doesn't react with celastrol. In **Table 6.1** are shown all the results from the HPLC-MS experiments. Celastrol reacts with GSH giving an adduct product with molecular weight (MW) equal to the sum of celastrol and GSH. Similarly, celastrol reacts with TCEP forming an adduct molecule. Last, celastrol seems to not interact with DTT or d10-DTT giving in water-based buffer a peak in HPLC that corresponds to the same molecular weight as celastrol. However, the retention time is different, indicating that the formed compound is different than celastrol, most probably is an isoform of it. In summary, it was concluded that celastrol doesn't bind covalently to DTT, otherwise the adduct molecule should have been seen in our experimental conditions.

Table 6.1 Results of the HPLC-MS measurements on celastrol with different nucleophiles.

Name of the LC-MS sample	Sample	MW of each reaction component		Experimental MW	Retention time (main peak)
		component	MW		
EIK-01	Celastrol	Celastrol	450.26	451.01	4.37min
EIK-02	Celastrol + GSH/GSSG (10:10:1)	Celastrol GSH GSSH	450.26 307.32 612.63	757.83 (complex of celastrol with GSH)	2.81min
EIK-03	Celastrol +DTT (excess of DTT)	Celastrol DTT	450.26 154.25	451.00	3.58min
EIK-04	Celastrol + d10-DTT (excess of DTT)	Celastrol D10-DTT	450.26 164.31	451.00	3.56min
EIK-05	Celastrol + TCEP	Celastrol TCEP	450.26 250.19	700.70 (complex of celastrol with TCEP)	2.72min

Since it was found that celastrol is not stable when DTT is present in the buffer conditions, all previously done experiments should be repeated in buffer conditions without DTT. The reason is that it's important to be sure that the inhibitory effect observed is due to celastrol and not due to its product from the reaction with DTT.

6.7 Activity assay

The DiFMUP activity assay was performed exactly the same way as previously described with the only difference being the elimination of DTT from the buffer conditions (**Figure 6.17**). Again, celastrol inhibits PTP1B and TCPTP constructs with low micromolar IC_{50} values (**Figure 6.17 A-D**). Using the same assay, the type of inhibition was determined and it was shown that celastrol is a non-competitive inhibitor for both phosphatases, since the K_m does not change and the V_{max} decreases (**Figure 6.17 E-F**). Reversibility of the inhibition was checked by incubating 1 nM protein with 5 µM celastrol, or with equivalent volume of DMSO in reaction buffer for 10 min (**Figure 6.17 G-H**). The reaction was started by addition of 5 µM DiFMUP and was monitored continuously for 40 min. Further addition of DiFMUP or DiFMUP and H_2O_2 revealed that the inhibition is reversible. H_2O_2 was used as a negative control (Salmeen et al. 2003).

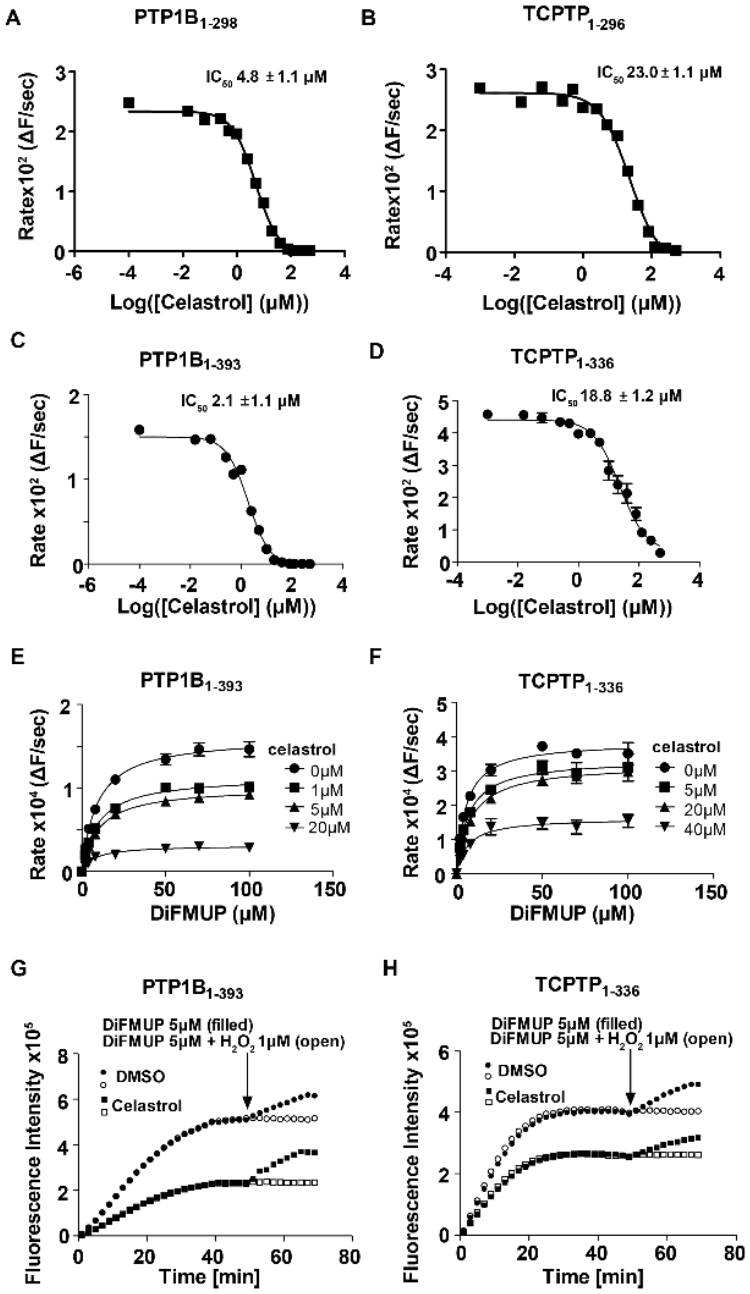

Figure 6.17 Activity assay results for celastrol without DTT in the buffer conditions.
(A-D) Inhibition curves of PTP1B **(left) (A,C)** and TCPTP **(right) (B,D)** constructs in the presence of celastrol using DiFMUP as a substrate. Biphasic fitting from nonlinear regression analysis was used to obtain IC50 values. **(E,F)** $PTP1B_{1-393}$ **(left)** and $TCPTP_{1-336}$ **(right)** were incubated with different amount of substrate DiFMUP (0-100 μM) in the absence and presence of celastrol at three different concentrations. Data were fitted with Michaelis-Menten equation. **(G,H)** Reversibility of inhibition by celastrol. 1 nM $PTP1B_{1-393}$ **(G)** and $TCPTP_{1-336}$ **(F)** were incubated with 5 μM celastrol (■□) and with an equivalent volume of DMSO (●○) for 10 min in buffer assay. Reactions were initiated by addition of 5 μM DiFMUP and monitored for 50 min. Reversibility of the reaction was checked by further addition of 5 μM DiFMUP (filled symbols) or 5 μM DiFMUP and 1 μM H_2O_2 (open symbols), indicated by an arrow.

6.8 NMR studies

The competitive STD experiments with celastrol and 4'-aminoxanilic acid (AOAC) was also repeated but without DTT in the buffer conditions. The results were the same in this case too. Either starting with celastrol or with AOAC, addition of the other compound, did not lead to reduction on the intensity of the signals of the first compound with both compounds showing signals simultaneously (**Figure 6.18**). This indicates that both compounds can simultaneously bind to the protein and do not compete with each other.

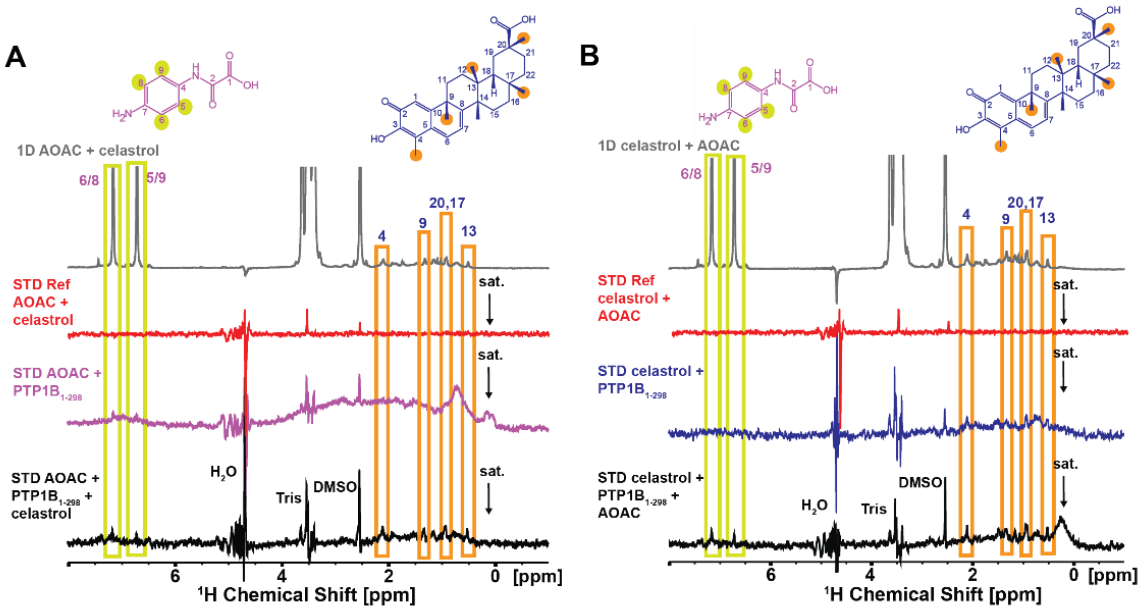

Figure 6.18 Competition STD NMR experiments without DTT were performed by adding celastrol and the active site inhibitor AOAC in different order.
(A) celastrol was added after AOAC, while on **(B)** AOAC was added after celastrol. The grey spectra are recorded with 500 µM celastrol and 500 µM AOAC in d11-Tris-HCl pH 7.5, 75 mM NaCl and 10% D_2O buffer (600 MHz, 20 ^oC, 128 scans), characteristic signals of the two compounds are highlighted. Red spectra correspond to the reference STD spectra of the two compounds in buffer. The violet spectrum **(A)** shows STD signals of the active site inhibitor AOAC, and the blue spectrum **(B)** shows STD signals for celastrol. Thus, both compounds can simultaneously bind to the protein. Addition of the second compound (celastrol, **(A)**; AOAC, **(B)**) leads to additional STD signals but does not decrease the STD signals observed upon addition of the first compound (black spectra), indicating that the compounds are non-competitive and can bind simultaneously to the protein. In all STD experiments, the arrow indicates the irradiation region (0.05 ppm) (600 MHz, 20 ^oC, 800 scans).

Then 2D ^1H-^{15}N TROSY NMR experiments were recorded using a NMR buffer without DTT to map the binding site of celastrol onto the structure of PTP1B. For many PTP1B amide resonances similar chemical shift perturbations (CSPs) were observed as well as line-broadening as before (**Figure 6.19**). The CSPs were mapped onto the crystal structure of $PTP1B_{1-321}$ and indicating that celastrol binds in the vicinity of the active site. A similar experiment was performed

for TCPTP$_{1-336}$, and also reveals chemical shift perturbations and line broadening upon addition of celastrol (**Figure 6.20**), thus confirming a similar binding to TCPTP, but the binding site could not yet be mapped due to lack of assignment.

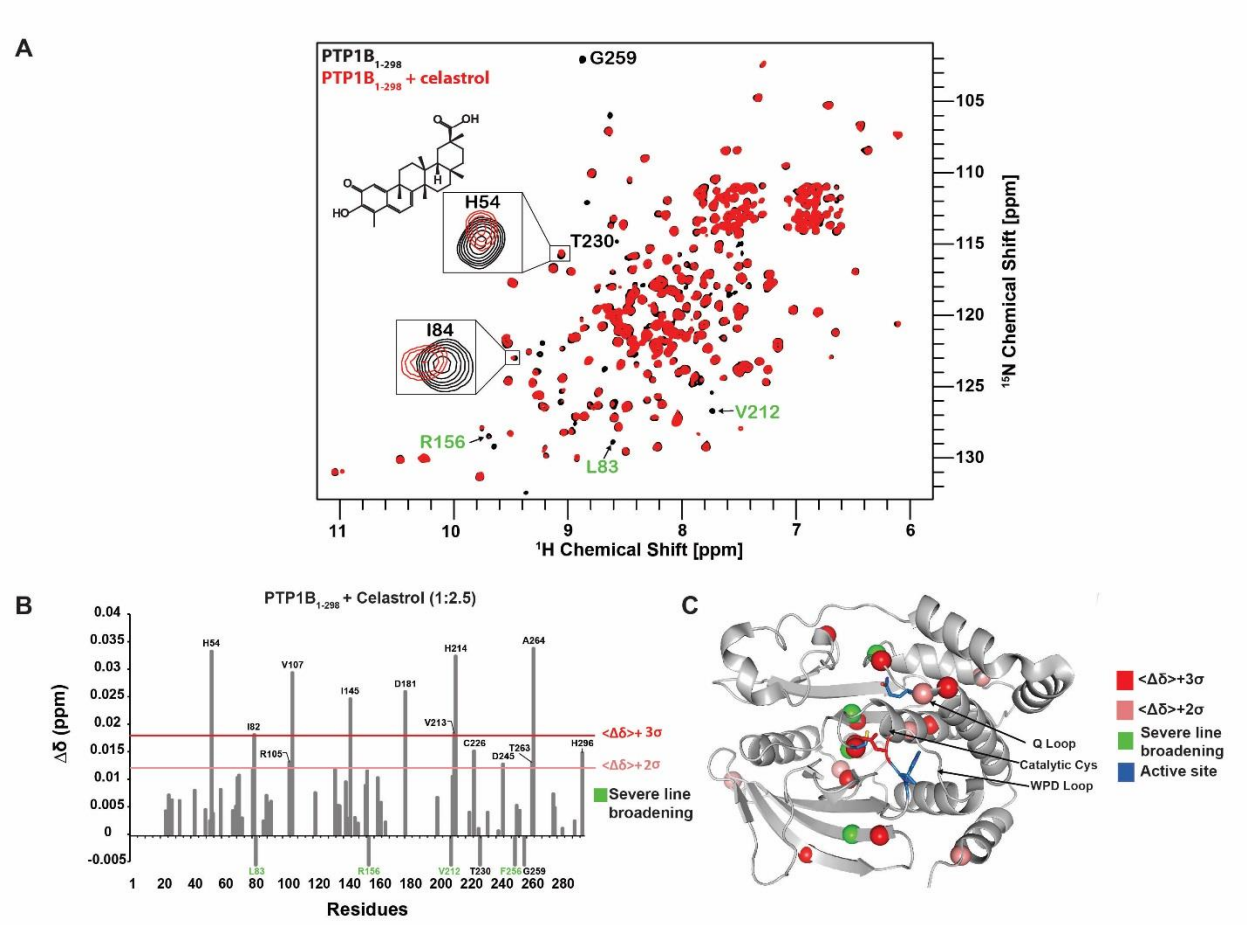

Figure 6.19 Mapping the binding site of celastrol into PTP1B crystal structure.
(A) Superposition of 2D ^{1}H-^{15}N correlation spectra of 100 μM PTP1B$_{1-298}$ recorded without (black) and with 500 μM celastrol (red) (800 MHz, 20 ^{o}C, 16 scans). **(B)** Chemical shift perturbations (CSP, Δδ) observed upon celastrol binding to PTP1B1-298. Colored lines indicate 2 and 3 σ standard deviation from the mean <Δδ>. **(C)** Mapping of the spectral changes upon titration of celastrol onto the structure of PTP1B (1WAX). NMR signals of amide groups in PTP1B$_{1-298}$ that experience CSPs above 2 and 3 standard deviations (SDs) from the mean <Δδ> are represented as spheres and colored salmon and red, respectively, with green color are represented residues with strong line broadening.

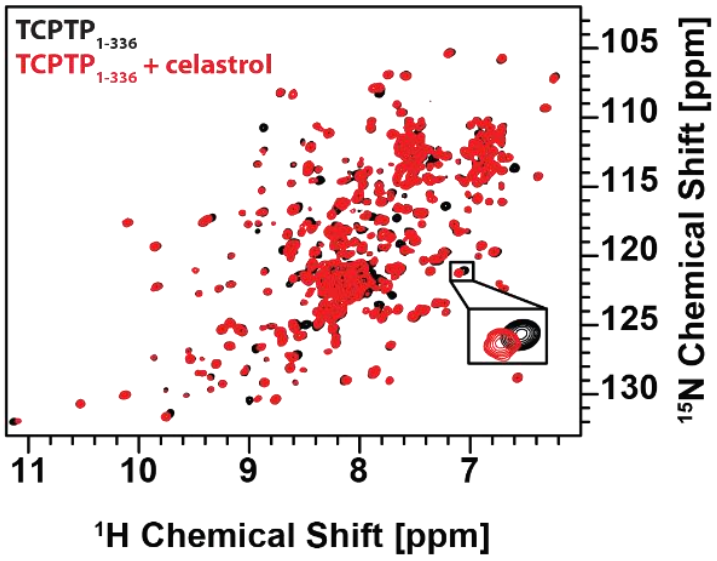

Figure 6.20 Overlay of the 2D $^{1}H,^{15}N$ correlation spectra spectra of 100 µM $TCPTP_{1-336}$ without (black) and with 500 µM celastrol (red). Insert: zoom of regions showing CSPs and line broadening upon celastrol binding

6.9 MALDI-TOF analysis

In order to evaluate what kind of interaction is taking place between PTP1B and celastrol, a mass spectrometry analysis of the mixture of $PTP1B_{1-298}$ with celastrol was performed in NMR buffer containing and without containing DTT (**Figure 6.21**). the molecular mass revealing that celastrol does not bind covalently to the protein, which is consistent with reversible inhibition.

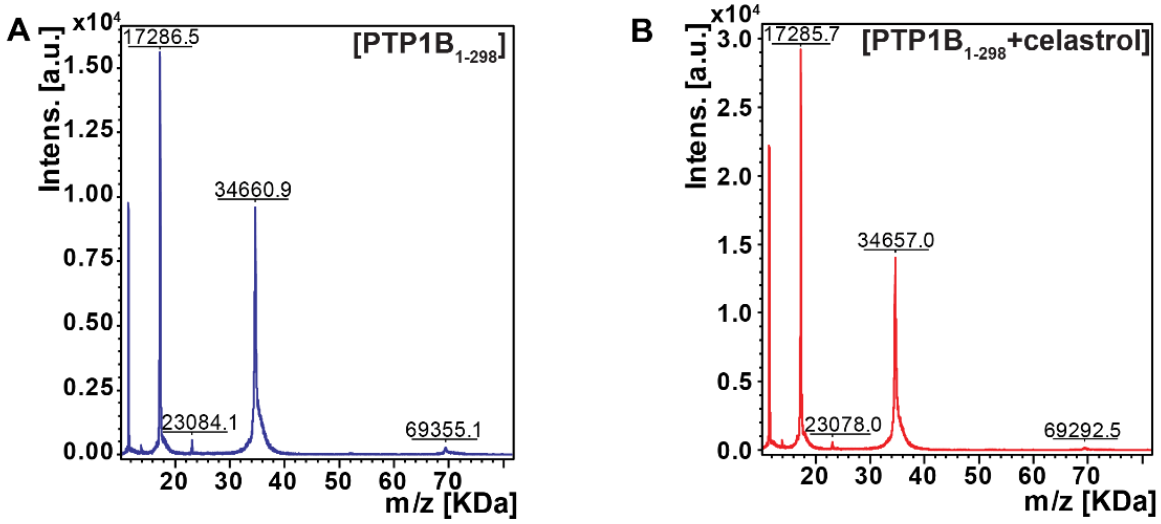

Figure 6.21 Mass spectrometry analysis.
Mass spectrometry analysis of $PTP1B_{1-298}$ with **(B)** and without **(A)** celastrol. After incubating $PTP1B_{1-298}$ with celastrol, the molecular weight of the $PTP1B_{1-298}$-celastrol complex was investigated by MALDI-TOF. There was no molecular mass difference, indicating that celastrol does not bind covalently to $PTP1B_{1-298}$.

6.10 SOCS3 protein

SOCS3 protein is a suppressor of the cytokine signaling 3 (White and Nicola 2013). Our collaborators in Australia aimed to assess whether celastrol mediates leptin resensitization via inhibition of hypothalamic PTP1B and TCPTP using mice genetically engineered to be homozygous for lox-P-flanked PTP1B (PTPN1), TCPTP (PTPN2) and Suppressor-of–cytokine-signaling-3 (SOCS3). Subsequent infusion of a Cre-expressing adeno-associated virus (AAV) into the arcuate nucleus (CreArc), which led to genetic deletion of PTP1B and TCPTP (CreArc), largely abolished the weight-lowering and hypophagic efficacy of celastrol (data not shown). SOCS3 was co-deleted to avoid previously reported compensatory mechanisms for the absence of PTP1B. To confirm that the loss of celastrol's weight lowering effects in mice with genetic ptpn1/ptpn2/socs3 deletion in ARC are derived only by PTP1B and TCPTP and not by SOCS3, SOCS3 protein, which was kindly provided by professor Jeffrey J. Babon, was expressed and purified. Purified SOCS3 protein was then used for NMR titration experiments of celastrol. CSPs or line broadening on SOCS3 upon celastrol addition (**Figure 6.23**) were not observed, confirming that celastrol does not bind to SOCS3.

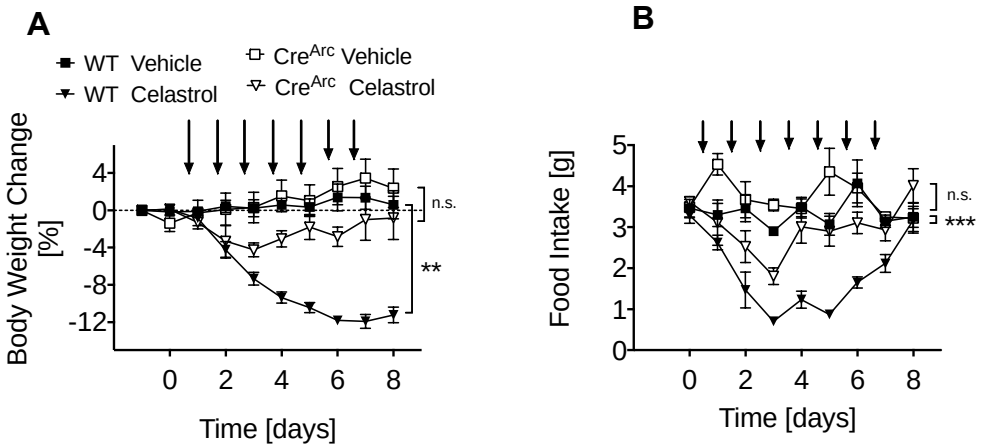

Figure 6.22 Celastrol drives weight loss via PTP1B and TCPTP.
Effects of daily celastrol treatment (100 µg/kg; sc injections indicated by arrows) on BW **(A)** and FI **(B)** in HFD-fed mice homozygous for loxP-flanked alleles of Ptpn1 (PTP1B), Ptpn2 (TCPTP) and SOCS3 (n=4; $Ptpn1^{fl/fl}Ptpn2^{fl/fl}Socs3^{fl/fl}$). Vehicle or celastrol was administered before (WT) and after infusion of a Cre-expressing adeno-associated virus (AAV-Cre) into the arcuate nucleus (Cre^{Arc}).

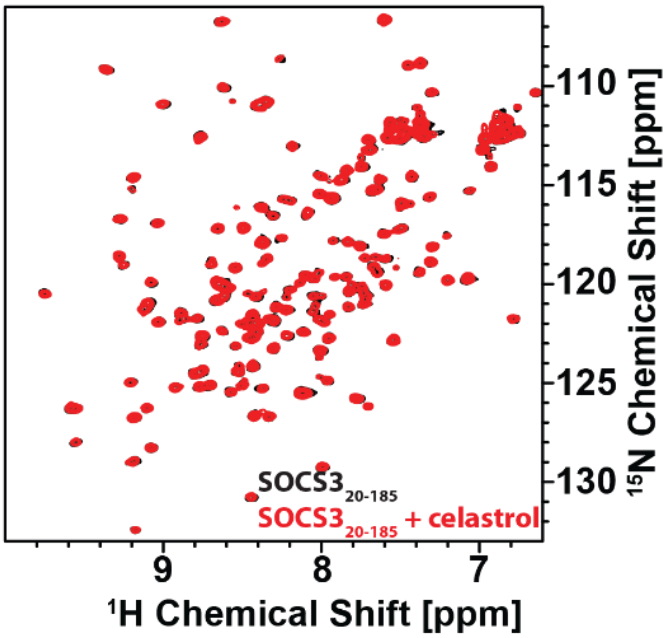

Figure 6.23 Overlay of the 2D ^{1}H-^{15}N correlation spectra spectra of 30 µM SOCS3$_{20-185}$ without (black) and with 500 µM celastrol (red). No changes are observed between the two spectra.

6.11 SwitchSENCE

SwitchSENSE technology (Langer et al. 2013) was used as an alternative method to confirm binding and determine the affinity of celastrol to surface-immobilized PTP1B$_{1-298}$. Protein conjugation to DNA nanolevers was successful and sufficient for about 420 full chip regeneration cycles. In **Figure 6.24** are shown all the hybridization traces that were recorded during the PTP1B experiments performed.

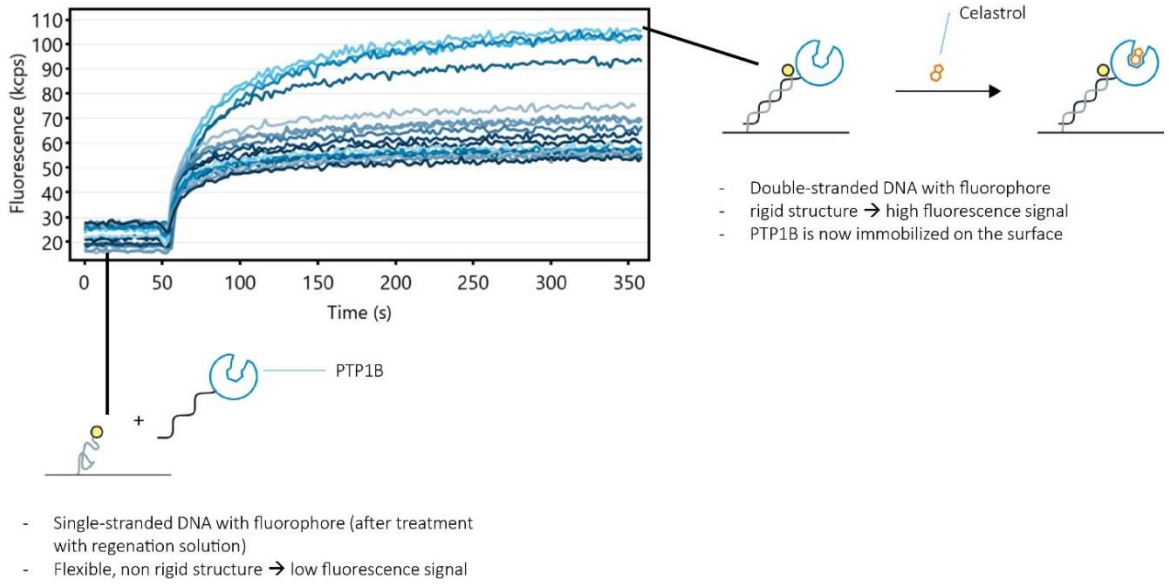

Figure 6.24 Hybridization traces of PTP1B$_{1-298}$ with single stranded DNA with fluorophore.

Initially, a sizing experiment of the protein was performed. In the switchSENSE technology, time resolved fluorescence intensity measurements are used to characterize the switching dynamics when the DNA nanolevers are electrically actuated, as shown in the **Figure 6.25** for the upward motion of double-stranded DNA. The transition of the DNA nanolevers from lying to standing state is marked by a distinct increase of the fluorescence intensity. A hydrodynamic model, called the lollipop model, evaluates these changes and yields the hydrodynamic diameter (D_H) of the attached protein. For covalently immobilized $PTP1B_{1-298}$ a D_H of 3.92 ± 0.03 nm was determined.

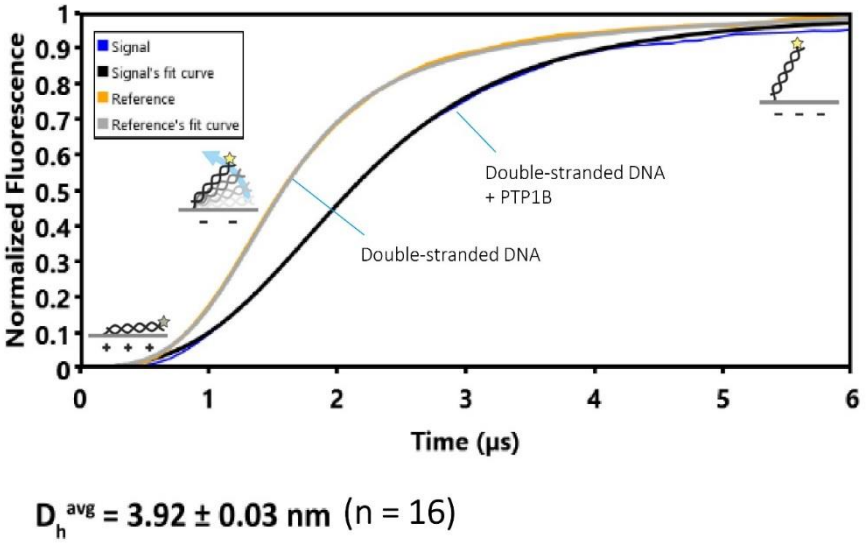

Figure 6.25 Sizing experiment of $PTP1B_{1-298}$.

Then the structural effects of celastrol on $PTP1B_{1-298}$ size were tested and the hydrodynamic diameter was compared with the size of different conformation protein structures. In presence of 50 µM celastrol, the hydrodynamic diameter of the protein increased significantly to 4.18 ± 0.09 nm (**Figure 6.26**). This indicates that the binding of celastrol to $PTP1B_{1-298}$ causes an increase in the hydrodynamic friction, potentially by triggering a conformational change of the molecular structure towards a less compact folding state. For evaluation of the hydrodynamic diameters, the switchANALYSIS software features an evaluation tool that can model the hydrodynamic properties based on a molecular structure (Ortega, Amorós, and García de la Torre 2011) in a comparison to hydrodynamic diameters that were modelled from PTP1B crystal structures in both open and closed conformation, the experimental D_H values determined by switchSENSE agree well to the theoretical data. Nevertheless, the hydrodynamic diameters that

were derived from PTP1B crystal structures exhibit values between 5.19 nm and 5.38 nm, suggesting an offset to the experimental data of about 1 nm (**Table 6.2**).

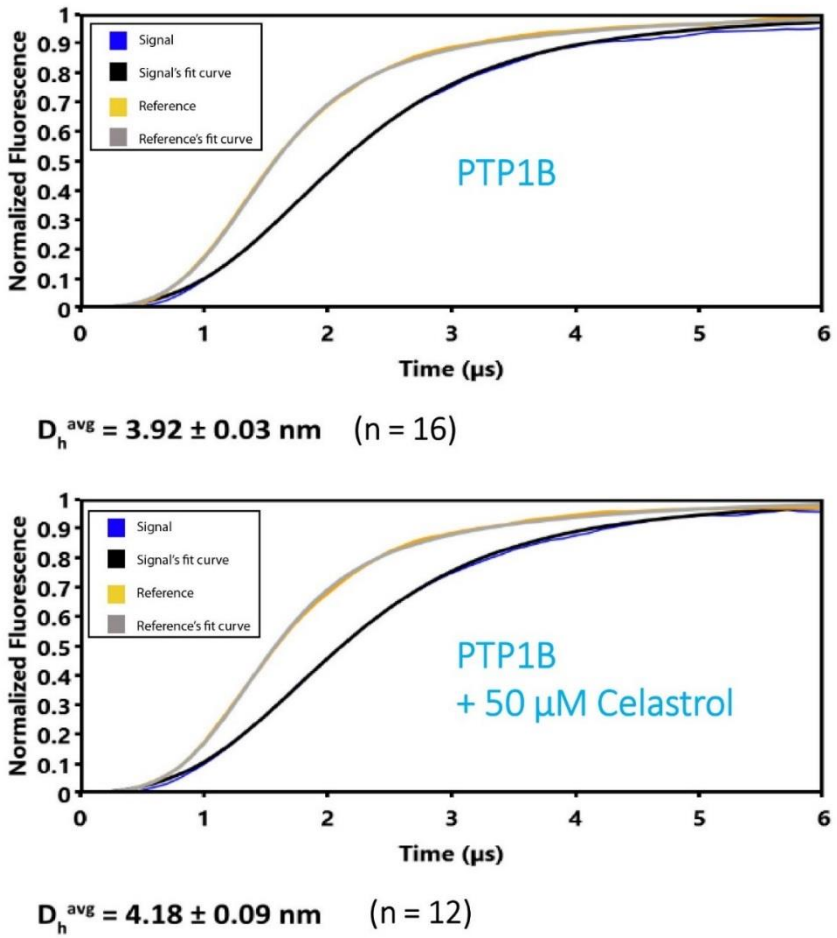

Figure 6.26 Celastrol changes the PTP1B conformation

Table 6.2 Theoritical DH values calculates from PTP1B crystal structures.

PDB	Residues*	Modeled D_H (nm)**	Conformation
2HNP	5-282	5.19	Open
1WAX	2-282	5.29	Closed
1T4J	1-298	5.38	Open

*Residues that are included in the crystal structure.

**Hydrodynamic diameter derived from crystal structure after Ortega et al., 2011.

Binding of celastrol to surface-immobilized PTP1B can be clearly detected by changes of the absolute fluorescence intensity. The binding signals can be well described by a global exponential fit, yielding a K_D of 6.1 µM (**Figure 6.27**). This is in agreement with a previously determined IC_{50} value of 4.8 µM. Celastrol binds to PTP1B with slow association and dissociation rates. This combination of slow association rate constant (K_{on}) with a slow dissociation rate

constant (K_{off}) is not very common. Typically, a slow K_{on} is indicative of a fairly weak affinity, whereas slow K_{off} values point to a strong affinity. An explanation might be a conformational change that stabilizes the state after celastrol binding as it was previously observed by Seo *et al.* for the interaction of maltose binding protein and maltose (Seo et al. 2014).

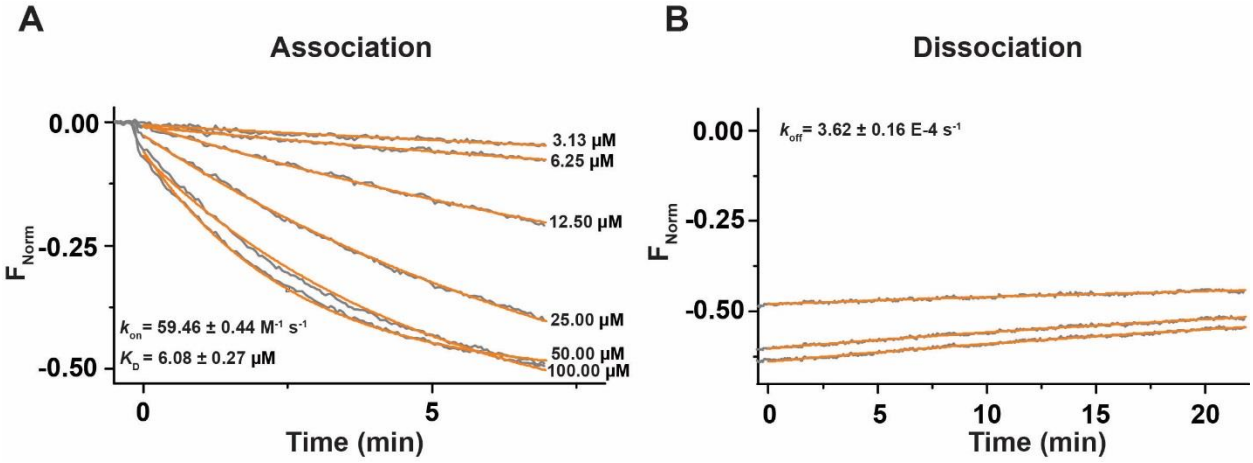

Figure 6.27 PTP1B – celastrol kinetic measurements using SwitchSENSE technology.
Association **(A)** and dissociation curves **(B)** of covalently immobilized $PTP1B_{1-298}$ at different celastrol concentrations.

7. Discussion

The main objective of this study was the identification and characterization of new allosteric compounds targeting PTP1B. For this purpose, a small library of 50 natural compounds described in the literature with anti-diabetic and anti-obesity activity was established. The compounds were classified depended on their scaffold into three groups: triterpenoids, steroids and their derivatives and a number of other compounds. The TCPTP protein was selected for testing for selectivity reasons and subsequently as a drug candidate itself for two reasons, firstly because is the most homologous phosphatase to PTP1B (Andersen et al. 2004) and because it plays complementary roles in insulin and leptin signaling in the hypothalamus (Tiganis 2013). Thus, both PTP1B and TCPTP should be studied as molecular targets against diabetes type 2 and obesity.

Several PTP1B and TCPTP constructs were successfully cloned, overexpressed and purified. All the protocols were optimized in order to produce sufficient amount of labeled and unlabeled proteins for structural studies. All proteins constructs are well folded as confirmed by NMR spectroscopy experiments. Different size constructs were produced in order to investigate the role of the C-terminal end of the proteins in their activity (**Figure 7.1**).

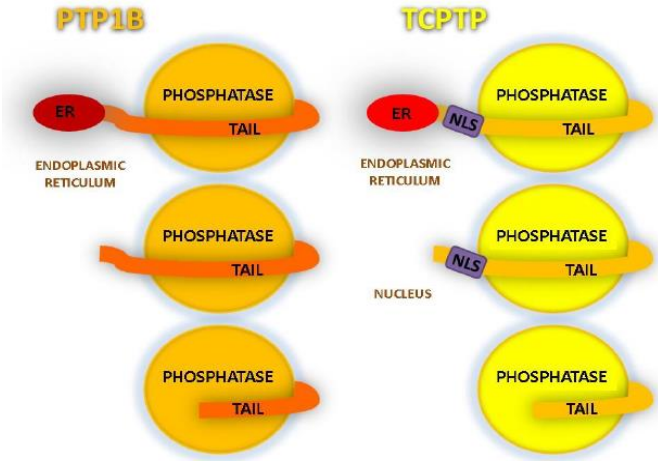

Figure 7.1 Role of the C-terminal part of PTP1Ba nd TCPT in the activity of the proteins.

The kinetic constants K_m and k_{cat} for different constructs were determined using the pNPP activity assay. It was shown that the K_m increases for longer constructs of PTP1B, while decreases for longer TCPTP constructs, indicating that the affinity worsens for longer PTP1B constructs and improves for longer TCPTP constructs. The k_{cat} values showed that both PTP1B and TCPTP longer

constructs are more active than the shorter ones. From these results it is obvious that the C-terminal part of the protein plays a role in the activity of the protein. A comparison of the two assigned constructs, $PTP1B_{1\text{-}393}$ and $PTP1B_{3\text{-}303}$, from Tonks were used for the calculation of the CSPs (**Figure 7.2**). It's obvious from these data that the C-terminal region of the protein affects the protein overall, presumably by transient and dynamic interactions of the intrinsically disordered polypeptide (residues 300-393, but not entirely unstructured, they they contained two α-helices) with the globular fold (Krishnan et al. 2014). There is no any specific cluster as can be seen in the **Figure 7.3**, the most strongly affected residue Gly183, is located Asp181 in the WPD loop that plays key role in the mechanism of the catalysis. In addition, Choy et al. have shown that PTP1B activity is regulated by rigidity, dynamics, and allostery. More specifically, catalysis including product hydrolysis requires both rigidity and slow dynamics, while its allosteric regulation requires fast dynamics, suggesting the existence of a communication pathway between the PTP1B active and allosteric sites (Choy et al. 2017).

The C-terminus seems to regulate the activity of the protein and definitely has to be more investigated.

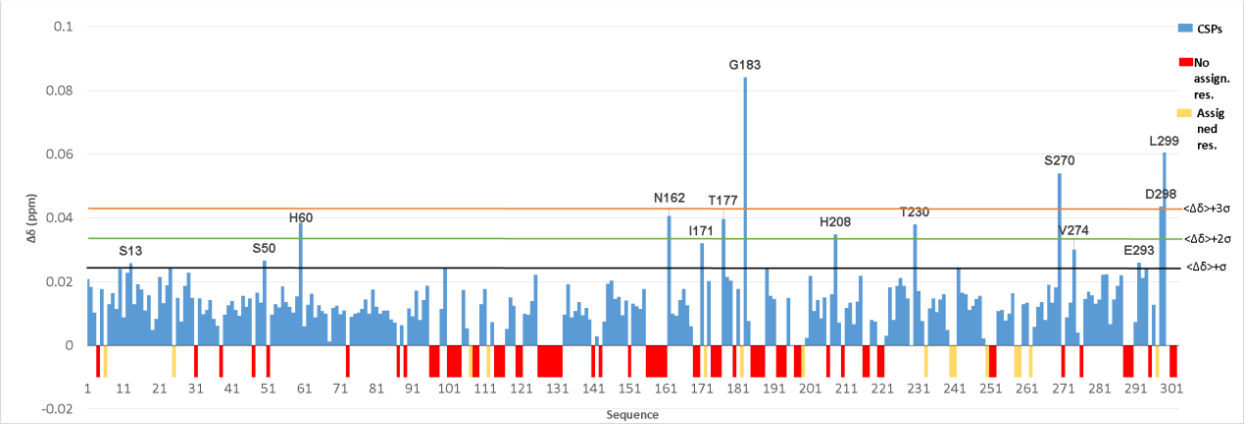

Figure 7.2 CSPs of the $PTP1B_{1\text{-}393}$ and $PTP1B_{3\text{-}303}$.

A combination of structure-based approaches and activity assays was used to characterize the binding modes of inhibitors. Firstly, an X-ray-based screening was used. Described conditions for PTP1B crystallization were reproduced and then many soaking and co-crystallization experiments were performed with relevant compounds from all the groups (**Table 5.7**). In total fifty-two datasets were acquired at the ESRF (Grenoble) and analyzed but no ligand was found bound to PTP1B. The only exception was for PTP1B inhibitor, which is a known allosteric inhibi-

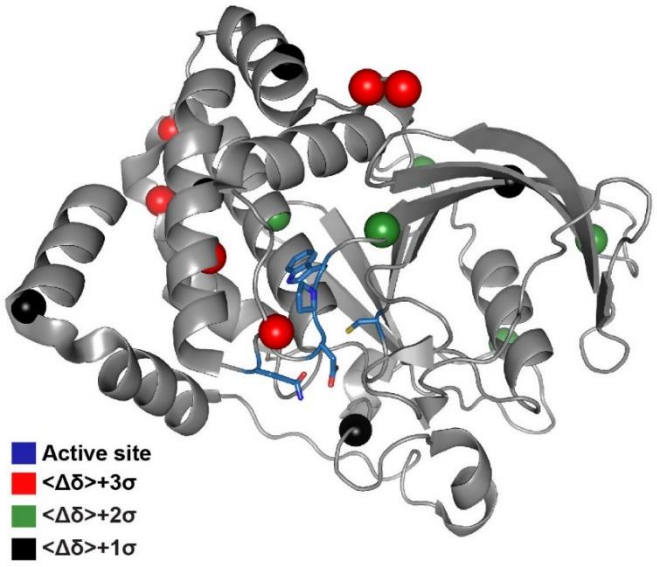

Figure 7.3 CSPs comparing short and long PTP1B proteins mapped onto the structure of a single conformer of PTP1B$_{1\text{-}298}$ (PDB: 1SUG).
1, 2 and 3 standard deviations (SDs) from the mean <Δδ> are represented as spheres and colored black, green and red, respectively. There is no any specific cluster, there are changes all over the protein.

tor of PTP1B and the crystal structure of the complex has been solved before (Wiesmann et al. 2004). This compound was used as a positive control in order to discriminate if the problem comes from the type of the crystallization conditions or from the compounds. It was then found that the compounds are not easy to be crystallized in complex with the protein, most probably due to the type of the interactions being developed between the protein side chains and the compound. Co-crystallization method used because it is usually chosen when the compounds are insoluble. However, there are different parameters that affect co-crystallization, such as temperature, use of additives and the ligand concentration, that need to be optimized. Soaking crystals with inhibitors is another commonly used method to obtain crystals of protein–ligand complexes. This method did not provide crystals with ligand density and that could be attributed to the soaking time and inhibitor concentration that also need to be optimized. Additives may be required to achieve effective ligand binding during the soak time and/or during the subsequent cryoprotectant exchange. A thermofluor screening was performed in order to determine the most stable buffer conditions of PTP1B. Thermofluor assay was also used for screening the binding of our compound library. For the screening all the aromatic compounds from the class C (**Figure 5.18**) were used, two of them are known inhibitors of PTP1B and were used as controls, in all cases an increase in the initial fluorescence is observed suggesting possible interference with the dye, which is also aromatic, with π stacking interactions. The rest compounds (section 5.2) tested, among them three

aminosterols (trodusquemine, SIXB, and NV673) and the same behavior was observed, which can be attributed to possible compound aggregation. A decrease of the melting point is also observed, which is also an indication of binding. However, the screening conditions still has to be optimized to sort out problem of possible compound aggregation and interference with the dye. For example, a possible solution could be an alternative dye that does not interfere with the aromatic compounds, or the usage of detergents to prevent aggregation.

NMR screenings were used to identify ligand binding to PTP1B protein. Compounds 18β-glycyrrthetinic acid, gymnemagenin, asiatic acid, oleanic acid, madecassic acid, hydrocortisone, cortisone, dehydroepiandrosterone sulfate, β-estradiol 3-sulfate, pregnenolone sulfate, cholesterol sulfate, cycloastragenol, trodusquemine, claramine, berberine, papaverine, AOAC and HePTP Inhibitor were found to bind to PTP1B both by STD NMR experiments and by recording 1D NMR experiments, where changes in the resonances after the protein addition were monitored.

The inhibitory ability of these compounds on the phosphatase activity of PTP1B and TCPTP constructs was tested by the pNPP phosphatase activity assay. Compounds for which it was not clear if they bind to proteins by STD experiments were also screened with the activity assay. The compounds that inhibit in low μM range the protein PTP1B were in descending order, cholesterol sulfate ($PTP1B_{1-298}$ 8.6 μM, $PTP1B_{1-321}$ 0.52 μM, $PTP1B_{1-393}$ 1.6 μM), SIXB ($PTP1B_{1-298}$ 130.3 μM, $PTP1B_{1-321}$ 3 μM, $PTP1B_{1-393}$ 2.1 μM), trodusquemine ($PTP1B_{1-298}$ 130.3 μM, $PTP1B_{1-321}$ 3 μM, $PTP1B_{1-393}$ 2.1 μM), ursolic acid ($PTP1B_{1-298}$ 14.9 μM, $PTP1B_{1-321}$ 7.6 μM, $PTP1B_{1-393}$ 6.8 μM), oleanic acid ($PTP1B_{1-298}$ 18.7 μM, $PTP1B_{1-321}$ 7.8 μM, $PTP1B_{1-393}$ 12.8 μM), diosgenin ($PTP1B_{1-298}$ 95.4 μM, $PTP1B_{1-321}$ 11.6 μM, $PTP1B_{1-393}$ 115 μM) and pregnenolone ($PTP1B_{1-321}$ 220 μM, $PTP1B_{1-393}$ 30.3 μM). Compounds vitamin D2 ($PTP1B_{1-321}$ 118 μM, $PTP1B_{1-393}$ 186.9 μM), asiatic acid ($PTP1B_{1-298}$ 133 μM, $PTP1B_{1-321}$ 135.8 μM, $PTP1B_{1-393}$ 128 μM), 18β-glycyrrthetinic acid ($PTP1B_{1-298}$ 127 μM, $PTP1B_{1-321}$ 200.3 μM, $PTP1B_{1-393}$ 255 μM), vitamin D3 ($PTP1B_{1-393}$ 160.8 μM) and madecassic acid ($PTP1B_{1-298}$ 262 μM, $PTP1B_{1-321}$ 238 μM) are following with higher IC_{50} values. Interestingly, compounds cholesterol ($PTP1B_{1-298}$ 6.8 μM, $PTP1B_{1-321}$ 4.3 μM), papaverine ($PTP1B_{1-298}$ 2.4 μM, $PTP1B_{1-321}$ 33.1 μM) and trigonelline ($PTP1B_{1-321}$ 75.9 μM) activate PTP1B in low μM range.

The compounds that inhibit in low μM range the protein TCPTP were in descending order cholesterol sulfate ($TCPTP_{1-296}$ 2.3 μM, $TCPTP_{1-336}$ 1.3 μM), ursolic acid ($TCPTP_{1-296}$ 20.9 μM, $TCPTP_{1-336}$ 6.3 μM), SIXB ($TCPTP_{1-296}$ 16.1 μM, $TCPTP_{1-336}$ 22.3 μM) and oleanic acid ($TCPTP_{1-}$

$_{296}$ 24.2 µM, TCPTP$_{1-336}$ 86.3 µM). Compounds pregnenolone (TCPTP$_{1-296}$ 195 µM, TCPTP$_{1-336}$ 57.5 µM), 18α-glycyrrthetinic acid (TCPTP$_{1-296}$ 125.8 µM, TCPTP$_{1-336}$ 158.2 µM) and diosgenin (TCPTP$_{1-296}$ 322.5 µM) are inhibiting TCPTP with relatively high IC_{50} values. Whilst, compounds vitamin D2 (TCPTP$_{1-296}$ 4.4 µM, TCPTP$_{1-336}$ 6 µM) and D3 (TCPTP$_{1-296}$ 11 µM, TCPTP$_{1-336}$ 7.7 µM), asiatic acid (TCPTP$_{1-296}$ 11.3 µM, TCPTP$_{1-336}$ 9.5 µM), cortisone (TCPTP$_{1-296}$ 31.5 µM) and hydrocortisone (TCPTP$_{1-296}$ 72.3 µM) are activating the protein giving low µM range IC_{50} values. Compounds cholesterol and pregnenolone sulfate are weak activators of the TCPTP protein.

In collaboration with Paul Pfluger (IDO), the most promising and interesting compounds hits (oleanolic acid, 18β-glycyrrthetinic acid, cholesterol sulfate, SIXB, Trodusquemine, PTP1B inhibitor 539741, ursolic acid, diosgenin, β-estradiol, 18α-glycyrrthetinic acid, cortisol, metformin and asiatic acid) were tested in cellular *in vitro* assays using hypothalamic CLU-177 neuronal cells (Adult Mouse Hypothalamus Cell Line) to evaluate the effect of hit compounds on insulin and leptin sensitivity. Compounds oleanolic acid, 18β-glycyrrthetinic acid, cholesterol sulfate, SIXB, trodusquemine, PTP1B inhibitor 539741, hydrocortisone, metformin and asiatic acid elicited insulin pathway activation in CLU-177 neuronal cells, by increasing the phosphorylation levels of AKT. These are discussed with more detail in the following.

7.1 Cholesterol and cholesterol sulfate

Cholesterol is a sterol compound synthesized by all animal cells. Cholesterol has a wide range of action. In the brain it makes up the myelin sheath that insulates against signal loss. In the membrane of all cells, it promotes cell-cell communication, prevents ions leaks and protects from pathogens (Haines 2001; Yeagle 1991). In the blood it is part of the lipoproteins (LDL, HDL) and it is essential for protecting contents in the blood from oxidation (free radicals) and glycation (inflammation) during transport to cells and organs. In the heart, it allows heart muscle to beat. It is the precursor to of all steroid hormones that regulate blood sugar (Glucocorticoids), mineral balance and blood pressure (mineral corticoids), sex hormones (testosterone, estrogen, etc), Vitamin D, Cortisone (the stress hormone) (Payne and Hales 2004).

Cholesterol sulfate is a form of cholesterol that is produced in the skin after exposure to the sun and is an important regulatory molecule (Seneff 2014). Sulfate makes cholesterol water soluble and therefore much easier to transport. It protects against cancer, diabetes and cardiovascular disease, improves the immune function and is used as substrate for the synthesis of sulfated steroids (Roberts et al. 1964; Strott and Higashi 2003). It is the most important known

sterol sulfate found in the human plasma in a concentration of 300 μg/100 mL or 320-535 μM (Strott and Higashi 2003). The determined IC_{50} values ($PTP1B_{1-393}$ 1.6 μM, $TCPTP_{1-336}$ 1.3 μM) are well below the physiological plasma levels and subsequently it can be considered that cholesterol sulfate inhibits both PTP1B and TCPTP in the body.

Krishnan et al. proposed that trodusquemine, an aminosterol, binds to the C-terminal of PTP1B in a similar way that cholesterol does to the β-adrenergic receptor, implying that cholesterol would bind to PTP1B in the same region as trodusquemine and therefore that is an allosteric inhibitor (Krishnan et al. 2014). However, in this thesis is shown that cholesterol is a strong activator of PTP1B, while it activates TCPTP very weakly, suggesting that is selective between the two proteins. That is consistent with the hypothesis that cholesterol binds to C-terminal part of PTP1B like trodusquemine, since the C-terminal parts of the two proteins differs from each other. The physiological serum levels of total cholesterol that is bound to low- and high-density lipoproteins are 5.18 mM, while the free cholesterol can be estimated to be around 13 μM based on the compound solubility in water and subsequently in blood. The free cholesterol concentration is higher than the concentration that can activate PTP1B ($PTP1B_{1-298}$ 6.8 μM, $PTP1B_{1-321}$ 4.3 μM). It is known that PTP1B is attached to the membrane and cholesterol is an important component of the membrane, thus one can expect that cholesterol might play an important role in the regulation of the PTP1B activity.

Interestingly cholesterol sulfate, which is the best-found inhibitor, inhibits both proteins with low IC_{50} values and always stronger the longer constructs, suggesting that the C-terminal part of the proteins plays an important role in the activity of the protein. However, the compound is not selective toward the two proteins, presumably as the compound binds to the catalytic domain of the proteins that they are highly homologous. NMR Spectroscopy data were used to map cholesterol sulfate binding site on the 3D structure of PTP1B. Most of the residues that are affected after the compound addition are indeed located around the catalytic site, while the residue Ser222 that belongs to the active site sequence and residue Ala264 that is very close to the Q loop are the residues that shift the most. From this data, can be suggested that cholesterol sulfate binds to the catalytic domain of the proteins, but not directly to the active center. However, additional experiments should be performed to lead to more reliable conclusions. Taking into account that structurally cholesterol sulfate is similar to cholesterol and trodusquemine (**Figure 7.4**), it is expected to be an allosteric inhibitor binding to the same region as trodusquemine. That is not the

case but that might be due to the fact that our NMR mapping studies have been done with the short length PTP1B. It should not be forgotten that in the activity assay the compound inhibits stronger the longest construct and that could be potentially attributed to binding in the C-terminal part of the protein.

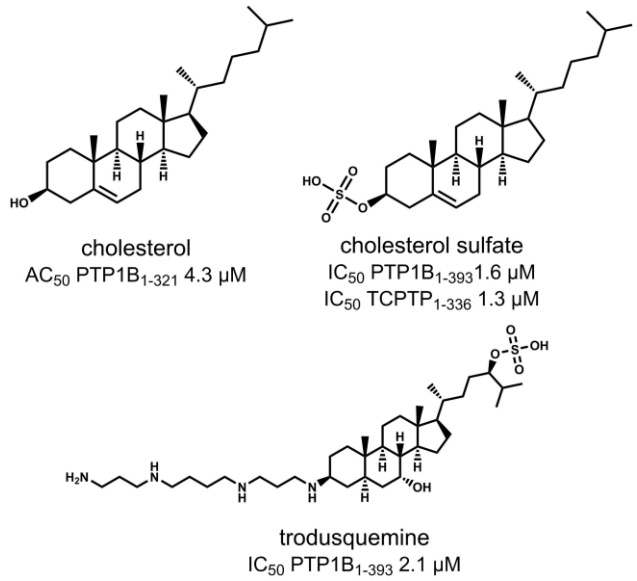

Figure 7.4 Cholesterol, cholesterol sulfate and trodusquemine structures and their inhibitory activity.

Neither cholesterol nor cholesterol sulfate have been connected with the PTP1B or TCPTP inhibition or activation. It has been only mentioned that cholesterol might increase the expression levels of PTP1B (Herre et al. 2015) and that cholesterol is essential for insulin release (Xia et al. 2008). Although cholesterol and cholesterol sulfate cannot be possibly considered as drugs, their physiological role in diabetes and obesity could be very interesting to explore.

Cholesterol sulfate was further evaluated in a cell assay using hypothalamic CLU-177 neuronal cells. Upon insulin stimulation, phosphorylation and activation of a linear signaling cascade IR/IRS1/PI3K lead to the phosphorylation of AKT. It is known that insulin signaling induces transient oxidation and inactivation of its inhibitor PTP1B (Meng et al. 2004), but this inactivation is defective in insulin resistance and type 2 diabetes, where PTP1B activity is elevated. Thus, blocking PTP1B activity would prevent dephosphorylation of AKT, which is a component of insulin signaling, and thereby augment insulin signaling. Here it was found that cholesterol sulfate enhances the phosphorylation of AKT, like insulin.

7.2 Trodusquemine and SIXB

Trodusquemine is an aminosterol isolated from the dogfish shark *Squalus acanthias*. It has been shown to reduce body weight in diet-induced obese mice (Lantz et al. 2010) and to suppress HER2-positive breast cancer (Krishnan et al. 2014) by inhibiting PTP1B that is involved in both insulin and leptin signaling but is also a tumor promoter, overexpressed in HER2-positive cancer.

Krishnan et al. (Krishnan et al. 2014) suggest that trodusquemine binds to the protein in two different parts, one is at the C-terminal part of construct $PTP1B_{1-393}$ (residues 371-375) and the other close to the catalytic segment (residues 299-310). He underlines that without the C-terminus trodusquemine is not able to bind to the protein anymore. To prove his hypothesis, the authors tested trodusquemine with a shorter construct ($PTP1B_{1-303}$) and they showed that there is no binding any more, something that comes in contrast to the results presented in this thesis. Clearly trodusquemine binds to the shorter construct ($PTP1B_{1-298}$) that does not include the C-terminal part that the compound supposes to bind to the protein, but not as strong as our longest construct ($PTP1B_{1-393}$). From the activity assay, it was determined that trodusquemine inhibits $PTP1B_{1-393}$ (IC_{50} 2.1 μM) almost 40-60 times stronger than the shorter constructs ($PTP1B_{1-298}$ 130.4 μM and $PTP1B_{1-321}$ 81.6 μM) with an IC_{50} of 2.1 μM which is comparable with the IC_{50} of 0.6 μM determined by Krishnan. The difference in the inhibitory capacity between the constructs, can be explained by the fact that there is another binding site of trodusquemine to the C-terminal part of PTP1B. In addition, our data agree with Qin and collaborators who also have not seen any inhibition activity of trodusquemine against TCPTP protein (Qin et al. 2015).

Novel analogues of trodusquemine have been identified that are potent inhibitors of PTP1B and have potential delivery route advantages. Compound SIXB is one of these analogues synthesized by Qin and collaborators and found to inhibit selectively PTP1B (Qin et al. 2015). In their paper, they have shown by using special PTP1B phosphatase Activity Assay Kit that SIXB inhibits PTP1B with an IC_{50} of 0.5 μM similar to 0.6 μM for trodusquemine determined by Krishnan (Krishnan et al. 2014). Our data show comparable inhibition values for SIXB with an IC50 of 3 μM. It was shown that SIXB can inhibit TCPTP as well but weaker than PTP1B, on contrast Qin has shown using the Human/Mouse/Rat Active TC-PTP DuoSet IC ELISA kit, that SIXB does not inhibit TCPTP. Based on the structural similarity between the compound SIXB and trodusquemine (**Figure 7.5**) one would expect that SIXB is also an allosteric selective inhibitor of

PTP1B and to bind at the same region as trodusquemine. Further investigation of the binding mode of SIXB against both full length proteins should be done.

Trodusquemine and SIXB were further evaluated in a cell assay using hypothalamic CLU-177 neuronal cells. It was found that cholesterol sulfate could increase phosphorylation of the key component AKT of the insulin-signaling cascade, confirming that the compounds act through inhibition of PTP1B.

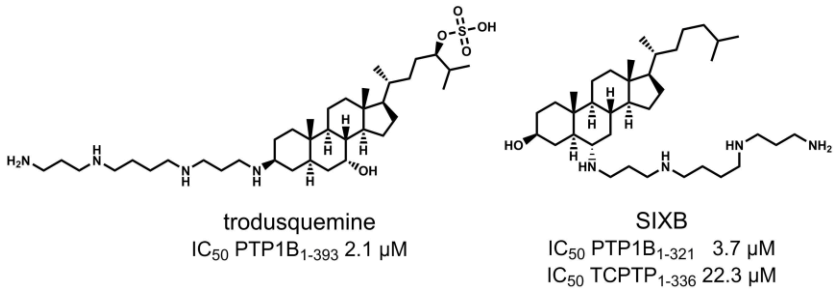

Figure 7.5 Trodusquemine and SIXB structures and their inhibitory activity.

7.3 Oleanolic and Ursolic acids

Oleanolic and ursolic acids are triterpenic acids extracted from several plants and fruits (Silva, Oliveira, and Duarte 2016). Both compounds are known among others for their antidiabetic and antiobesity properties (Castellano et al. 2013; Wu et al. 2015; de Melo et al. 2010; Rao et al. 2011). They act as hypoglycemic and antiobesity agents by reducing the absorption of glucose, decreasing endogenous glucose production, increasing insulin sensitivity, improving lipid homeostasis and promoting body weight regulation (Silva, Oliveira, and Duarte 2016).

There are reports that show that both compounds inhibit directly PTP1B (Ramírez-Espinosa et al. 2011, 2014; Na et al. 2006; W. Zhang et al. 2006). For oleanolic acid, Na et al. have found using the pNPP activity assay (Buffer conditions: 50 mM citrate pH 6.0, 0.1 M NaCl, 1 mM EDTA, 1 mM DTT) that it inhibits PTP1B (IC_{50}: 3.37 μM) in a comparable way to TCPTP (IC_{50}: 3.40 μM) (Na et al. 2006). Using the same activity assay for the determination of the inhibitory activity of oleanic acid, it was found that it inhibits $PTP1B_{1-321}$ with IC_{50}: 7.80 μM, while the longer and the shorter constructs are inhibited weaker (IC_{50}: 18.70 μM and 12.80 μM for $PTP1B_{1-298}$ and $PTP1B_{1-393}$ respectively). On the other hand, our data show that oleanolic acid inhibits stronger the PTP1B protein than TCPTP (IC_{50}: 24.20 μM and 86.30 μM for $TCPTP_{1-296}$ and $TCPTP_{1-336}$ respectively). Na et al. did not specify which PTP1B and TCPTP constructs they used

for the inhibitory activity determination. The differences in the buffer conditions and most probably differences in the constructs, can probably explain why our data differ.

Ursolic acid is one of our inhibitors exhibiting inhibitory activity in low μM range, though it inhibits both proteins without being selective (IC_{50}:6.80 μM and 6.30 μM for $PTP1B_{1-393}$ and $TCPTP_{1-336}$ respectively). Our data are in agreement with Zhang and his collaborators who have shown that ursolic acid inhibits both phosphatases in the same range (IC_{50}: 3.08 μM and 3.33 μM for $PTP1B_{1-298}$ and $TCPTP_{1-415}$ respectively) (W. Zhang et al. 2006). However, our data support that there is an effect from the C-terminal part since it is seen that the longer constructs are inhibited stronger in comparison to the shorter ones (IC_{50}:14.90 μM and 20.90 μM for $PTP1B_{1-298}$ and $TCPTP_{1-296}$ respectively).

Structurally oleanolic and ursolic acid only differ in the substituents of the carbons C20 and C21 (**Figure 7.6**). In case of oleanolic acid there is a dimethyl group at carbon C21 while in ursolic acid there is only a methyl group and one extra in the carbon C20. They are inhibiting both phosphatases in a low μM range thus they are not selective. Therefore, the differences in their structures are not important and they do not affect their inhibitory activity. What we have found is that the important groups affecting the inhibitory activity of the triterpenoids are the hydroxyl group at C2 position, an alkyl substitution of C18 in R conformation and a carboxyl or an ether group substitution at C17 position in S conformation (**Figure 7.6**). Previous reports claim that indeed the hydroxyl group at position C2 and the carboxylate group at position C17 are required for the activity (Ramírez-Espinosa et al. 2014; M. Na et al. 2006).

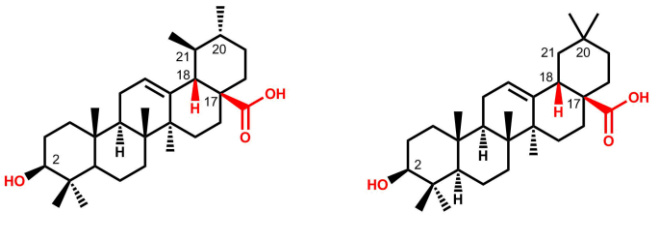

Figure 7.6 Ursolic and oleanic acid structures and their inhibitory activity. In red are highlighted the important groups for the activity.

Improvement of the antidiabetic properties of ursolic and oleanolic acid have been extensively performed, but only one derivative of oleanolic acid, bardoxolone methyl, has been tested in clinical trials. It successfully passed the Phase II trials (Pergola, Krauth, et al. 2011;

Pergola, Raskin, et al. 2011) but not the Phase III trials due to a higher incidence of cardiovascular event (de Zeeuw et al. 2013). However, the strong antidiabetic properties of ursolic and oleanolic acid still make them very good candidates for treatment of diabetes type 2. Possibly the low bioavailability problem in combination to very limited number of clinical trials are the reasons that new strategies for development of new derivatives with better bioavailability and efficacy and testing of their effects in clinical trials with type 2 diabetes patients need to be done.

Ursolic and oleanolic acid ability to activate insulin signaling in neuronal hypothalamic cells was investigated. It was found that only oleanolic acid enhances significantly the phosphorylation levels of AKT, while ursolic acid does not. It would have been expected that ursolic acid would also enhance AKT phosphorylation levels, since is stronger inhibitor of both PTP1B and TCPTP. However, the dose and the time of cell incubation with the compound could affect the activation of insulin signaling and they need to be optimized for the future. In summary, our data concerning the important for the inhibition groups can be used for the optimization of the compound structure. Further NMR structural studies will be more useful for the development of more potent derivatives.

7.4 Diosgenin

Diosgenin is a steroidal sapogenin found in several plants, such as *Dioscorea* and *Trigonella* (Raju et al. 2004; Y. Chen et al. 2015). It is known for its industrial importance since it's used as a starting material for the production of steroidal drugs and as a precursor for the synthesis of sex hormones and corticosteroids (Jasem et al. 2014; Djerassi et al. 1952). Apart from its industrial use, it is an important molecule for its bioactivity. It has been reported that it has anti-inflammatory and antioxidant properties and it can be used in blood and cerebral disorders, cardiovascular and allergic diseases, cancer and in diabetes and obesity (Y. Chen et al. 2015; Raju and Mehta 2009; Roghani-Dehkordi, Roghani, and Baluchnejadmojarad 2015; Jesus et al. 2016).

It has been reported that diosgenin can be useful for diabetes treatment through its ability to inhibit inflammation in adipose tissues (Jesus et al. 2016). Therefore, diosgenin may be useful to improve the patient's condition in the glucose metabolic disorder associated with obesity (Uemura et al. 2010). Ghosh et al have shown that the antidiabetic properties of diosgenin are due to its inhibitory activity against α-amylase and α-glucosidase, which leads to a reduction of high blood glucose levels (Ghosh et al. 2014).

There is no available study about inhibition of PTP1B from diosgenin. However, our data have shown for the first time that diosgenin binds directly to $PTP1B_{1-321}$ strongly (IC50: 11.6 μM), instead the other two PTP1B constructs are inhibited weaker (IC50: 95.4 μM, IC50: 115.0 μM for $PTP1B_{1-298}$ and $PTP1B_{1-393}$ respectively) revealing that the compound might bind in the C-terminal part of the $PTP1B_{1-321}$ construct and that the C-terminal part of the $PTP1B_{1-393}$ construct affects the inhibitory activity of the compound. In addition, the compound seems to be selective between PTP1B and TCPTP, since TCPTP is inhibited in high μM range. Diosgenin appears as a very interesting compound that can be used as and antidiabetic and anti-obesity agent and binding to PTP1B can provide and explanation of its mechanism of action. Further studies for the specific determination of the binding mode and site of the compound should be performed.

Diosgenin was also evaluated in a cell assay using hypothalamic CLU-177 neuronal cells, where it was found that that it doesn't enhance significantly the phosphorylation levels of AKT. But that could be because of the short incubation time of the cells with the compound, as well as the concentration of the compound used for the treatment of the cells. The experiment should be repeated in different doses and longer incubation times.

7.5 Pregnenolone

Pregnenolone is a steroid synthesized from the conversion of cholesterol by the cytochrome P450 enzyme (Vallée 2016) within the brain, adrenal glands and gonads (Baulieu 1997). It is used as a precursor in the biosynthesis of most of the steroid hormones. Pregnenolone is involved in various metabolic pathways, which differ between animal and human. In animals pregnenolone is converted to pregnenolone sulfate and progesterone, while in human is converted additionally into 17-hydropregnenolone (Luu-The 2013). It is surprising that pregnenolone and its sulfated derivative either act differently or they have different targets. For example, progesterone acts as an inhibitory steroid while the sulfated forms of pregnenolone and 17-hydropregnenolone act as excitatory steroids. Moreover, pregnenolone sulfate and 17-hydropregnenolone sulfate are inhibiting acide γ-aminobutyrique (GABA) and NMDAN-methyl-d-aspartate (NMDA) receptors, while pregnenolone expresses a poor affinity for these two receptors (Vallée 2016).

Pregnenolone is known as a neurosteroid that affects the functions of neurons by acting on nuclear steroid hormone receptors (Krohmer et al. 2017). More specifically, it targets Sigma 1 receptor, microtubules and type-1 cannabinoids receptor.

There is no study correlating pregnenolone and its derivatives with diabetes and obesity. Our results though are showing that pregnenolone binds relatively strong to the $PTP1B_{1-393}$ construct (IC_{50}: 30.3 μM) and almost 2-fold stronger than the $TCPTP_{1-336}$ construct (IC_{50}: 57.5 μM) revealing that it might be an allosteric inhibitor of PTP1B protein binding to the C-terminal part of the protein or that the C-terminal part of the protein is stabilizing its binding in the catalytic domain of the protein. On the other hand, the sulfate form of pregnenolone inhibits very weakly the PTP1B protein whilst it seems to activate very weakly the TCPTP protein. The different behavior of the two compounds is not very surprising since it's known that although they are structurally very similar they exhibit different action as it's described above. It will be very interesting from the biological point of view to explore further whether pregnenolone and its derivatives play a role in insulin and leptin pathways via regulation of PTP1B and TCPTP activity.

However, it has been reported that the physiological levels of pregnenolone in the blood serum is 33-248 ng/dL or 1.05-7.83 nM, which is much lower than the IC_{50} values determined for PTP1B and TCPTP, meaning that pregnenolone would not be sufficient to inhibit the activity of PTP1B and TCPTP in the body.

7.6 18β-glycyrrhetinic acid and 18α-glycyrrhetinic acid

18β-glycyrrhetinic and 18α-glycyrrhetinic acid are two pentacyclic triterpenoid stereoisomers. They are the main bioactive substances of licorice, with 18β-glycyrrhetinic (enoxolone) used as cicatrizant and anti-inflammatory drug and as clinical drug for the gastrointestinal system (Shibata 2000).

18β-glycyrrhetinic acid shows anti-inflammatory, antivirus, antiulcer and adrenal cortical hormone kind function (Lin et al. 2012). It has been reported to have a positive effect against dermatitis, purulent scar disease, and hair follicle infection. It can cure gingivitis, esophagus inflammatory disease, lipemia and antiatherosclerotic. It also prevents from atherosclerosis (Lin et al. 2012). In addition, it inhibits many enzymes in the corticosteroid metabolic process. More specifically, it inhibits both 11β-hydroxysteroid dehydrogenase enzyme 1 and 2 (11β-HSD1 and 11β-HSD2) that catalyze the interconversion of hormonally active cortisol and inactive cortisone (Armanini et al. 2005).

18α-glycyrrhetinic acid on the other hand has been only reported to inhibit reversibly the gap-junction intercellular communication in the alveolar epithial cells in parallel with the

dephosphorylation of the entire connexin (Cx) 43 protein signal (Guo et al. 1999). It also inhibits 11β-HSD but only the 11β-HSD1 (Classen-Houben et al. 2009).

In this study, 18β and 18α-glycyrrhetinic acid have been tested as PTP1B and TCPTP inhibitors. Given the high similarity of their structures, one would expect that they would show same activity. However, our results reveal that 18β-glycyrrhetinic acid is inhibiting only PTP1B protein while 18α-glycyrrhetinic acid inhibits only TCPTP protein. This is not the first time that the two stereoisomers exhibit different action. Guo et al. have shown that 18α-glycyrrhetinic acid dephosphorylates the whole Cx43 signal whereas 18β-glycyrrhetinic acid dephosphorylates only the Cx43-P2 protein (Guo et al. 1999). The inhibitory activity of 18β-glycyrrhetinic acid against PTP1B protein has been tested before by Scott and collaborators (Scott et al. 2011), who have shown that 18β-glycyrrhetinic acid is a potent inhibitor of Shp2 phosphatase and 4 times more selective in comparison to PTP1B protein with IC_{50} values of 9.6 and 45.8 μM respectively. Our IC_{50} values for PTP1B constructs differ from Scott results, it was found that the compound inhibits PTP1B with an IC_{50} of 127 μM and 255 μM for $PTP1B_{1-298}$ and $PTP1B_{1-393}$ construct respectively. CSPs of 18β-glycyrrhetinic acid induced on the $PTP1B_{1-298}$ construct were calculated in an attempt to map the binding site of the compound. There it can be seen that the residues that were affected by the compound are not close to the active site, indicating that is probably an allosteric inhibitor. Further investigation of the role of the two stereoisomers in the inhibition pathways of the two phosphatases by NMR and another activity assay would be very interesting for future studies.

By using neuronal CLU-177 cells we showed that only 18β-glycyrrhetinic acid has an insulin-like effect, increasing AKT phosphorylation. That was expected, since only 18β-glycyrrhetinic acid inhibits PTP1B.

7.7 Madecassic acid and Asiatic acid

Madecassic acid is a natural triterpenic acid isolated from the *Centella asiatica* (Singh 1990). Madecassic acid has anti-inflammatory activity via suppressing the nuclear factor kappa B pathway (Won et al. 2010). It has been also suggested that has anti-oxidative action (Tabassum et al. 2013). Recently Hsu et al. reported that madecassic acid improved glycemic control and hemostatic imbalance, lowered lipid accumulation, and attenuated oxidative and inflammatory stress in diabetic mice (Hsu et al. 2015). Thus, madecassic acid could be considered as an antidiabetic agent.

Until now the mechanism and the targets of the madecassic acid that can explain its antidiabetic properties are not known. There is only one QSAR study where it was pointed that its target might be PTP1B with IC_{50}: 12.8 μM (Joshi et al. 2012). However, our study has revealed that madecassic acid inhibits only PTP1B with relatively high IC_{50} values ($PTP1B_{1-321}$ IC_{50}: 238 μM). Indeed, binding to PTP1B protein might be the reason of its antidiabetic activity. Therefore, madecassic acid can be considered as a potential selective inhibitor of PTP1B. Although it should bind in a similar region as ursolic and oleanolic acid due to their structural similarities it could be that these differences are enough to develop interactions in another region most possibly allosteric due to its selectivity towards the two highly homologous proteins and it can be used as a scaffold for the design of better affinity derivatives. Mapping the binding site of the compound to the protein structure and investigation of the binding mode using activity assays will be considered for future studies.

Asiatic acid is also an ingredient of the *Centella asiatica* (Hong et al. 2005) commonly used in wound healing (Maquart et al. 1999). It has like madecassic acid antioxidant and anti-inflammatory properties, and additionally it has shown protection effects against glutamate- or β-amyloid-induced neurotoxicity and neuroprotective benefits against stroke (Krishnamurthy et al. 2009). It has also been found to induce cell cycle arrest and apoptosis in breast cancer cells and block angiogenesis in cells and tumors from glioblastomas (Kavitha et al. 2011). There are also studies showing that asiatic acid has antidiabetic effects. It has been shown that it improves the level of plasma insulin, decreases glucose level, reverses the changes in the levels of the key carbohydrate metabolizing enzymes and also prevents lipid peroxidation and improves antioxidant status in rats with streptozotocin-induced diabetes (Ramachandran, Saravanan, and Senthilraja 2014).

However, there are no biochemical and structural data showing the molecular target of asiatic acid. Based on the structural similarities between asiatic acid and ursolic and oleanolic acid here is investigated whether the compound inhibits PTP1B and TCPTP proteins. Indeed, the compound inhibits all PTP1B constructs with around 100 μM inhibition activity, which is 2 times better than madecassic acid. Interestingly, they only differ in one hydroxyl group which madecassic acid has additionally at position 7 (**Figure 7.7**). The inhibitory activity of both asiatic and madecassic acid is worse than that of oleanic and ursolic acid. This can lead us to the conclusion that the less -OH groups at the ring A of the triterpenoid the better binding to the protein.

Due to the structural similarities with oleanolic and ursolic acid, it is expected that both madecassic and asiatic acid bind in the same region of the protein as the former compounds (**Figure 7.7**). Most of the residues in this region are hydrophobic (Phe52, Ala27), giving an explanation of loss of affinity when the compound is more hydrophilic. On the other hand, in the case of asiatic acid we have seen that activates TCPTP protein in low micromolar range. This is surprising, since it would be expected to have similar action to the other three triterpenoids, which is either weak affinity or no interaction with the TCPTP protein at all. The experiments should be repeated in order to lead to reliable conclusions.

Asiatic acid was also shown to enhance the phosphorylation levels of the insulin-signaling key component AKT, when tested in neuronal hypothalamic cells, most probably through PTP1B inhibition.

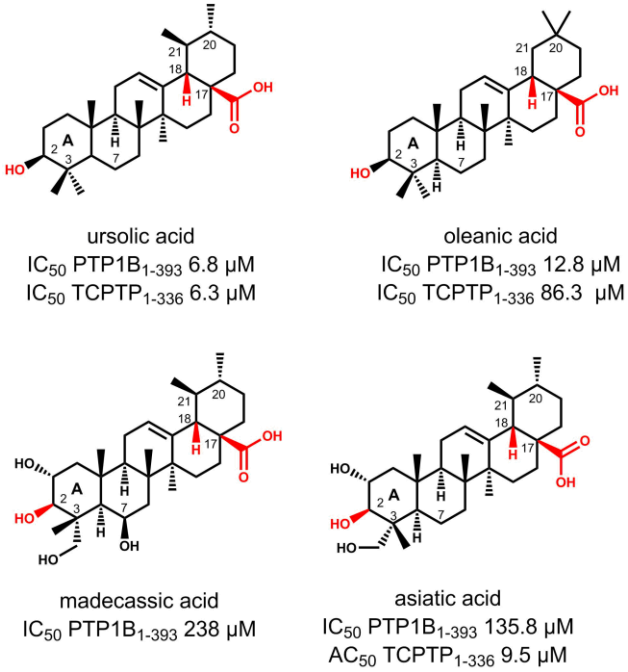

Figure 7.7 Ursolic, oleanic, madecassic and asiatic acid structures and their inhibitory activity. In red are highlighted the important groups for the activity.

7.8 Trigonelline and Papaverine

Trigonelline and papaverine are plant alkaloids existing in the *Trigonella foenum-graecum L.* (fenugreek) and the *Papaver somniferum* respectively. Both compounds activate $PTP1B_{1-321}$ with low IC_{50} values (IC_{50}:75.95 μM for trigonelline and IC_{50}:33.1 μM for papaverine). Their activity against TCPTP needs to be tested.

Trigonelline has hypoglycemic, hypolipidemic, neuroprotective, antimigraine, sedative, memory-improving, antibacterial, antiviral, and anti-tumor activities, and it has been shown to reduce diabetic auditory neuropathy and platelet aggregation (J. Zhou, Chan, and Zhou 2012). It has demonstrated direct antidiabetic properties in clinical studies by improving β-cells regeneration, insulin secretion and enzymes related to glucose metabolism (Koupý, Kotolová, and Rudá Kučerová 2015). However, the mechanism of its action is unknown. Based on our results the antidiabetic properties of trigonelline cannot be attributed to the inhibition of PTP1B since it's activating the protein. It will be interesting to further explore the biological role of the trigonelline and test its activity with TCPTP or other proteins that could potentially be its target.

Papaverine is used as antispasmodic drug in the treatment of spasm and vasospasm. The mechanism of its pharmacological actions is not clear, but it apparently can inhibit phosphodiesterases and it may have direct actions on calcium channels (Ohmura 1976). Papaverine has also hypoglycemic action (Bustanji, Taha, Al-Masri, et al. 2009). It has been tested before as an inhibitor of PTP1B due to its structural similarity with the known berberine inhibitor (IC_{50}: 156 nM) (Bustanji et al. 2006) and it was found that inhibits PTP1B nearly 10 folds weaker that of berberine with an IC_{50} of 1.25 μM (Bustanji, Taha, Al-Masri, et al. 2009). The difference in the inhibitory ability of the two compounds was assigned to the permanently cationic charge of berberine combined with the fact that berberine is more rigid than papaverine. Both papaverine and berberine bind to the active site of the protein according to docking simulation studies (Bustanji, Taha, Al-Masri, et al. 2009; Bustanji et al. 2006). Our results though are contradicting the above results. Papaverine was found to activate relatively strongly the protein PTP1B. The opposite results between our data and the literature could be due to the different activity assays used for the determination of the inhibitory activity of the compound. Bunstanji et al. have used malachite green ammoniummolybdate, whereas the pNPP assay was used in my case. That could be due to solubility issues. Anyhow, the experiments with the compound papaverine should be repeated with both pNPP and DiFMUP assays and it will also be interesting to determine its binding pocket by running NMR experiments and compare the results with the docking data of the literature.

7.9 Vitamins D2 and D3

Vitamin D2 (ergocarciferol) and Vitamin D3 (cholecalciferol) are the two main forms of vitamin D. Vitamin D2 is synthesized by plants, while vitamin D3 is synthesized in skin when it

is exposed to UV rays of the sun (Martin and Campbell 2011). Both forms are inactive and they have to be converted into active forms primarily in liver forming 25-hydroxyvitamin D mediated by 25-hydroxylase and second in kidney mediated by 1 α-hydroxylase forming the final activated product calcitriol (1,25 dihydroxyvitamin D) (Papandreou and Hamid 2015). 25-hydroxyvitamin D3 is the most abundant circulating form of vitamin D and is used as a biomarker to determine vitamin D levels (Carlberg and Campbell 2013).

There are many research studies linking vitamin D to T2D and T1D. Vitamin D indirect effects are via regulation of calcium effects on various mechanisms related to the pathophysiology of type 2 diabetes, including pancreatic beta cell dysfunction, impaired insulin action and systemic inflammation (Mitri and Pittas 2014; Papandreou and Hamid 2015; Schwalfenberg 2008). It has been reported that vitamin D can improve insulin production by promoting pancreatic beta cell function in several ways (Kadowaki and Norman 1984; Norman et al. 1980) and it can increase the insulin sensitivity by stimulating the expression of insulin receptors and/or by activating peroxisome proliferator-activated receptor (Maestro et al. 2002, 2003).

Therefore, there is increasing evidence suggesting that vitamin D plays a significant role in diabetes type 2, inhibiting NF-kB through direct binding to the C-terminal part of VDR and IKKβ. It is known that VDR binding causes TCPTP transcription and translation (Ramagopalan et al. 2010), therefore TCPTP could form a complex with VDR regulating DNA binding. However, there are no published clinical trials specifically designed to test the safety and efficacy of long-term vitamin D administration on the risk of reducing development of type 2 diabetes; thus, clear conclusions cannot be drawn regarding the role of vitamin D for prevention or treatment of diabetes. In addition, there are no studies about the molecular targets of vitamin D.

Here vitamin D2 and D3 were tested as potential inhibitors of PTP1B and TCPTP proteins. It was found that both vitamins are inhibiting $PTP1B_{1-393}$ construct with similar IC_{50} values (IC_{50}:186.9 μM and 160.8 μM for vitamin D2 and D3 respectively), whilst only vitamin D2 inhibits the $PTP1B_{1-321}$ construct with IC_{50}:118 μM. Interestingly both vitamins are activating TCPTP constructs in low μM range. The antidiabetic properties of the two vitamins could be due to this action and it should be confirmed with further experiments.

7.10 Cortisone and hydrocortisone

Cortisone and hydrocortisone are corticosteroids, which is a class of steroids hormones. They are both secreted by the adrenal gland and they are released in response to stress. They are

used for the treatment of inflammation and allergies due to their action of suppressing the immune system. It has been published that corticosteroids cause increasing glucose blood levels and enhance insulin resistance (Vondra and Hampl 2006; Blackburn, Hux, and Mamdani 2002). It is also known that chronic or extensive use of corticosteroids can develop what is called "steroid-induced diabetes" (Hwang and Weiss 2014). It is clear that there is a connection between corticosteroids and diabetes. They cannot be used as drugs since it's shown that they can cause diabetes but it will be interesting to investigate the biology behind this action.

The activity of both compounds with PTP1B and TCPTP have been tested. It was found that hydrocortisone inhibits very weakly only $PTP1B_{1-393}$ in millimolar range, while cortisone is inhibiting both the intermediate and the longest PTP1B construct with around 150 μM IC_{50} value. On the other hand, both compounds activate protein $TCPTP_{1-296}$ in relatively low micromolar range (AC_{50}:72.3 μM and 31.6 μM for hydrocortisone and cortisone respectively). Activation of protein TCPTP can explain the anti-inflammatory properties of the compound and at the same time their ability to increase insulin resistance, which could be due to the dephosphorylation of the insulin receptor by the TCPTP protein. The cortisol physiological blood levels are 193.13-689.75 nM, meaning that it's not sufficient to inhibit PTP1B or activate TCPTP in the body.

In addition, it was found that hydrocortisone enhances the phosphorylation levels of AKT in the used cell assay, which is surprising since it inhibits PTP1B weakly while activates TCPTP stronger. Then, it would be expected that suppresses insulin cascade and subsequently decreases phosphorylation levels of AKT. The experiment should be repeated looking for phosphorylation of leptin-signaling key components that TCPTP is stronger involved.

7.11 Celastrol

Celastrol is a pentacyclic triterpene natural compound with antidiabetic and antiobesity properties (J. Liu et al. 2015b). It has been also reported to have anti-neurodegenerative (J. Wang et al. 2005), anti-inflammatory (Allison et al. 2001) and anticancer (Klaić et al. 2011; Abbas et al. 2007) properties.

In reducing conditions, it was shown using NMR experiments that celastrol binds to both PTP1B and TCPTP proteins. Furthermore, using a fluorescence assay, it was shown that inhibits both PTP1B and TCPTP in low micro molar range and that it is a non-competitive compound. Then protein-detected NMR experiments were used to map the binding site of celastrol onto the structure of PTP1B. The CSPs were mapped onto the crystal structure of $PTP1B_{1-321}$ and indicate

that celastrol binds in the vicinity of the active site. An information-driven docking approach (HADDOCK) gave similar results, based on the best score structure, the compound is bound to the actual active site. This last *in vitro* experiment with celastrol and $TCPTP_{1-336}$ was repeated, where the same profile is observed, chemical shifts and line broadening. Western blotting for celastrol was performed, firstly it was found that 1 μM is the best dose. Then proteins p-AKT, p-STAT3, p-STAT5, p-JAK2 and p-ERK1/2 were detected. It was shown that celastrol clearly enhances phosphorylation levels of AKT, while it does not affect the ERK1/2 phosphorylation at all. p-STAT3 was not detected, due to low protein expression levels. For p-STAT5 and p-JAK2 no big effect from the treatment of the cells with celastrol was seen, but that could be because of the short time of incubation of the cells with the stimulus.

Since it's known that celastrol it is not very stable, the reactivity of celastrol under different buffer conditions was then investigated. Specifically, the effect of DTT on the structure of celastrol was studied. To clarify if celastrol is converted to dihydrocelastrol in reducing conditions, it was decided to synthesize the dihydrocelastrol compound that according to literature is supposed to be the reduction product of celastrol. I have found that celastrol in presence of DTT differs from dihydrocelastrol. The full assignment of celastrol in the presence of DTT in DMSO-d6 is not completely done due to overlap effect, but it was concluded that there is more than one species one of which is the complex of celastrol with DTT. However, mass spectrometry analysis shows that celastrol doesn't form a covalent bond with DTT, which does not explain why the adduct product by NMR is detected. One explanation could be that the adduct molecule can be formed only in the absence of water. Further analysis of the spectra for the complete assignment of the species structures needs to be done.

Due to the observation that celastrol changes whenever DTT is present, all the experiments without DTT were repeated in order to check if still the effects of celastrol can be seen. Repeating the experiments, it was found that still our *in vitro* and *in vivo* findings support a model whereby celastrol enhances leptin regulation via direct inhibition of PTP1B and TCPTP in oxidized conditions as well. The exact nature of the active molecule *in vivo* needs still to be clarified, since in the blood there are reduced conditions that might alter the molecule. Celastrol when is mixed with glutathione/glutathione disulfide (GSH/GSSG) in a ratio of 1:10, which corresponds to the physiological ratio in the blood plasma (Aquilano, Baldelli, and Ciriolo 2014), forms an adduct product complex with GSH.

In addition, our collaborator in Australia showed that celastrol mediates leptin resensitization via inhibition of hypothalamic PTP1B and TCPTP using mice genetically engineered to be homozygous for lox-P-flanked PTP1B, TCPTP and SOCS3. SOCS3 protein was expressed and purified in order to rule out any in vivo effect of celastrol mediated by SOCS3 using an in vitro assay with purified SOCS3 protein. Indeed, running 2D TROSY NMR experiments it was found that celastrol doesn't induce any chemical shift perturbation on the protein spectra. Suggesting that the observed effect *in vivo* are mediated largely by PTP1B and TCPTP.

7.12 Summary

In this study, I aimed to identify new inhibitors/ modulators of PTP1B and TCPTP proteins, which are involved in insulin and leptin signaling. For this purpose, PTP1B was soaked or cocrystallized with several hit compounds, coming from our new established library with compounds with antidiabetic or anti-obesity properties. A total of 52 datasets were acquired at the ESRF (Grenoble), but unfortunately no compound density was found in the electron density maps. Therefore, I decided to focus more on NMR spectroscopy analysis of protein-compound interaction. Two activity assays were used to find several hit molecules that regulate PTP1B or TCPTP activity, a colorimetric assay using pNPP as a substrate and a fluorimetric assay using DiFMUP as a substrate. It was found that out of the 50 compounds from our library, 3 compounds (trodusquemine, madecassic acid and 18β-glycyrrhetinic acid) inhibit only PTP1B, 6 compounds (pregnenolone sulfate, vitamin D2, vitamin D3, cortisol, cortisone and asiatic acid) inhibit PTP1B while activate TCPTP, 6 compounds (SIXB, diosgenin, cholesterol sulfate, ursolic acid, oleanoic acid and pregnenolone) inhibit both PTP1B and TCPTP and 18α-glycyrrhetinic acid inhibits only TCPTP. They were found several molecules that inhibit PTP1B and TCPTP in the high nM to low µM range.

The best hits were validated by NMR studies. In order to map the compound binding site on PTP1B and TCPTP 3D structures, triple resonance assignment spectra were recorded. In total, 75% of the backbone assignments resonances of $PTP1B_{1-298}$ were assigned. The binding site of several hit compounds was subsequently mapped onto the crystal structure of PTP1B based on chemical shift perturbations observed in the 2D spectra upon titration of the small compounds. Trodusquemine was tested, a known noncompetitive inhibitor (Krishnan et al. 2014), and some derivatives of it (collaboration with Dr. Jean-Michel Brunel, Université de la Mediterranée, Marseille, France), cholesterol sulfate, 18β-glycyrrthetinic acid and celastrol. It was observed that

the tested molecules bind to different binding sites on PTP1B: from close to the active site, as celastrol, to sites far from the active site and possibly allosteric.

Then our hits were validated in cellular assays at IDO in collaboration with Paul Pfluger to test the effect of hit compounds on insulin and leptin sensitivity. I observed that several of the tested compounds had a strong effect on insulin sensitivity. Among these are hit molecules with possible therapeutic application on T2D and obesity, and biological molecules (steroid hormones, vitamins) important in metabolism. Interestingly, I found some biological molecules (hormones, vitamins) that enhance TCPTP activity and/or inhibit PTP1B activity and compounds with the opposite effect. These compounds could be important for the metabolic integration of several signaling pathways in a way not previously described. It will be very interesting to evaluate the role of these molecules in metabolic integration, such us the VDR receptor, in future studies.

Importantly, for the compound celastrol, it was shown that its weight-lowering effects are mediated via reversible non-competitive inhibition of hypothalamic PTP1B and TCPTP, and are independent from UCP1-mediated thermogenesis. Our collaborator Paul Pfluger has shown that the *in vivo* relevance of PTP1B binding and inhibition by celastrol as global PTP1B-deficient mice were significantly resistant to celastrol-induced hypophagia and weight loss. In addition, our collaborator Michael Cowley (Monash University, Australia) was able to show that mice with genetic deletion of PTP1B and TCPTP in the mediobasal hypothalamus are resistant to the weight-lowering and hypophagic efficacy of celastrol. These results encourage reconsideration of therapeutic anti-obesity strategies built upon leptin sensitization and PTP inhibition.

Our findings demonstrate that it is possible to find new scaffolds targeting PTP1B which has been considered for a long time as non-druggable because of *in vivo* compound efficacy problems of polar hits targeting the active site. In this project, I found that new scaffolds (triterpenoids, steroids, among others) with reduced polarity bind to PTP1B at different binding sites that can be explored in the future.

Of particular interest is also the role of some hormones and vitamins screened by us that modulate PTP1B and TCPTP, either activating or inhibiting their activity and could be important for the metabolic integration of several signaling pathways (steroid hormones, leptin and insulin) in a way not previously described. The role of these molecules would be interesting to be evaluated in metabolic integration in future studies.

Bibliography

Abbas, Sabiha, Anindita Bhoumik, Russell Dahl, Stefan Vasile, Stan Krajewski, Nicholas D.P. Cosford, and Ze'ev A. Ronai. 2007. "Preclinical Studies of Celastrol and Acetyl Isogambogic Acid in Melanoma." *Clinical Cancer Research : An Official Journal of the American Association for Cancer Research* 13 (22 Pt 1): 6769–78. doi:10.1158/1078-0432.CCR-07-1536.

Allison, Anthony C., Ramon Cacabelos, Valter R. M. Lombardi, Xoan A. Álvarez, and Carmen Vigo. 2001. "Celastrol, a Potent Antioxidant and Anti-Inflammatory Drug, as a Possible Treatment for Alzheimer's Disease." *Progress in Neuro-Psychopharmacology and Biological Psychiatry* 25 (7): 1341–57. doi:10.1016/S0278-5846(01)00192-0.

Alonso, Andres, Joanna Sasin, Nunzio Bottini, Ilan Friedberg, Iddo Friedberg, Andrei Osterman, Adam Godzik, Tony Hunter, Jack Dixon, and Tomas Mustelin. 2004. "Protein Tyrosine Phosphatases in the Human Genome." *Cell* 117 (6): 699–711. doi:10.1016/j.cell.2004.05.018.

Andersen, Jannik N., Peter G. Jansen, Søren M. Echwald, Ole H. Mortensen, Toshiyuki Fukada, Robert Del Vecchio, Nicholas K. Tonks, and Niels Peter H. Møller. 2004. "A Genomic Perspective on Protein Tyrosine Phosphatases: Gene Structure, Pseudogenes, and Genetic Disease Linkage." *FASEB Journal: Official Publication of the Federation of American Societies for Experimental Biology* 18 (1): 8–30. doi:10.1096/fj.02-1212rev.

Aquilano, Katia, Sara Baldelli, and Maria R. Ciriolo. 2014. "Glutathione: New Roles in Redox Signaling for an Old Antioxidant." *Frontiers in Pharmacology* 5 (August). doi:10.3389/fphar.2014.00196.

Armanini, Decio, Davide Nacamulli, Francesco Francini-Pesenti, Giuliana Battagin, Eugenio Ragazzi, and Cristina Fiore. 2005. "Glycyrrhetinic Acid, the Active Principle of Licorice, Can Reduce the Thickness of Subcutaneous Thigh Fat through Topical Application." *Steroids* 70 (8): 538–42. doi:10.1016/j.steroids.2005.01.007.

Babon, Jeffrey J., Shenggen Yao, David P. DeSouza, Christopher F. Harrison, Louis J. Fabri, Edvards Liepinsh, Sergio D. Scrofani, Manuel Baca, and Raymond S. Norton. 2005. "Secondary Structure Assignment of Mouse SOCS3 by NMR Defines the Domain Boundaries and Identifies an Unstructured Insertion in the SH2 Domain." *The FEBS Journal* 272 (23): 6120–30. doi:10.1111/j.1742-4658.2005.05010.x.

Barr, Alastair J. 2010. "Protein Tyrosine Phosphatases as Drug Targets: Strategies and Challenges of Inhibitor Development." *Future Medicinal Chemistry* 2 (10): 1563–76. doi:10.4155/fmc.10.241.

Baskaran, Sarath Kumar, Nabajyoti Goswami, Sudhagar Selvaraj, Velusamy Shanmuganathan Muthusamy, and Baddireddi Subhadra Lakshmi. 2012. "Molecular Dynamics Approach to Probe the Allosteric Inhibition of PTP1B by Chlorogenic and Cichoric Acid." *Journal of Chemical Information and Modeling* 52 (8): 2004–12. doi:10.1021/ci200581g.

Baulieu, E. E. 1997. "Neurosteroids: Of the Nervous System, by the Nervous System, for the Nervous System." *Recent Progress in Hormone Research* 52: 1–32.

Blackburn, David, Janet Hux, and Muhammad Mamdani. 2002. "Quantification of the Risk of Corticosteroid-Induced Diabetes Mellitus Among the Elderly." *Journal of General Internal Medicine* 17 (9): 717–20.

Brandão, Tiago A. S., Alvan C. Hengge, and Sean J. Johnson. 2010. “Insights into the Reaction of Protein-Tyrosine Phosphatase 1B.” *The Journal of Biological Chemistry* 285 (21): 15874–83. doi:10.1074/jbc.M109.066951.

Buettner, Christoph, Alessandro Pocai, Evan D. Muse, Anne M. Etgen, Martin G. Myers, and Luciano Rossetti. 2006. “Critical Role of STAT3 in Leptin’s Metabolic Actions.” *Cell Metabolism* 4 (1): 49–60. doi:10.1016/j.cmet.2006.04.014.

Burguera, Bartolome, Khawla F. Ali, and Juan P. Brito. 2017. “Antiobesity Drugs in the Management of Type 2 Diabetes: A Shift in Thinking?” *Cleveland Clinic Journal of Medicine* 84 (7 Suppl 1): S39–46. doi:10.3949/ccjm.84.s1.05.

Bustanji, Yasser, Mutasem O. Taha, Al-Motassem Yousef, and Amal G. Al- Bakri. 2006. “Berberine Potently Inhibits Protein Tyrosine Phosphatase 1B: Investigation by Docking Simulation and Experimental Validation.” *Journal of Enzyme Inhibition and Medicinal Chemistry* 21 (2): 163–71. doi:10.1080/14756360500533026.

Bustanji, Yasser, Mutasem Omar Taha, Ihab Mustafa Al-masri, and Mohammad Khalil Mohammad. 2009. “Docking Simulations and *in Vitro* Assay Unveil Potent Inhibitory Action of Papaverine against Protein Tyrosine Phosphatase 1B.” *Biological and Pharmaceutical Bulletin* 32 (4): 640–45. doi:10.1248/bpb.32.640.

Bustanji, Yasser, Mutasem Omar Taha, Ihab Mustafa Al-Masri, and Mohammad Khalil Mohammad. 2009. “Docking Simulations and in Vitro Assay Unveil Potent Inhibitory Action of Papaverine against Protein Tyrosine Phosphatase 1B.” *Biological & Pharmaceutical Bulletin* 32 (4): 640–45.

Cala, Olivier, Florence Guillière, and Isabelle Krimm. 2014. “NMR-Based Analysis of Protein–ligand Interactions.” *Analytical and Bioanalytical Chemistry* 406 (4): 943–56. doi:10.1007/s00216-013-6931-0.

Carlberg, Carsten, and Moray J. Campbell. 2013. “Vitamin D Receptor Signaling Mechanisms: Integrated Actions of a Well-Defined Transcription Factor.” *Steroids* 78 (2): 127–36. doi:10.1016/j.steroids.2012.10.019.

Carlomagno, Teresa. 2005. “Ligand-Target Interactions: What Can We Learn from NMR?” *Annual Review of Biophysics and Biomolecular Structure* 34 (1): 245–66. doi:10.1146/annurev.biophys.34.040204.144419.

Castellano, Jose M., Angeles Guinda, Teresa Delgado, Mirela Rada, and Jose A. Cayuela. 2013. “Biochemical Basis of the Antidiabetic Activity of Oleanolic Acid and Related Pentacyclic Triterpenes.” *Diabetes* 62 (6): 1791–99. doi:10.2337/db12-1215.

Cefalu, William T. 2004. “Evolving Strategies for Insulin Delivery and Therapy.” *Drugs* 64 (11): 1149–61.

Chantemèle, Eric J. Belin de, Kenjiro Muta, James Mintz, Michel L. Tremblay, Mario B. Marrero, David Fulton, and David W. Stepp. 2009. “Protein Tyrosine Phosphatase 1B, a Major Regulator of Leptin-Mediated Control of Cardiovascular Function.” *Circulation* 120 (9): 753–63. doi:10.1161/CIRCULATIONAHA.109.853077.

Chen, Chunhua, Yuebo Zhang, and Cheng Huang. 2010. “Berberine Inhibits PTP1B Activity and Mimics Insulin Action.” *Biochemical and Biophysical Research Communications* 397 (3): 543–47. doi:10.1016/j.bbrc.2010.05.153.

Chen, Yan, You-Mei Tang, Su-Lan Yu, Yu-Wei Han, Jun-Ping Kou, Bao-Lin Liu, and Bo-Yang Yu. 2015. “Advances in the Pharmacological Activities and Mechanisms of Diosgenin.” *Chinese Journal of Natural Medicines* 13 (8): 578–87. doi:10.1016/S1875-5364(15)30053-4.

Cheng, Alan, Noriko Uetani, Paul D. Simoncic, Vikas P. Chaubey, Ailsa Lee-Loy, C. Jane McGlade, Brian P. Kennedy, and Michel L. Tremblay. 2002. “Attenuation of Leptin Action and Regulation of Obesity by Protein Tyrosine Phosphatase 1B.” *Developmental Cell* 2 (4): 497–503. doi:10.1016/S1534-5807(02)00149-1.

Cho, Hyeongjin. 2013. “Chapter Seventeen - Protein Tyrosine Phosphatase 1B (PTP1B) and Obesity.” In *Vitamins & Hormones*, edited by Gerald Litwack, 91:405–24. Obesity. Academic Press. doi:10.1016/B978-0-12-407766-9.00017-1.

Choy, Meng S., Yang Li, Luciana E. S. F. Machado, Micha B. A. Kunze, Christopher R. Connors, Xingyu Wei, Kresten Lindorff-Larsen, Rebecca Page, and Wolfgang Peti. 2017. “Conformational Rigidity and Protein Dynamics at Distinct Timescales Regulate PTP1B Activity and Allostery.” *Molecular Cell* 65 (4): 644–658.e5. doi:10.1016/j.molcel.2017.01.014.

Cimmperman, Piotras, and Daumantas Matulis. 2011. “Protein Thermal Denaturation Measurements via a Fluorescent Dye.” In *Biophysical Approaches Determining Ligand Binding to Biomolecular Targets*, 1st ed., 247–74. RSC Biomolecular Sciences 22. RSCPublishing.

Classen-Houben, Dirk, Daniela Schuster, Thierry Da Cunha, Alex Odermatt, Gerhard Wolber, Ulrich Jordis, and Bernhard Kueenburg. 2009. “Selective Inhibition of 11β-Hydroxysteroid Dehydrogenase 1 by 18α-Glycyrrhetinic Acid but Not 18β-Glycyrrhetinic Acid.” *The Journal of Steroid Biochemistry and Molecular Biology* 113 (3): 248–52. doi:10.1016/j.jsbmb.2009.01.009.

Dadke, Shrikrishna, and Jonathan Chernoff. 2003. “Protein-Tyrosine Phosphatase 1B as a Potential Drug Target for Obesity.” *Current Drug Targets. Immune, Endocrine and Metabolic Disorders* 3 (4): 299–304.

Dalvit, C., G. Fogliatto, A. Stewart, M. Veronesi, and B. Stockman. 2001. “WaterLOGSY as a Method for Primary NMR Screening: Practical Aspects and Range of Applicability.” *Journal of Biomolecular NMR* 21 (4): 349–59.

Dalvit, C., P. Pevarello, M. Tatò, M. Veronesi, A. Vulpetti, and M. Sundström. 2000. “Identification of Compounds with Binding Affinity to Proteins via Magnetization Transfer from Bulk Water.” *Journal of Biomolecular NMR* 18 (1): 65–68.

Delaglio, F., S. Grzesiek, G. W. Vuister, G. Zhu, J. Pfeifer, and A. Bax. 1995. “NMRPipe: A Multidimensional Spectral Processing System Based on UNIX Pipes.” *Journal of Biomolecular NMR* 6 (3): 277–93.

Dixon, C. J., T. Knight, E. Binns, B. Ihaka, and D. O’Brien. 2017. “Clinical Measures of Balance in People with Type Two Diabetes: A Systematic Literature Review.” *Gait & Posture* 58 (August): 325–32. doi:10.1016/j.gaitpost.2017.08.022.

Djerassi, Carl, G. Rosenkranz, J. Pataki, and S. Kaufmann. 1952. “STEROIDS XXVII. SYNTHESIS OF ALLOPREGNANE-3β,11β,17α,20β,21-PENTOL FROM CORTISONE AND DIOSGENIN.” *Journal of Biological Chemistry* 194 (1): 115–18.

Dominguez, Cyril, Rolf Boelens, and Alexandre M. J. J. Bonvin. 2003. “HADDOCK: A Protein−Protein Docking Approach Based on Biochemical or Biophysical Information.” *Journal of the American Chemical Society* 125 (7): 1731–37. doi:10.1021/ja026939x.

Elchebly, Mounib, Paul Payette, Eva Michaliszyn, Wanda Cromlish, Susan Collins, Ailsa Lee Loy, Denis Normandin, et al. 1999. “Increased Insulin Sensitivity and Obesity Resistance in Mice Lacking the Protein Tyrosine Phosphatase-1B Gene.” *Science* 283 (5407): 1544–48. doi:10.1126/science.283.5407.1544.

Eleftheriou, Phaedra. 2016. “The Protein Tyrosine Phosphatase 1b as a Drug Target for the Treatment of Diabetes Type II. Developing Effective and Selective PTP1B Inhibitors.” *ChemXpress* 2 (2). http://www.tsijournals.com/abstract/the-protein-tyrosine-phosphatase-1b-as-a-drug-target-for-the-treatment-of-diabetes-type-ii-developing-effective-and-sele-1426.html.

Emsley, P., and K. Cowtan. 2004. “Coot: Model-Building Tools for Molecular Graphics.” *Acta Crystallographica Section D: Biological Crystallography* 60 (12): 2126–32. doi:10.1107/S0907444904019158.

Erbe, David V., Suyue Wang, Yan-Ling Zhang, Kimberly Harding, Leslie Kung, May Tam, Leslie Stolz, et al. 2005. “Ertiprotafib Improves Glycemic Control and Lowers Lipids via Multiple Mechanisms.” *Molecular Pharmacology* 67 (1): 69–77. doi:10.1124/mol.104.005553.

Ericsson, Ulrika B., B. Martin Hallberg, George T. Detitta, Niek Dekker, and Pär Nordlund. 2006. “Thermofluor-Based High-Throughput Stability Optimization of Proteins for Structural Studies.” *Analytical Biochemistry* 357 (2): 289–98. doi:10.1016/j.ab.2006.07.027.

Esquivel, Mary Angelynne, and M. Cecilia Lansang. 2017. “Optimizing Diabetes Treatment in the Presence of Obesity.” *Cleveland Clinic Journal of Medicine* 84 (7 Suppl 1): S22–29. doi:10.3949/ccjm.84.s1.04.

Evans, Philip, and Airlie McCoy. 2008. “An Introduction to Molecular Replacement.” *Acta Crystallographica Section D: Biological Crystallography* 64 (Pt 1): 1–10. doi:10.1107/S0907444907051554.

Feldhammer, Matthew, Noriko Uetani, Diego Miranda-Saavedra, and Michel L. Tremblay. 2013. “PTP1B: A Simple Enzyme for a Complex World.” *Critical Reviews in Biochemistry and Molecular Biology* 48 (5): 430–45. doi:10.3109/10409238.2013.819830.

Feng, Brian Y, and Brian K Shoichet. 2006. “A Detergent-Based Assay for the Detection of Promiscuous Inhibitors.” *Nature Protocols* 1 (2): 550–53. doi:10.1038/nprot.2006.77.

Flint, Andrew J., Tony Tiganis, David Barford, and Nicholas K. Tonks. 1997. “Development of ‘Substrate-Trapping’ Mutants to Identify Physiological Substrates of Protein Tyrosine Phosphatases.” *Proceedings of the National Academy of Sciences of the United States of America* 94 (5): 1680–85.

Foster, Mark P., Craig A. McElroy, and Carlos D. Amero. 2007. “Solution NMR of Large Molecules and Assemblies.” *Biochemistry* 46 (2): 331–40. doi:10.1021/bi0621314.

Frühbeck, Gema. 2006. “Intracellular Signalling Pathways Activated by Leptin.” *Biochemical Journal* 393 (Pt 1): 7–20. doi:10.1042/BJ20051578.

Fu, Weiqi, Jianping Lin, and Peilin Cen. 2007. “5-Aminolevulinate Production with Recombinant Escherichia Coli Using a Rare Codon Optimizer Host Strain.” *Applied Microbiology and Biotechnology* 75 (4): 777–82. doi:10.1007/s00253-007-0887-y.

Galic, Sandra, Manuela Klingler-Hoffmann, Michelle T. Fodero-Tavoletti, Michelle A. Puryer, Tzu-Ching Meng, Nicholas K. Tonks, and Tony Tiganis. 2003. “Regulation of Insulin Receptor Signaling by the Protein Tyrosine Phosphatase TCPTP.” *Molecular and Cellular Biology* 23 (6): 2096–2108. doi:10.1128/MCB.23.6.2096-2108.2003.

Gasteiger, E., C. Hoogland, A. Gattiker, S. Duvaud, M. R. Wilkins, R. D. Appel, and A. Bairoch. 2005. “Protein Identification and Analysis Tools on the ExPASy Server.” In *The Proteomics Protocols Handbook*, 571–607. Humana Press.

Gebregiworgis, Teklab, and Robert Powers. 2012. “Application of NMR Metabolomics to Search for Human Disease Biomarkers.” *Combinatorial Chemistry & High Throughput Screening* 15 (8): 595–610.

Ghosh, Sougata, Piyush More, Abhishek Derle, Ajay B. Patil, Pramod Markad, Adersh Asok, Navanath Kumbhar, et al. 2014. "Diosgenin from Dioscorea Bulbifera: Novel Hit for Treatment of Type II Diabetes Mellitus with Inhibitory Activity against α-Amylase and α-Glucosidase." *PLoS ONE* 9 (9). doi:10.1371/journal.pone.0106039.

Goldstein, Barry J., Anna Bittner-Kowalczyk, Morris F. White, and Mark Harbeck. 2000. "Tyrosine Dephosphorylation and Deactivation of Insulin Receptor Substrate-1 by Protein-Tyrosine Phosphatase 1B POSSIBLE FACILITATION BY THE FORMATION OF A TERNARY COMPLEX WITH THE GRB2 ADAPTOR PROTEIN." *Journal of Biological Chemistry* 275 (6): 4283–89. doi:10.1074/jbc.275.6.4283.

Guo, Yihe, Cara Martinez-Williams, Kirk A. Gilbert, and D. Eugene Rannels. 1999. "Inhibition of Gap Junction Communication in Alveolar Epithelial Cells by 18α-Glycyrrhetinic Acid." *American Journal of Physiology - Lung Cellular and Molecular Physiology* 276 (6): L1018–26.

Haines, Thomas H. 2001. "Do Sterols Reduce Proton and Sodium Leaks through Lipid Bilayers?" *Progress in Lipid Research* 40 (4): 299–324. doi:10.1016/S0163-7827(01)00009-1.

Hampton research Index. n.d. "Https://Hamptonresearch.Com/Documents/Product/Hr008507_binder1.Pdf."

Hartshorn, Michael J., Christopher W. Murray, Anne Cleasby, Martyn Frederickson, Ian J. Tickle, and Harren Jhoti. 2005. "Fragment-Based Lead Discovery Using X-Ray Crystallography." *Journal of Medicinal Chemistry* 48 (2): 403–13. doi:10.1021/jm0495778.

He, Yaqin, Hexin Yan, Hui Dong, Peng Zhang, Liang Tang, Xiuhua Qiu, Mengchao Wu, and Hongyang Wang. 2005. "Structural Basis of Interaction between Protein Tyrosine Phosphatase PCP-2 and Beta-Catenin." *Science in China. Series C, Life Sciences* 48 (2): 163–67.

Heinonen, Krista M., Frederick P. Nestel, Evan W. Newell, Gabrielle Charette, Thomas A. Seemayer, Michel L. Tremblay, and Wayne S. Lapp. 2004. "T-Cell Protein Tyrosine Phosphatase Deletion Results in Progressive Systemic Inflammatory Disease." *Blood* 103 (9): 3457–64. doi:10.1182/blood-2003-09-3153.

Herre, David J., J. Blake Norman, Ruchi Anderson, Michel L. Tremblay, Anne-Cecile Huby, and Eric J. Belin de Chantemèle. 2015. "Deletion of Protein Tyrosine Phosphatase 1B (PTP1B) Enhances Endothelial Cyclooxygenase 2 Expression and Protects Mice from Type 1 Diabetes-Induced Endothelial Dysfunction." *PLoS ONE* 10 (5). doi:10.1371/journal.pone.0126866.

Hoang, Duc Manh, Tran Minh Ngoc, Nguyen Tien Dat, Do Thi Ha, Young Ho Kim, Hoang Van Luong, Jong Seog Ahn, and KiHwan Bae. 2009. "Protein Tyrosine Phosphatase 1B Inhibitors Isolated from Morus Bombycis." *Bioorganic & Medicinal Chemistry Letters* 19 (23): 6759–61. doi:10.1016/j.bmcl.2009.09.102.

Hobiger, Kirstin, and Thomas Friedrich. 2015. "Voltage Sensitive Phosphatases: Emerging Kinship to Protein Tyrosine Phosphatases from Structure-Function Research." *Frontiers in Pharmacology* 6. doi:10.3389/fphar.2015.00020.

Hong, Soon-Sun, Jong-Ho Kim, Hong Li, and Chang-Koo Shim. 2005. "Advanced Formulation and Pharmacological Activity of Hydrogel of the Titrated Extract of C. Asiatica." *Archives of Pharmacal Research* 28 (4): 502–8.

Hsu, Yuan-Man, Yi-chih Hung, Lihong Hu, Yi-ju Lee, and Mei-chin Yin. 2015. "Anti-Diabetic Effects of Madecassic Acid and Rotundic Acid." *Nutrients* 7 (12): 10065–75. doi:10.3390/nu7125512.

Huijsduijnen, Rob Hooft van, Sébastien Wälchli, Mark Ibberson, and Axel Harrenga. 2002. "Protein Tyrosine Phosphatases as Drug Targets: PTP1B and Beyond." *Expert Opinion on Therapeutic Targets* 6 (6): 637–47. doi:10.1517/14728222.6.6.637.

Hwang, Jessica L., and Roy E. Weiss. 2014. "Steroid-Induced Diabetes: A Clinical and Molecular Approach to Understanding and Treatment." *Diabetes/Metabolism Research and Reviews* 30 (2): 96–102. doi:10.1002/dmrr.2486.

Iversen, Lars Fogh, Karin Bach Møller, Anja K. Pedersen, Günther H. Peters, Annette S. Petersen, Henrik Sune Andersen, Sven Branner, Steen B. Mortensen, and Niels Peter Hundahl Møller. 2002. "Structure Determination of T Cell Protein-Tyrosine Phosphatase." *Journal of Biological Chemistry* 277 (22): 19982–90. doi:10.1074/jbc.M200567200.

Jacobsen, Neil E. 2007. *NMR Spectroscopy Explained: Simplified Theory, Applications and Examples for Organic Chemistry and Structural Biology*. 1st ed. Wiley-Interscience. http://gen.lib.rus.ec/book/index.php?md5=BF651B9A6981D743A209CC72554123A6.

Jasem, Yosef Al, Mubashar Khan, Ahmed Taha, and Thies Thiemann. 2014. "Preparation of Steroidal Hormones with an Emphasis on Transformations of Phytosterols and Cholesterol - a Review." *Mediterranean Journal of Chemistry* 3 (2): 796–830.

Jesus, Mafalda, Ana P. J. Martins, Eugenia Gallardo, and Samuel Silvestre. 2016. "Diosgenin: Recent Highlights on Pharmacology and Analytical Methodology." Research article. *Journal of Analytical Methods in Chemistry*. doi:10.1155/2016/4156293.

Jiang, Cheng-shi, Lin-fu Liang, and Yue-wei Guo. 2012. "Natural Products Possessing Protein Tyrosine Phosphatase 1B (PTP1B) Inhibitory Activity Found in the Last Decades." *Acta Pharmacologica Sinica* 33 (10): 1217–45. doi:10.1038/aps.2012.90.

Johnson, Theodore O., Jacques Ermolieff, and Michael R. Jirousek. 2002. "Protein Tyrosine Phosphatase 1B Inhibitors for Diabetes." *Nature Reviews Drug Discovery* 1 (9): 696–709. doi:10.1038/nrd895.

Joshi, Prashant, Omprakash Tanwar, Sujit Rambhade, Mukesh Bhaisare, and Deepti Jain. 2012. "2-D QSAR Studies of Steroidal Natural Products Oleanic Acid and Their Semisynthetic Derivatives as Potent Protein Tyrosine Phosphatase 1B Inhibitors." *Medicinal Chemistry Research* 21 (3): 351–61. doi:10.1007/s00044-010-9529-5.

Jung, Hyun Ah, Himanshu Kumar Bhakta, Byung-Sun Min, and Jae Sue Choi. 2016. "Fucosterol Activates the Insulin Signaling Pathway in Insulin Resistant HepG2 Cells via Inhibiting PTP1B." *Archives of Pharmacal Research* 39 (10): 1454–64. doi:10.1007/s12272-016-0819-4.

Jung, Hyun Ah, Md. Nurul Islam, Chan Mi Lee, Sang Ho Oh, Sanghyuk Lee, Jee H. Jung, and Jae Sue Choi. 2013. "Kinetics and Molecular Docking Studies of an Anti-Diabetic Complication Inhibitor Fucosterol from Edible Brown Algae Eisenia Bicyclis and Ecklonia Stolonifera." *Chemico-Biological Interactions* 206 (1): 55–62. doi:10.1016/j.cbi.2013.08.013.

Jung, Hyun Ah, Pradeep Paudel, Su Hui Seong, Byung-Sun Min, and Jae Sue Choi. 2017. "Structure-Related Protein Tyrosine Phosphatase 1B Inhibition by Naringenin Derivatives." *Bioorganic & Medicinal Chemistry Letters* 27 (11): 2274–80. doi:10.1016/j.bmcl.2017.04.054.

Kadowaki, S, and A W Norman. 1984. "Dietary Vitamin D Is Essential for Normal Insulin Secretion from the Perfused Rat Pancreas." *Journal of Clinical Investigation* 73 (3): 759–66.

Kavitha, Chandagirikoppal V., Chapla Agarwal, Rajesh Agarwal, and Gagan Deep. 2011. "Asiatic Acid Inhibits Pro-Angiogenic Effects of VEGF and Human Gliomas in Endothelial Cell Culture Models." *PLoS ONE* 6 (8). doi:10.1371/journal.pone.0022745.

Keeler, James. 2005. *Understanding NMR Spectroscopy*. 1st edition. Wiley. http://gen.lib.rus.ec/book/index.php?md5=F8B7FA7221956D42874781559D5BDE0A.

Klaić, Lada, Paul C. Trippier, Rama K. Mishra, Richard I. Morimoto, and Richard B. Silverman. 2011. "Remarkable Stereospecific Conjugate Additions to the Hsp90 Inhibitor Celastrol." *Journal of the American Chemical Society* 133 (49): 19634–37. doi:10.1021/ja208359a.

Klaman, Lori D., Olivier Boss, Odile D. Peroni, Jason K. Kim, Jennifer L. Martino, Janice M. Zabolotny, Nadeem Moghal, et al. 2000. "Increased Energy Expenditure, Decreased Adiposity, and Tissue-Specific Insulin Sensitivity in Protein-Tyrosine Phosphatase 1B-Deficient Mice." *Molecular and Cellular Biology* 20 (15): 5479–89.

Koupý, David, Hana Kotolová, and Jana Rudá Kučerová. 2015. "[Effectiveness of phytotherapy in supportive treatment of type 2 diabetes mellitus II. Fenugreek (Trigonella foenum-graecum)]." *Ceska a Slovenska Farmacie: Casopis Ceske Farmaceuticke Spolecnosti a Slovenske Farmaceuticke Spolecnosti* 64 (3): 67–71.

Krishnamurthy, Rajanikant G., Marie-Claude Senut, Daniel Zemke, Jiangyong Min, Mark B. Frenkel, Eric J. Greenberg, Seong-Woon Yu, et al. 2009. "Asiatic Acid, a Pentacyclic Triterpene From Centella Asiatica, Is Neuroprotective in a Mouse Model of Focal Cerebral Ischemia." *Journal of Neuroscience Research* 87 (11): 2541–50. doi:10.1002/jnr.22071.

Krishnan, Navasona, Dorothy Koveal, Daniel H. Miller, Bin Xue, Sai Dipikaa Akshinthala, Jaka Kragelj, Malene Ringkjøbing Jensen, et al. 2014. "Targeting the Disordered C-Terminus of PTP1B with an Allosteric Inhibitor." *Nature Chemical Biology* 10 (7): 558–66. doi:10.1038/nchembio.1528.

Krohmer, Anna, Martin Brehm, Volker Auwärter, and Bela Szabo. 2017. "Pregnenolone Does Not Interfere with the Effects of Cannabinoids on Synaptic Transmission in the Cerebellum and the Nucleus Accumbens." *Pharmacological Research* 123 (Supplement C): 51–61. doi:10.1016/j.phrs.2017.04.032.

Laemmli, U. K. 1970. "Cleavage of Structural Proteins during the Assembly of the Head of Bacteriophage T4." *Nature* 227 (5259): 680–85.

Langer, Andreas, Paul A. Hampel, Wolfgang Kaiser, Jelena Knezevic, Thomas Welte, Valentina Villa, Makiko Maruyama, et al. 2013. "Protein Analysis by Time-Resolved Measurements with an Electro-Switchable DNA Chip." *Nature Communications* 4 (July): ncomms3099. doi:10.1038/ncomms3099.

Lantz, Kristen A., Susan G. Emeigh Hart, Sonia L. Planey, Mitchell F. Roitman, Inez A. Ruiz-White, Henry R. Wolfe, and Michael P. McLane. 2010. "Inhibition of PTP1B by Trodusquemine (MSI-1436) Causes Fat-Specific Weight Loss in Diet-Induced Obese Mice." *Obesity* 18 (8): 1516–23. doi:10.1038/oby.2009.444.

Lee, Jaemin, Junli Liu, Xudong Feng, Mario Andrés Salazar Hernández, Patrick Mucka, Dorina Ibi, Jae Won Choi, and Umut Ozcan. 2016. "Withaferin A Is a Leptin Sensitizer with Strong Antidiabetic Properties in Mice." *Nature Medicine* 22 (9): 1023–32. doi:10.1038/nm.4145.

Liau, Nicholas P. D., Artem Laktyushin, and Jeffrey J. Babon. 2017. "Purification of SOCS (Suppressor of Cytokine Signaling) SH2 Domains for Structural and Functional Studies." *Methods in Molecular Biology (Clifton, N.J.)* 1555: 173–82. doi:10.1007/978-1-4939-6762-9_10.

Lin, Dan, Wei Sun, Zhe Wang, Lian-Guo Chen, Xiao-Le Chen, Shuang-Hu Wang, Wan-Shu Li, Ren-Shan Ge, and Guo-Xin Hu. 2012. "The Effect of Glycyrrhetinic Acid on Pharmacokinetics of Cortisone and Its Metabolite Cortisol in Rats." Research article. *BioMed Research International*. doi:10.1155/2012/856324.

Lipchock, James M., Heidi P. Hendrickson, Bonnie B. Douglas, Kelly E. Bird, Patrick S. Ginther, Ivan Rivalta, Nicholas S. Ten, Victor S. Batista, and J. Patrick Loria. 2017. "Characterization of Protein Tyrosine Phosphatase 1B Inhibition by Chlorogenic Acid and Cichoric Acid." *Biochemistry* 56 (1): 96–106. doi:10.1021/acs.biochem.6b01025.

Liu, Gang, Zhili Xin, Heng Liang, Cele Abad-Zapatero, Philip J. Hajduk, David A. Janowick, Bruce G. Szczepankiewicz, et al. 2003. "Selective Protein Tyrosine Phosphatase 1B Inhibitors: Targeting the Second Phosphotyrosine Binding Site with Non-Carboxylic Acid-Containing Ligands." *Journal of Medicinal Chemistry* 46 (16): 3437–40. doi:10.1021/jm034088d.

Liu, Junli, Jaemin Lee, Mario Andres Salazar Hernandez, Ralph Mazitschek, and Umut Ozcan. 2015a. "Treatment of Obesity with Celastrol." *Cell* 161 (5): 999–1011. doi:10.1016/j.cell.2015.05.011.

Los, Evan, and Andrew S. Wilt. 2017. "Diabetes Mellitus, Type 1, Pediatric." In *StatPearls*. Treasure Island (FL): StatPearls Publishing. http://www.ncbi.nlm.nih.gov/books/NBK441918/.

Luu-The, Van. 2013. "Assessment of Steroidogenesis and Steroidogenic Enzyme Functions." *The Journal of Steroid Biochemistry and Molecular Biology* 137 (Supplement C): 176–82. doi:10.1016/j.jsbmb.2013.05.017.

Maestro, B., Norma Dávila, M. Carmen Carranza, and Consuelo Calle. 2003. "Identification of a Vitamin D Response Element in the Human Insulin Receptor Gene Promoter." *The Journal of Steroid Biochemistry and Molecular Biology*, Proceedings of the 15th International Symposium of the Journal of Steroid Biochemistry and Molecular Biology - Poster Presentations, 84 (2): 223–30. doi:10.1016/S0960-0760(03)00032-3.

Maestro, B., S. Molero, S. Bajo, N. Dávila, and C. Calle. 2002. "Transcriptional Activation of the Human Insulin Receptor Gene by 1,25-Dihydroxyvitamin D(3)." *Cell Biochemistry and Function* 20 (3): 227–32. doi:10.1002/cbf.951.

Maquart, F. X., F. Chastang, A. Simeon, P. Birembaut, P. Gillery, and Y. Wegrowski. 1999. "Triterpenes from Centella Asiatica Stimulate Extracellular Matrix Accumulation in Rat Experimental Wounds." *European Journal of Dermatology: EJD* 9 (4): 289–96.

Martin, Teresa, and R. Keith Campbell. 2011. "Vitamin D and Diabetes." *Diabetes Spectrum* 24 (2): 113–18. doi:10.2337/diaspect.24.2.113.

Max Planck Crystallization Facility. n.d. "Inhouse Screenings Crystal Platform Magic1 and Magic2. (The Composition of the Screens Is Confidential, Contact the Facility for Information)."

Mayer, Moriz, and Bernd Meyer. 2001. "Group Epitope Mapping by Saturation Transfer Difference NMR To Identify Segments of a Ligand in Direct Contact with a Protein Receptor." *Journal of the American Chemical Society* 123 (25): 6108–17. doi:10.1021/ja0100120.

McCance, David R. 2015. "Diabetes in Pregnancy." *Best Practice & Research. Clinical Obstetrics & Gynaecology* 29 (5): 685–99. doi:10.1016/j.bpobgyn.2015.04.009.

McFarlane, Samy I. 2009. "Antidiabetic Medications and Weight Gain: Implications for the Practicing Physician." *Current Diabetes Reports* 9 (3): 249–54.

McPherson, Alexander. 2009. *Introduction to Macromolecular Crystallography*. 2nd ed. Wiley-Blackwell. http://gen.lib.rus.ec/book/index.php?md5=55C80ECE553F76711C9597E297FE11A0.

Meier, Sebastian, Yu-Chin Li, James Koehn, Isidoros Vlattas, James Wareing, Wolfgang Jahnke, Lawrence P. Wennogle, and Stephan Grzesiek. 2002. "Backbone Resonance Assignment of the 298 Amino Acid Catalytic Domain of Protein Tyrosine Phosphatase 1B (PTP1B)." *Journal of Biomolecular NMR* 24 (2): 165–66.

Melo, Célio L. de, Maria Goretti R. Queiroz, Said G. C. Fonseca, Ayla M. C. Bizerra, Telma L. G. Lemos, Tiago S. Melo, Flavia A. Santos, and Vietla S. Rao. 2010. "Oleanolic Acid, a Natural Triterpenoid Improves Blood Glucose Tolerance in Normal Mice and Ameliorates Visceral Obesity in Mice Fed a High-Fat Diet." *Chemico-Biological Interactions* 185 (1): 59–65. doi:10.1016/j.cbi.2010.02.028.

Meng, Tzu-Ching, Deirdre A. Buckley, Sandra Galic, Tony Tiganis, and Nicholas K. Tonks. 2004. "Regulation of Insulin Signaling through Reversible Oxidation of the Protein-Tyrosine Phosphatases TC45 and PTP1B." *The Journal of Biological Chemistry* 279 (36): 37716–25. doi:10.1074/jbc.M404606200.

Mitri, Joanna, and Anastasios G. Pittas. 2014. "Vitamin D and Diabetes." *Endocrinology and Metabolism Clinics of North America* 43 (1): 205–32. doi:10.1016/j.ecl.2013.09.010.

Moorhead, Greg B. G., Veerle De Wever, George Templeton, and David Kerk. 2009. "Evolution of Protein Phosphatases in Plants and Animals." *Biochemical Journal* 417 (2): 401–9. doi:10.1042/BJ20081986.

Moorhead, Greg B. G., Laura Trinkle-Mulcahy, and Annegret Ulke-Lemée. 2007. "Emerging Roles of Nuclear Protein Phosphatases." *Nature Reviews Molecular Cell Biology* 8 (3): 234–44. doi:10.1038/nrm2126.

Myers, Michael P., Jannik N. Andersen, Alan Cheng, Michel L. Tremblay, Curt M. Horvath, Jean-Patrick Parisien, Annette Salmeen, David Barford, and Nicholas K. Tonks. 2001. "TYK2 and JAK2 Are Substrates of Protein-Tyrosine Phosphatase 1B." *Journal of Biological Chemistry* 276 (51): 47771–74. doi:10.1074/jbc.C100583200.

Na, Min Kyun, Seungmi Yang, Long He, Hyuncheol Oh, Beom Seok Kim, Won Keun Oh, Bo Yeon Kim, and Jong Seog Ahn. 2006. "Inhibition of Protein Tyrosine Phosphatase 1B by Ursane-Type Triterpenes Isolated from Symplocos Paniculata." *Planta Medica* 72 (03): 261–63. doi:10.1055/s-2005-873194.

Na, MinKyun, Long Cui, Byung Sun Min, KiHwan Bae, Jae Kuk Yoo, Bo Yeon Kim, Won Keun Oh, and Jong Seog Ahn. 2006. "Protein Tyrosine Phosphatase 1B Inhibitory Activity of Triterpenes Isolated from Astilbe Koreana." *Bioorganic & Medicinal Chemistry Letters* 16 (12): 3273–76. doi:10.1016/j.bmcl.2006.03.036.

Nguyen, Quang T., Karmella T. Thomas, Katie B. Lyons, Loida D. Nguyen, and Raymond A. Plodkowski. 2011. "Current Therapies and Emerging Drugs in the Pipeline for Type 2 Diabetes." *American Health & Drug Benefits* 4 (5): 303–11.

Norman, A. W., J. B. Frankel, A. M. Heldt, and G. M. Grodsky. 1980. "Vitamin D Deficiency Inhibits Pancreatic Secretion of Insulin." *Science (New York, N.Y.)* 209 (4458): 823–25.

Ohmura, I. 1976. "[Action mechanisms of the contracting drugs, K, acetylcholine, histamine and Ba and of the antispasmodics, isoproterenol and papaverine in the isolated guinea pig ileum, particularly in relation to Ca]." *Nihon Yakurigaku Zasshi. Folia Pharmacologica Japonica* 72 (2): 201–10.

Ortega, A., D. Amorós, and J. García de la Torre. 2011. “Prediction of Hydrodynamic and Other Solution Properties of Rigid Proteins from Atomic- and Residue-Level Models.” *Biophysical Journal* 101 (4): 892–98. doi:10.1016/j.bpj.2011.06.046.

Papandreou, Dimitrios, and Zujaja-Tul-Noor Hamid. 2015. “The Role of Vitamin D in Diabetes and Cardiovascular Disease: An Updated Review of the Literature.” *Disease Markers* 2015. doi:10.1155/2015/580474.

Parker, M.W. 2003. “Protein Structure from X-Ray Diffraction.” *Journal of Biological Physics* 29 (4): 341–62. doi:10.1023/A:1027310719146.

Patterson, Kate I., Tilman Brummer, Philippa M. O’brien, and Roger J. Daly. 2009. “Dual-Specificity Phosphatases: Critical Regulators with Diverse Cellular Targets.” *Biochemical Journal* 418 (3): 475–89. doi:10.1042/BJ20082234.

Payne, Anita H., and Dale B. Hales. 2004. “Overview of Steroidogenic Enzymes in the Pathway from Cholesterol to Active Steroid Hormones.” *Endocrine Reviews* 25 (6): 947–70. doi:10.1210/er.2003-0030.

Pedersen, A. K., G. H. Peters, K. B. Møller, L. F. Iversen, and J. S. Kastrup. 2004. “Water-Molecule Network and Active-Site Flexibility of Apo Protein Tyrosine Phosphatase 1B.” *Acta Crystallographica Section D: Biological Crystallography* 60 (9): 1527–34. doi:10.1107/S0907444904015094.

Pergola, Pablo E., Melissa Krauth, J. Warren Huff, Deborah A. Ferguson, Stacey Ruiz, Colin J. Meyer, and David G. Warnock. 2011. “Effect of Bardoxolone Methyl on Kidney Function in Patients with T2D and Stage 3b–4 CKD.” *American Journal of Nephrology* 33 (5): 469–76. doi:10.1159/000327599.

Pergola, Pablo E., Philip Raskin, Robert D. Toto, Colin J. Meyer, J. Warren Huff, Eric B. Grossman, Melissa Krauth, et al. 2011. “Bardoxolone Methyl and Kidney Function in CKD with Type 2 Diabetes.” *New England Journal of Medicine* 365 (4): 327–36. doi:10.1056/NEJMoa1105351.

Peters, Günther H, Sven Branner, Karin B Møller, Jannik N Andersen, and Niels Peter H Møller. 2003. “Enzyme Kinetic Characterization of Protein Tyrosine Phosphatases.” *Biochimie* 85 (5): 527–34. doi:10.1016/S0300-9084(03)00036-1.

Popov, Doina. 2011. “Novel Protein Tyrosine Phosphatase 1B Inhibitors: Interaction Requirements for Improved Intracellular Efficacy in Type 2 Diabetes Mellitus and Obesity Control.” *Biochemical and Biophysical Research Communications* 410 (3): 377–81. doi:10.1016/j.bbrc.2011.06.009.

Powell, D. R. 2006. “Obesity Drugs and Their Targets: Correlation of Mouse Knockout Phenotypes with Drug Effects in Vivo.” *Obesity Reviews: An Official Journal of the International Association for the Study of Obesity* 7 (1): 89–108. doi:10.1111/j.1467-789X.2006.00220.x.

QIAGEN screenings. n.d. “Https://Www.Qiagen.Com/Products/Protein/Crystallization/Compositiontables/Default.Aspx.”

Qin, Zhaohong, Nihar R. Pandey, Xun Zhou, Chloe A. Stewart, Aswin Hari, Hua Huang, Alexandre F. R. Stewart, Jean Michel Brunel, and Hsiao-Huei Chen. 2015. “Functional Properties of Claramine: A Novel PTP1B Inhibitor and Insulin-Mimetic Compound.” *Biochemical and Biophysical Research Communications* 458 (1): 21–27. doi:10.1016/j.bbrc.2015.01.040.

Raju, Jayadev, and Rekha Mehta. 2009. “Cancer Chemopreventive and Therapeutic Effects of Diosgenin, a Food Saponin.” *Nutrition and Cancer* 61 (1): 27–35. doi:10.1080/01635580802357352.

Raju, Jayadev, Jagan M. R. Patlolla, Malisetty V. Swamy, and Chinthalapally V. Rao. 2004. “Diosgenin, a Steroid Saponin of Trigonella Foenum Graecum (Fenugreek), Inhibits Azoxymethane-Induced Aberrant Crypt Foci Formation in F344 Rats and Induces Apoptosis in HT-29 Human Colon Cancer Cells.” *Cancer Epidemiology and Prevention Biomarkers* 13 (8): 1392–98.

Ramachandran, Vinayagam, Ramalingam Saravanan, and Poomalai Senthilraja. 2014. “Antidiabetic and Antihyperlipidemic Activity of Asiatic Acid in Diabetic Rats, Role of HMG CoA: In Vivo and in Silico Approaches.” *Phytomedicine* 21 (3): 225–32. doi:10.1016/j.phymed.2013.08.027.

Ramagopalan, Sreeram V., Andreas Heger, Antonio J. Berlanga, Narelle J. Maugeri, Matthew R. Lincoln, Amy Burrell, Lahiru Handunnetthi, et al. 2010. “A ChIP-Seq Defined Genome-Wide Map of Vitamin D Receptor Binding: Associations with Disease and Evolution.” *Genome Research* 20 (10): 1352–60. doi:10.1101/gr.107920.110.

Ramírez-Espinosa, Juan José, Maria Yolanda Rios, Sugey López-Martínez, Fabian López-Vallejo, José L. Medina-Franco, Paolo Paoli, Guido Camici, Gabriel Navarrete-Vázquez, Rolffy Ortiz-Andrade, and Samuel Estrada-Soto. 2011. “Antidiabetic Activity of Some Pentacyclic Acid Triterpenoids, Role of PTP–1B: In Vitro, in Silico, and in Vivo Approaches.” *European Journal of Medicinal Chemistry* 46 (6): 2243–51. doi:10.1016/j.ejmech.2011.03.005.

Ramírez-Espinosa, Juan José, Maria Yolanda Rios, Paolo Paoli, Virginia Flores-Morales, Guido Camici, Vianey de la Rosa-Lugo, Sergio Hidalgo-Figueroa, Gabriel Navarrete-Vázquez, and Samuel Estrada-Soto. 2014. “Synthesis of Oleanolic Acid Derivatives: In Vitro, in Vivo and in Silico Studies for PTP-1B Inhibition.” *European Journal of Medicinal Chemistry* 87 (Supplement C): 316–27. doi:10.1016/j.ejmech.2014.09.036.

Rao, Vietla S., Celio L. de Melo, Maria Goretti R. Queiroz, Telma L.G. Lemos, Dalgimar B. Menezes, Tiago S. Melo, and Flavia A. Santos. 2011. “Ursolic Acid, a Pentacyclic Triterpene from Sambucus Australis, Prevents Abdominal Adiposity in Mice Fed a High-Fat Diet.” *Journal of Medicinal Food* 14 (11): 1375–82. doi:10.1089/jmf.2010.0267.

Roberts, Kenneth D., Lajos Bandi, Harold I. Calvin, William D. Drucker, and Seymour Lieberman. 1964. “Evidence That Steroid Sulfates Serve as Biosynthetic Intermediates.* IV. Conversion of Cholesterol Sulfate in Vivo to Urinary C19 and C21 Steroidal Sulfates†.” *Biochemistry* 3 (12): 1983–88. doi:10.1021/bi00900a034.

Roghani-Dehkordi, Farshad, Mehrdad Roghani, and Tourandokht Baluchnejadmojarad. 2015. “Diosgenin Mitigates Streptozotocin Diabetes-Induced Vascular Dysfunction of the Rat Aorta: The Involved Mechanisms.” *Journal of Cardiovascular Pharmacology* 66 (6): 584–92. doi:10.1097/FJC.0000000000000308.

Salmeen, Annette, Jannik N. Andersen, Michael P. Myers, Tzu-Ching Meng, John A. Hinks, Nicholas K. Tonks, and David Barford. 2003. “Redox Regulation of Protein Tyrosine Phosphatase 1B Involves a Sulphenyl-Amide Intermediate.” *Nature* 423 (6941): 769–73. doi:10.1038/nature01680.

Saltiel, Alan R. 2016. “New Therapeutic Approaches for the Treatment of Obesity.” *Science Translational Medicine* 8 (323): 323rv2. doi:10.1126/scitranslmed.aad1811.

Sanchez-Rangel, Elizabeth, and Silvio E. Inzucchi. 2017. “Metformin: Clinical Use in Type 2 Diabetes.” *Diabetologia* 60 (9): 1586–93. doi:10.1007/s00125-017-4336-x.

Sattler, Michael, Jürgen Schleucher, and Christian Griesinger. 1999. “Heteronuclear Multidimensional NMR Experiments for the Structure Determination of Proteins in Solution Employing Pulsed Field Gradients.” *Progress in Nuclear Magnetic Resonance Spectroscopy - PROG NUCL MAGN RESON SPECTROS* 34 (March): 93–158. doi:10.1016/S0079-6565(98)00025-9.

Schauer, Philip R., Deepak L. Bhatt, John P. Kirwan, Kathy Wolski, Ali Aminian, Stacy A. Brethauer, Sankar D. Navaneethan, et al. 2017. “Bariatric Surgery versus Intensive Medical Therapy for Diabetes — 5-Year Outcomes.” *The New England Journal of Medicine* 376 (7): 641–51. doi:10.1056/NEJMoa1600869.

Schmidt, Stefanie. 2016. “Modulation of PTP1B and TCPTP Activity by Small Molecules.” Master’s Thesis, Technical University of Munich.

Schwalfenberg, Gerry. 2008. “Vitamin D and Diabetes.” *Canadian Family Physician* 54 (6): 864–66.

Scott, Latanya M., Liwei Chen, Kenyon G. Daniel, Wesley H. Brooks, Wayne C. Guida, Harshani R. Lawrence, Said M. Sebti, Nicholas J. Lawrence, and Jie Wu. 2011. “Shp2 Protein Tyrosine Phosphatase Inhibitor Activity of Estramustine Phosphate and Its Triterpenoid Analogs.” *Bioorganic & Medicinal Chemistry Letters* 21 (2): 730–33. doi:10.1016/j.bmcl.2010.11.117.

Seneff, Stephanie. 2014. “Cholesterol, Sulfate, and Heart Disease.” presented at the Wise Traditions Workshop, London, February 9.

Seo, Moon-Hyeong, Jeongbin Park, Eunkyung Kim, Sungchul Hohng, and Hak-Sung Kim. 2014. “Protein Conformational Dynamics Dictate the Binding Affinity for a Ligand.” *Nature Communications* 5 (April): ncomms4724. doi:10.1038/ncomms4724.

Shen, Kui, Yen-Fang Keng, Li Wu, Xiao-Ling Guo, David S. Lawrence, and Zhong-Yin Zhang. 2001. “Acquisition of a Specific and Potent PTP1B Inhibitor from a Novel Combinatorial Library and Screening Procedure.” *Journal of Biological Chemistry* 276 (50): 47311–19. doi:10.1074/jbc.M106568200.

Shibata, S. 2000. “A Drug over the Millennia: Pharmacognosy, Chemistry, and Pharmacology of Licorice.” *Yakugaku Zasshi: Journal of the Pharmaceutical Society of Japan* 120 (10): 849–62.

Silva, Filomena S. G., Paulo J. Oliveira, and Maria F. Duarte. 2016. “Oleanolic, Ursolic, and Betulinic Acids as Food Supplements or Pharmaceutical Agents for Type 2 Diabetes: Promise or Illusion?” *Journal of Agricultural and Food Chemistry* 64 (15): 2991–3008. doi:10.1021/acs.jafc.5b06021.

Simoncic, Paul D., Ailsa Lee-Loy, Dwayne L. Barber, Michel L. Tremblay, and C. Jane McGlade. 2002. “The T Cell Protein Tyrosine Phosphatase Is a Negative Regulator of Janus Family Kinases 1 and 3.” *Current Biology* 12 (6): 446–53. doi:10.1016/S0960-9822(02)00697-8.

Singh, B. R. 1990. “Identification of Specific Domains in Botulinum and Tetanus Neurotoxins.” *Toxicon: Official Journal of the International Society on Toxinology* 28 (8): 992–96.

Sivashanmugam, Arun, Victoria Murray, Chunxian Cui, Yonghong Zhang, Jianjun Wang, and Qianqian Li. 2009. “Practical Protocols for Production of Very High Yields of Recombinant Proteins Using Escherichia Coli.” *Protein Science : A Publication of the Protein Society* 18 (5): 936–48. doi:10.1002/pro.102.

Skinner, Simon P., Rasmus H. Fogh, Wayne Boucher, Timothy J. Ragan, Luca G. Mureddu, and Geerten W. Vuister. 2016. “CcpNmr AnalysisAssign: A Flexible Platform for Integrated NMR Analysis.” *Journal of Biomolecular Nmr* 66 (2): 111–24. doi:10.1007/s10858-016-0060-y.

Smyth, Simon, and Andrew Heron. 2006. “Diabetes and Obesity: The Twin Epidemics.” *Nature Medicine* 12 (1): 75–80. doi:10.1038/nm0106-75.

Sorli, Christopher. 2014. “Insulin Therapy in Type 2 Diabetes: A Reflection on the State of the Art Today and the Potential Journeys yet to Come.” *The American Journal of Medicine* 127 (10 Suppl): S1-2. doi:10.1016/j.amjmed.2014.07.007.

Soulsby, Matthew, and Anton M. Bennett. 2009. “Physiological Signaling Specificity by Protein Tyrosine Phosphatases.” *Physiology* 24 (5): 281–89. doi:10.1152/physiol.00017.2009.

Sprangers, Remco. 2014. “Large Complexes/2H.” presented at the G-NMR School, Helmholtz-Center, Neuheberg, Germany, October 13.

Stier, G. n.d. “PETM Vectors. Unpublished Work.” EMBL.

Strott, Charles A., and Yuko Higashi. 2003. “Cholesterol Sulfate in Human Physiology What’s It All about?” *Journal of Lipid Research* 44 (7): 1268–78. doi:10.1194/jlr.R300005-JLR200.

Studier, F. William. 2005. “Protein Production by Auto-Induction in High Density Shaking Cultures.” *Protein Expression and Purification* 41 (1): 207–34.

Swarbrick, Michael M., Peter J. Havel, Arthur A. Levin, Andrew A. Bremer, Kimber L. Stanhope, Madeline Butler, Sheri L. Booten, et al. 2009. “Inhibition of Protein Tyrosine Phosphatase-1B with Antisense Oligonucleotides Improves Insulin Sensitivity and Increases Adiponectin Concentrations in Monkeys.” *Endocrinology* 150 (4): 1670–79. doi:10.1210/en.2008-0885.

Tabassum, Rizwana, Kumar Vaibhav, Pallavi Shrivastava, Andleeb Khan, Md Ejaz Ahmed, Hayate Javed, Farah Islam, et al. 2013. “Centella Asiatica Attenuates the Neurobehavioral, Neurochemical and Histological Changes in Transient Focal Middle Cerebral Artery Occlusion Rats.” *Neurological Sciences: Official Journal of the Italian Neurological Society and of the Italian Society of Clinical Neurophysiology* 34 (6): 925–33. doi:10.1007/s10072-012-1163-1.

Tamrakar, Akhilesh Kumar, Chandan K. Maurya, and Amit K. Rai. 2014. “PTP1B Inhibitors for Type 2 Diabetes Treatment: A Patent Review (2011 - 2014).” *Expert Opinion on Therapeutic Patents* 24 (10): 1101–15. doi:10.1517/13543776.2014.947268.

Tanti, Jean-François, and Jennifer Jager. 2009. “Cellular Mechanisms of Insulin Resistance: Role of Stress-Regulated Serine Kinases and Insulin Receptor Substrates (IRS) Serine Phosphorylation.” *Current Opinion in Pharmacology* 9 (6): 753–62. doi:10.1016/j.coph.2009.07.004.

Tautz, Lutz, and Eduard A. Sergienko. 2013. “High-Throughput Screening for Protein Tyrosine Phosphatase Activity Modulators.” *Methods in Molecular Biology (Clifton, N.J.)* 1053 (July): 223–40. doi:10.1007/978-1-62703-562-0_14.

Tiganis, Tony. 2013. “PTP1B and TCPTP – Nonredundant Phosphatases in Insulin Signaling and Glucose Homeostasis.” *FEBS Journal* 280 (2): 445–58. doi:10.1111/j.1742-4658.2012.08563.x.

Tiganis, Tony, and Anton M. Bennett. 2007. “Protein Tyrosine Phosphatase Function: The Substrate Perspective.” *Biochemical Journal* 402 (Pt 1): 1–15. doi:10.1042/BJ20061548.

Uemura, Taku, Shizuka Hirai, Noriko Mizoguchi, Tsuyoshi Goto, Joo-Yong Lee, Keiko Taketani, Yuki Nakano, et al. 2010. “Diosgenin Present in Fenugreek Improves Glucose Metabolism

by Promoting Adipocyte Differentiation and Inhibiting Inflammation in Adipose Tissues." *Molecular Nutrition & Food Research* 54 (11): 1596–1608. doi:10.1002/mnfr.200900609.

Vallée, Monique. 2016. "Neurosteroids and Potential Therapeutics: Focus on Pregnenolone." *The Journal of Steroid Biochemistry and Molecular Biology*, SI:Steroids & Nervous System, 160 (Supplement C): 78–87. doi:10.1016/j.jsbmb.2015.09.030.

Viegas, Aldino, João Manso, Franklin L. Nobrega, and Eurico J. Cabrita. 2011. "Saturation-Transfer Difference (STD) NMR: A Simple and Fast Method for Ligand Screening and Characterization of Protein Binding." *Journal of Chemical Education* 88 (7): 990–94. doi:10.1021/ed101169t.

Vliet, Catherine van, Patricia E. Bukczynska, Michelle A. Puryer, Christine M. Sadek, Benjamin J. Shields, Michel L. Tremblay, and Tony Tiganis. 2005. "Selective Regulation of Tumor Necrosis Factor–induced Erk Signaling by Src Family Kinases and the T Cell Protein Tyrosine Phosphatase." *Nature Immunology* 6 (3): 253–60. doi:10.1038/ni1169.

Vogt, Merly C., and Jens C. Brüning. 2013. "CNS Insulin Signaling in the Control of Energy Homeostasis and Glucose Metabolism - from Embryo to Old Age." *Trends in Endocrinology and Metabolism: TEM* 24 (2): 76–84. doi:10.1016/j.tem.2012.11.004.

Vondra, K., and R. Hampl. 2006. "[Glucocorticoids and diabetes mellitus]." *Vnitrni Lekarstvi* 52 (5): 493–97.

Wang, Jin, Silvia Gines, Marcy E MacDonald, and James F Gusella. 2005. "Reversal of a Full-Length Mutant Huntingtin Neuronal Cell Phenotype by Chemical Inhibitors of Polyglutamine-Mediated Aggregation." *BMC Neuroscience* 6 (January): 1. doi:10.1186/1471-2202-6-1.

Wang, Yi-Wei, Si-Jia He, Xiao Feng, Jin Cheng, Yun-Tao Luo, Ling Tian, and Qian Huang. 2017. "Metformin: A Review of Its Potential Indications." *Drug Design, Development and Therapy* 11 (August): 2421–29. doi:10.2147/DDDT.S141675.

Welte, Stefan, Karl-Heinz Baringhaus, Wolfgang Schmider, Günter Müller, Stefan Petry, and Norbert Tennagels. 2005. "6,8-Difluoro-4-Methylumbiliferyl Phosphate: A Fluorogenic Substrate for Protein Tyrosine Phosphatases." *Analytical Biochemistry* 338 (1): 32–38. doi:10.1016/j.ab.2004.11.047.

White, Christine A, and Nicos A Nicola. 2013. "SOCS3. An Essential Physiological Inhibitor of Signaling by Interleukin-6 and G-CSF Family Cytokines." *JAK-STAT* 2 (4). doi:10.4161/jkst.25045.

Wiede, Florian, Benjamin J. Shields, Sock Hui Chew, Konstantinos Kyparissoudis, Catherine van Vliet, Sandra Galic, Michel L. Tremblay, Sarah M. Russell, Dale I. Godfrey, and Tony Tiganis. 2011. "T Cell Protein Tyrosine Phosphatase Attenuates T Cell Signaling to Maintain Tolerance in Mice." *The Journal of Clinical Investigation* 121 (12): 4758–74. doi:10.1172/JCI59492.

Wiesmann, Christian, Kenneth J. Barr, Jenny Kung, Jiang Zhu, Daniel A. Erlanson, Wang Shen, Bruce J. Fahr, et al. 2004. "Allosteric Inhibition of Protein Tyrosine Phosphatase 1B." *Nature Structural & Molecular Biology* 11 (8): 730–37. doi:10.1038/nsmb803.

Wilkins, M. R., E. Gasteiger, A. Bairoch, J. C. Sanchez, K. L. Williams, R. D. Appel, and D. F. Hochstrasser. 1999. "Protein Identification and Analysis Tools in the ExPASy Server." *Methods in Molecular Biology (Clifton, N.J.)* 112: 531–52.

Winn, Martyn D., Garib N. Murshudov, and Miroslav Z. Papiz. 2003. "Macromolecular TLS Refinement in REFMAC at Moderate Resolutions." In *Methods in Enzymology*, 374:300–

321. Macromolecular Crystallography, Part D. Academic Press. doi:10.1016/S0076-6879(03)74014-2.

Won, Jong-Heon, Ji-Sun Shin, Hee-Juhn Park, Hyun-Ju Jung, Duck-Jae Koh, Baek-Geon Jo, Jin-Yong Lee, Kijoo Yun, and Kyung-Tae Lee. 2010. "Anti-Inflammatory Effects of Madecassic Acid via the Suppression of NF-KappaB Pathway in LPS-Induced RAW 264.7 Macrophage Cells." *Planta Medica* 76 (3): 251–57. doi:10.1055/s-0029-1186142.

Wu, Panpan, Jie Zheng, Tianming Huang, Dianmeng Li, Qingqing Hu, Anming Cheng, Zhengyun Jiang, Luoying Jiao, Suqing Zhao, and Kun Zhang. 2015. "Synthesis and Evaluation of Novel Triterpene Analogues of Ursolic Acid as Potential Antidiabetic Agent." *PLoS ONE* 10 (9). doi:10.1371/journal.pone.0138767.

Xia, Fuzhen, Li Xie, Anton Mihic, Xiaodong Gao, Yi Chen, Herbert Y. Gaisano, and Robert G. Tsushima. 2008. "Inhibition of Cholesterol Biosynthesis Impairs Insulin Secretion and Voltage-Gated Calcium Channel Function in Pancreatic β-Cells." *Endocrinology* 149 (10): 5136–45. doi:10.1210/en.2008-0161.

Yeagle, P. L. 1991. "Modulation of Membrane Function by Cholesterol." *Biochimie* 73 (10): 1303–10.

You-Ten, Kong E., Eric S. Muise, Annick Itié, Eva Michaliszyn, John Wagner, Serge Jothy, Wayne S. Lapp, and Michel L. Tremblay. 1997. "Impaired Bone Marrow Microenvironment and Immune Function in T Cell Protein Tyrosine Phosphatase–deficient Mice." *The Journal of Experimental Medicine* 186 (5): 683–93.

Zeeuw, Dick de, Tadao Akizawa, Paul Audhya, George L. Bakris, Melanie Chin, Heidi Christ-Schmidt, Angie Goldsberry, et al. 2013. "Bardoxolone Methyl in Type 2 Diabetes and Stage 4 Chronic Kidney Disease." *The New England Journal of Medicine* 369 (26): 2492–2503. doi:10.1056/NEJMoa1306033.

Zhang, Sheng, and Zhong-Yin Zhang. 2007. "PTP1B as a Drug Target: Recent Developments in PTP1B Inhibitor Discovery." *Drug Discovery Today* 12 (9–10): 373–81. doi:10.1016/j.drudis.2007.03.011.

Zhang, Wei, Di Hong, Yueyang Zhou, Yinan Zhang, Qiang Shen, Jing-ya Li, Li-hong Hu, and Jia Li. 2006. "Ursolic Acid and Its Derivative Inhibit Protein Tyrosine Phosphatase 1B, Enhancing Insulin Receptor Phosphorylation and Stimulating Glucose Uptake." *Biochimica et Biophysica Acta (BBA) - General Subjects* 1760 (10): 1505–12. doi:10.1016/j.bbagen.2006.05.009.

Zhang, Zhong-Yin. 1998. "Protein-Tyrosine Phosphatases: Biological Function, Structural Characteristics, and Mechanism of Catalysis." *Critical Reviews in Biochemistry and Molecular Biology* 33 (1): 1–52. doi:10.1080/10409239891204161.

Zhang, Zhong-Yin, Garron T. Dodd, and Tony Tiganis. 2015. "Protein Tyrosine Phosphatases in Hypothalamic Insulin and Leptin Signaling." *Author*, October. https://scholarworks.iupui.edu/handle/1805/9440.

Zhou, J., L. Chan, and S. Zhou. 2012. "Trigonelline: A Plant Alkaloid with Therapeutic Potential for Diabetes and Central Nervous System Disease." *Current Medicinal Chemistry* 19 (21): 3523–31.

Zhou, Yingjiang, and Liangyou Rui. 2013. "Leptin Signaling and Leptin Resistance." *Frontiers of Medicine* 7 (2): 207–22. doi:10.1007/s11684-013-0263-5.

Appendix

Abbreviations

1D, 2D, 3D	1/ 2/ 3 dimension
AC	Activator concentration
ACC	Acetyl-coenzyme-A carboxylase
AEBSF	4-(2-aminoethyl)benzenesulfonyl fluoride hydrochloride
AgRP	Agouti-related protein
AKT	Protein kinase B
Amb	Ambiguous
AOAC	4'-aminoxanilic acid
ASOs	Antisense-based oligonucleotides
bp	Base pair
Cdc	Cell division control proteins
Cdks	Cyclin-dependent kinases
CLU-177	Adult mice hypothalamic cells
COSY	Correlation spectroscopy
CreArc	Arcuate nucleus
CSA	Chemical Shift Anisotropy
C-Src	Proto-oncogene tyrosine-protein kinase Src
CSP	Chemical shift perturbation
DFMP	Difluoromethylene phosphate
DiFMUP	Difluorinated 4-methylumbelliferyl phosphate
DMSO	Dimethyl sulfoxide
DPP-4	Dipeptidyl peptidase-4 inhibitor
DTT	Dithiothreitol
DUSPs	Dual specificity PTPs
EDTA	Ethylenediaminetetraacetic acid
ER	Endoplasmic reticulum
ESRF	European Synchrotron Radiation Facility
F2pmp	Phosphonodifluoromethyl phenyl group
FDA	Food and Drug Administration
MAPK	Mitogen-activated protein kinase
MES	2-(N-morpholino)ethanesulfonic acid
MKSPs	MAPK phosphatases
NF-kB	nuclear factor kappa-light-chain-enhancer of activated B cells
Ni-NTA	Nickel-charged affinity resin
NMR	Nuclear magnetic resonance
FID	Free induction decay
FPS	Fluorescence proximity sensing
GABA	gamma-Aminobutyric acid
GF	Gel filtration
GLP-1	Glucagon-like peptide-1
GLUT4	Glucose transporter type 4
GSH/GSSG	Glutathione/ glutathione disulfide
GSK3	Glycogen synthase kinase 3
HADDOCK	high ambiguity driven protein-protein docking
HDL	high-density lipoprotein
HepG2	Liver hepatocellular cells
HPLC-MS	Liquid chromatography–mass spectrometry
HSQC	Heteronuclear Single Quantum Coherence
IC	Inhibitor concentration
IDO	institute of diabetes and obesity
IKKβ	inhibitor of nuclear factor kappa-B kinase subunit beta
IMAC	Immobilized Metal Affinity Chromatography
IPTG	Isopropyl β-D-1-thiogalactopyranoside
IR	Insulin receptor
IRS	Insulin receptor substrate
IZD	Isothiazolidinone
JAK1, JAK2, JAK3	Janus kinase 1, 2 and 3
KO	Knock-out
LB	Ligase buffer or Lysogeny broth
LC-MS	Liquid chromatography–mass spectrometry
LDL	Low-density lipoprotein
LMW-PTPs	Low molecular weight PTPs
MALDI	Matrix-assisted laser desorption/ionization
MAPK	Mitogen-activated protein kinase
TAE	Tris-acetate-EDTA
TCEP	tris(2-carboxyethyl)phosphine
TCPTP	T-cell protein tyrosine phosphatase
NLS	Nuclear localization signal
NMDA	N-methyl-D-aspartate receptor

NOESY	Nuclear Overhauser and exchange spectroscopy
NP-40	Nonidet-P40
Obr	Astrocyte leptin receptor
OD	Optical density
PBS	Phosphate-buffered saline
PCR	Polymerase chain reaction
p-ERK1/2	Phospho extracellular signal–regulated kinases
p-ERK1/2	Phospho extracellular signal–regulated kinases
PI3K	Phosphatidylinositol-4,5-bisphosphate 3-kinase
p-JAK2	Phospho Janus kinase 2
p-JAK2	Phospho Janus kinase 2
pNP	p-Nitrophenylene anion
pNPH	p-Nitrophenol
pNPP	p-Nitrophenyl phosphate
POMC	Pro-opiomelanocortin
PSPs	Protein serine/threonine phosphatases
pThr	Phosphothreonine
PTKs	Protein Tyrosine Kinases
PTP1B	Protein tyrosine phosphatase
PTPs	Protein Tyrosine Phosphatases
pTyr	Phosphotyrosine
S/N	Signal to noise
SAR	Structure-activity relationship
SDS	Sodium dodecyl sulphate
SDS-PAGE	sodium dodecyl sulphate-polyacrylamide gel electrophoresis
SEC	Size-exclusion chromatography
SGLT-2	Sodium-glucose co-transporter-2
SOCS3	Suppressor of cytokine signaling 3
STAT3, STAT5	Signal transducer and activator of transcription 3 and 5
STD	Saturation Transfer Difference
T1D	Type 1 diabetes
T2D	Type 2 diabetes
TEV	Tobacco Etch Virus protease
TMS	Tetramethylsilane
TOCSY	Total correlation spectroscopy
TROSY	Transverse Relaxation Optimized Spectroscopy
TEV	Tobacco Etch Virus protease
TMS	Tetramethylsilane
TOCSY	Total correlation spectroscopy
TROSY	Transverse Relaxation Optimized Spectroscopy
TZD	Thiadiazolidinone
VDR	Vitamin D receptor
WaterLOG	Water-Ligand Observed via Gradient
SY	SpectroscopY
WT	Wild type

Acknowledgments

First of all, I would like to thank Prof. Dr. Michael Sattler for giving me the opportunity to work in his group. I am thankful for his support, valuable comments and suggestions about my work and specially for always finding time to discuss the project.

I would then like to express my deep gratitude to my supervisor Dr. Ana Messias, who entrusted me such an interesting and challenging project. She has been much more than just a tremendous mentor for me. With her continuous support, encouragement, inspiring advice and immense knowledge, she provided my first exposure to the world of advanced scientific research and guided me at every step throughout my Ph.D. work. Without her input it would have been impossible to complete this thesis. I would also like to thank her for all sorts of valuable discussions around different topics we had that contributed to my scientific as well as personal development. I will always admire her for her dedication toward work and family life. This, along with her pleasant and excellent personality are great inspirations to my life.

I am really grateful to the member of my thesis advisory committee Dr. Paul Pfluger (NBD, Research Unit NeuroBiology of Diabetes), for his guidance and support during my studies. His always positive and enthusiastic attitude and his perspective towards my work, contributed to the establishment of an excellent collaboration. I will never forget the warm reception by him and his group, while I was working at his lab. My special thanks go to Dr. Dhiraj Kabra and Katrin Pfuhlmann for providing me the necessary practical and theoretical knowledge around western-blotting. I am really thankful for their always ready to help attitude and their very useful suggestions. I would also like to thank the whole NBD group for the nice environment and for making me feel part of their team.

I would really like to thank Prof. Dr. Franz Hagn and Prof. Dr. Dierk Neissing for kindly accepting my invitation for participation in my examination committee.

I have to thank sincerely Helmholtz Zentrum München Diabetes Portfolio Project for funding my Ph. D. project for the first three and a half years. I am also grateful to my graduate school, HELENA, which provided the funding in order to participate in international scientific conferences and soft skills courses and then continued to fund my Ph.D. for the next one and a half years.

I am really thankful to Arie Geerlof for helping me with cloning, protein expression and protein purification and all his very useful advice. I will never forget that he insisted to perform SLS measurements for me until late night even if it was Friday. I always felt very lucky to have a colleague like Arie. I owe a special thanks to Astrid Lauxen, who together with Arie organized the lab in a way that even for new people it is easy to start working. Her positive energy made our work in HMGU more enjoyable and memorable.

I would like to thank the whole Sattler group for the nice interaction. Mainly, I would like to acknowledge Gerd Gemmecker for helpful discussions about celastrol reactivity and the NMR experiments useful for the compound assignment. I would also like to thank him and Sam Asami for their support and their suggestion when I gave an NMR seminar. Dominik Lenhart, who helped me with the synthesis of the dihydrocelastrol and for performing all the LC-MS analyses. I also want to thank Grzegorz Popowicz and Andreas Bracher for collecting X-ray diffraction data for me at ESRF, Grenoble and especially Grzegorz for training me how acquire these data myself. I also want to thank Rainer Häßner, for maintaining the NMR-spectrometers and the IT-system. I owe a thank you to Waltraud for taking care of the administration and for her valuable help during my first days in Germany.

During my stay in the lab I was lucky to collaborate with the student Steffi Schmidt who contributed a lot to my work.

I would also like to thank Anna Diller and Jenny Halander for the good time we had in our office. I should also thank all the colleagues at HMGU and TUM for providing a wonderful environment to work, especially Pravin, Komal, Carolina, Martin and Nishtha for their generosity and friendship over the years. I want to thank Janosch Hennig and Hyun Seo Kang for the warm welcome to the group and the great parties. With particular gratitude, I would like to thank my colleague and friend Leonidas Emmanoulidis, the most optimistic person I know, whose support and encouragement was more than valuable to me.

I want to thank Stratis, Panos, Nektaria, Dafni, Petros, Nikoleta and John, who made my life in Munich so much easier and enjoyable.

Last but not least, I would like to thank my family with all my heart, my parents, Antonia and Vassilis, Aliki and Stelios, my beloved grandparents, Antigoni and Joseph, my sister Ioanna and my brother Vaggelis for their unconditional support all my years of studies. It was them who encouraged me to follow my interests and stood next to me by providing me help in all aspects. I

am also really grateful to Loukas, who has been my family during the last four years in Munich, for his patience, his support and his love during this period. To them I dedicate my dissertation with all my love.